TECHNICAL REPORT STANDARD TITLE PAGE

1. Report No. FHWA/TX-87/44+415-2F	2. Government Accession No.	3. Recipient's Catalog No.
4. Title and Subtitle STUDY OF DESIGN METHOD FOR VERTICAL DRILLED SHAFT RETAINING WALLS		5. Report Date August 1986 6. Performing Organization Code
7. Author(s) Shin-Tower Wang and Lymon C. Reese		8. Performing Organization Report No. Research Report 415-2F
9. Performing Organization Name and Address Center for Transportation Research, The University of Texas at Austin, Austin, Texas 78712-1075		10. Work Unit No. 11. Contract or Grant No. Research Study 3-5-85-415
12. Sponsoring Agency Name and Address Texas State Department of Highways and Public Transportation; Transportation Planning Division, P. O. Box 5051, Austin, Texas 78763-5051		13. Type of Report and Period Covered Final 14. Sponsoring Agency Code

15. Supplementary Notes
Study conducted in cooperation with the U. S. Department of Transportation, Federal Highway Administration
Research Study Title: "Analysis of Drilled Shafts"

16. Abstract

A method is presented for the design of drilled shafts that are employed as a retaining wall. The method considers the height of the wall, the soil characteristics, the diameter and reinforcing of the drilled shaft, the clear spacing between drilled shafts, and the length of the shaft.

17. Key Words drilled shafts, sand, clay, p-y curves, bending stiffness, ultimate bending moment, retaining wall, lateral earth pressure, deflection, cantilever, model tests	18. Distribution Statement No restrictions. This document is available to the public through the National Technical Information Service, Springfield, Virginia 22161.

19. Security Classif. (of this report)	20. Security Classif. (of this page)	21. No. of Pages	22. Price
Unclassified	Unclassified	374	

Form DOT F 1700.7 (8-69)

STUDY OF DESIGN METHOD FOR VERTICAL DRILLED SHAFT RETAINING WALLS

by

Shin-Tower Wang
Lymon C. Reese

Research Report 415-2F

Analysis of Drilled Shafts
Employed in Earth-Retaining Structures

Research Study 3-5-85-415

conducted for

Texas
State Department of Highways and Public Transportation

in cooperation with the

U. S. Department of Transportation
Federal Highway Administration

by the

CENTER FOR TRANSPORTATION RESEARCH
THE UNIVERSITY OF TEXAS AT AUSTIN

August 1986

The contents of this report reflect the views of the authors, who are responsible for the facts and the accuracy of the data presented herein. The contents do not necessarily reflect the official views or policies of the Federal Highway Administration. This report does not constitute a standard, specification, or regulation.

There was no invention or discovery conceived or first actually reduced to practice in the course of or under this contract, including any art, method, process, machine, manufacture, design or composition of matter, or any new and useful improvement thereof, or any variety of plant which is or may be patentable under the patent laws of the United States of America or any foreign country.

PREFACE

The writers extend special thanks to Dr. Stephen G. Wright for his enthusiastic support of the project and for his valuable suggestions. Thanks are also extended to Dr. Kenneth H. Stokoe, Dr. Richard L. Tucker, and Dr. Ching-Hsie Yew for their contributions to the work.

The assistance of Messrs. Chris Swan, T.C. Lee, and William Isenhower is also acknowledged. Appreciation is expressed to University personnel: Messrs. Leon Snider and James Stewart for their help in construction of the equipment that was used in the small-scale tests. Special thanks go to Ms. Lola Williams for the expeditious handling of numerous administrative details and Ms. Annette Guillen for her careful typing and preparing of this report.

The writers wish to express appreciation to The Texas State Department of Highways and Public Transportation for the financial support of this project and to the Department of Civil Engineering of The University of Texas for the computer and laboratory facilities.

Shin-Tower Wang
Lymon C. Reese

August 1986

ABSTRACT

A method is presented for the design of drilled shafts that are employed as a retaining wall. The method considers the height of the wall, the soil characteristics, the diameter and reinforcing of the drilled shaft, the clear spacing between drilled shafts, and the length of the shaft.

Key Words: drilled shafts, sand, clay, p-y curves, bending stiffness, ultimate bending moment, retaining wall, lateral earth pressure, deflection, cantilever, model tests.

SUMMARY

Recently, drilled shafts at close spacing have become widely used as a ground-support system because of several specific advantages. The drilled-shaft retaining wall has been especially appropriate in congested urban areas where noise and the effect on adjacent property are of importance. While the drilled-shaft wall is widely utilized in many different areas, the design method has been based principally on limit-equilibrium theory. The research described in this report presents a method of design of drilled-shaft retained walls based on the modern concepts of soil-structure interaction. The design method includes consideration of soil conditions and the details of the structure system. Factors that are taken into account are the nonlinear soil-resistance-displacement relationships, shaft spacing, the depth of penetration, and structural properties. Procedures are presented for estimating the loads due to earth pressures, for assessing the resistance of the soil (p-y curves), and for estimating the response (deflection, bending moment, and shear) of the drilled shafts in the wall.

In order to verify the proposed p-y criteria for drilled-shaft retaining walls, small-scale experiments were conducted. Results were predicted from methods that were developed and compared with the measured data. The agreement was good to excellent. In addition, the suitability of the proposed method was examined by collecting the results of full-scale measurements reported in the literature. The results of case studies indicate that the new method, based on the p-y analysis with the group-effect taken into account, is very promising.

IMPLEMENTATION STATEMENT

The method of design of drilled shafts that are used for a retaining wall as presented herein can be employed in the near future. It will be necessary for the computer program that is presented to be put into use and for design personnel to assess the various concepts that are presented.

The writers are of the opinion that the method is superior to any other one presently available.

TABLE OF CONTENTS

LIST OF TABLES

LIST OF FIGURES

LIST OF SYMBOLS

A_y, B_y	nondimensional coefficients for piles of infinite length and finite length, constant pile stiffness, constant soil stiffness, on axial loading
b	pile diameter or width of foundation (L)
c	undrained shear strength (F/L^2)
C	distance used in the Mindlin equation (L)
D	width of a square-shape pile (L)
D_r	relative density
D_1	center to center spacing between two piles (L)
E_c	Young's modulus of concrete (F/L^2)
E_s	soil modulus (secant to p-y curve) (F/L^2)
EI	flexural rigidity of pile (F/L^2)
EI_g	gross section of EI $(F-L^2)$
f_c'	compressive strength of concrete (F/L^2)
f_r	modulus of rupture of concrete, (F/L^2)
f_s	friction on the pile surface (F/L^2)
F_h	Horizontal component from the side of the wedge
F_a	Horizontal force due to active earth pressure (F)
F_p	force against a pile from wedge of soil (F)
F_s	Horizontal resistance from the base of the wedge (F)
F_1, F_2, F_3, F_4	Horizontal components employed in the derivation of ultimate soil resistance in clay (F)
F_5, F_6, F_7	Horizontal components employed in the derivation of ultimate soil resistance in clay (F)
G	coefficient employed in the Ito et al equation shear modulus from pressurement (F/L^2)
G	shear modulus (F/L^2)
h	increment length (L)
H	hight of the wall (L)

H_1	interference depth employed in the derivation of ultimate soil resistance (L)
I	moment of nertia (L^4)
I_{cr}	moment of inertia of the transformed cracked section (L^4)
I_e	effective moment of inertia (L^4)
I_g	moment of inertia of gross concrete section (L^4)
$I_{\rho F}$	elastic influence coefficient for fixed-head pile
$I_{\rho H}$	elastic influence coefficient for deflection caused by horizontal load
$I_{\rho M}$	elastic influence coefficient for deflection caused by moment
$I_{\rho P}$	elastic influence coefficient for deflection caused by horizontal load
J	the polar moment of inertia (L^4)
k	$=bk_o$, soil modulus (F/L^2)
k_o	subgrade modulus (F/L^3)
K_a	minimum coefficient of active earth pressure
K_0	coefficient of earth pressure at rest
K_p	Rankine coefficient of passive pressure
K_1, K_2, K_3, K_4	coefficient employed in the derivation of ultimate soil resistance
L	length of pile (L)
m	number of piles in group
m	pile node number
m	coefficient for the position of surcharge
M	bending moment (F-L)
M_a	maximum moment in member at stage deflection is computed (F-L)
M_{cr}	cracking moment (F-L)
M_m	bending moment at node m (F-L)
M_u	ultimate bending moment in pile (F-L)
n	exponent used in Spangler's equation
n	depth coefficient

N_q	bearing capacity factor
N_q^*	bearing capacity factor including the effect from the adjacent footing
N_ϕ	$= K_p^2$, coefficient employed in the Ito et al equation
p	soil resistance (F-L)
P_a	active earth pressure ($F-L^2$)
P_p	passive earth pressure ($F-L^2$)
P_u	ultimate soil resistance or ultimate soil reaction (F/L)
P_x	axial load at pile top (F)
P_z	soil resistance at the yielding point (F/L)
P_{h2}'	effective confining pressure in the Brom equation (F/L^2)
q	line load (F-L)
q	$= (\sigma_1 + \sigma_3)/2$, average of the principal stresses (F/L^2)
Q	point load (F)
Q_{mj}	resultant force on the increment j of pile m (F)
R_m	$= E_m I_m$, flexural rigidity at pile section m ($F-L^2$)
R_1, R_2, R_3	distance defined in the Mindlin equation
T	relative stiffness factor (1/L)
V	shear (F)
w	distributed load (F/L)
x	coordinate along pile, beam (L)
y	pile deflection and for y-coordinate (L)
y_{gp}	deflection of a pile in a group (L)
y_{sp}	deflection of a single pile (L)
y_{ip}	deflection of a single imaginary pile (L)
y_t	pile top deflection (L)
z	depth (L)
α	angle used in defining geometry of soil wedge
α_g	group factor
α_p	coefficient of earth pressure due to surcharge

β	angle used in defining geometry of soil wedge
γ	average unit weight of soil (F/L^3)
γ'	bouyant unit weight or average unit weight used in computing effective stress (F/L^3)
γ_e	equivalent fluid density (F/L^3)
ε_{50}	axial strain of soil corresponding to one-half the maximum principal stress difference
θ	angle between a particular stress and a principal stress
$\theta_A, \theta_B, \theta_C, \theta_D$	angle θ between the slope line and the x-axis
ν	Poisson's ratio
ρ	steel ratio
ρ_k	deflection of the "k-th" pile (L)
ρ_F	the unit reference displacement of a single pile under a unit horizontal load, computed by using elastic theory (L)
ρ_x	lateral displacement due to the horizontal point load acting beneath the surface of a semi-infinite elastic mass (L)
σ	normal stress (F/L^2)
σ_a	minimum active stress (F/L^2)
σ_f	normal stress on the failure plane (F/L^2)
σ_h	horizontal effective stress (F/L^2)
σ_n	radial pressure (F/L^2)
σ_p	maximum passive stress (F/L^2)
σ_v	average effective stress (F/L^2)
σ_x	stress in the x-direction (F/L^2)
σ_y	stress in the y-direction (F/L^2)
τ	shear stress (F/L^2)
τ_f	shear stress on the failure plane (F/L^2)
τ_{xy}	shear stress on the xy plane
ϕ	angle of internal friction of sand
ϕ	curvature
ξ	constant

η	constant
ω	$= \sin^{-1}(f_s/c)$, ratio of surface friction versus cohesive strength

CHAPTER 1. INTRODUCTION

STATEMENT OF PROBLEM

There are many types of retaining structures such as gravity walls, sheet-pile walls, diaphragm walls, and reinforced-earth walls that are used to retain earth. Each type of wall has its specific advantages and disadvantages, depending on constraints in design and construction.

Recently, drilled shafts at close spacing have become widely used as a ground-support system. The drilled-shaft wall has been especially appropriate in congested urban areas where the movements of the ground near the construction site are limited in magnitude. The use of cantilevered drilled-shaft wall has provided a common and economical solution for excavations of 15 to 25 ft depths in the Houston area when the wall is also incorporated as an integral part of the finished structure (Williams and Shamooelian, 1981). In London, drilled shafts were adopted for the Dunton Green retaining wall because of the specific ground and subsurface conditions (Garrett and Barnes, 1984). The Dunton Green wall was designed with cantilever action for economic and other reasons and the interspaces between the drilled shafts provide the possible drainage of water in Gault clay, which has high shrinkage and swelling associated with the changes of moisture content. In particular, a varying wall height and stiffness could be more readily provided by this design. Another advantage generally given by this type of retaining wall is that the installation can be carried out at almost any site, regardless of ground conditions.

Construction of a drilled-shaft wall has an inherent flexibility. This method is used in built-up areas where noise of construction and effect on adjacent property are of importance. This method is frequently used for underground excavation for basements for buildings, in industrial complexes where access, headroom, or a restriction on vibration are limited, and at places where other types of walls are unsuitable or more expensive. The drilled-shaft wall is related particularly to another important application: the construction of underpasses for highways. In Japan and in the United States, drilled-shaft walls are designed to prevent the failure of earth slopes.

While the drilled-shaft wall is widely utilized for different purposes in the world, the design method has not been well documented. Consequently, there have been questions concerning the guidelines for design. The conventional method of design is based on a limit-equilibrium theory that has a theoretical weakness for soil-structure-interation problems. The behavior of retaining structures is largely a matter of soil conditions and the details of the structural system. Therefore, a rational method of design must include the nonlinear soil-resistance-displacement relationships, shaft spacing, penetration depth, and structural properties. The development of methods of analysis is highly desirable in order to satisfy the requirements of safety and economy.

OBJECTIVE

The objective of this study is to develop a rational method for the design of drilled shafts used for earth retaining walls. This method will logically include procedures for estimating the loads due to earth pressures, procedures for assessing the resistance of the soil (p-y curves), and procedures for estimating the response (deflection, bending moment, and shear) of the drilled shafts in the wall.

This method will include guidelines for selecting the spacing, diameter, flexural rigidity, and penetration for given backfill material, foundation soils, and height of the wall.

STUDY PLAN

As mentioned above, the complete solution of drilled-shaft retaining structures involves predictions of lateral pressures and deformations by considering the initial stress condition in the soil, the stress-strain relationships of the soil, and the boundary conditions describing soil-structure interaction. Such a rigorous solution is extremely complex; therefore, five tasks are planned in order to accomplish the stated objective. These tasks are:

(1) prediction of the load from the earth pressure,

(2) presentation of the effects of nonlinear moment-curvature relationship of the drilled shaft on the behavior of the system,

(3) development of soil resistance curves (p-y) for drilled shafts with the group-effect taken into account,

(4) study of the effects of penetration of the drilled shaft below the cut line*, and

(5) verification and amplification of the theoretical studies by performing small-scale experiments in the laboratory.

The specific aspects and potential problems involved in each task are discussed and the significant results and recommendation are presented in this report. Although these studies are aimed at providing an engineer with a rational method to design a drilled-shaft retaining wall, the approach and concept stressed herein also can form the basis for the design of other types of flexible retaining structures.

---

* A companion report (Swan, Wright, and Reese, 1986) deals with the penetration below the cut line in considerable detail and the results of that report are summarized herein.

CHAPTER 2. BACKGROUND AND LITERATURE REVIEW

BEHAVIOR OF FLEXIBLE RETAINING WALLS

Flexible retaining structures have received much attention since 1940 because of the widespread use in engineering construction. Flexible retaining walls, in contrast to more-or-less rigid, gravity walls, usually mean a single row of sheet piles that may be of timber, reinforced concrete, or steel that are driven by hammers and have their lower ends embedded in soil. There are two principal types of sheet-pile walls commonly in use; namely, simple cantilever walls, and walls which are tied to anchors behind the wall. The response of closely spaced drilled-shaft retaining walls is fundamentally similar to the response of sheet-pile walls. Therefore, a number of the publications on the behavior of sheet-pile walls will provide useful information for this study.

In 1948 Tschebotarioff presented the result of his famous large-scale model tests. One of the most important conclusions was that the distribution of earth pressure on sheet piles is highly influenced by the deformations of walls. Some years later, Rowe (1955) published the results of his medium-scale model tests that confirmed Tschebotarioff's results. Based on these model tests as well as some full-scale measurements, the deflection and the earth pressure on sheet-pile walls can be generally represented as shown in Fig. 2.1. The pressure distribution varies with the wall deflection and it becomes more complicated if the wall deflection is constrained by anchors.

After the classic experiments conducted by Tschebotarioff and Rowe, the measurements of soil deformations behind sheet-pile walls became possible due to the development of the X-ray technique. Deformations of the soil are of interest not only because of the effect of such deformation on adjacent buildings

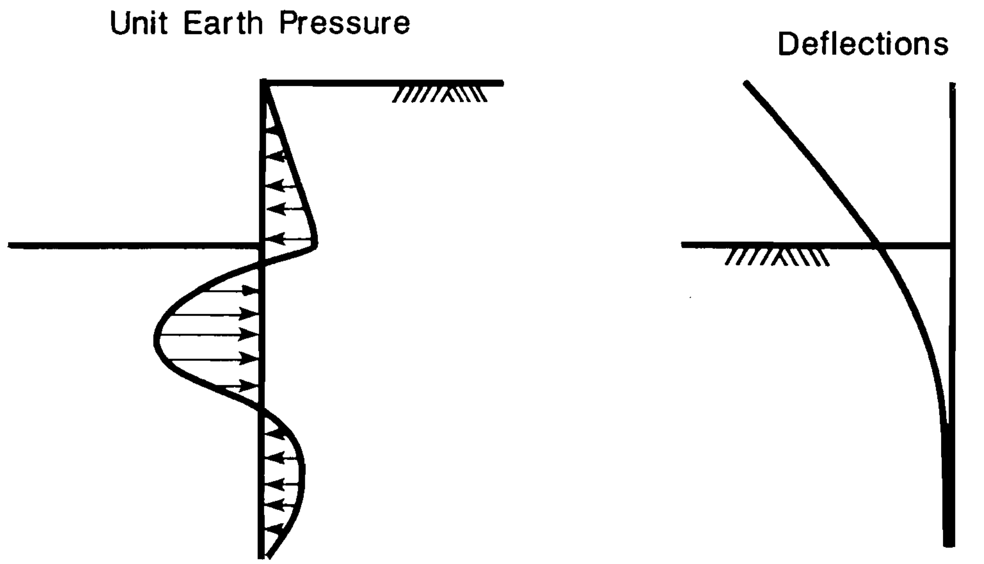

(a) Free-standing sheet piles

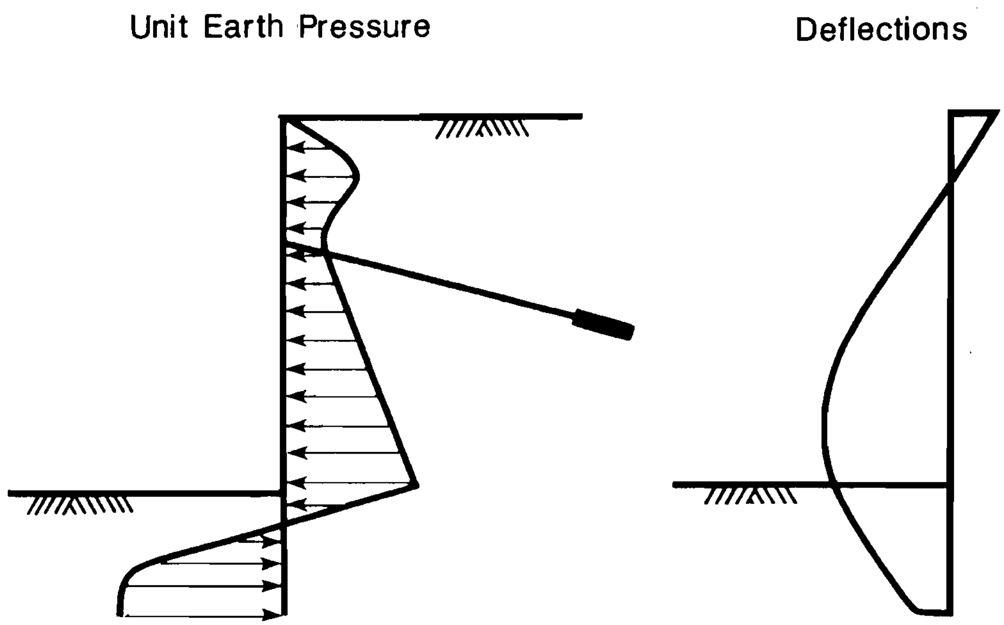

(b) Sheet piles with anchors

Fig. 2.1. The earth pressure and deflection on sheet-pile walls.

but also stresses on the wall will be intimately linked with the soil deformations. The earth pressures on the wall can only be predicted with confidence once both the soil deformations behind the wall and the stress-strain properties of the soil are known. Roscoe, Arthur, and James (1963) were the first researchers to apply X-ray technique to measure the deformations in soil. Essentially, this method consists of burying a regular grid of lead markers within the sand and then exposing radiographs of the sample at different stages of testing. The positions of the images of lead markers on the radiographs are measured and the displacements of each markers may be determined between exposures. Once the displacements of the nodes of the grid are known, the strains within each mesh of the grid may then be calculated. The typical results of soil deformations near cantilever sheet-pile walls, shown in Fig. 2.2, were measured by Bransby and Milligan (1975) in their model tests. As can be seen, the contours of shear strains measured in the experiments established clear patterns of soil deformations on both the active and passive sides of the wall.

Deformations in the active zone behind the wall are confined approximately to a triangular area bounded by a line at about $\pi/4-\phi/2$ to the vertical direction, in which ϕ is the internal friction angle of sand. Deformations in the passive zone are confined to a flat area close to the wall and immediately below the dredge line. The triangular area for passive pressures is bounded by a line at about $\pi/4+\phi/2$ to the vertical direction. The patterns of soil deformations near the walls are similar for tests in dense sand or in loose sand. But the behavior between walls in dense and loose sand were not similar from the measured curves of wall deflections. In loose sand, the wall seemed to be relatively very rigid; thus, the deflection was due largely to rigid body rotation of the wall, and the deflection due to the bending of the wall was small. However, the wall in dense sand behaved as if the end of the wall below the dredge level was fixed, and the deflection of the top of the wall was due entirely to the bending of the wall itself. The cantilever action of the wall in dense sand resulted

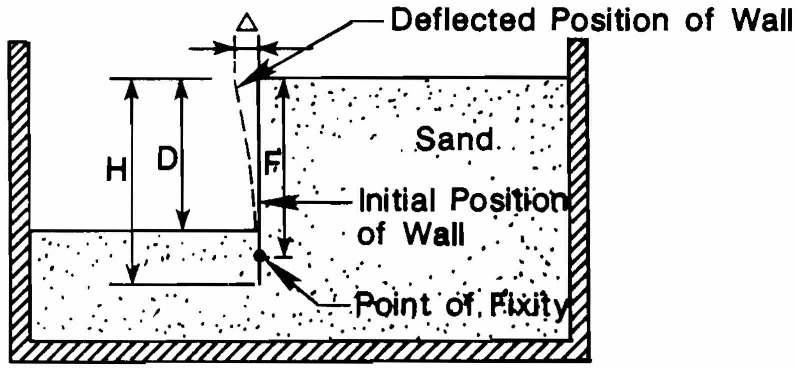

(a) Schematic section of model wall and sand tank

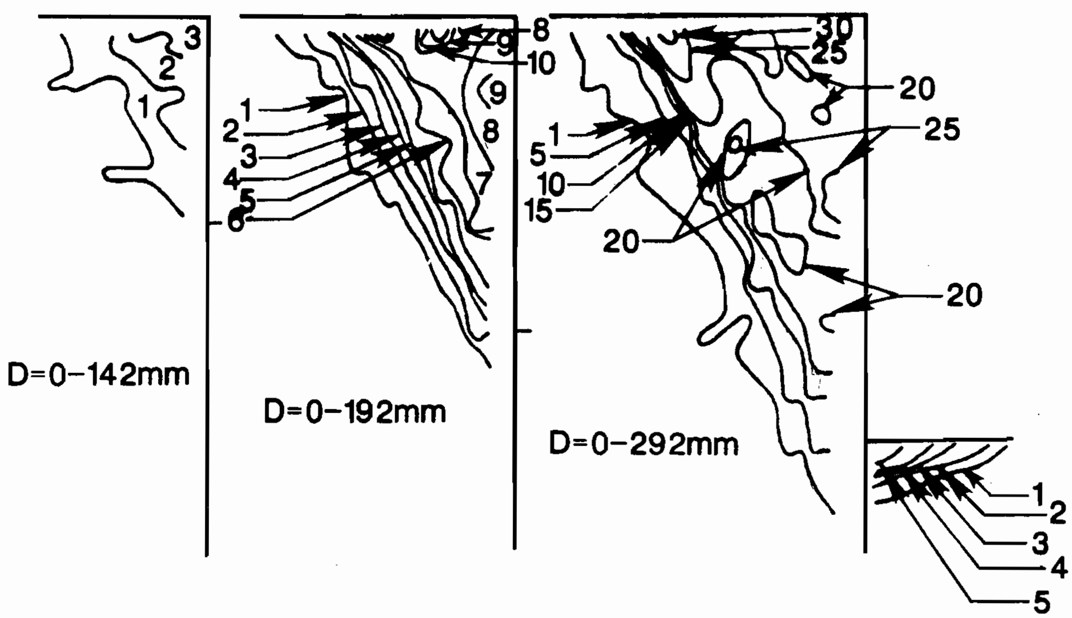

(b) Numbers in figures show observed contours of shear strain (%)

Fig. 2.2. Contours of cumulative shear strain γ (%) for soil near cantilever sheet-pile walls (after Bransby and Milligan, 1975).

in a higher bending moment along the wall than for loose sand. While the rigid rotation of the wall in loose sand led to a smaller bending moment, the deflection of the top of a wall in loose sand was greater than for a wall in dense sand.

Milligan (1983) investigated the deformations of sand behind a wall by performing a series of model tests of flexible sheet-pile walls that were restrained against deflection at the top of the wall. The contours of strains and the location of the rupture surface in the soil are presented in Fig. 2.3. Unlike the measured results for cantilever sheet piles, the strains are very large in a narrow band along the edge of the deforming zone, and relatively small between this band and the wall. The upper part of the deforming zone is complex due to the constraint at the top of the wall. The effects of arching associated with anchored flexible walls have been discussed by a number of authors (Stroyer, 1935; Bjerrum et al., 1972; and Rowe, 1972). Arching likely happened in the soil near the top of the wall in the Milligan tests because the sand had a tendency to dilate, but was confined between the unyielding top of the wall and the almost rigid soil outside the deforming zone. The studies by Milligan and others have indicated the complicated nature of the interactions between a retaining wall and the surrounding soil. Such interaction must be considered in the design of retaining structures.

AVAILABLE METHODS OF DESIGN AND ANALYSIS

Limit-Equilibrium Analysis

The magnitude and the distribution of earth pressure, as mentioned before, is a function of the displacements of the soil and the related deflections of the structure. Because the problem involved is statically indeterminate, the real stress-deformation relations of soils have been ignored and designs have been based on simple assumptions. Most of the so-called conventional methods employ the hydrostatic pressure-distribution theory in the limit-equilibrium analysis. This simplification is agreed to be used

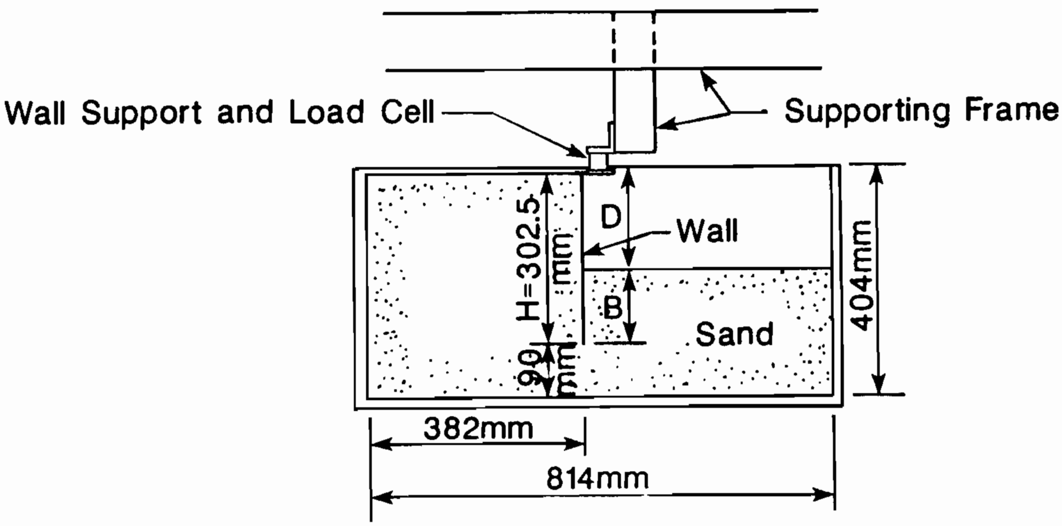

(a) Schematic section of model wall and sand tank

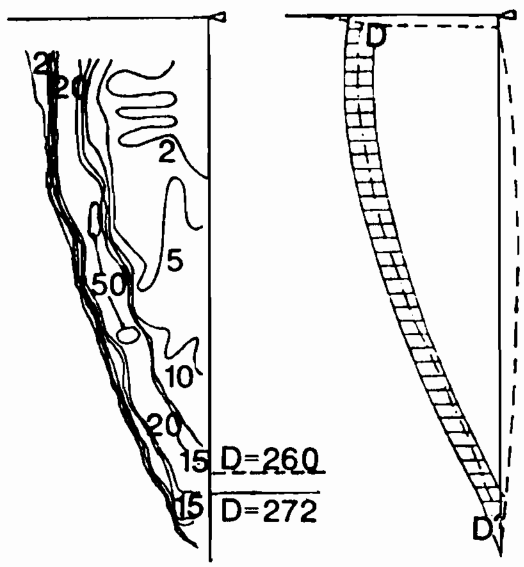

(b) Numbers in figures show observed contours of shear strain (%)

Fig. 2.3. Contours of cumulative shear strain γ (%) for soil near proped sheet-pile walls (after Milligan, 1983).

only if the interaction between the soil and structure is not of concern in the analysis.

Cantilever sheet-pile walls. Walls that are classified in this group depend on an adequate embedment into the soil below the dredge line so that a driven line of sheet piles acts as a wide cantilever beam in resisting the lateral earth pressures that developed above the dredge line. In the conventional design of this type of wall, the hydrostatic-pressure distribution is assumed for the active and passive pressures on the wall. If wall is assumed to rotate under the influence of the earth pressures above the dredge line, a pivot or rotation point C on the wall is found at certain distance below the dredge line. Above point C, the method assumes full active pressures on the back side and full passive pressures on the front side, as shown in Fig. 2.4. The net pressures above point C are shown by a hatched zone. Below this point, it appears that passive pressures should be on the back side, and active pressures should be on the front side. Because the states of stress cannot have an immediate change at the pivot point, a linear variation in the net pressure at point C to the net pressure developed at point J at the bottom of the wall is assumed in the analysis. The net pressures along the depth shown in the figure are computed by one of the classical methods for the design of cantilever walls.

Sheet piles in cohesive soil are treated somewhat similarly to those in granular soil. The typical net-pressure diagram for cohesive soils is presented in Fig. 2.5. There are, however, certain phenomena associated with cohesive soils which require additional consideration. For example, tension cracks may form in the active zone and become filled with water; thus, increasing the lateral pressure considerably. If this situation occurs, the equilibrium equations have to be modified appropriately. Obviously, there are two unknowns involved in the determination of static equilibrium of the system; namely, the depth of embedment, D, and the distance, Z, between the pile tip and the assumed point of rotation, as shown in Figs. 2.4 and 2.5. These two values can be solved by two equilibrium equations; one is from the

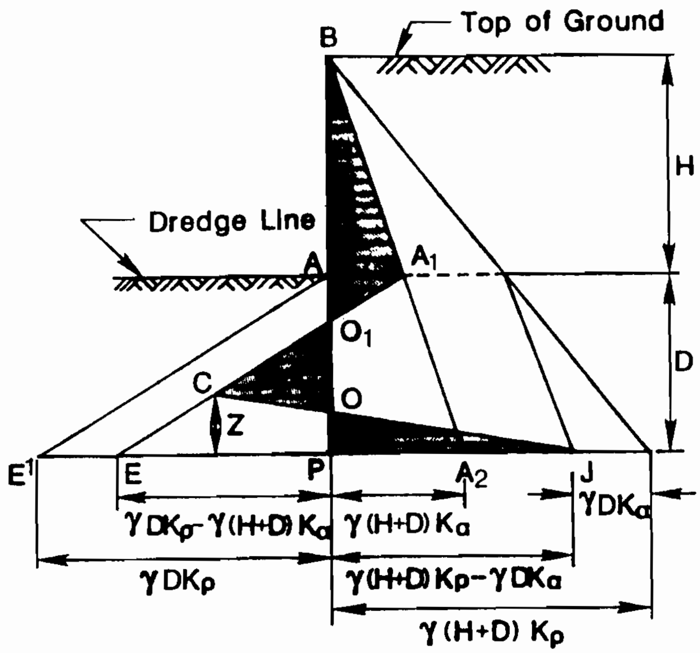

Fig. 2.4. The pressure distribution for the cantilever sheet-pile walls in cohesionless soil (c=0) from the limit-equilibrium analysis.

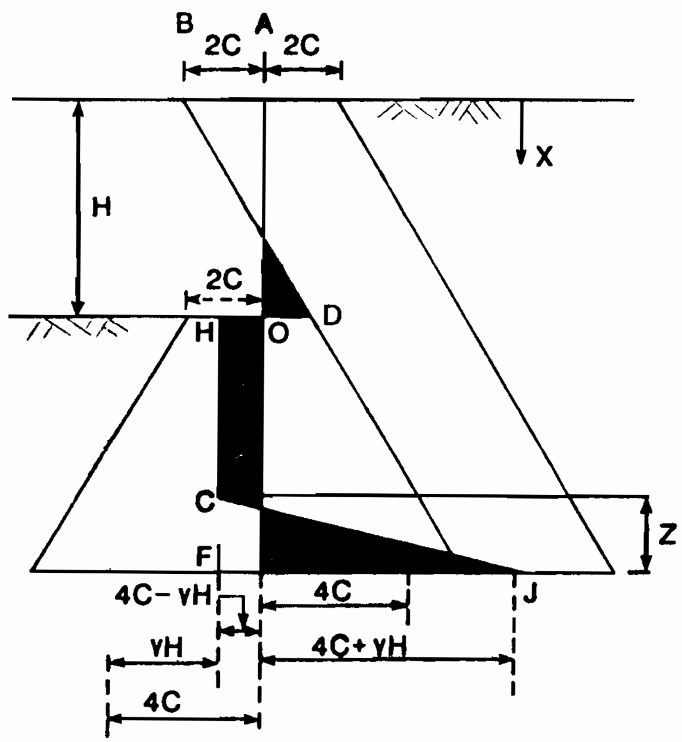

Fig. 2.5. The pressure distribution for the cantilever sheet-pile walls in cohesive soil (ϕ=0) from the limit-equilibrium analysis.

equilibrium of the horizontal forces and the other from the equilibrium of the moments. Because the bending moment increases with the cube of the distance from the top of the wall, the required section modulus increases rapidly with increase in the wall height. The required section modulus is an important factor that must be considered before selecting a cantilever reaction wall. The lateral deflection of this type of wall will be relatively large due to the cantilever action. In general, excessive deflections can cause distress in neighboring structures, but deflection cannot be computed in the limit-equilibrium analysis.

Sheet-pile walls with an anchor (flexible bulkhead). In some instances sheet-pile walls have anchors to reduce the lateral deflection, the bending moment, and the depth of penetration. The analysis of flexible bulkheads is quite different from that for cantilever walls because of the more complex deformations of the flexible-bulkhead system. One of the most important contributions to this type of walls was made by Terzaghi (1954). He described two types of deformations in regard to flexible structures with bulkheads. If sheet piles are driven to shallow depths, the deflections along a sheet pile are assumed similar to those of a simply supported beam. Bulkheads satisfying this condition are said to have free earth support (Fig. 2.6a). If sheet piles are driven to a considerable depth, the lower end of the sheet pile is assumed to be more-or-less fixed in position. Bulkheads of this type are said to have fixed-earth support (Fig. 2.6b). Assuming adequate anchorage, the former case can fail by either bending or sliding of the base of the wall; whereas, the latter case can fail only in bending.

Design of the sheeting for a flexible bulkhead is generally accomplished using the free-earth support concept. The assumption is made that the driving force is active pressure and resistances come from anchor pull and passive pressure near the toe. The unknowns are the depth of penetration and the tie rod force. These unknowns can be found by summing the moments about the tie

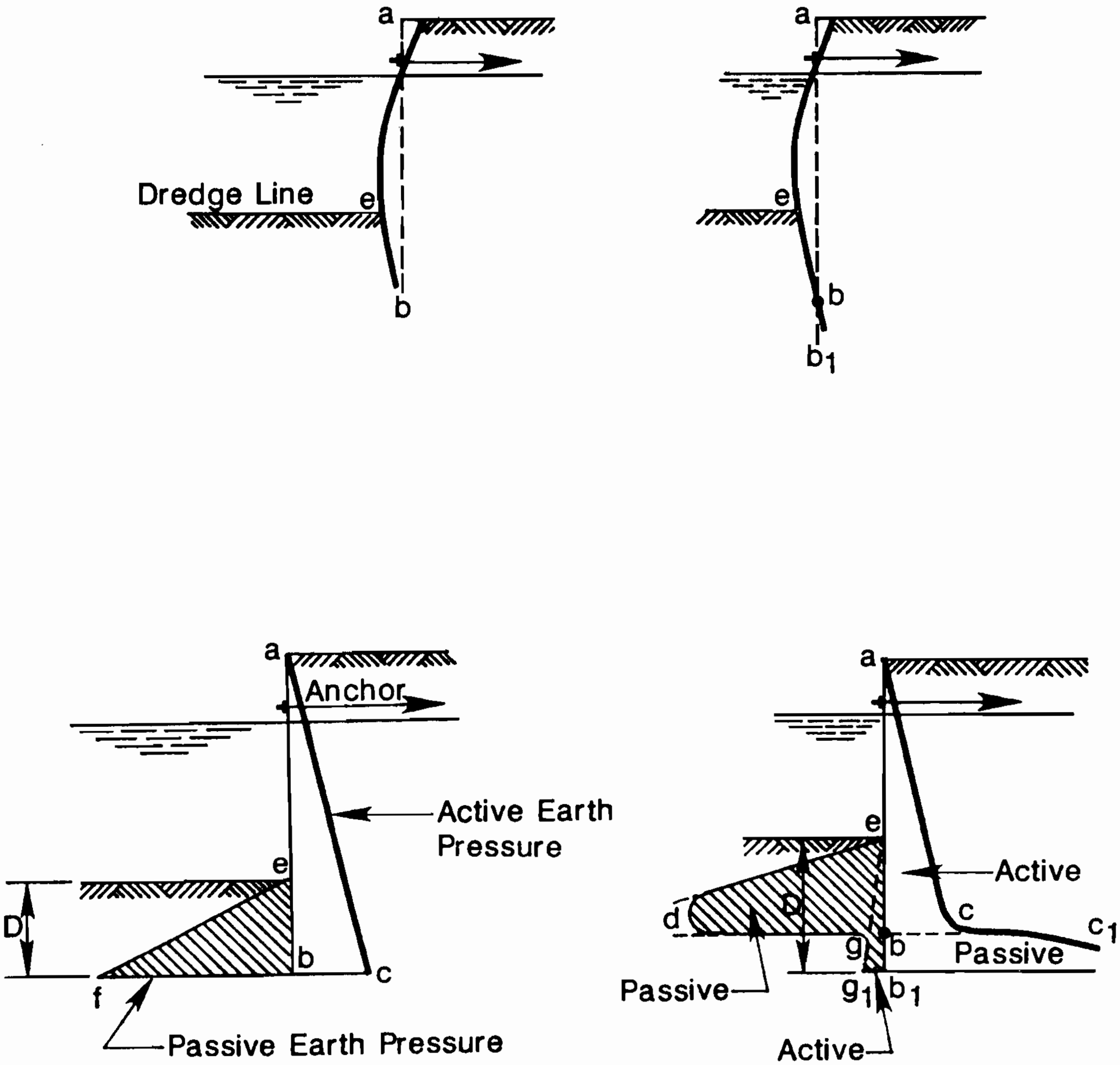

(a) Free earth support

(b) Fixed earth support

Fig. 2.6. Sheet piles with bulkheads (a) free earth support (b) fixed earth support (after Terzaghi, 1954).

rod to get the depth of penetration and summing the horizontal forces to find the tie-rod pull.

In either type of sheet-pile wall, a hydrostatic-type of active earth pressure and of passive earth pressure is assumed and the design is simplified because the effect of wall deformations on the magnitude or the distribution of the soil pressure is ignored. Unfortunately, the principles of soil-structure-interation are violated and an unrealistic pressure distribution can result. While a large number of flexible retaining structures have been designed as indicated above and have given good service, a more rational solution should be achieved.

Subgrade Reaction Method

The desire for improving analysis to consider the development of soil resistance with wall deflection has led to the subgrade reaction method. The method solves the differential equation of the bending beam with the soil represented as linear springs providing resisting forces that increase with lateral deflection. The method became popular and accepted by engineers after Terzaghi published a comprehensive document in 1955 discussing the application of this method and predictions of the subgrade modulus for a variety of cases. Both Rowe(1955) and Richart(1957) published methods of analysis for sheet-pile walls based on the elastic, subgrade-reaction theory.

Rowe took advantage of computer technique at that time and developed solutions for three different cases of loading on a sheet-pile wall as:

Case 1: cantilever pile subjected to a line load at the top.
Case 2: cantilever pile subjected to triangular loading above the dredge line.
Case 3: cantilever pile subjected to a rectangular loading above the dredge line.

The superposition of these results leads to solutions of sheet-pile walls with a variety of boundary conditions. An anchorage system, a surcharge behind a wall, or other combination of loading can be treated.

Richart's method of analysis considers the sheet pile separately above and below the dredge line. Newmark's numerical procedure for beams, plus the assumption of zero deflection at the tie-rod level, is used to determine shear, moment, and pressure at the dredge line. After forces at the boundary are calculated, the theory of subgrade reaction is used to solve the beam below the dredge line.

The subgrade reaction method discussed above is probably accurate for elastic materials but these materials cannot generally represent the real soils. However, it can be seen that this method might be much improved if the linear soil reaction could be replaced by nonlinear soil reaction that is based on realistic test results. The resulting problem can be described as a beam on a nonlinear foundation. Rauhut (1966) and Haliburton (1968) both made attempts at the numerical analysis of flexible retaining walls where the soil response was a nonlinear function of wall deflection. The utility of such solutions is considerable in the design of flexible retaining walls so that ways can be found to protect soil response as a function of wall deflection.

Finite-Element Method

It is well recognized that the determination of the actual earth pressure on a wall is extremely complicated, because it depends on the relative movement of the wall and the soil. The finite-element method has been found to be a powerful tool for solving problems which involve equilibrium and the compatibility of stresses and strains in a continuum. Most of the flexible retaining walls pose typical two-dimensional problems and solutions to these problems have been obtained and well documented in many texts. The use of finite element methods has allowed attempts to be made at the complete solution of the retaining-wall problem, including the computation of stresses and deformations in both the wall and the adjoining soil. The recent development of high-speed computers has opened up the possibility of obtaining improved solutions to the problem of interaction between a flexible structure and the nonlinear, inelastic soil medium. The problems that now can be handled by the finite-element analysis range from simple retaining structures to such complex problems as anchored and braced excavations (Clough and Tsui, 1971).

The significant advantage of the finite-element analysis over the other methods is the capability of studying the stresses and strains developed on the entire system and this provides a better understanding of the behavior of the soil and the wall. However, the outcome of this method seems to depend strongly on the use of the correct soil data. Limitations in using this method primarily derive from the inability to describe an appropriate constitutive law for soil and to determine the parameters needed for the constitutive models. Although the finite-element analysis is still not developed far enough to be used for design purposes, it has already at the present stage of development proved to represent a valuable tool in a study of the interaction between the soil and structures.

CONCLUSION

As mentioned above, the interactions between the structure and the soil on retaining walls will be governed by the retained soil at the back, supporting soil in the front, as well as the structure itself. The response of the soil is a function of the soil-structure system and of the permissible deflections of this system. It is recognized that the limit-equilibrium analysis does not take into account the nonlinear mobilization of soil reaction with wall deflection in the analysis and should not be recommended for the appropriate design procedure. The finite-element method shows promise to handle the complicated stress-strain relationship for the retaining system. However, the constitutive law of soil has not been understood well enough for this method to be used in engineering practice with confidence.

Recently, the method of analysis for beams on nonlinear foundations, that employs the soil response curves derived from full-scale experiments, has been accepted as a rational design method by many engineers. The method commonly is referred to as p-y method and has been very successful for the design of laterally loaded piles. Basically, drilled shafts that are used in an earth-retaining structure are similar to piles loaded by lateral forces. The present state-of-the-art p-y curves have considerable promise for use in the design of drilled-shaft walls in a variety of soils. The next chapter will discuss this method in further detail.

CHAPTER 3. THEORY OF p-y ANALYSIS

THE DIFFERENTIAL EQUATION OF THE BEAM ON ELASTIC FOUNDATION

A straight beam, subjected to tranverse distributed loading and supported along its entire length by an elastic foundation, is shown in Fig. 3.1. The beam will deflect due to the external loads and produce continuously distributed reaction forces from the supporting medium. The reaction forces will be assumed to be acting perpendicularly to the original axis of the beam and opposite in direction to the deflection. The intensity of the reaction at every point is, in general, a function of the magnitude of the deflection at the same point and can be expressed as

$$p = bk_o y = ky \qquad (3.1)$$

where b is the width of the beam and k_o is generally called as the subgrade modulus. The subgrade modulus is defined as the force which, distributed over a unit area, will cause a deflection equal to unity.

For the sake of brevity the symbol k with the unit force/length^2 will be used to replace b(length) $\times k_o$ (force/length^3) in the following derivations, but it is important to note that this k includes the effect of the width of the beam and will be numerically equal to k_o only if the beam has a unit width. If an infinitely small element is cut from the beam, the forces associated with the element are shown in Fig. 3.2. Summation of forces in the vertical direction leads to a relation between the applied loads and the shear resistance.

$$V - (V + dV) + kydx - wdx = 0 \qquad (3.2)$$

where

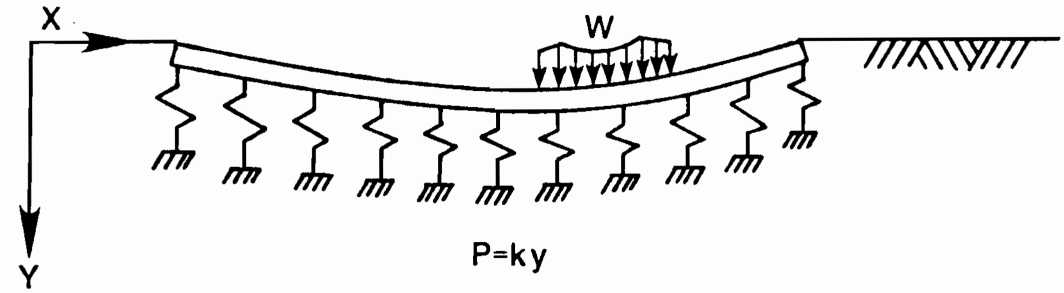

Fig. 3.1. Beam on elastic foundation

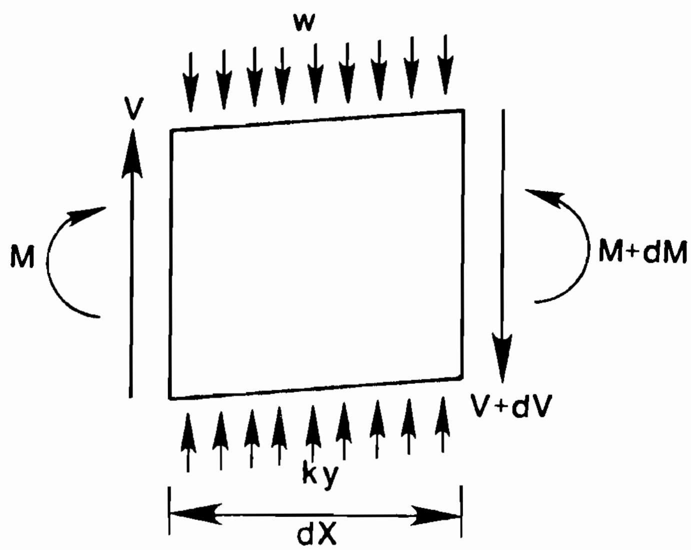

Fig. 3.2. Section of a beam under transverse distributed load.

$$\frac{dV}{dx} = ky - w \tag{3.3}$$

The moment equilibrium equation about the right side of the element gives

$$- M + (M + dM) - Vdx + wdx \frac{dx}{2} - ky\,dx \frac{dx}{2} = 0 \tag{3.4}$$

or

$$\frac{dM}{dx} = V + \frac{1}{2} kydx - \frac{1}{2} wdx \tag{3.5}$$

when dx is infinitesimally small, the above expression becomes

$$\frac{dM}{dx} = V \tag{3.6}$$

If shear deformation is ignored, from beam theory, the bending moment M is the value of flexural rigidity EI times the second derivative of the deflection y as

$$M = - EI \frac{d^2y}{dx^2} \tag{3.7}$$

Hence by using Eq. 3.3, the differential equation for the deflection curve of a beam supported on an elastic foundation can be expressed

$$\frac{d^2 (EI \frac{d^2y}{dx^2})}{dx^2} = -ky + w \tag{3.8}$$

If the flexural rigidity is constant along the beam, the equation will have the form of

$$EI \frac{d^4y}{dx^4} + ky - w = 0 \tag{3.9}$$

The equations derived above do not in general consider the effects of any axial load. In many cases a beam is acted upon by both an axial load and a lateral load. The governing equation that includes the axial loading can be derived in a manner that is similar to the above procedures and leads to another basic fourth order differential equation for beam-columns.

$$EI \frac{d^4y}{dx^4} + P_x \frac{d^2y}{dx^2} + P - w = 0 \qquad (3.10)$$

where

P_x = axial load on the pile, F

y = lateral deflection of structures, L

p = ky, soil reaction per unit length, F/L

EI = flexural rigidity, F-L2

w = distributed load, F/L

A detailed derivation of Eq. 3.10 can be found in Hetenyi (1956).

THE p-y METHOD

The deformation of a pile under axial and lateral loading can be found by solving Eq. 3.10. The physical definition of the soil reaction p on the pile is important in the p-y method and is illustrated in Fig.3.3. Figure 3.3a shows a profile of a pile that has been installed by driving or by other methods. The soil resistance is examined for a thin slice of soil at some depth x below the ground surface, as shown in Fig. 3.3a. The assumption is made that the pile has been installed without bending so that the initial soil stresses at the depth x are uniformly distributed, as shown in Fig. 3.3b. If the pile is loaded laterally so that a pile deflection y occurs at the depth x, the soil stresses will become unbalance as shown in Fig. 3.3c. Integration of the soil stresses will yield the soil reaction p with units of F/L.

It is convenient to express the soil reaction p in the same form of Eq. 3.1 as:

$$p = -ky$$

where

k = a parameter with the units F/L , relating pile deflection y and soil reaction p.

It is evident that the soil reaction p will reach a limiting value (and perhaps decrease) with increasing deflection. Furthermore,

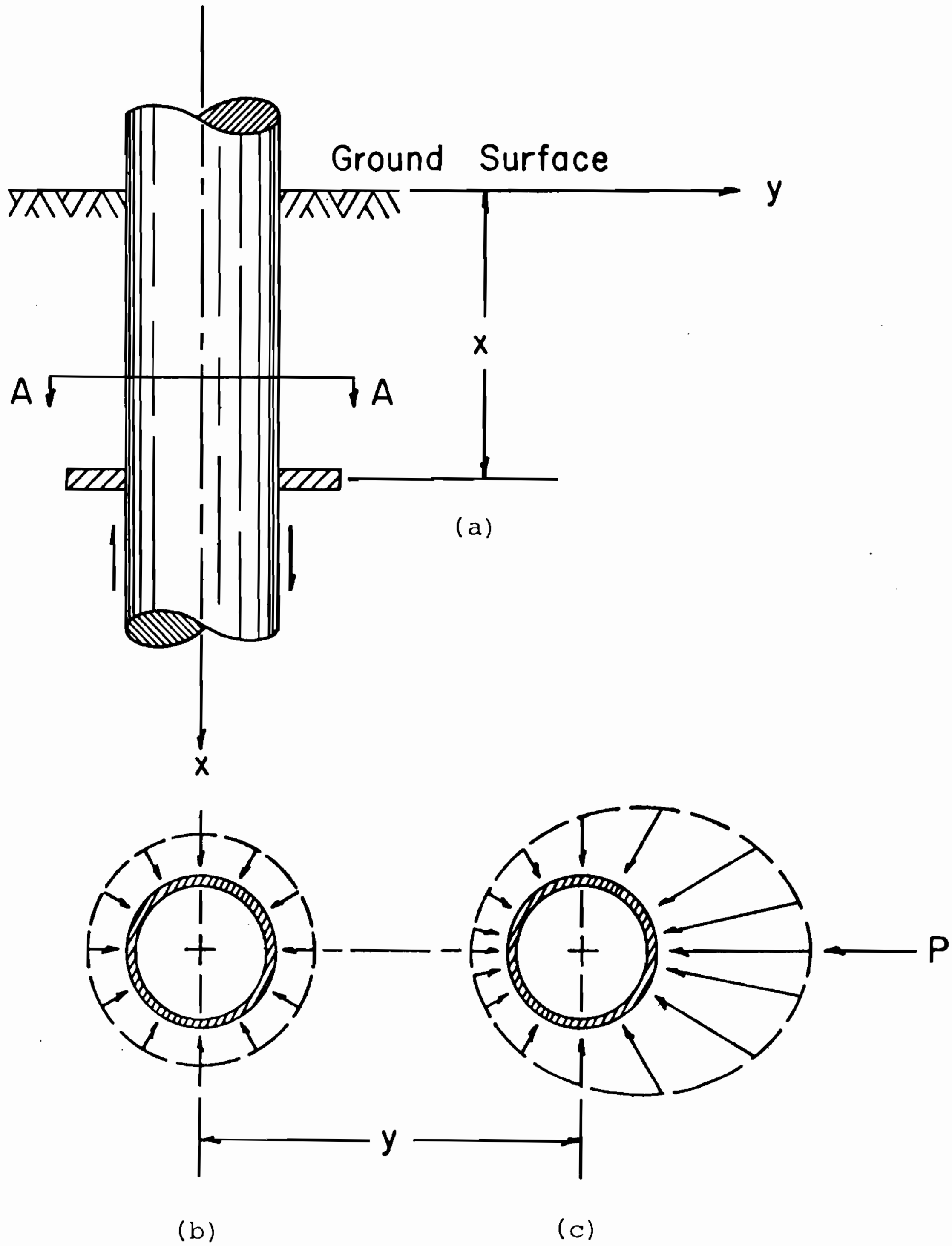

Fig. 3.3. Definition of p and y as related to the response of a pile to lateral loading (after Reese, 1984).

the soil strength in the general case will vary with depth; therefore, only in rare cases will k be constant with depth.

In view of the nonlinearities of Eq. 3.10, it cannot be solved with any closed-form solution and numerical methods must be utilized. The finite difference method can be employed to convert the differential equations to difference forms and solved with good results. Equation 3.11 is the differential equation in difference form

$$y_{m-2}R_{m-1} + y_{m-1} (- 2R_{m-1} - 2R_m + P_x h^2) \quad (3.11)$$
$$+ y_m (R_{m-1} + 4R_m + R_{m+1} - 2P_x h^2 +$$
$$K_m h^4) + y_{m+1} (-2R_m - 2R_{m+1} + P_x h^2)$$
$$+ y_{m+2}R_{m+1} - w_m h^4 = 0$$

where

y = finite deflection at point m along the pile, L
$R_m = E_m I_m$, F-L
h = increment length, L

The pile is sub-divided into n increments and n+1 equations can be written of the form of Eq.3.11, yielding n+5 unknown deflections. The axial load P_x is assumed to be known and to be constant with depth. In addition, two boundary conditions at the bottom of the pile and two at the top of the pile allow for a solution of the n+5 equations with selected values of R and k. The value of n and the number of significant figures in y can be selected to give results that give appropriate accuracy. The solution of the equations proceeds as illustrated in Fig. 3.4. Figure 3.4b shows a family of p-y curves where the curves are in the second and fourth quadrants because soil resistance is opposite in direction to pile deflection. Also in Fig. 3.4b is a dashed line showing the deflection of the pile, either assumed or computed on the basis of an estimated soil response. Figure 3.4c shows the upper p-y curve enlarged with the pile deflection at that depth represented by the vertical, dashed line. A line is drawn to the soil resistance p

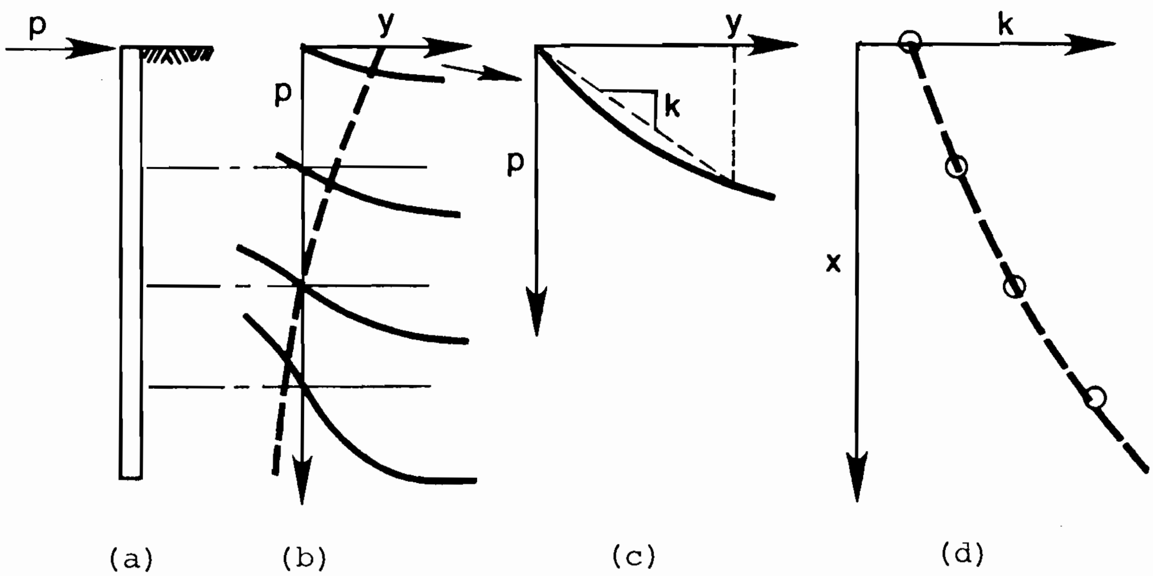

Fig. 3.4. Procedure for determining value of k.

corresponding to the deflection y with the slope of the line indicated by the symbol k. Figure 3.4d shows the values of k plotted as a function of depth x. In performing a computation, the computer utilizes the computed values of k and iterates until the differences in the deflections for the last two computations are less than a specified tolerance. After deflections have been computed, difference equations can be employed to compute rotation, bending moment, shear, and soil reaction along the pile.

SOIL-RESISTANCE CURVES

With regard to soil response, the assumptions are made (1) that there is no shear stress at the surface of the pile parallel to its axis (the direction of the soil resistance is perpendicular to the axis of the pile) and (2) that any lateral resistance or moment at the base of the pile can be accounted for by a p-y curve perpendicular to the axis of the pile near the base. Any errors due to these assumptions are thought to be negligible.

Soil-response curves have been obtained primarily from several full-scale experiments. The piles were instrumented for the measurement of bending moment as a function of depth. Loads were applied in increments and a bending-moment curve was obtained for each load. Two integrations of each curve yielded pile deflection and two differentiations yielded soil reaction. The cross-plotting of deflection and soil resistance yielded p-y curves at different depths. Examples of such curves are shown in Figs. 3.5 and 3.6 (Cox et al, 1974). The curves in Figs. 3.5 and 3.6 were used to develop prediction equations for p-y curves in sand (Reese et al, 1974). Theory has been used to assist in developing prediction equations for those curves obtained from the full-scale measurements. The theory of elasticity has been used to give an indication of the slope of the early part of the curve and the equations of limit equilibrium have been used to yield approximate values for the ultimate resistance as a function of depth. These theoretical expressions have allowed results from full-scale experiments to be interpreted with the consequence that

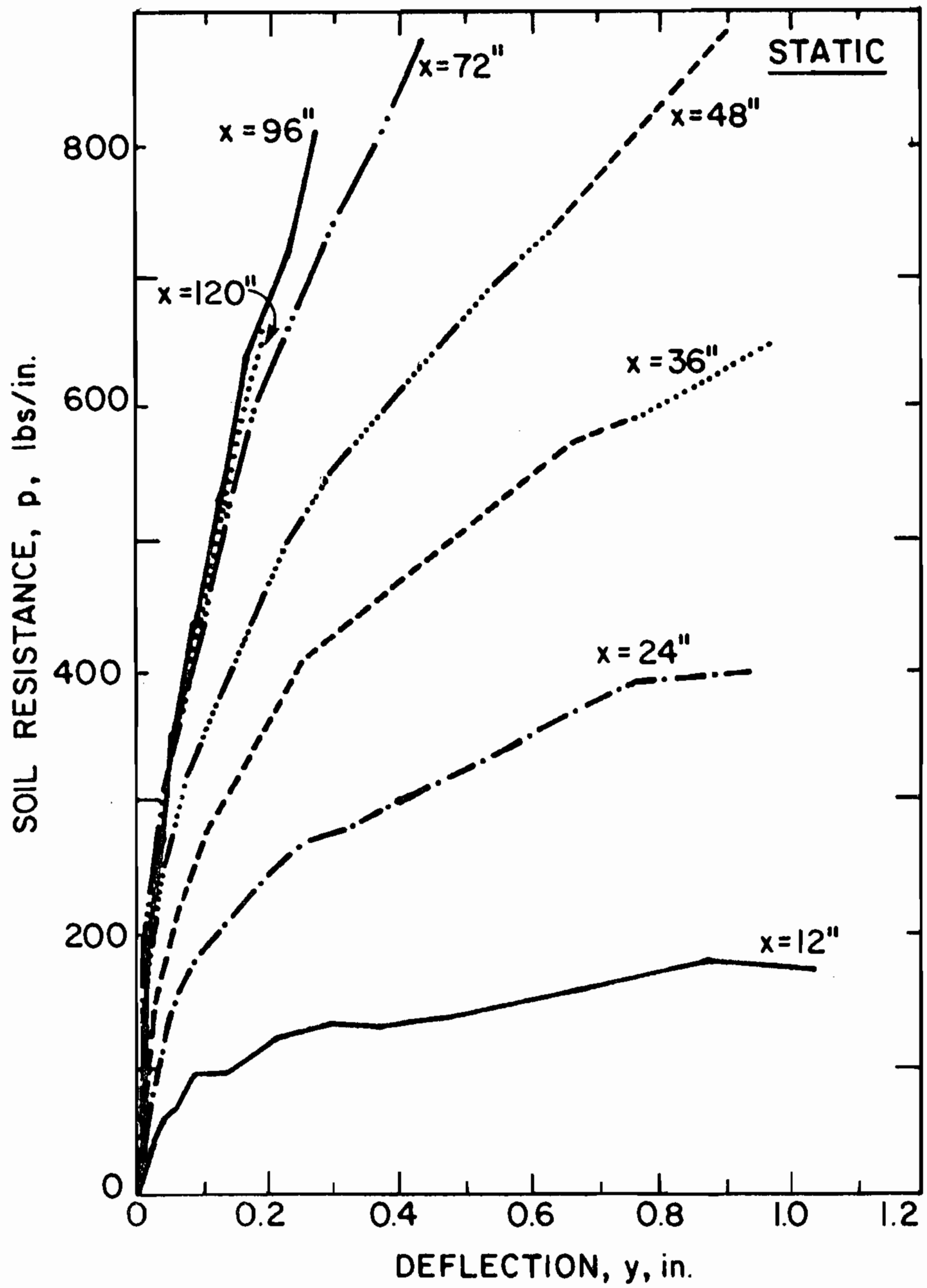

Fig. 3.5. p-y curves developed from static-load test of 24-in. O.D. pile in sand (after Cox et al, 1974).

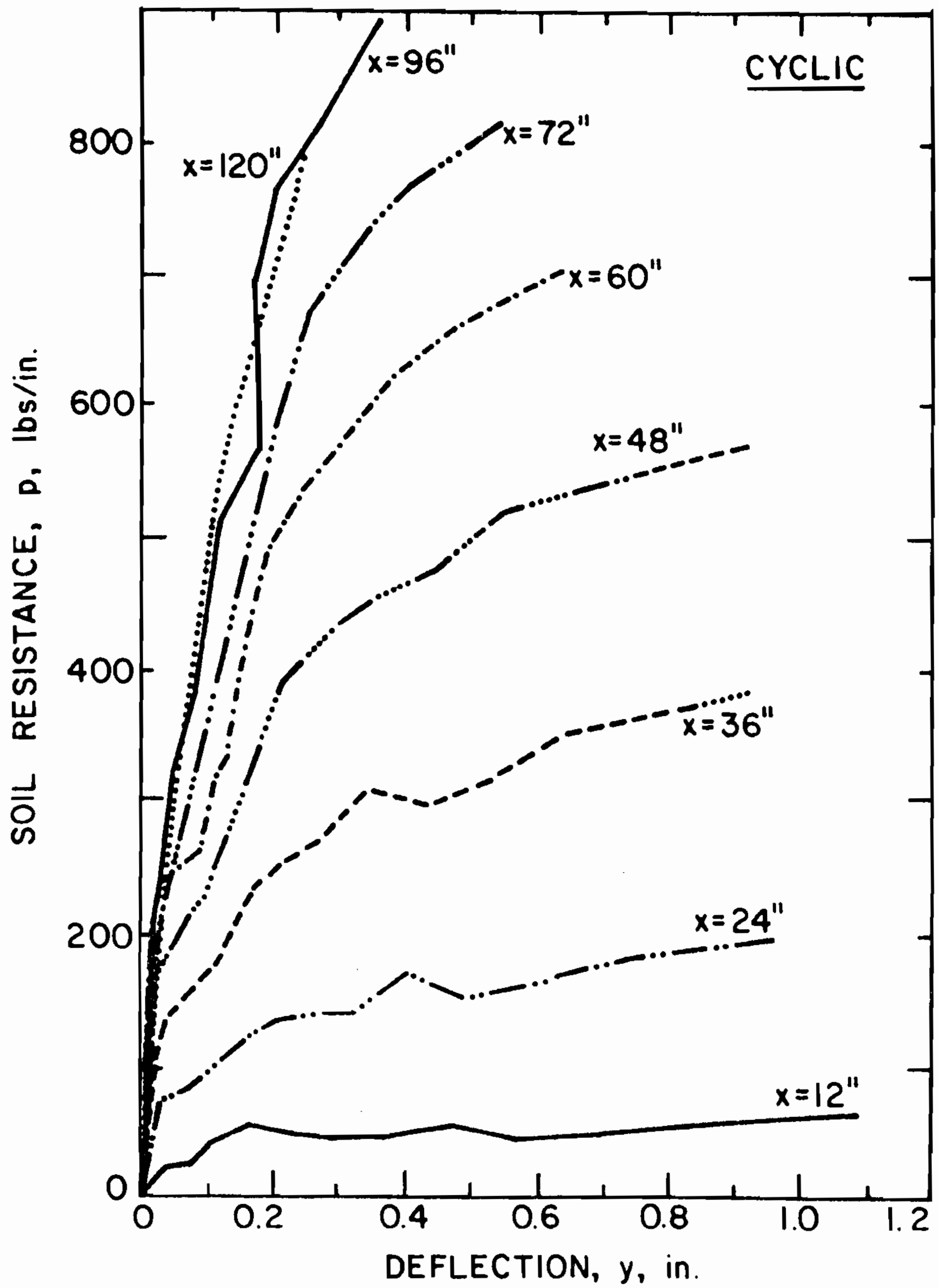

Fig. 3.6. p-y curves developed from cyclic-load test of 24-in. O.D. pile in sand (after Cox et al, 1974).

predictions have been developed for soil-response curves for a variety of subsurface soil conditions.

Predictions for p-y curves have been worked out, by the procedure outlined above for soft clay (Matlock, 1970), for stiff clay with free water (Reese et al, 1975), for stiff clay without free water (Welch and Reese, 1972), for sand (Cox et al, 1974), and for rock (Nyman, 1980). Other writers have made use of reports in the technical literature on instrumented tests and on uninstrumented tests to make other recommendations (Parker and Reese, 1971; Sullivan, 1977; Bhushan et al, 1981; Murchison and O'Neill, 1984; Gazioglu and O'Neill, 1984). The details of existing recommendations for constructing p-y curves will not be discussed further here, and the reader is referred to the cited references.

The importance of obtaining correct soil information to generate p-y curves is evident from the results of parametric studies. For cohesive soil, the undrained shearing strength is employed in the analyses. The initial stiffness of the soil as well as ε_{50} are also required to establish the p-y curves, where ε_{50} is the strain corresponding to one-half the maximum principal-stress difference from a laboratory unconsolidated-undrained test. If no stress-strain curves are available, typical values of ε_{50} and the initial stiffness are given by Reese (1984). For cohesionless soils, the angle of internal friction is the relevant strength parameter that is needed. The initial stiffness of cohesionless soil can best be related to the relative density and is required to define the initial slope of the p-y curve. Representative values of initial stiffness k for sand are also recommended by Reese (1984).

The p-y method, based on the Winkler assumption, is used in the majority of the current design procedures due to the fact that this method is simple and accounts for nonlinear soil response in a realistic manner. Some objection has been given to the Winkler assumption because it can not reflect the condition of continuity. However, p-y curves recommended above are based directly on experimental results and the conditions of continuity were automatically satisfied in the experiments. The p-y method has been used to compare computed results to measured results for a sizeable number of experiments where piles were installed in different soils (Reese and Wang, 1986). The comparisons have shown the p-y method to be very useful and is thought to be the best one presently available for the analysis of piles under lateral loading.

CHAPTER 4. ESTIMATING LOAD FROM EARTH PRESSURE

EARTH-PRESSURE THEORY

The state of stress of a point under the ground can be indicated in a Mohr diagram as shown in Fig. 4.1. Referring to the element in Fig. 4.1a, the initial vertical and horizontal stresses are σ_v and σ_h, respectively, under conditions of zero lateral strain. The active failure state is developed by reducing the horizontal effective stress until failure occurs, i.e. until the Mohr circle becomes tangent to the failure envelope (Fig. 4.1b). The passive state of failure is developed by increasing the horizontal effective stress until failure occurs. The horizontal stresses which correspond to the active state and passive state are commonly represented by σ_a and σ_p, respectively.

The earth pressure against a wall is directly related to the movement of the wall. The relationship between wall movement and earth pressure is shown qualitatively in Fig. 4.2. A long, frictionless wall of height H, as shown in Fig. 4.2a, is assumed to have been placed in a sand deposit. If the wall is placed without causing any deformations in the sand, the wall is subjected to the in-situ stresses of the soil. The soil pressure against a unit area of the wall can be defined by the following equation.

$$\sigma_o = K_o \gamma Z \qquad (4.1)$$

where

σ_o = lateral at-rest earth pressure,

K_o = coefficient of at-rest earth pressure,

γ = soil unit weight,

Z = the distance from the ground surface.

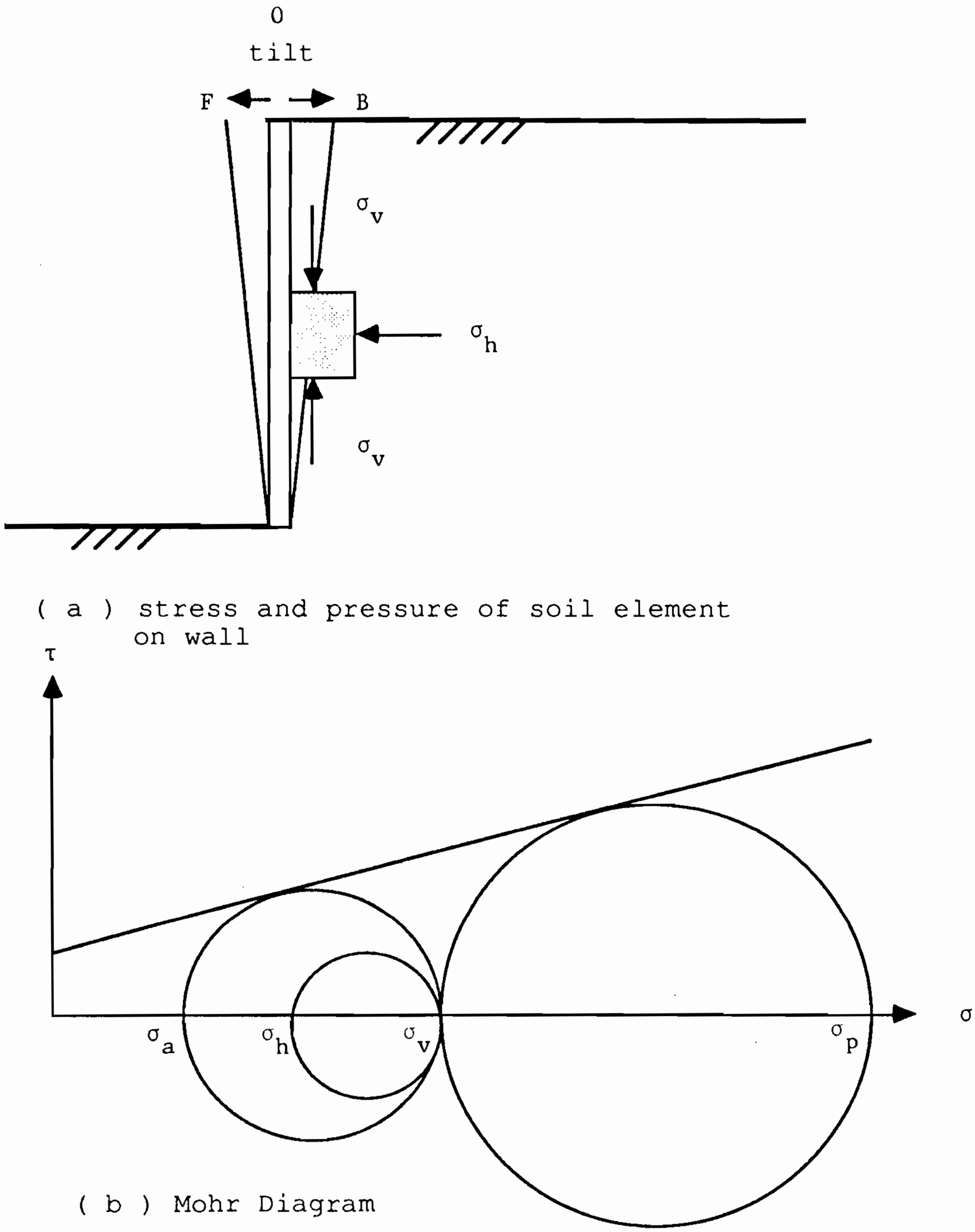

(a) stress and pressure of soil element on wall

(b) Mohr Diagram

Fig. 4.1. States of stresses of active and passive conditions.

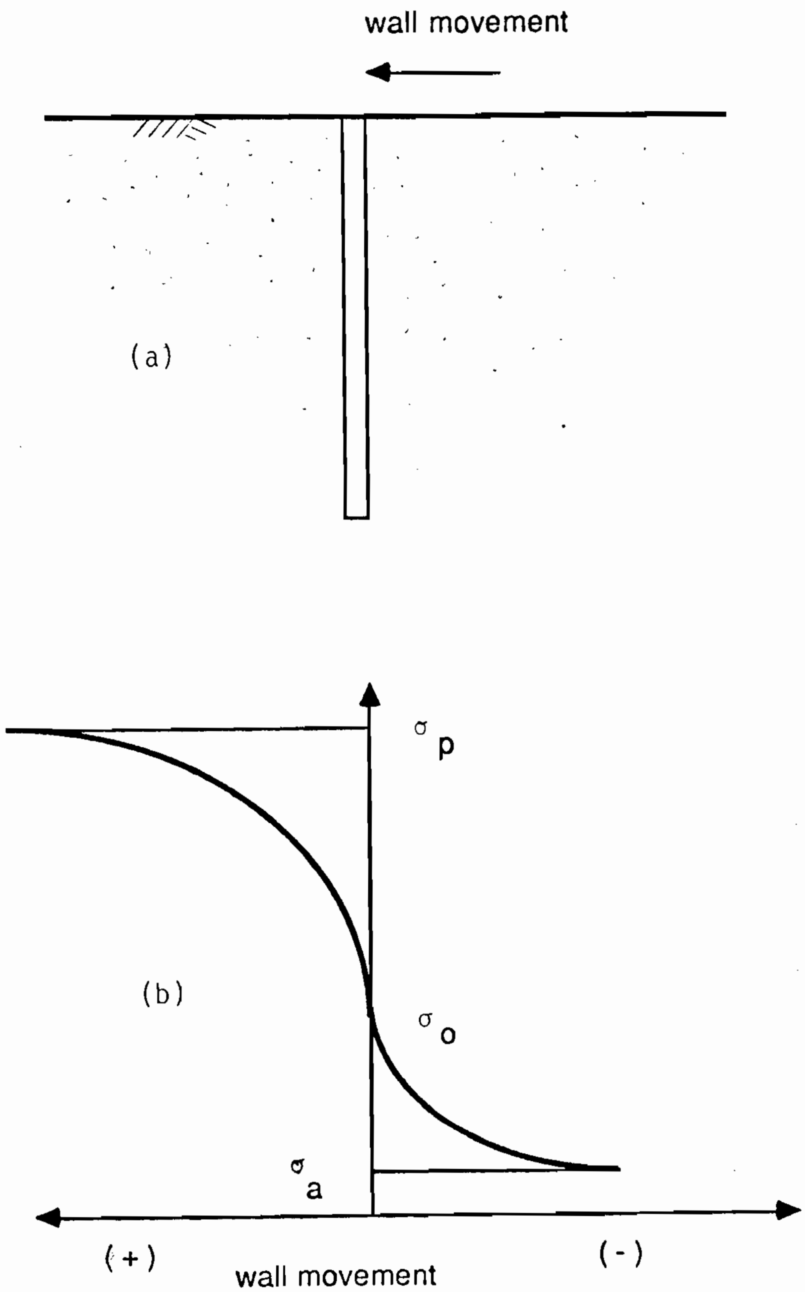

Fig. 4.2. The variation of earth pressures with the movements of the wall.

The lateral earth pressure σ_o corresponding to the zero deflection of the wall is represented by a point on the vertical axis in Fig. 4.2b. If the wall is moved in the direction as indicated in the figure, the pressure on the left face of the wall will increase, as shown in the sketch, until it reaches the limiting value

$$\sigma_p = K_p \gamma Z \qquad (4.2)$$

where

σ_p = passive earth pressure, and
K_p = coefficient of passive earth pressure

If the movement is enough, the value of earth pressure on the right face of the wall will decrease until it reaches the limiting value

$$\sigma_a = K_a \gamma Z \qquad (4.3)$$

where

σ_a = active earth pressure, and
K_a = coefficient of active earth pressure.

Earth pressures σ_p and σ_a represent the limiting values as shown in Fig. 4.2b.

In general, the earth pressure coefficients are not known for the entire range of the deflection of the wall. However, a theoretical solution exists, along with some experimental evidence, for estimating the coefficients of active and passive pressures. The earth pressures in between the active and passive states can be estimated from correlations of measured pressures and movements on full-size structures.

A drilled-shaft retaining wall must support the horizontal earth pressure at-rest if no wall movements are allowed. However, as soil is removed from one side, the wall will tilt. If the movement of the wall is insufficient to develop the active condition, the lateral pressure will be between the at-rest and active values. If the wall continues to tilt outward, the movement will reach or exceed the point where the active state is developed.

The two classical theories of earth pressure are those due to Coulomb (1776) and Rankine (1857). Rankine's theory considers the stress in a semi-infinite mass of soil with a horizontal surface when it reaches a state of plastic equilibrium. The total active earth resultant from Rankine's theory can be expressed by the following equation:

$$P_a = 0.5\ K_a\ \gamma\ H^2 - 2\ c\ \sqrt{K_a}\ \ H \qquad (4.4)$$

where

γ = the soil unit weight,
H = the depth from the top of the wall,
K_a = the coefficient of active earth pressure,
c = the cohesive strength, and
P_a = the total active earth resultant.

Three important assumptions in the Rankine solution are: (1) the backfill must be a plane surface; (2) the wall must not interfere with the failure wedge; and (3) there is no friction between the wall and soil. The Rankine solution is often used because the equation is simple. In practice, considerable friction may be developed between the wall and the adjacent soil. Rankine's assumptions result in an overestimation of the active earth pressure. More accurate methods are available that include the effects of wall friction. Some of these methods are the Coulomb-wedge analysis, in all of its variations; the more sophisticated log-spiral, wedge analysis; and the finite element analysis.

Coulomb's theory considers the stability of the soil wedge between the wall and a trial-failure plane. The method is not exact because only force equilibrium is analyzed and moment equilibrium is not considered. In this method, a number of trial-failure planes are selected and the critical force between the soil and the wall is determined (Fig. 4.3). One advantage of the trial-wedge analysis is the capability to handle more generalized conditions. For example the surface of the backfill

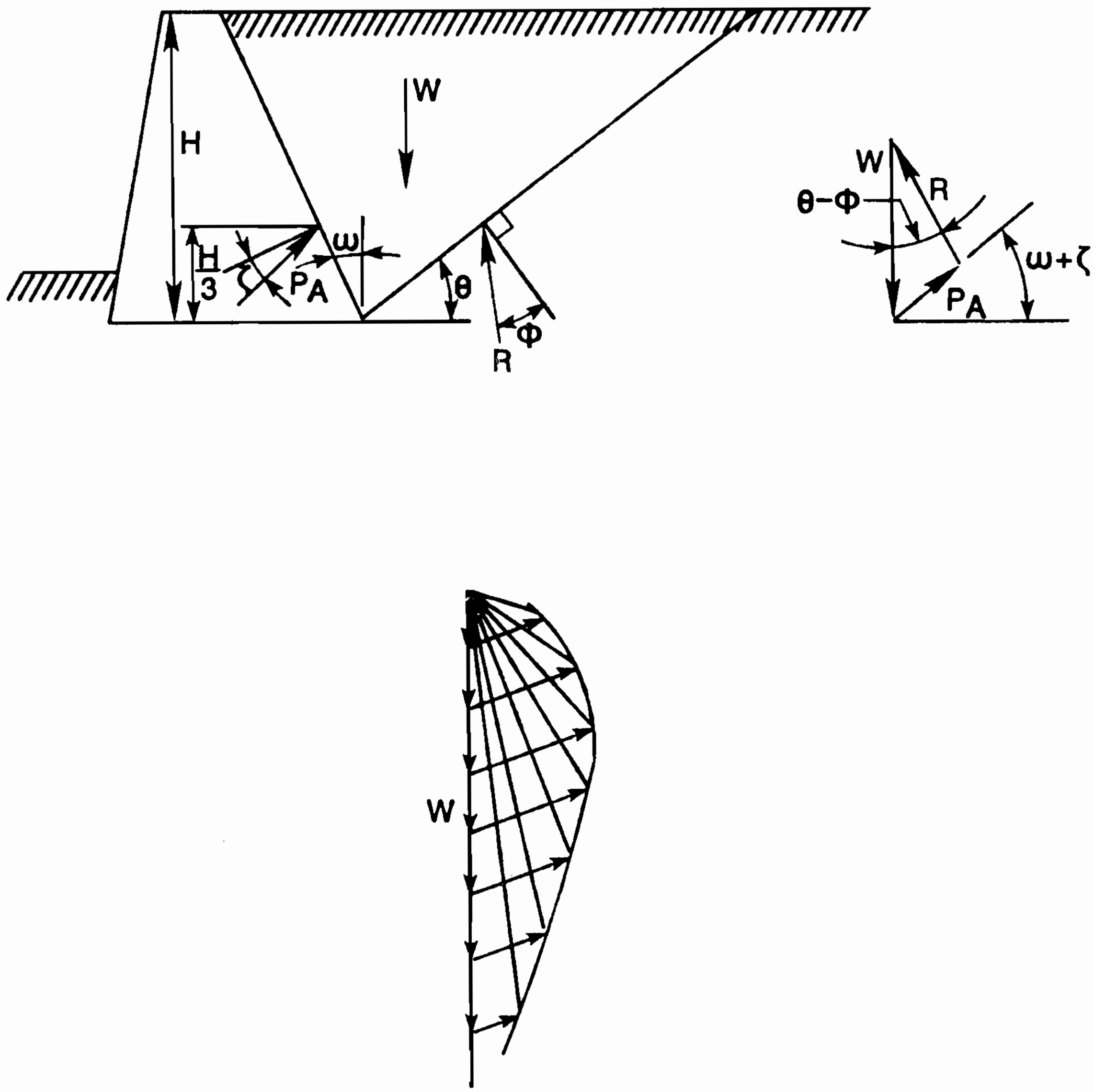

Fig. 4.3. Coulomb "Trial Wedge" analysis for active pressure on a solid gravity wall.

may be sloped, may have an irregular surface, or may be loaded with a surcharge. It is only necessary to take the appropriate forces into account when a trial wedge includes a particular force. Further, variable densities of soil can be easily taken into account. If conditions are complicated, the analysis is usually performed graphically. In general, the Coulomb analysis is slightly in error because moment equilibrium is not satisfied, but the error is usually small enough to be ignored. Another potential error from Coulomb's method is assuming the failure surface to be plane. However, the effect of this assumption is negligible for the active case.

Development of the active state of stress requires that the soil mass deforms sufficiently so that failure strains develop within the soil. This requires substantial movements of the wall. In general, a triangular soil-deformation pattern is found behind a retaining wall. The movements required to develop the full active condition are maximum at the top and minimum at the base. The required amount of the wall movement is usually expressed by the rotation of the wall. Because soils have nonlinear stress-strain behavior, most of the knowledge regarding wall movement versus earth pressure is based primarily on experimental work instead of on theoretical analyses. A substantial quantity of research work has been directed toward developing experimental methods to measure the earth pressure and the corresponding structural movements. Significant findings from some studies will be reviewed in the next section.

MEASUREMENT OF ACTIVE EARTH PRESSURE AND STRUCTURAL DEFORMATION

Tests of Terzaghi

In 1954 Terzaghi reported the results of a series of tests where dry sand was placed against a rigid retaining wall. The rigid wall was rotated about its base in both an active and passive sense and the variation of the earth pressure with rotation was measured. Tests were conducted for loose and dense sand. The well-known relationships between the movements, earth pressure, and relative density are shown in Fig. 4.4. A major point of interest is the small displacement required to reduce the earth pressure to values close to the fully active state. The active state was observed at top displacement of 0.06% of wall height for dense sand and 0.5% of wall height for loose sand. The corresponding K_a values that were measured were 0.10 for dense sand and 0.25 for loose sand.

Tests of Rowe

Rowe (1969) reported on a series of active earth-pressure tests for a model wall of 1.5m high, equipped with pressure cells. He made the measurements on a central wall that had guard walls on each side. The side walls of the tanks were covered with aluminum foil and grease. The pressure cells indicated a triangular pressure distribution on the wall. Tests were performed using a sand in both the dense (ϕ = 43°) and loose (ϕ = 32.5°) states. The corresponding deflections at the top of the wall at failure were about 0.2% and 2% of wall height, respectively. The coefficients of active earth pressure was 0.16 for dense sand and 0.30 for loose sand.

Tests of Moore and Spencer

Moore and Spencer(1972) used wet kaolinite as backfill. Their test wall was 19-in. high and 63-in. wide. The kaolinite had a liquid limit of 75 and plastic limit of 35, and a range in water content of 80% to 101%. The wall was translated in the active direction through distance of 1/16 in. to 1 1/4 in. (0.33% to 6.6% of the wall height). Measurements were made as a function of time. An interesting observation was that both the total stress and the pore water pressure decreased when the wall was translated. Both total stress and pore water pressure gradually rose with time and after a long period produced values close to those that would have occurred at the at-rest condition.

Tests of Bros

Bros (1972) presented experimental investigations concerning the influence of different kinds of movement and deformation of a

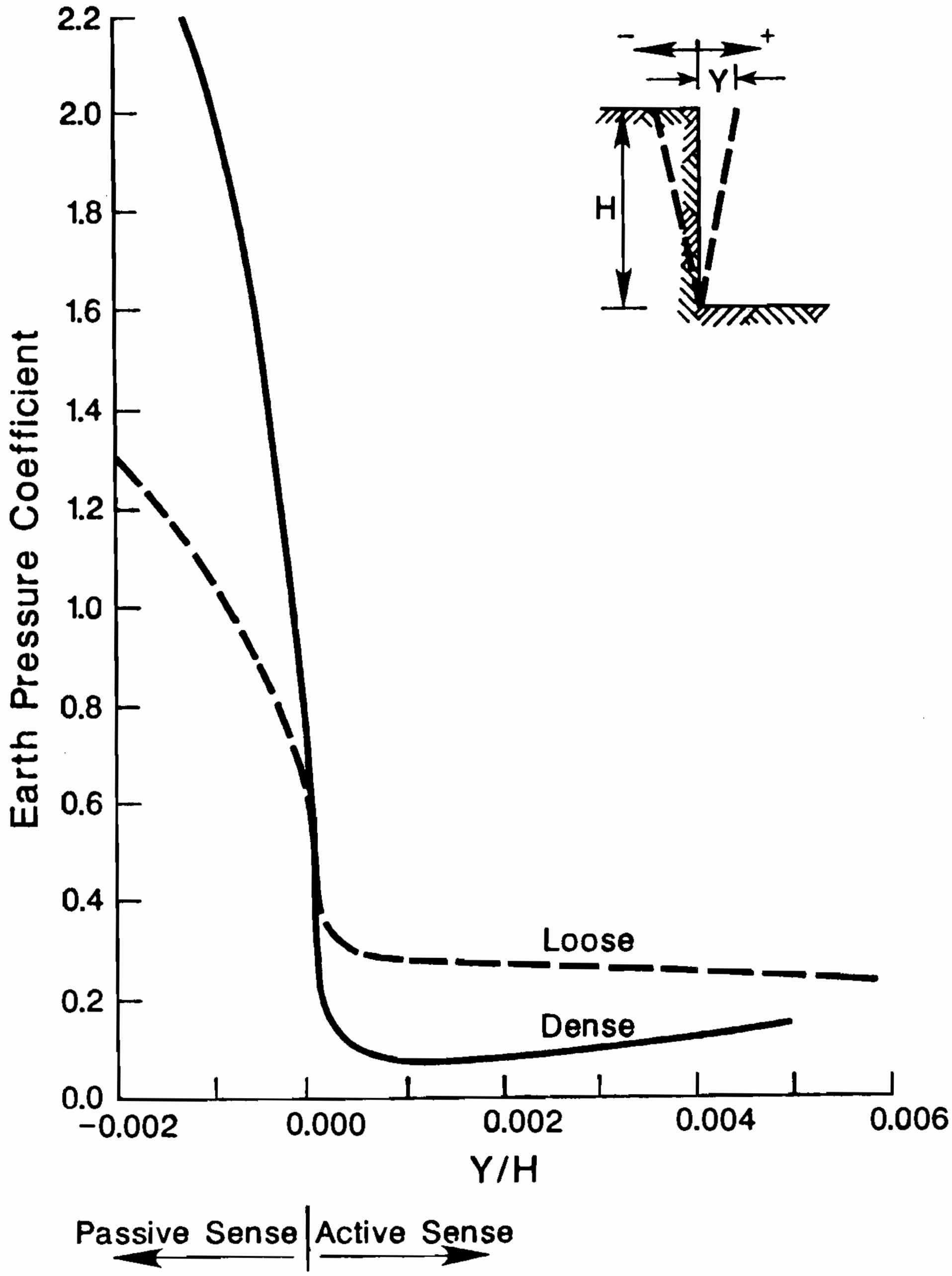

Fig. 4.4. Relation between movement of a wall and earth pressure for different densities (after Terzaghi, 1954).

model wall on earth pressures. The magnitude and the distribution of active and passive pressures were reported. Clean, dry quartz sand with a friction angle of about 35° was used in the tests. The sand was densified by vibrating each 12 to 15 cm layer. The studies found that K_a was about 0.24 for the model wall for a horizontal translation of 0.06% of the wall height, and K_a was about 0.30 when the model wall was rotated about the bottom with a top movement of about 0.35% of the wall height.

Tests of Mastsuo, Kennochi, and Yagi

Mastsuo, Kennochi, and Yagi (1978) investigated the active earth pressures on a retaining wall of 10 m high using two backfill materials, dense silty sand and slag. The coefficient of earth pressure at rest for the silty sand was 0.35 to 0.45 and 0.3 to 0.5 for slag. The active state for silty sand was observed at a top displacement of 0.64% to 0.77% of wall height and the active state for slag was observed at a top displacement of 0.3% to 0.5% of wall height. The corresponding K_a-values displacement of were 0.25 for silty sand and 0.1 to 0.25 for slag.

Tests of Sherif, Ishibashi, and Lee

Sherif, Ishibashi, and Lee (1982) measured the active earth pressure on a wall 40-in. wide by 41-in. high in a wooden bin that was 6 ft by 8 ft by 4 feet. The bin was placed on a shaking table and dry Ottawa sand was densified by shaking. The mode of wall movement to reach the active state was translation without rotation. For a movement of 0.1% of wall height, they found that Coulomb's method predicted the measured value accurately for both dense and loose sand.

Discussion

The magnitude of the earth pressure against a wall strongly depends on the movement of the wall. Theory is of little use in making predictions of earth pressure unless deformations in the soil cause either the active or passive states to be developed. The case studies that were reviewed earlier in this chapter, for walls in sand, show that theory can be used to make an approximate prediction of active earth pressure. Laboratory data for walls in clay are so meager that no verification can be made of the theory and reliance must be placed on field studies. Williams and Baka (1985) studied the performance of cantilevered retaining structures in overconsolidated, stiff clay and indicated the displacement at the top of the wall needed to mobilize the active pressure is about 0.4 to 1.2 percent of the wall height, depending on the wall stiffness, as shown in Fig. 4.5. The wall stiffness was defined as EI divided by the cube of the wall height with units of force/length. It was recognized that, for a wall with a lower stiffness, a large deflection at the top is needed for soils near the lower part of the wall to be strained enough to induce the active state of stress, as illustrated in Fig 4.6. Based on existing test data and on recommendations in the literature (Sowers and Sowers, 1970), a simplified table (Table 4.1) is presented that shows the approximate values of wall rotation needed to mobilize active earth pressure.

LOADING FROM ACTIVE EARTH PRESSURE

General Concept of Computing Load from Active Earth Pressure

A retaining wall needs be designed only to support the active pressure if the wall movements are tolerable. The design of drilled shafts is simplified if the active pressure is assumed to be the driving force that is acting. The deflection of the top of the drilled shafts should be at least as large as the values shown in Table 4.1. Because the deflection of drilled shafts is affected by many factors such as spacing, wall height, foundation soil, and flexural rigidity, proper selection of these variables is important.

The example that follows is intended to demonstrate conceptually the selection of variables in order to achieve the active state. A row of 48-in.-diameter drilled shafts (Fig. 4.7) are designed to resist the earth pressure of a sand fill ($\phi=35^\circ$). For simplicity, the drilled shafts at the excavation line are assumed to be fixed against rotations. The bending stiffness of each drilled shaft was computed to be 8.1×10^{11} lb-in^2. A design

TABLE 4.1. APPROXIMATE VALUES OF ROTATION NEEDED TO DEVELOP THE ACTIVE STATE

Description of backfill	Rotation (y/H)*	K_a
Sand and gravel, dense, fully drained	0.0005	0.20
Sand and gravel, loose, fully drained	0.002	0.35
Stiff clay (undrained), or clay compacted at a low moisture content	0.01	0.50
Soft clay (undrained), or clay compacted at a high moisture content	0.02	1.00

* y = horizontal displacement at the top of the wall

H = height of the wall

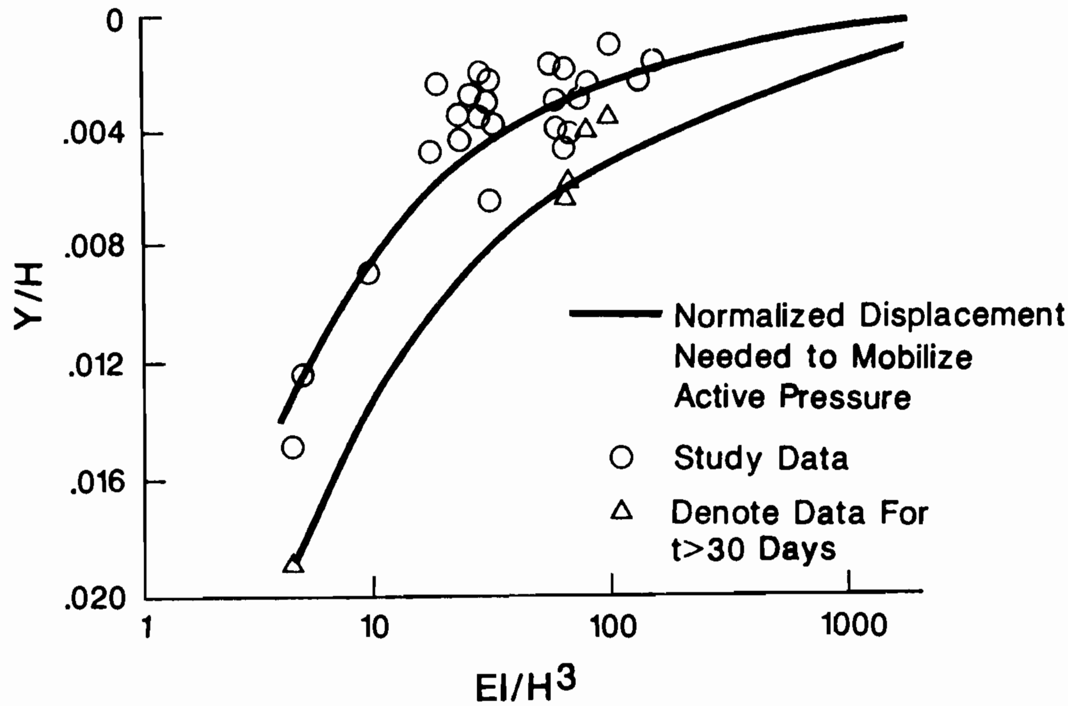

Fig. 4.5. Measured normalized displacement needed to mobilize active earth pressure (after Williams and Baka, 1985).

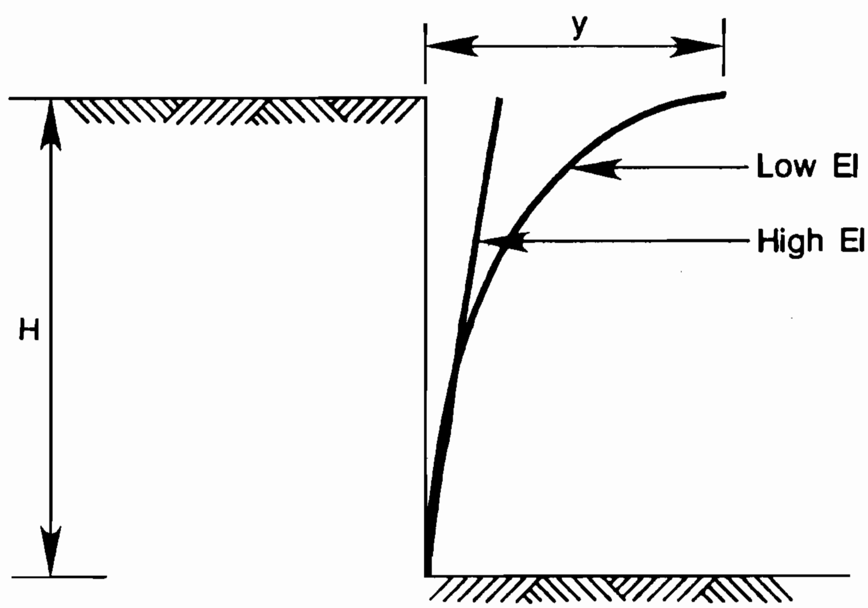

Fig. 4.6. Wall deflection under different system stiffness.

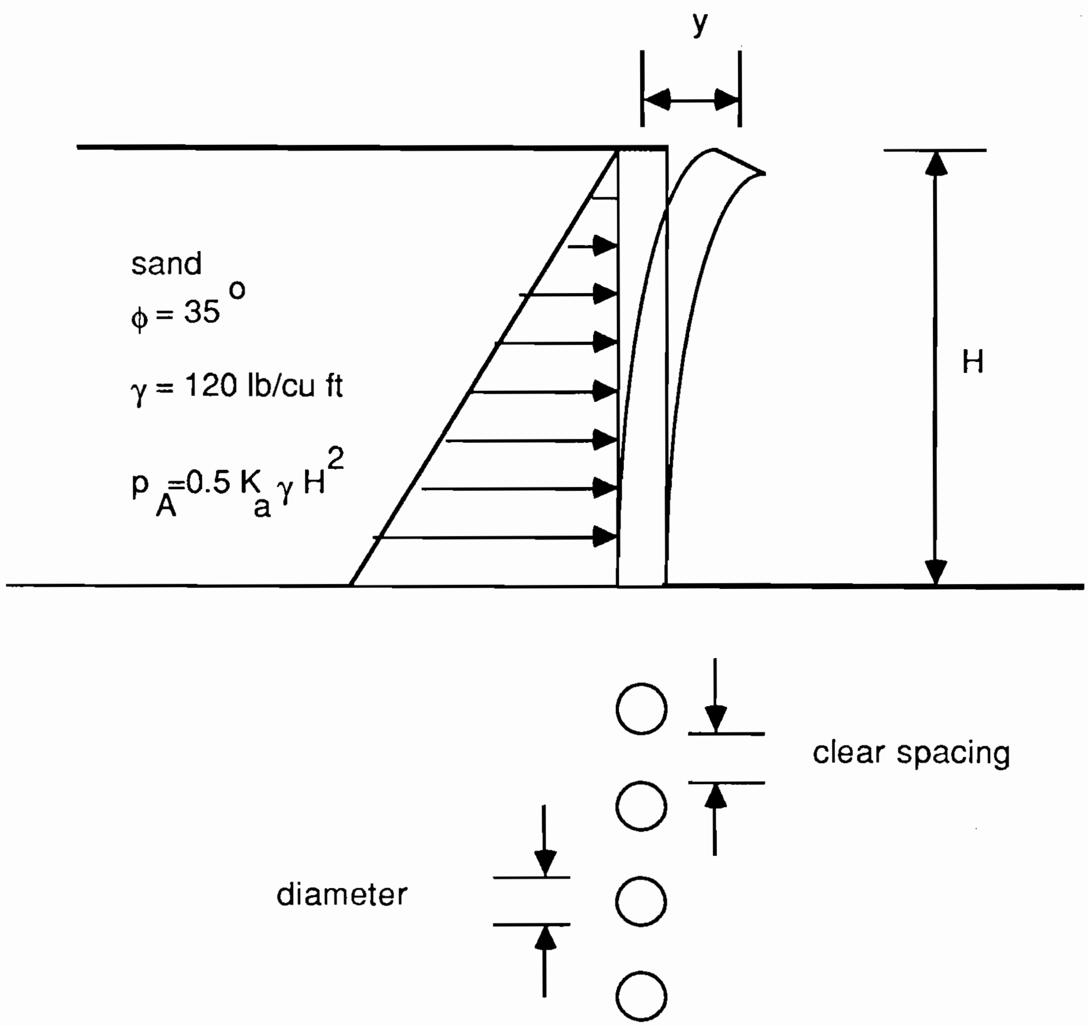

Fig. 4.7. Detailed informations of drilled-shaft walls in the example study.

chart (Fig. 4.8) which includes the relationships between displacement at the top of the wall, shaft spacing, and height of the wall, was developed. The moment capacity of each drilled shaft with 1% of steel and 3000 psi concrete was computed as 4.58×10^6 in-lb. If the spacing of the shafts or the height of the wall is large, the earth pressure acting on the wall produces a bending moment large enough to fail the shafts. Any point above the line AA in Fig. 4.8 indicates a structural failure due to overloading. On the other hand, a wall rotation larger than 0.002 is required from Table 4.1 to develop the active earth pressure. As may be noted, both restrictions mentioned above can only be satisfied by the hatched zone shown in Fig. 4.8. Any combination of variables selected in this zone is acceptable for design. An increase of the percentage of steel, concrete strength, and shaft diameter can result in a member with a higher bending resistance. With a higher bending capacity, the working zone becomes larger as shown in Fig. 4.9. It is apparent that a large working zone provides more design alternatives and improved safety conditions.

In the conventional design method, the active earth pressure is always to be employed as the driving force without examining whether the lateral displacement of the wall is sufficient to develop those pressure. Such designs may result in underestimating the earth pressures. Schultz, Einstein, and Azzouz (1984) conducted an extensive empirical investigation of the behavior of diaphragm walls and found the displacements associated with diaphragm walls in all soil categories are not sufficient to develop active earth pressures. They conclude that the earth pressure used to design diaphragm retaining walls should be between the earth pressure at-rest and the active condition. However, the spacing used for a drilled-shaft wall may be varied so that the active state can be achieved. The limitation, of course, is whether or not the deflections that are necessary are tolerable.

Influence of Water Pressure on Loading

Water pressure is an important factor in the prediction of load from the backfill. The effects of water in the backfill can

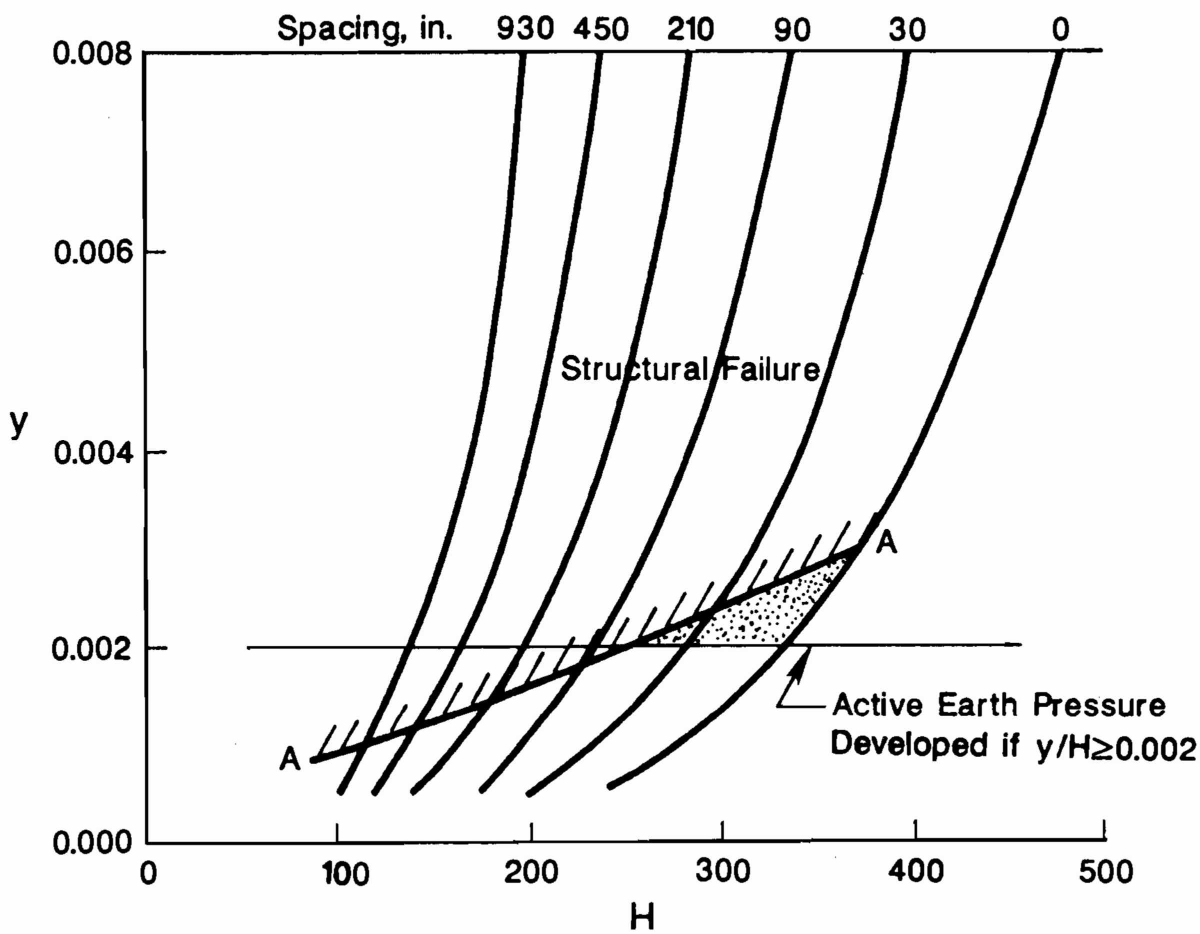

Fig. 4.8. The selection of the active earth pressure under various geometry conditions for section A (ρ = 1.3%).

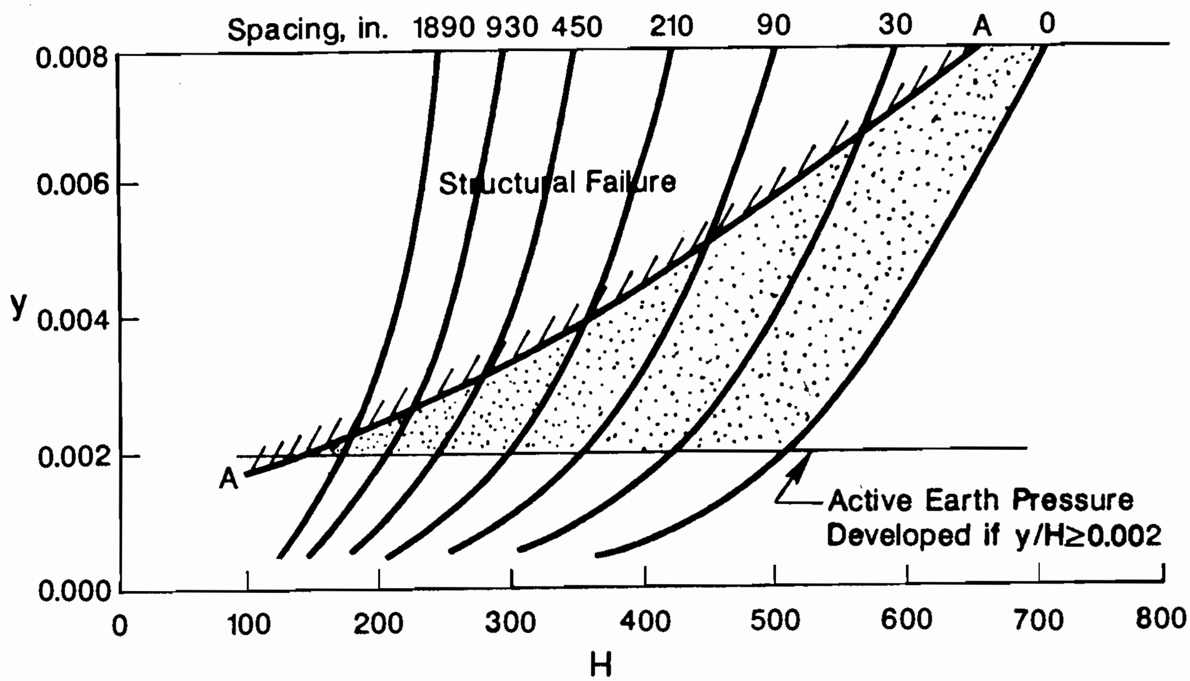

Fig. 4.9. The selection of the active earth pressure under various geometry conditions for section B (ρ = 2.3%).

be twofold. First, there is a direct effect from the hydrostatic pressure, and second, there is an indirect effect due to the influence of pore water pressure on soil strength. The complex problem is simplified if the backfill is a cohesionless soil. The effective-stress analysis for cohesionless soil is illustrated in Fig. 4.10. The pressure exerted by dry sand is shown in Fig. 4.10a. If the soil behind the same wall becomes inundated, the hydrostatic pressure is developed in addition to the effective pressure as shown in Fig. 4.10b. Because the effective weight of the soil is reduced by submergence, the effective pressure exerted by the sand grains is reduced proportionally. However, the presence of water in typical sands increases the total pressure to 2.5 to 3 times that for dry sands.

The direct effect of water on pressures from a saturated cohesive soil is more complex. In the active state, a saturated cohesive soil initially develops a pressure distribution as shown by the solid line and its extension in Fig. 4.11a. Cracks tend to form in the tension zone. If the cracks fill with water, as shown in Fig. 4.11b, the water pressure adds greatly to the pressures acting on the wall. It appears to be clear that the inundated conditions give significantly different results when computing wall loading when water is present in the clay. In general, inundated soil behind a drilled-shaft wall will not occur because of the interspace between two drilled shafts. If the space between the shafts is covered, weepholes should be installed. For either sand or clay, the load from the most critical condition, that may exist during the service life of the wall, is always selected for design.

Lateral Pressure Induced by Surcharge

In many occasions, the earth pressure of backfill is not the only load acting on a retaining wall. Surcharge, from either concentrated or distributed loads, causes additional lateral loads. Terzaghi (1954) pointed out that the Coulomb-wedge analysis may not provide satisfactory results if the surcharges are applied at some distance behind the wall. However, tests by Spangler (1936), Spangler and Mickle (1956), and others indicate that the

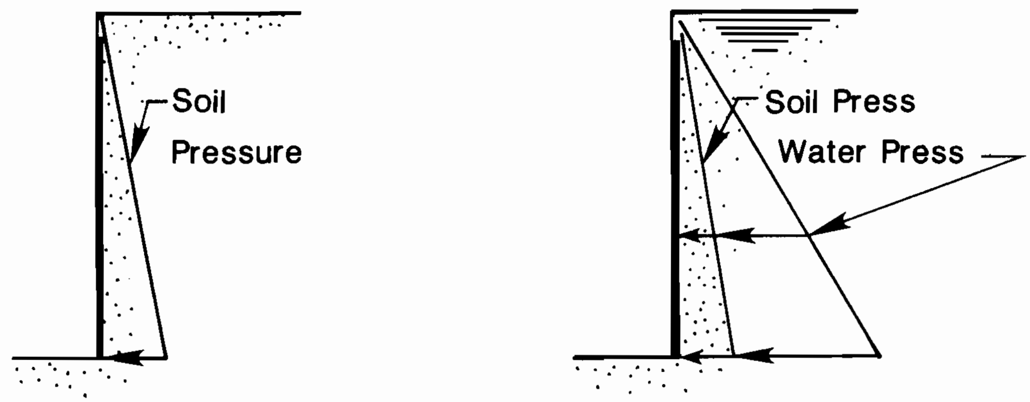

(a) Dry Cohesionless (b) Inundated Cohesionless

Fig. 4.10. The additional pressure induced by water for cohesionless soil.

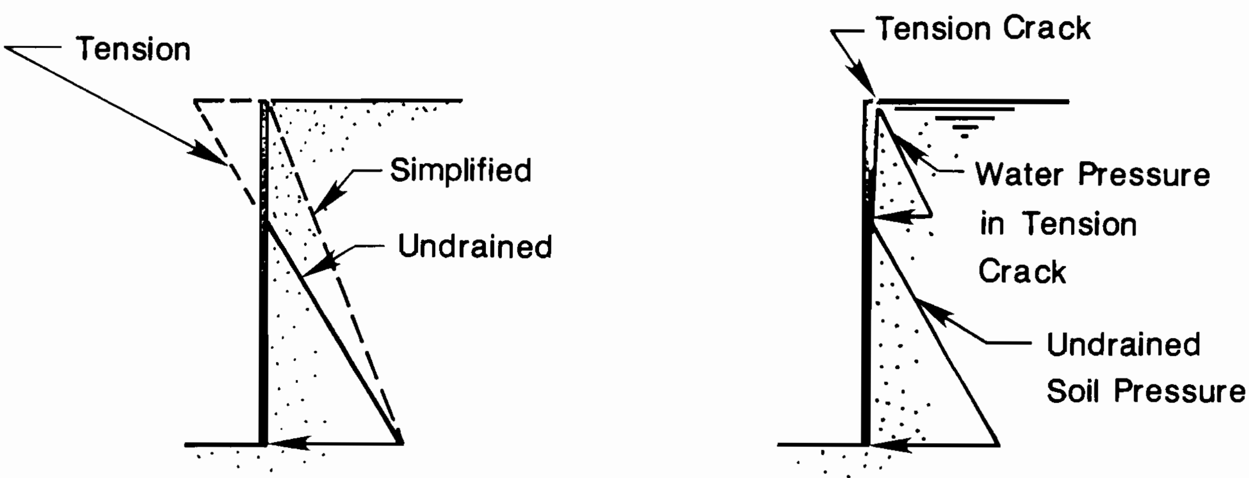

(a) Saturated Cohesive (b) Inundated Sat. Cohesive

Fig. 4.11. The additional pressure induced by water for cohesive soil.

lateral pressures can be calculated for a variety of surcharges by using modified forms of the Boussinesq equations. In these attempts, the stresses on the wall due to surcharge were calculated by assuming the backfill was a homogenerous, linearly-elastic material. The error introduced by this assumption is evident because the backfill near the wall is close to the plastic state of stress. Furthermore, the Boussinesq equations were derived for a semi-infinite body, which does not take into account the presence of the wall. However, if the elastic equations can be calibrated by experimental results, approximate solutions can be obtained. The equations for computing the lateral pressure resulting from surcharge have been reported in the technical literature and are summarized in Appendix A.

AVAILABLE DATA ON ACTIVE EARTH PRESSURES IN OVER-CONSOLIDATED STIFF CLAY

Drilled shafts are often used in earth-retaining structures in overconsolidated, stiff clay because there are few seepage or soil-collapse problems during construction. However, care should be employed in computing the lateral earth pressure. In general, the initial driving force is low as based on the undrained properties of the clay with high resistance to lateral deflection below the cut line. With time, negative pore pressures, induced by unloading due to the excavation, are dissipated and there will be an increase in active pressures and a decrease in lateral resistance near the cut line. Therefore, design procedures for cantilever-retaining walls in the overconsolidated clay typically use active pressures from drained properties.

Williams and Baka (1985) studied the performance of cantilever retaining walls in overconsolidated stiff clay in the Houston area and obtained some useful information regarding earth pressures. They did not measure the earth pressures directly; instead, they measured the slope of the cantilever wall using slope indicators embedded in the wall. By assuming a constant flexural rigidity and a triangular distribution of active pressure on the wall above the cut line, the active pressures were back-calculated by integrating the beam equation shown in Fig. 4.12.

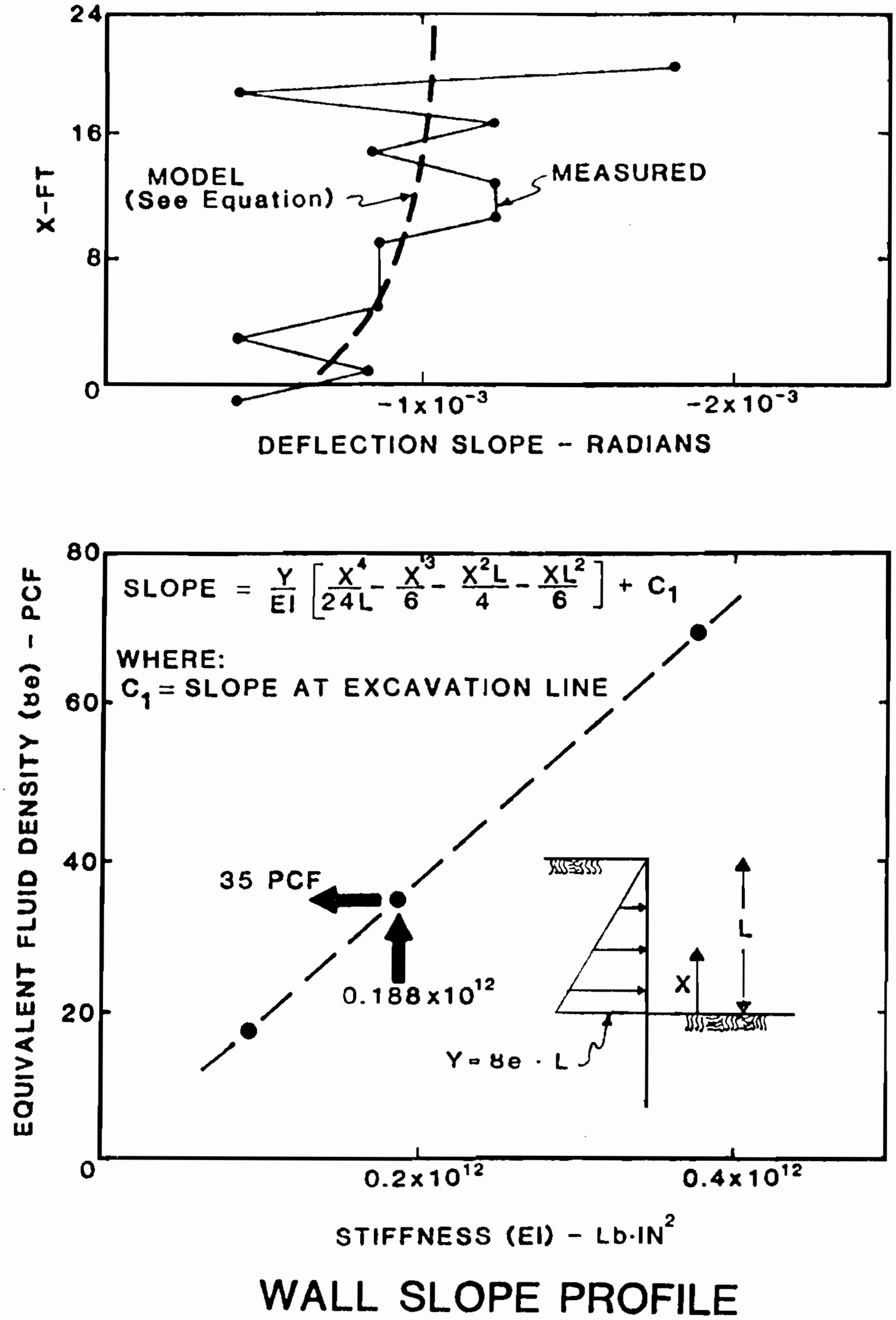

Fig. 4.12. Back-calculated earth pressure from the measured slope profile of a wall (after Williams and Baka, 1985).

The classical Rankine equation for cohesionless soil has the same form as the hydrostatic-pressure-resultant equation. Thus,

$$P_a = 0.5\ \gamma K_a H^2 = 0.5\ \gamma_e H^2 \qquad (4.5)$$

where the γK_a term is analogous to the unit weight of an equivalent fluid γ_e. Eighteen case histories, including thirteen drilled-shaft walls and five soldier-pile-and-lagging systems, were studied. The range of the equivalent fluid is from 13 to 57 lb/cu ft. The comparisons of these data with the undrained and drained active earth pressures are presented in Fig. 4.13. It appears that active earth pressure, based on the drained analysis, has a much close correspondence to the measured data.

An increase in active pressures with time was observed by Williams and Baka, but the elapsed time was limited to about 120 days only. This duration is typically sufficient for the construction of temporary retaining walls, but more time is necessary for long-term increases to be measured. Nevertheless, the measured data have provided guidance in the design of drilled-shaft walls in overconsolidated, stiff clay for short-term performance.

CONCLUDING COMMENT

It has been shown that the lateral earth pressures are the result of a complex interaction between the soil and retaining structures. The appropriate evaluation of this problem requires a knowledge of the stress-strain and stress-failure characteristics of both the soil and the structure. The active and passive states of stresses are well-known, based on limit analyses. How lateral earth pressures vary between the active and passive states is not so well-defined. The concept of employing the active states of stress, proposed here, provides a simple and rational way to estimate the load from earth pressure and avoids complications due to the stress-strain behavior of the soil.

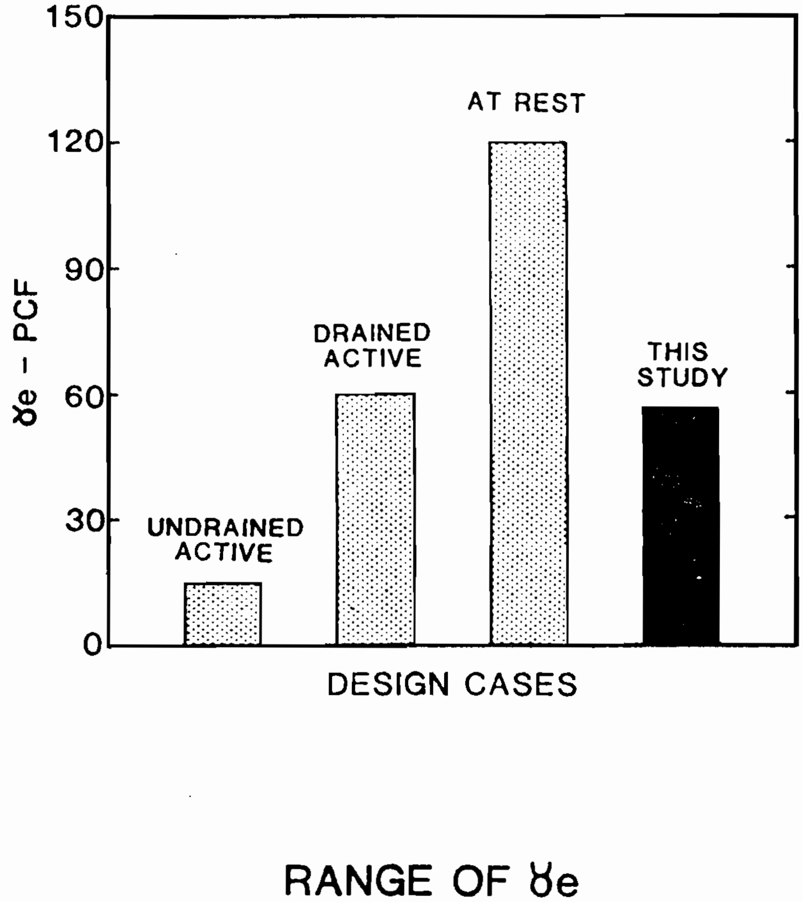

Fig. 4.13. Comparison between measured and predicted earth pressures (after Williams and Baka, 1985).

CHAPTER 5. THE EFFECT OF NONLINEAR MOMENT-CURVATURE RELATIONSHIP ON STRUCTURE BEHAVIOR

FLEXURAL RIGIDITY

The flexural behavior of a structural element such as a beam, column, or a pile subjected to bending is dependent on its flexural rigidity which is expressed as the product, EI, of the modulus of elasticity of the material of which it is made and the moment of inertia of the cross section about the axis of bending. In some instances, EI is constant for the level of loading to which the member is subjected, but there are situations where both E and I vary as the stress conditions change. This variation is most pronounced in reinforced-concrete members. For concrete, the value of E varies because of nonlinearity in stress-strain relationships, and the value of I is reduced because the concrete in the tensile zone below the neutral axis becomes ineffective due to cracking. The tensile weakness of concrete and the ensuing cracking is the major factor contributing to the nonlinear behavior of reinforced concrete elements.

Flexural rigidity, EI, is computed from the moment-curvature diagram when the values of moment, M, and curvature ,ϕ, are known.

$$EI = \frac{M}{\phi} \tag{5.1}$$

The calculation of moment for an assumed ϕ can be done by dividing the cross section of the structural member into a number of strips parallel to the neutral axis, and summing the products of strip areas times the bending stress times the distance from the neutral axis. Thus, values of M and EI can be obtained for given values of ϕ. The relationships of M versus ϕ and EI versus M for a reinforced-concrete beam with no axial load were computed and are shown in Figs. 5.1 and 5.2. It is noted that initially EI is nearly constant until excessive curvature causes the section to

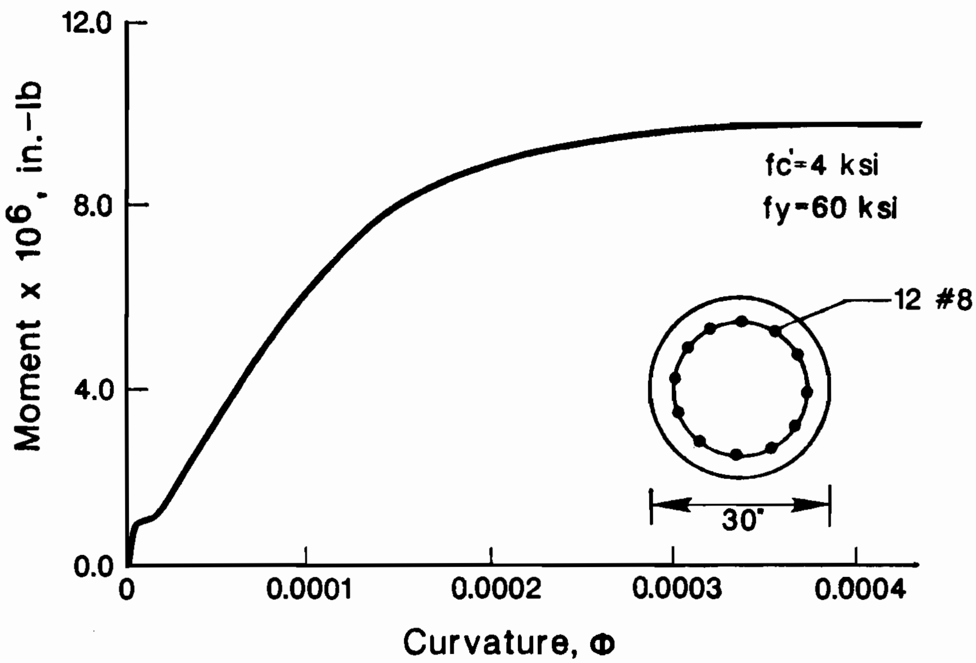

Fig. 5.1. Moment-curvature diagram for a circular cross section.

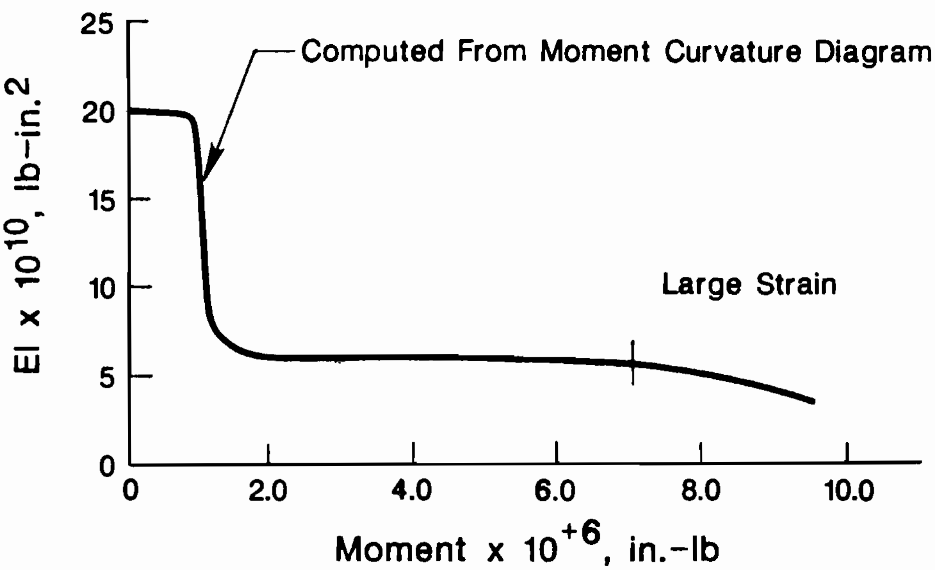

Fig. 5.2 Relationship between bending moment versus flexural rigidity for a circular cross section.

crack. After cracking occured, EI was calculated using the transformed cracked-section, in which no tensile stresses in the concrete section were taken into account. A large change in EI at the point of cracking is shown in Fig. 5.2. Generally, the range of ϕ for an intact section is very small; most concrete beams behave nonlinearly even under service-loading conditions.

Cracks form when the flexural stress due to bending exceeds the tensile strength of concrete. Immediately after formation of the first crack, the stresses in the concrete near the cracking zone are redistributed and cracks propagate along the member. As loading continues, additional cracks open up on occasion, but in general the initial cracks penetrate more deeply with increase in load. Many variables affect the development and characteristics of cracks. The major ones are: percentage of reinforcement, bond characteristics, and tensile strength of concrete. Since concrete is a heterogeneous material and as cracks occur at random, location and spacing of cracks are subjected to considerable variation. Studies have shown that the crack spacing and crack width follow a normal distribution and are influenced by each other. The crack patterns of a typical beam after tests are shown in Fig. 5.3 (Clark,1956; Mathey and Watstein, 1960). As cracking is a random behavior subject to a large degree of scatter, statistical studies based on the accumulation of experimental data are necessary and important.

The variation of EI with the magnitude of the bending moment in a general manner was studied by Eppes (1959) and his results are presented in Fig. 5.4. Three different stages of behavior can be distinguished from these measured relationships between EI and bending moment. They are:

(1) Uncracked stage: the concrete is uncracked and the full uncracked section is available to carry stress and provide rigidity. The EI is more-or-less constant and is equal to the calculated EI for the gross section.

(2) Crack-propagated stage: in this region the EI value is considerably reduced due to the deformation of flexural

(after Clark, 1956)

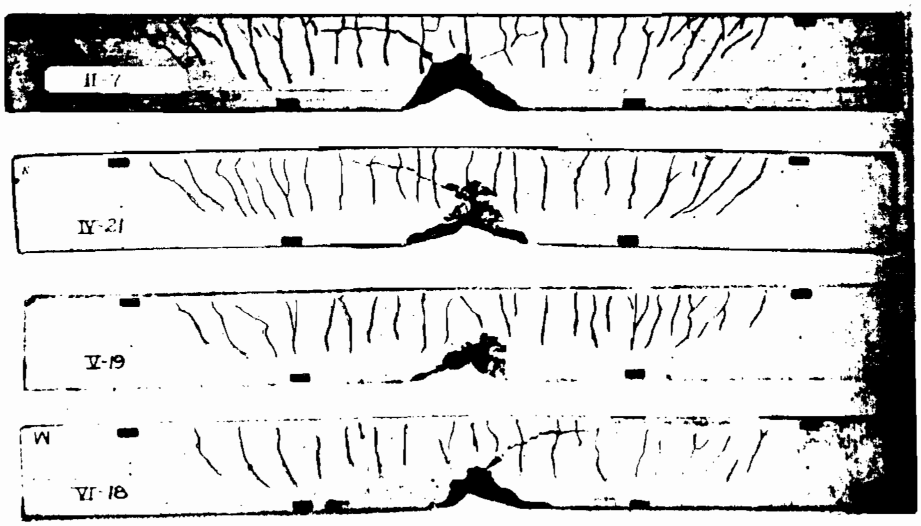

(after Mathey and Watstein, 1960)

Fig. 5.3. The general crack patterns of beams after testing.

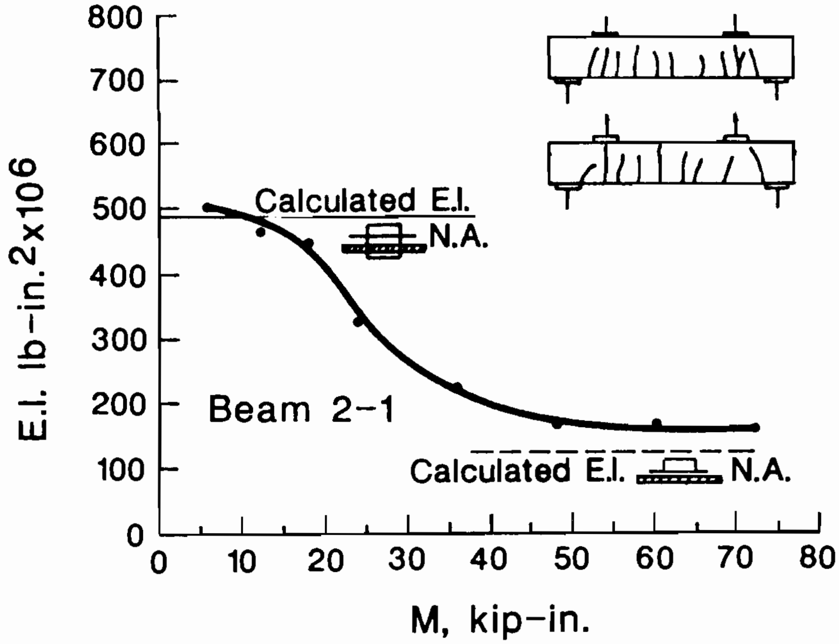

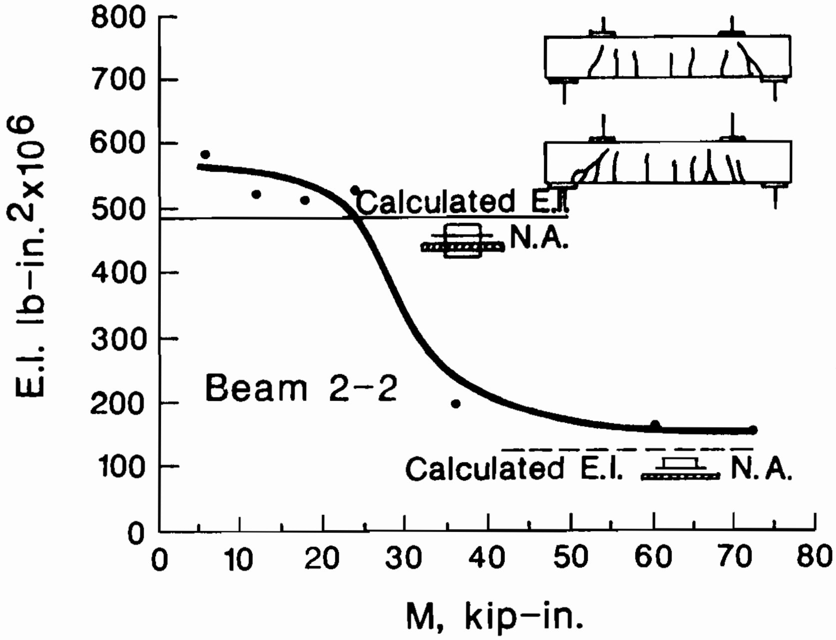

Fig. 5.4. Measured relationship between the flural rigidity and bending moment (after Eppes, 1959).

cracks. The rate of decrease depends mainly on the amount of reinforcement of the section, which controls the rate of penetration of cracks towards the neutral axis. Propagation is faster for beams with lower steel ratio. The moment at the beginning of this stage is called the cracked moment.

(3) Fully-cracked stage: a further decrease in the EI value takes place as cracks continue propagating, and some additional cracks are formed thus reducing the EI to a value which is close to that of a fully cracked section. The calculated EI by the cracked section method is close to the measured results.

It is evident that the use of the crack-transformed section for the computation of the EI at loads above that of cracking will overestimate deflection. The reason for this is that the stresses obtained by concrete theory, neglecting the tensile resistance, are not representative of the real action of reinforced-concrete beams under loads. Many experiments have indicated that the discrepancy between measured and calculated stresses is due to the presence of cracks and the effects produced by the concrete between cracks which resist part of the tension and thus reduce deformations.

EQUATION RECOMMENDED BY ACI CODE

The tension-stiffening effect of the concrete must be considered to make a more realistic prediction of short-term deflections of reinforced concrete beams. The America Concrete Institute has made extensive studies of the results of beam tests and has developed an approximate method to compute EI taking into account the effect of crack propagation (ACI, 1983). This method is the following.

$$E_c I_e = E_c \left[\left(\frac{M_{cr}}{M_a} \right)^3 I_g + \left(1 - \left(\frac{M_{cr}}{M_a} \right)^3 \right) I_{cr} \right] \quad (5.2)$$

where

$$M_{cr} = \frac{f_r I_g}{y_t};$$

and for normal weight concrete

$$f_r = 7.5\sqrt{f_c'}$$

where

f_c' = specified compressive strength of concrete, psi,
f_r = modulus of rupture of concrete, psi,
I_{cr} = moment of inertia of the transformed cracked section of concrete,
I_e = effective moment of inertia for computation of deflection,
I_g = moment of inertia of gross concrete section about centroidal axis, neglecting reinforcement,
E_c = modulus of elasticity of concrete,
M_a = maximum moment in member at stage deflection is computed,
M_{cr} = cracking moment, and
y_t = distance from centroidal axis of gross section, neglecting reinforcement, to extreme fiber in tension.

The effective moment of inertia, I_e, described in Eq. 5.2 provides a transition between the upper and lower bounds of I_g and I_{cr} as a function of the level of cracking in the form of M_{cr}/M_a.

The flexural rigidity computed directly from the transformed cracked-section, in terms of EI of instantaneous cracking, has been recognized to be unrealistic in use. With the modification recommended by the ACI code, the flexural rigidity first shows a constant range of stiffness for an uncracked section. After the cracks are initiated by a higher moment, a rather smooth transition of EI, in terms of progressive cracking, is represented as shown in Fig. 5.5. When the section is fully cracked, EI reaches a minimum value that can be calculated by the transformed cracked-section method.

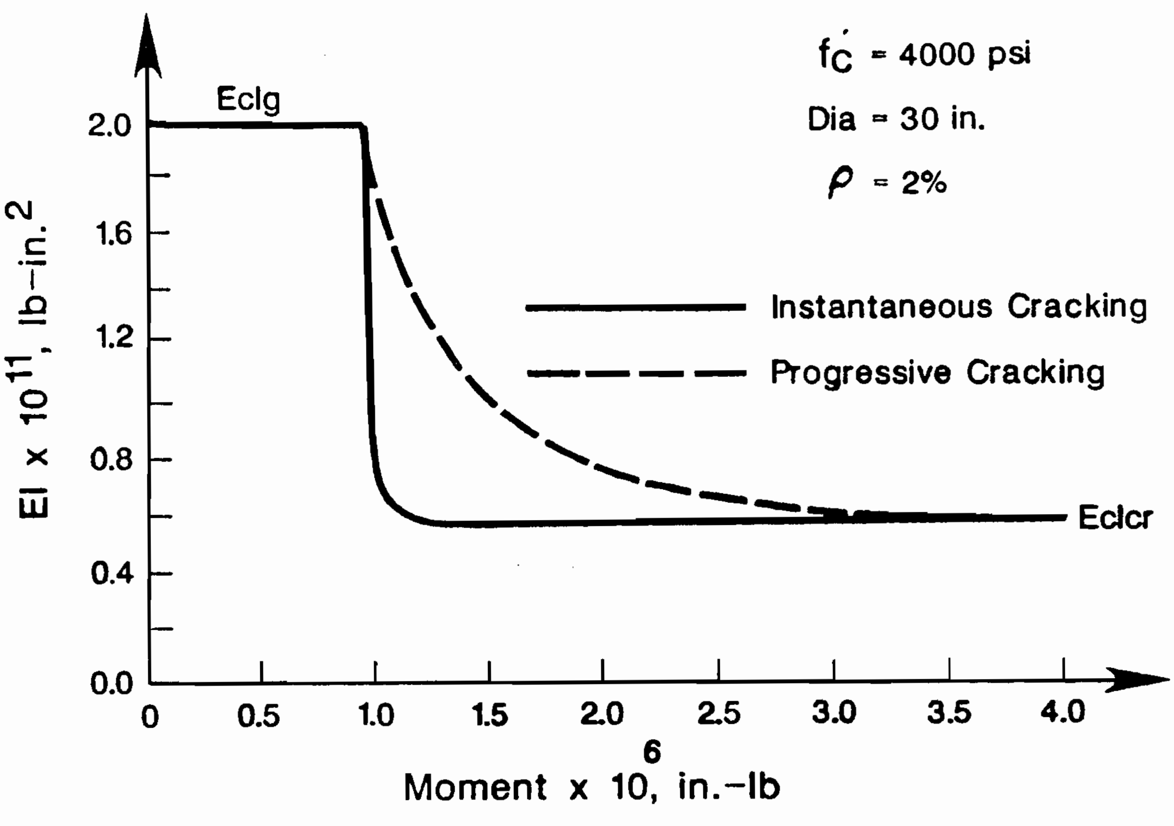

Fig. 5.5. Comparison between the EI-values of instantaneous cracking and progressive cracking.

DIFFERENCE EQUATIONS WITH NONLINEAR EI

The deformation of a drilled shaft under axial and lateral loadings can be found by solving Eq. 5.3.

$$\frac{d^2M}{dx^2} + P_x \frac{d^2y}{dx^2} + ky - w = 0 \qquad (5.3)$$

Since $M = EI\ (d^2y\ /\ dx^2)$, Eq. 5.3 can be rewritten as

$$\frac{d^2}{dx^2} \left(EI \frac{d^2y}{dx^2} \right) + P_x \frac{d^2y}{dx^2} + ky - w = 0 \qquad (5.4)$$

where

- P_x = axial load on the pile,
- y = lateral deflection of the pile at a point x along the length of the pile,
- k = soil stiffness,
- EI = flexural rigidity, and
- w = distributed load along the length of the pile.

If the flexural rigidity, EI, in the first term of Eq. 5.4 is a constant, then Eq. 5.4 can be written the same as Eq. 3.9.

$$EI \frac{d^4y}{dx^4} + P_x \frac{d^2y}{dx^2} + ky - w = 0 \qquad (5.5)$$

If, instead of maintaining EI as a constant, EI is considered to vary along the length of the pile, the resulting differentiations give

$$EI \frac{d^4y}{dx^4} + 2 \frac{d(EI)}{dx} \frac{d^3y}{dx^3} + \frac{d^2(EI)}{dx^2} \frac{d^2y}{dx^2} + P_x \frac{d^2y}{dx^2} + ky - w = 0 \qquad (5.6)$$

Writing each of the derivatives in finite difference form yields the following expression:

$$y_{m-2} (2R_m + R_{m-1} - R_{m+1}) + y_{m-1} (-12R_m + 4R_m + 2P_xh^2) + y_m (-4R_{m-1} + 20R_m - 4R_{m+1} - 4P_xh^2 + 2kh^4) + y_{m+1} (4R_{m-1} - 12R_m + 2P_xh^2) + y_{m+2} (2R_m - R_{m-1} + R_{m+1}) -2w_mh^4 = 0 \qquad (5.7)$$

where

$$R_m = E_m I_m$$

It is important to realize that, in developing Eq. 5.4, derivatives of certain products were taken that were subjected to the limitation of the assumption that the functions are smoothly continuous along the pile. If the flexural rigidity changes abruptly at some computing stations, Eq. 5.6 may not converge to a correct result. Therefore, instead of using Eq. 5.6, (d^2M/dx^2) is written in Eq. 5.4 as:

$$\frac{d^2M}{dx^2} = \frac{-2M_m + M_{m-1} + M_{m+1}}{h^2} \tag{5.8}$$
$$= \frac{-2R_m (y_{m-1} - 2y_m + y_{m+1}) + R_{m-1} (y_{m-2} - 2y_{m-1}}{h^4} \times \frac{+ y_m) + R_{m+1} (y_m - 2y_{m+1} + y_{m+2})}{1}$$

A fourth-order finite difference form is developed that is different from Eq. 5.7.

$$y_{m-2}R_{m-1} + y_{m-1} (-2R_{m-1} - 2R_m + P_x h^2) + y_m (R_{m-1} + 4R_m + R_{m+1} - 2P_x h^2 + k_m h^4) + y_{m+1} (-2R_m - 2R_{m+1} + P_x h^2) + y_{m+2}R_{m+1} - w_m h^4 = 0 \tag{5.9}$$

Equation 5.9 is a cruder approximation for a pile with varying EI than Eq. 5.7, but it has a distinct advantage in that it is not restricted against sharp changes in the flexural rigidity. Because EI may decrease sharply due to changes of dimension, or cracks in the concrete, Eq. 5.9 is believed to be more efficient in handling the nonlinear problem of laterally loaded pile and was employed in this study.

NONLINEAR EI EMPLOYED IN THE LOAD-DEFLECTION ANALYSIS

In most cases, the EI-value is assumed to be constant in the analysis. Little information is available in the literature to guide in selecting a reasonable EI-value for the analysis. A parametric study that varied the percentage of EI of the gross-section with concrete only has found some influence on the behavior of piles. The results of the study for different selections of EI-values are shown in Figs. 5.6 and 5.7.

A study was conducted to find the effect of the rigorous procedure with nonlinear variation of EI along a pile. The results for a particular pile and a particular soil are shown in Fig. 5.8. For comparison, an analysis using the assumption of a constant gross-section EI was also made and is shown in Fig. 5.8. This figure is a plot of deflection at the top of the pile versus lateral load. It is apparent that there are significant differences in the load-deflection curves and these differences increase with load. On the other hand, it is interesting to note that variation in EI has little influence on the maximum bending moment. In fact, bending moment along a pile does not depend strongly on its structural properties. If the pile becomes stiffer by increasing steel ratio by 1%, the cracking zone is limited to a small range. Conseqently, the differences due to the EI-selections are small as shown in Fig. 5.9.

The structural analysis can be much more simplified by using the assumption of constant EI. However, selection of the precise value of EI to use in a particular problem is, of course, a complex matter. Based on the comparisons shown in Figs. 5.8 and 5.9, EI varies with load amplitude, concrete strength, and steel ratio. Detailed studies regarding the influence of these variables have been conducted for this research. Steel ratios were selected as 1%, 2%, and 3% respectively, and concrete with a strength of 3000 psi and 4000 psi were employed in the analysis. It is necessary to know the ultimate moment of a structural member to vary properly the loading amplitude. The ultimate bending moment, M_u, can be selected as the ultimate moment that the section can sustain, or it can be selected as a particular value of a corresponding compressive strain in the extreme fibers of the concrete, say 0.003. The failure load is defined generally as the loading that produces the ultimate bending moment for the structural member. Based on the failure load obtained above, 25%,

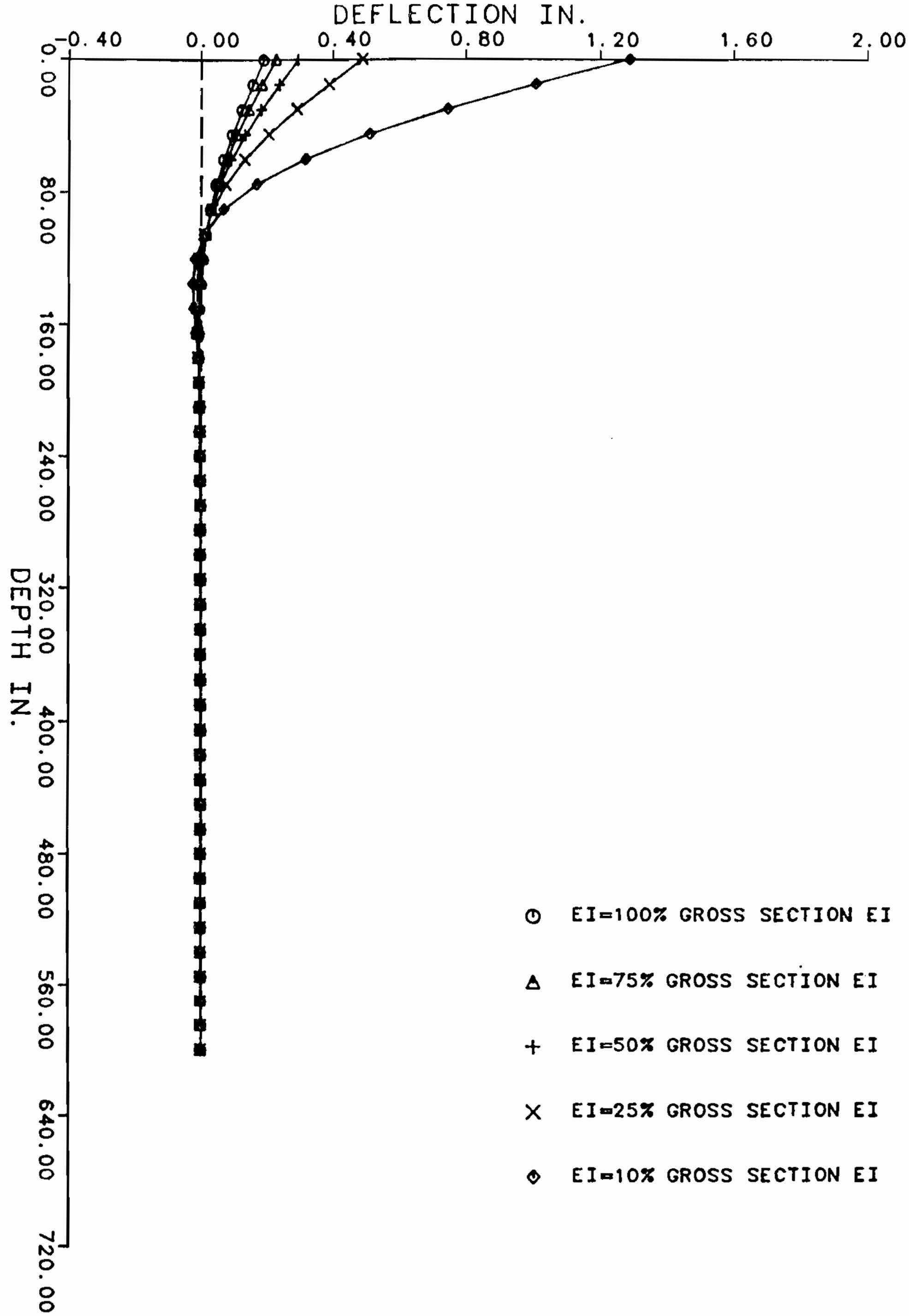

Fig. 5.6. Comparison of the pile deflection curves under different EI-values.

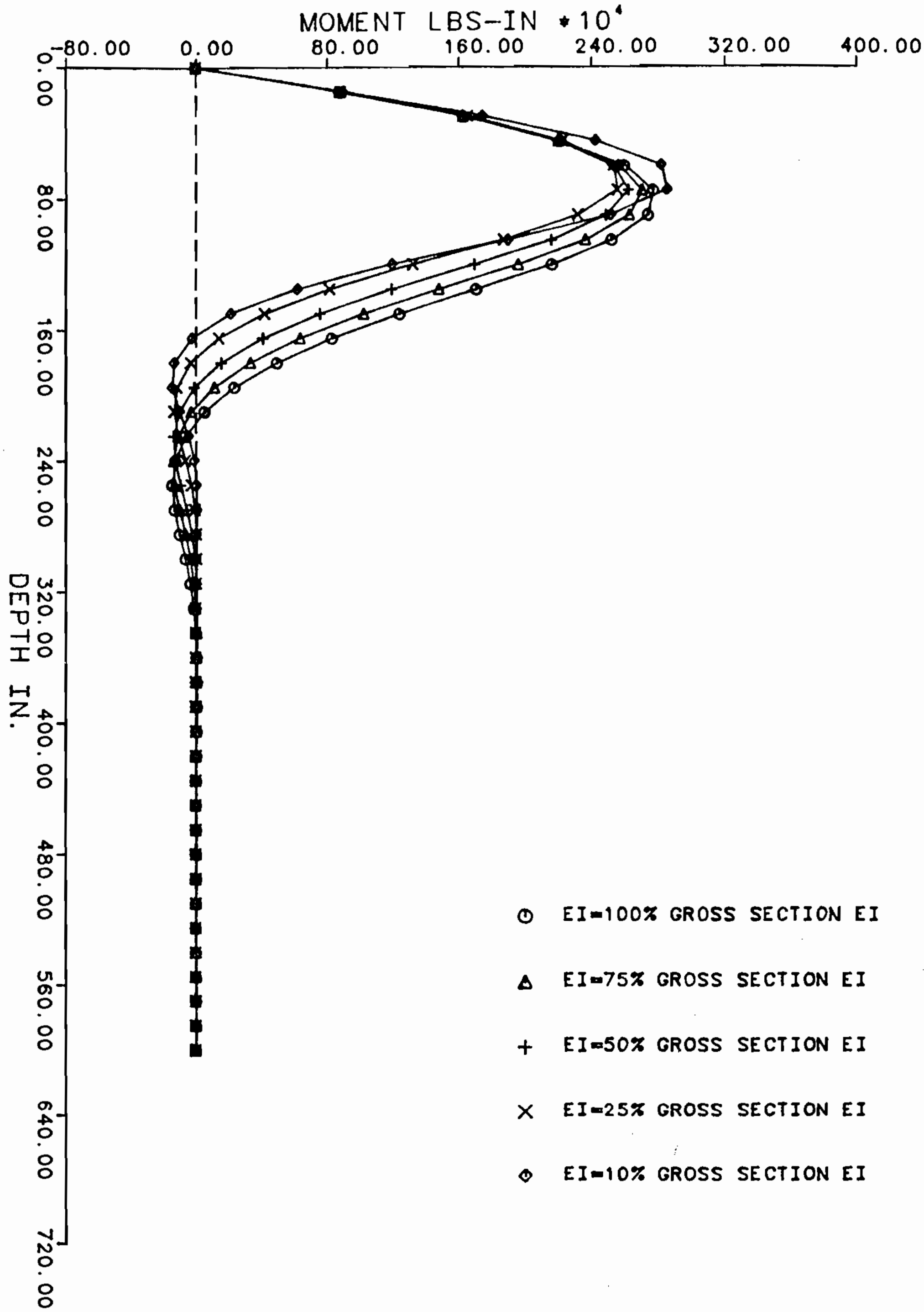

Fig. 5.7. Comparison of the bending moment curves along a pile under different EI-values.

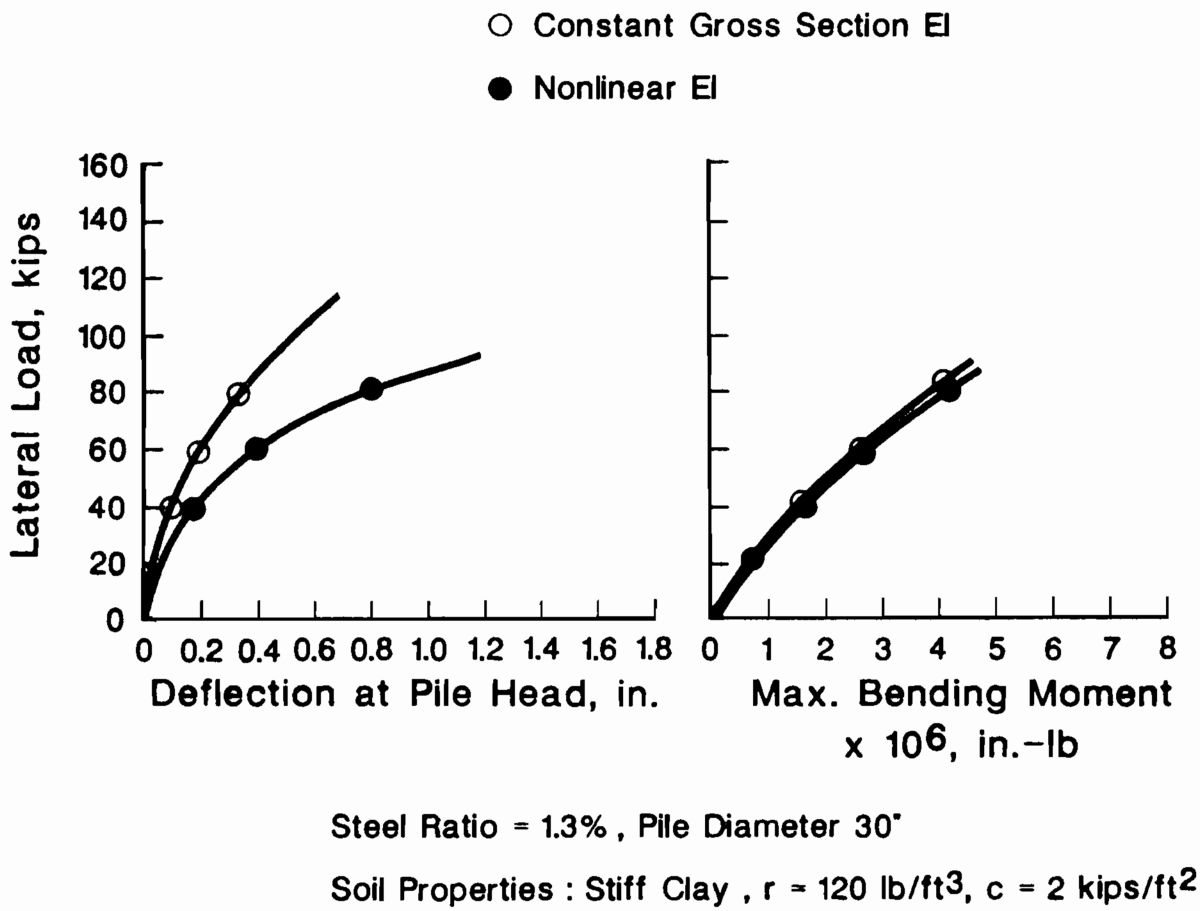

Fig. 5.8. The deflection at the pile top and the maximum bending moment in a pile with the consideration of nonlinear EI (ρ = 1.3%).

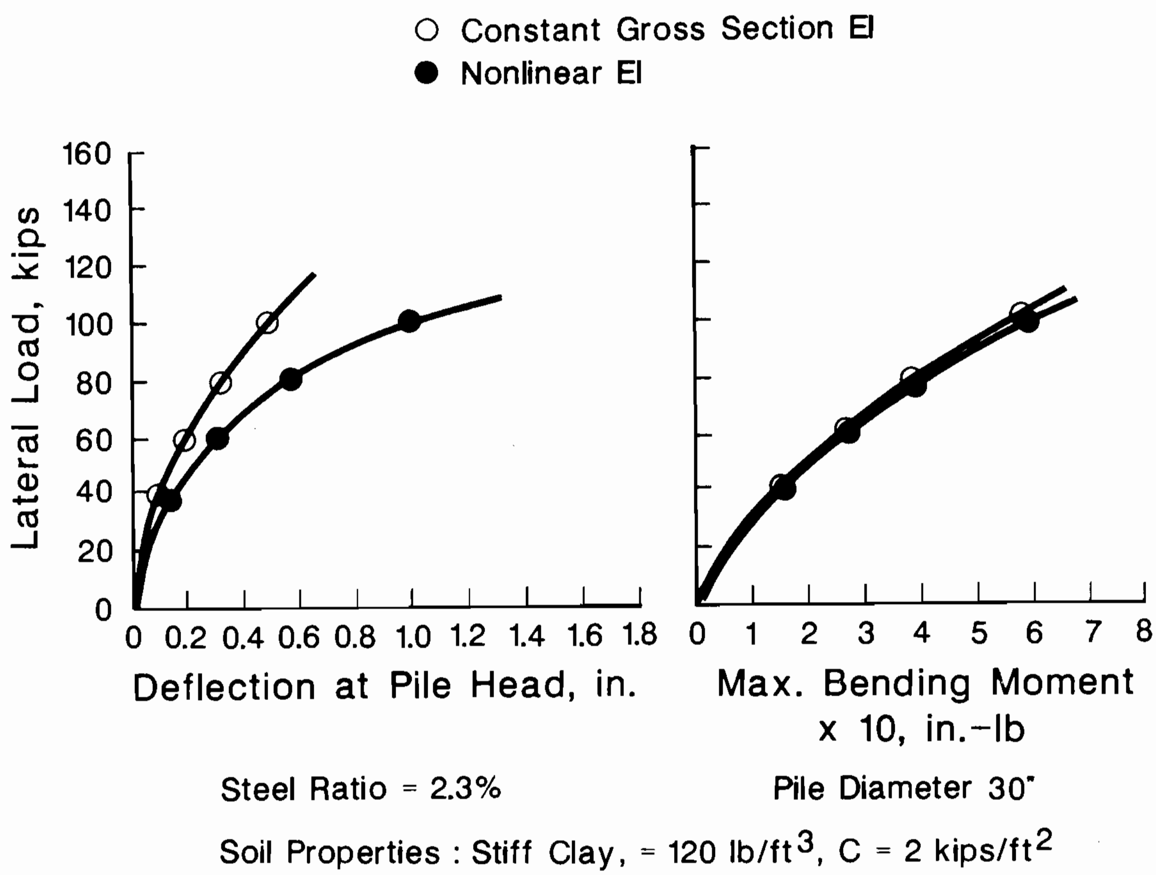

Fig. 5.9. The deflection at the pile top and the maximum bending moment in a pile with the consideration of nonlinear EI (ρ = 2.3%).

50%, and 75% of the failure load were selected in studying the influence of the loading conditions.

The first step in making the comparison was to select a homogenerous soil deposit and the geometry of a pile that were the same for every case. The deflection at the pile head was found by taking into account the nonlinearity of structural properties for the specified value of loading, steel ratio, and concrete strength. The second step was to find a constant value of EI to produce the same pile deflection that was obtained from the first step for the same loading and soil conditions. The values of constant EI obtained from the second step were normalized by the EI of the gross section with concrete only, identified as E_cI_g. The normalized values are plotted versus loading range, steel ratio, and compressive strength of concrete in Figs. 5.10 and 5.11.

The constant EI for analyses of the different cases, was found to have a wide range of variation. Generally, it is most variable when the steel ratio was less than 1%. The EI-value can vary from 110% of the gross section E_cI_g for 25% of the failure load to about 35% of E_cI_g for 75% of the failure load. The reason for this is that the structural behavior is dominated by the properties of the concrete. When the steel ratio increases from 1% to 2% or 3%, the structural member is less influenced by the cracks of the concrete. The selection of a constant EI-value can vary from approximately 80% of EI_g in the lower loading range to approximately 50% of E_cI_g in the higher loading range. It is also interesting to note that variation of compressive strength of concrete and the surrounding soil medium has little effect on the flexural rigidity.

In the analysis of a pile under lateral loading, only the upper portion of the pile will be subjected to a large moment. The flexural rigidity in that portion dramatically changes with moment (Fig. 5.12). Because the upper portion of the pile needs greater stiffness, reinforcing steel is used only as required by bending moment rather than over the entire length of the pile. This procedure, with the consideration of nonlinear bending resistance,

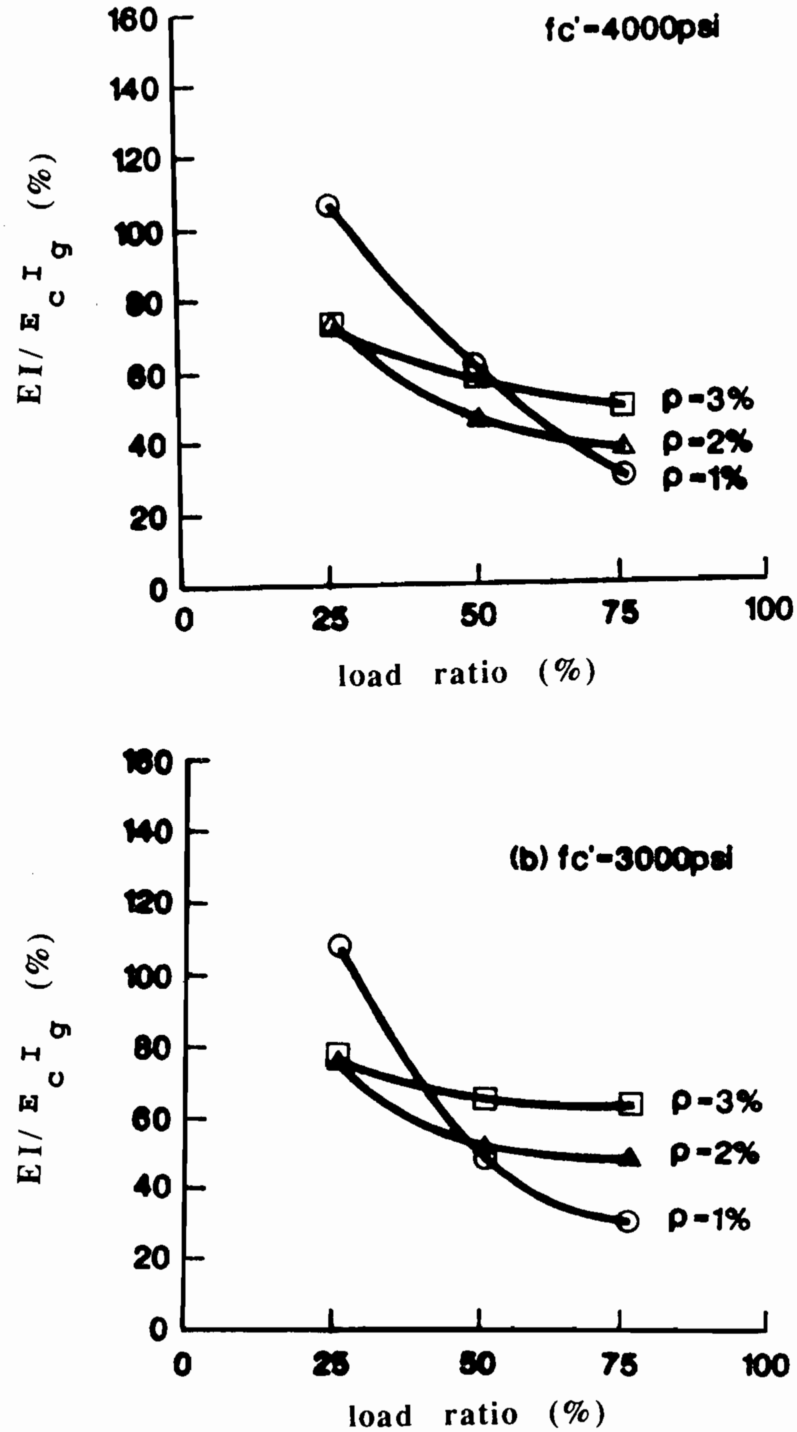

Fig. 5.10. The proposed constant EI-values of concrete piles in sand.

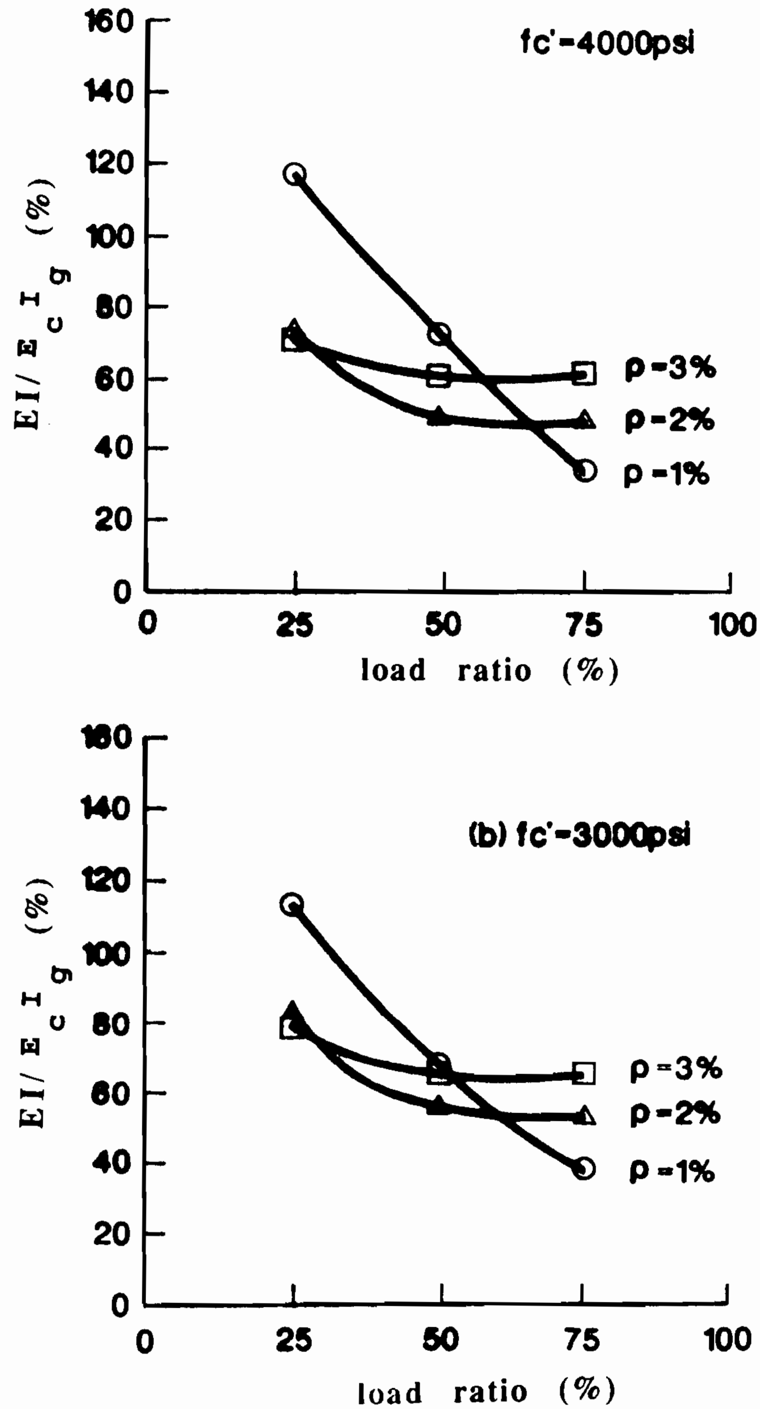

Fig. 5.11. The proposed constant EI-values of concrete piles in stiff clay.

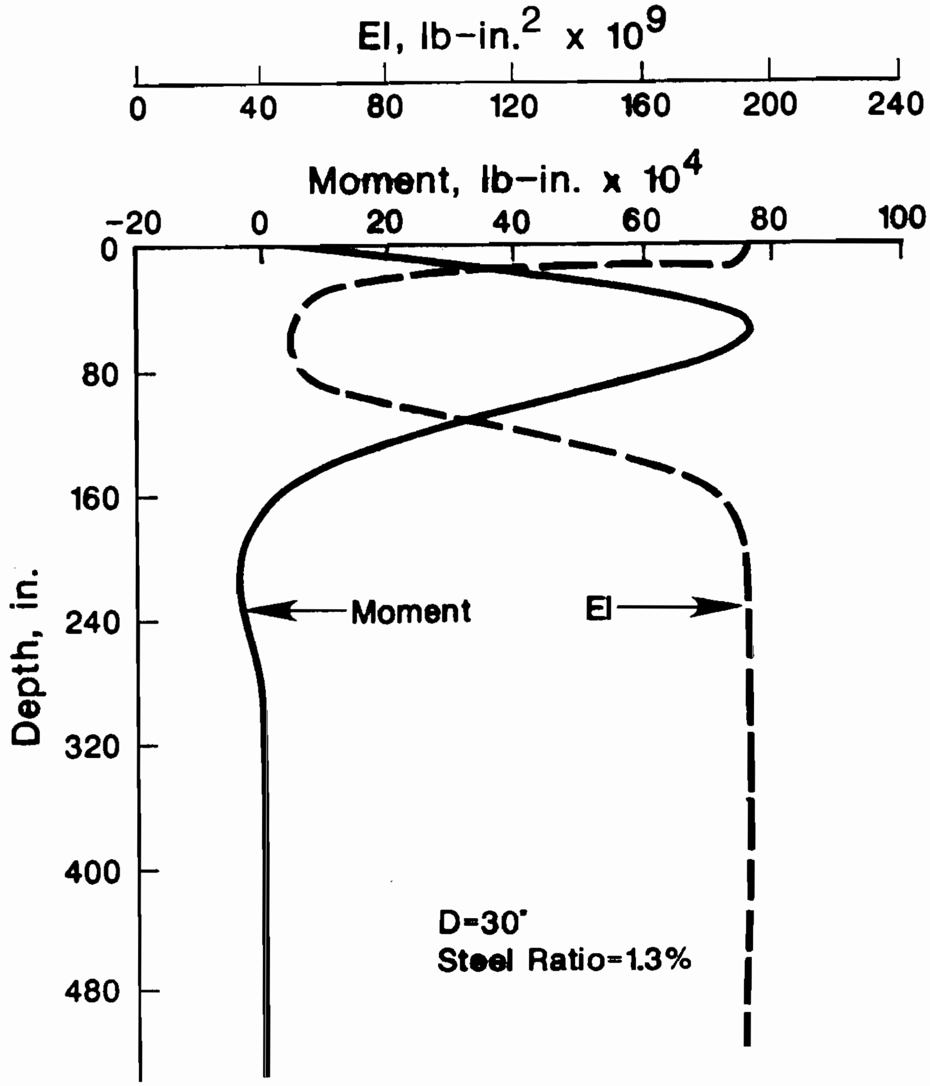

Fig. 5.12. Bending moment and flexural rigidity versus depth for a laterally loaded pile .

should allow drilled-shaft walls to be designed with increased confidence and with decreased cost.

CHAPTER 6. SOIL RESISTANCE (p-y) CURVES FOR LATERALLY LOADED DRILL SHAFTS IN A ROW

ANALYTICAL MODEL

When piles are in a group and are subjected to lateral loading, stresses will be transferred through the soil from one pile to the next. This phenomenon is termed "pile-soil-pile" interaction. The change of the stress and strain by these interactions is quite complicated due to the nonlinear and inelastic soil properties. How to quantify the influence of the pile-soil-pile interaction for pile-group design has become an important subject for many studies. Generally, the effect of one pile on another is dependent on the distance between piles, the relative direction from one pile to the next, and the stiffness of the piles and soils.

Several methods have been published in technical literature for the analysis of pile groups loaded by lateral forces. These methods provide an overview of current development on the design of pile groups under lateral load. The commonly used analytical methods for groups of closely spaced piles subjected to lateral loads are identified as follows:

(1) finite-element model,
(2) continuum model,
(3) hybrid model,and
(4) imaginary single pile model

Finite-Element Model

The development of the finite-element method during the last two decades has provided a powerful tool for mechanical analysis. This method is particularly attractive due to its applicability to any boundary and geometric conditions. Desai and Appel (1976) developed a three-dimensional finite-element code for the analysis of piles in a group. This code performs nonlinear analysis for the soil and linearly-elastic analysis for piles. The nonlinear behavior of soil is usually obtained from a series of triaxial tests under various confining pressures, and often at different relative densities. The finite-element method can also simulate a gap and other interface problems between soils and piles.

Although this method is a powerful analytical solution, it is inadequate for design purposes because of high computer costs. Furthermore, the uncertainty of the constitutive laws for soils is a limitation to this method. The recent development of super computers can lower computer cost, but, unless a better constitutive model for soils is established, this method will have limited application for many practical problems.

Continuum Model

The analytical solutions for the behavior of a single, elastic pile embedded in an elastic continuum have been extended to model the behavior of pile group by Poulos(1971). The method of solution for the isotropic medium is to integrate Mindlin's equations for the stresses caused by a point load acting within an elastic continuum, and to predict the interaction between two piles. The interaction of any number of piles then be computed by repeated superpositions. Poulos produced design charts to obtain the group-reduction factors for computing the deflection and load on each of piles in a group. The deflection of the k-th pile can be calculated for a group of m piles from

$$\rho_k = \rho_F \sum_{\substack{j=1 \\ j \neq k}}^{m} (H_j \alpha_{\rho F k j} + H_k) \qquad (6.1)$$

where

ρ_k = deflection of the k-th pile,

ρ_F = the unit reference displacement of a single pile under a unit horizontal load, computed by using elastic theory,

H_j = lateral load on pile j,

$\alpha_{\rho Fkj}$ = the coefficient to get the influence of pile j on pile k in computing the deflection ρ (the subscript F pertains to the fixed-head case and is used here for convenience; there are also influence coefficients as shown later where shear is applied, $\alpha_{\rho Hkj}$, and where moment is applied, $\alpha_{\rho Mkj}$),

H_k = lateral load on pile k, and

m = number of piles in group.

The influence factor $\alpha_{\rho Fkj}$ is a function of pile length-to-diameter ratio, pile flexural rigidity, Poisson's ratio of the soil, pile spacing-to-diameter ratio, and direction of load relative to the pair of piles being considered.

Poulos' method can only predict the pile-head response. Variations in deflection and bending moment along the piles are not considered. While such methods are instructive, there is evidence to show that soils cannot generally be characterized as linear, homogenerous, elastic materials. Consequently, this method can only be used with confidence when the loads are small and the stress and stain of the soil is in the linearly elastic range.

Hybrid Model

The continuum model is based on the assumptions that soils must be elastic and have constant and uniform properties with depth. It is well recognized that such assumptions are not appropriate for practical problems. Focht and Koch (1974) proposed another model that combined the well-documented p-y approach of a single pile with the elastic-group effects from Poulos' work. Focht and Koch's modification begins by introducing a term R into Eq. 6.2 as

$$\rho_k = \rho_F \sum_{\substack{j=1 \\ j \neq k}}^{m} \left(H_j \alpha_{\rho Fkj} + RH_k \right) \qquad (6.2)$$

where R is the ratio of the groundline deflection of a single pile computed by the p-y curve method to the deflection ρ_i, computed by the Poulos method, that assumes an elastic soil.

The above equation can be used to solve for group deflection, Y_g and loads on individual piles. With the known group deflection, Y_g, the p-y curves at each depth for a single pile can be multiplied by a factor, termed the "Y" factor, to match the pile-head deflection of a single pile with the group deflection, Y_g, by repeated trials. The "Y" factor is a constant multiplier employed to increase the deflection values of each point on each p-y curves; thus, generating a new set of p-y curves that include the group effects. The modification of p-y curves as described above for piles in the group allow the computation of deflection and bending moment as a function of depth.

From a theoretical viewpoint, group effects for the initial part of p-y curves can be obtained from elastic theory. The ultimate resistance of soil on a pile is also affected by the adjacent piles due to the interference of the shear failure planes, called shadowing effects. Focht and Koch suggested a p-factor may need to be applied to the p-y curves in cases where shadowing effects occur. The p-factor should be less than one and the magnitude depends on the configuration of piles in a group. Ha and O'Neill (1981) suggested a modification of the work of Focht and Koch and developed a computer code PILGP1 to model three-dimensional group of piles. The model differs from the Focht-Koch procedure in that the influence of the stresses from nearby piles was obtained directly by integrating Mindlin's equation in place of using Poulos' charts. There are no comprehensive studies on the shadowing effect for closely spaced piles, therefore, PILGP1 can only provide reasonable information about behavior under working loads.

Imaginary Single-Pile Model

The imaginary-pile model is based on the assumption that the soil contained between the piles moves with the group as a whole. Thus, the pile group with the contained soil can be treated as a single pile of large diameter. This method has been accepted by engineers for many years and was well-described by Reese (1984). The diameter of this imaginary pile is taken as the perimeter of the group divided by π. The stiffness is determined as the sum of the stiffnesses of the individual piles. All piles in the group are assumed to have the same deflection at the top and to have the same deflected shape. The existing p-y method is used to compute the soil resistance, pile deflection, shear, and bending moment. The shear and bending moment are then equally distributed to the individual piles. The results of this solution are compared to that of a single pile analysis and the worst case (normally the group solution) is used for design.

Bogard and Matlock (1983) have extended the concept of the imaginary pile to describe the behavior of a closely spaced pile group in soft clay. When the piles are spaced widely, the behavior of each pile can be treated as a single pile without any effect from the others. For a group in which the piles are close together, the group would tend to behave like an imaginary large-diameter pile as mentioned earlier. Bogard and Matlock believe that the deflection of the piles in a group is related to both the deflection of the piles acting individually and the deflection of this large imaginary pile. They recommended criteria to construct p-y curves (Fig. 6.1) at various depths based on the p-y curves of a single individual pile and a single imaginary pile as follows:

$$Y_{gp} = Y_{sp} + (Y_{ip} / D_1) \qquad (6.3)$$

where

Y_{gp} = deflection of a pile in a group,
Y_{sp} = deflection of a single individual pile,
Y_{ip} = deflection of a single imaginary pile, and
D_1 = center-to-center spacing between the two piles.

If the pile spacing is small, group effects completely dominate and the contribution from a single individual pile is only a small part of the total deflection as shown in Fig. 6.2. With this model, Bogard and Matlock were able to compare the predicted results with the measured results obtained by them on a

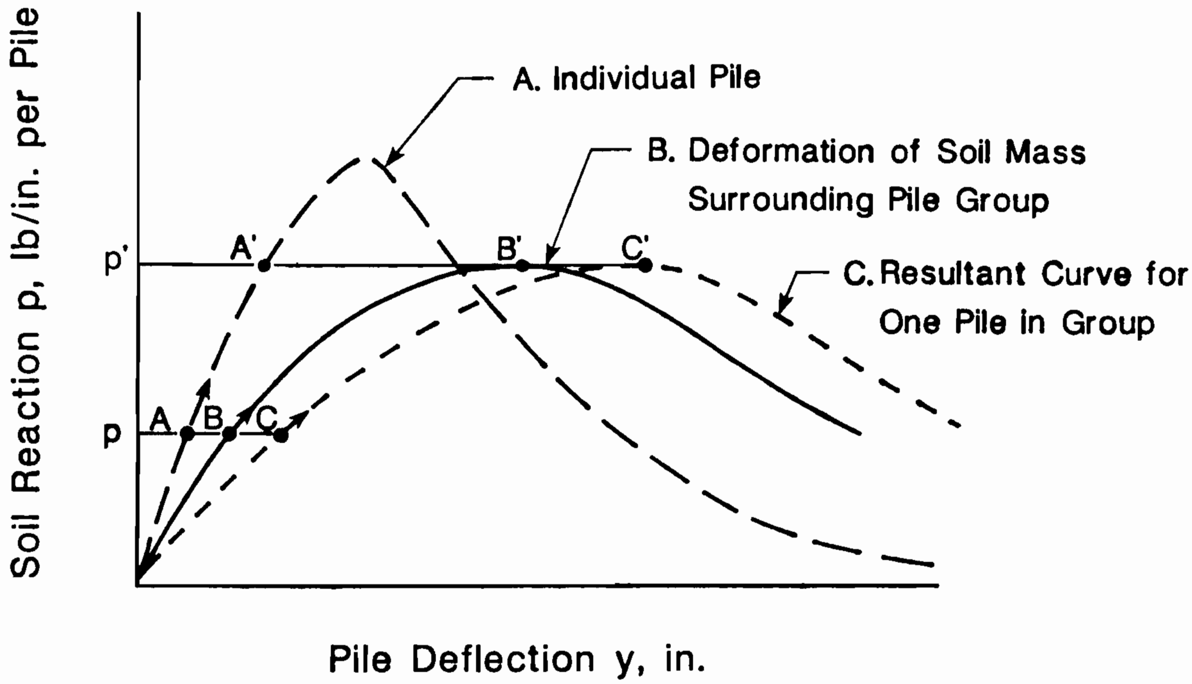

Fig. 6.1. Conceptual Construction of p-y curves for piles within groups (after Bogard and Matlock, 1983).

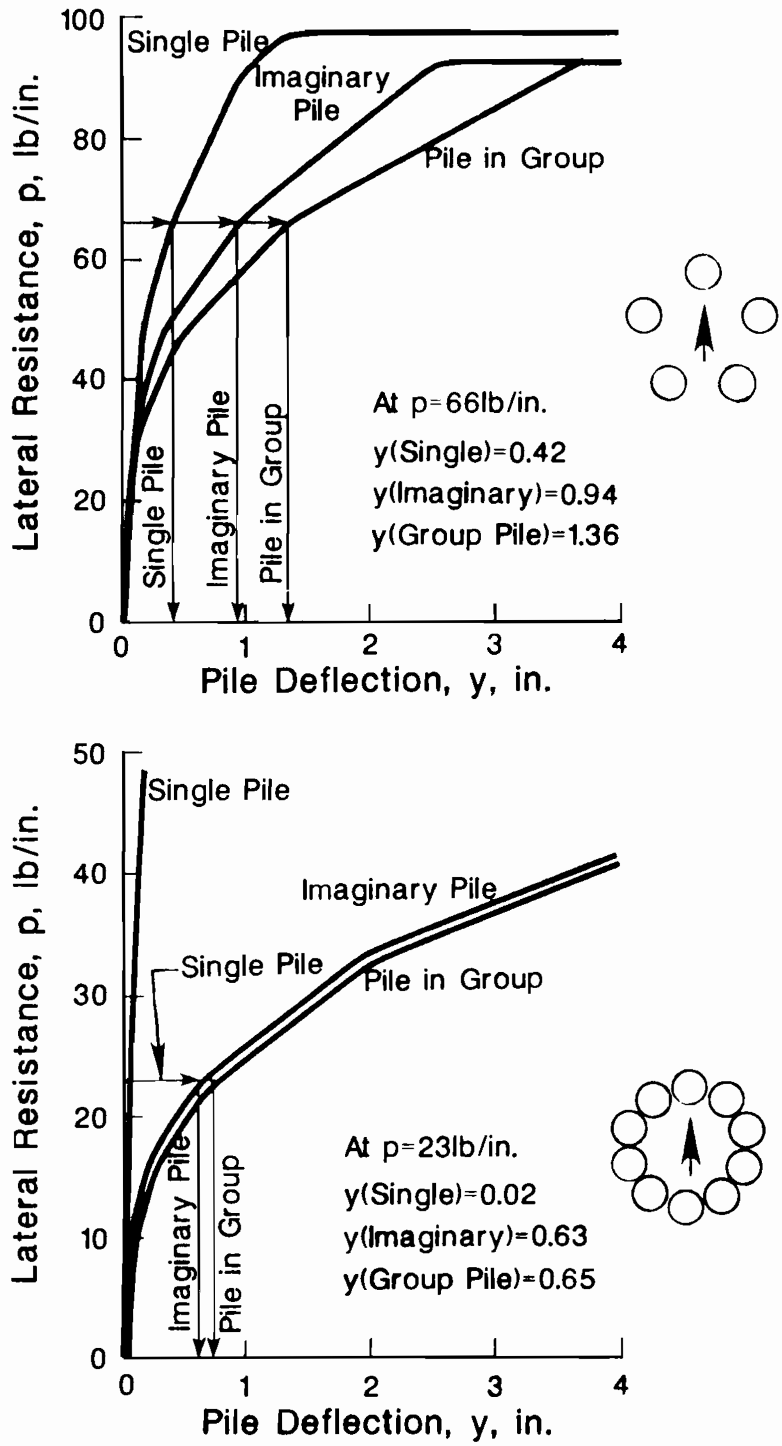

Fig. 6.2. p-y curves for pile groups from Bogard and Matlock procedures (after Bogard and Matlock).

group of piles in a very soft clay at Harvey, Louisiana in 1981. There is a good agreement between the measured and predicted results.

It is recognized that this model is a crude approximation and has proved to be sucessful only for piles in a circular pattern in very soft clay. If piles stand in a row, the concept of the imaginary pile is inadequate due to the geometric problems. It is questionable for this method to be employed in the research described herein.

After reviewing the common methods for the analysis of pile groups, it seems that the hybrid model is the most adequate method for the design of drilled-shaft walls. The group reactions from elastic theory can be added to the p-y curves of a single pile. If shadowing effects do not exist, the p-y curves with or without elastic-group reactions should reach the same ultimate resistance as shown in Fig. 6.3. However, it is realized that a larger deflection is needed when group action is present to develop the same ultimate resistance because the supporting soil is forced to deform by the stresses from nearby piles. When piles are in a closely spaced group, the shear-failure planes resulting from the movement of each pile will overlap and the ultimate resistance for piles in a group may be less than that of a single pile. Generally, the ultimate resistance can be derived from limit analysis or by other approximate methods. Thus, the complete p-y curves for piles in a group can be constructed as shown in Fig. 6.4. The following sections will discuss equations for computing the ultimate soil resistance for piles in a row. The elastic interactions between piles will be studied after that.

ULTIMATE SOIL RESISTANCE FROM LIMIT-EQUILIBRIUM ANALYSIS

Using observations in the field and in the laboratory, soil failure around a laterally loaded pile can be distinguished into

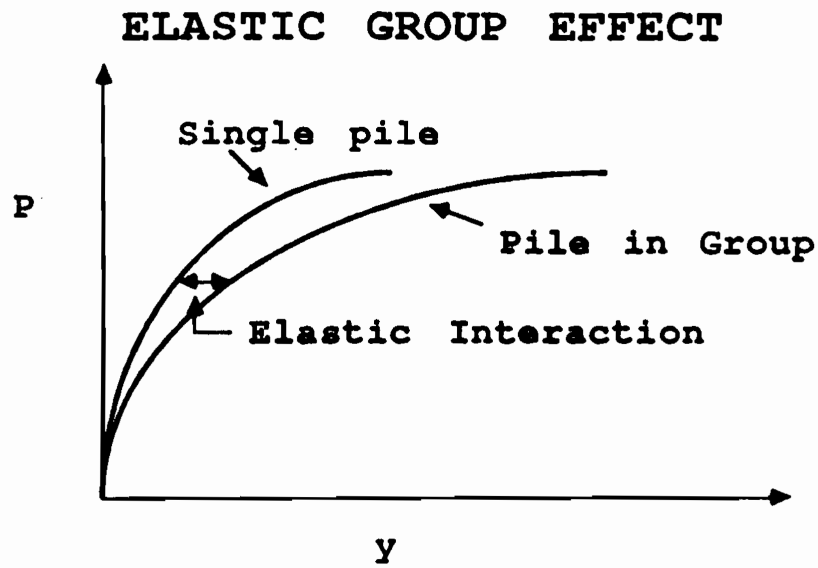

Fig. 6.3. p-y curves for single pile and pile group without shadowing-effect.

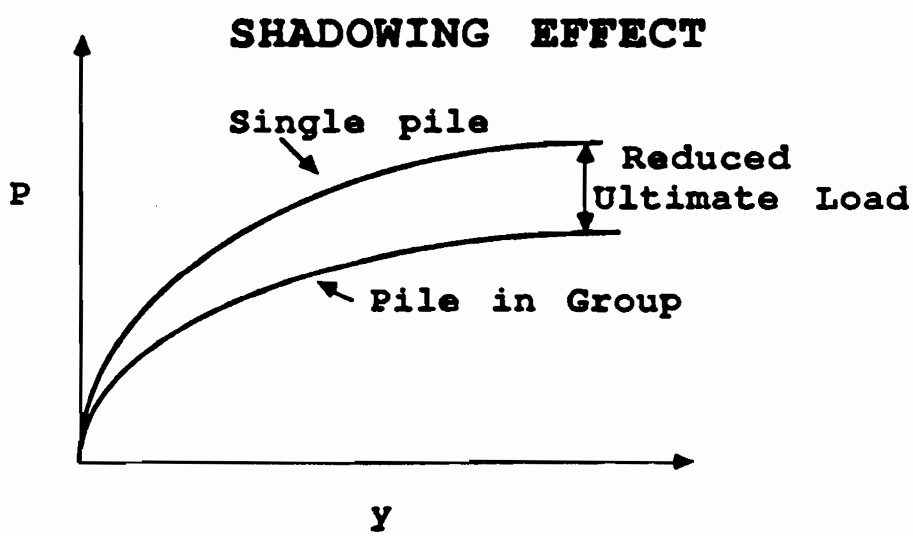

Fig. 6.4. p-y curves for single pile and pile group with shadowing-effect.

two failure conditions as shown in Fig. 6.5. First, a passive wedge-failure occurs near the ground surface and a wedge of soil is moved up and away from the pile. Second, failure surfaces are generated by the pile several diameters below the ground surface. Here the soils are limited to plane-strain behavior and are forced to move in a flow-around manner.

Wedge-Type Failure

Ultimate soil resistance in cohesionless soil (c=0). The soil model for computing the ultimate resistance on a single pile near the ground surface in sand is shown in Fig. 6.6 (Reese,Cox, and Koop, 1974). The horizontal force against the pile can be computed by summing the horizontal components of the forces on the sliding surfaces, taking into account the force of gravity on the wedge of soil. Differentiation of the resulting horizontal force with respect to the depth of this wedge yields an expression for the ultimate soil resistance on a single pile as follows.

$$P_u = K_p \gamma b H + K_p \gamma \tan\alpha \tan\beta \ H^2 + K_o \gamma \tan\beta \ (\tan\phi - \tan\alpha) \ H^2 - K_a \gamma b H \tag{6.4}$$

in which angle α and β are indicated in Fig.6.6. A detailed derivation can be found in the paper by Reese et al (1974).

For a row of drilled shafts with a small spacing (Fig. 6.7), the sliding surfaces interfere with each other and result in the so-called shadowing effect. Figure 6.7 shows a general view of this interference. A plan view of the sliding surface is shown in Fig. 6.8. As the piles move laterally, the horizontal stresses of the soils in front of piles increase until a maximum value is reached. From the Mohr's diagram (Fig.6.9), the normal and shear stresses on the failure plane, σ_f and, τ_f can be obtained:

$$\sigma_f = \frac{1}{2} (K_p \gamma Z + \gamma Z) - \frac{1}{2} (K_p \gamma Z - \gamma Z) \sin\phi \tag{6.5}$$

$$\tau_f = \frac{1}{2} (K_p \gamma Z - \gamma Z) \cos\phi \tag{6.6}$$

where

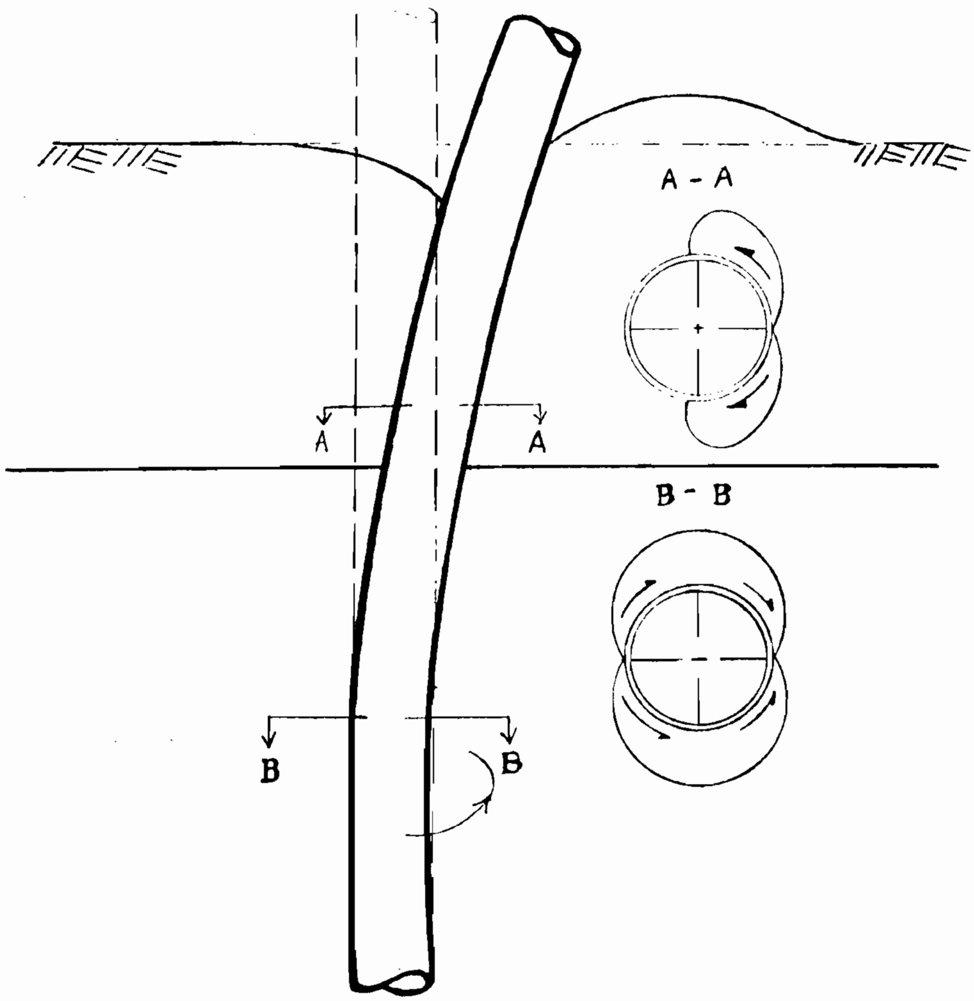

Fig. 6.5. Pile and soil deformation under lateral load.

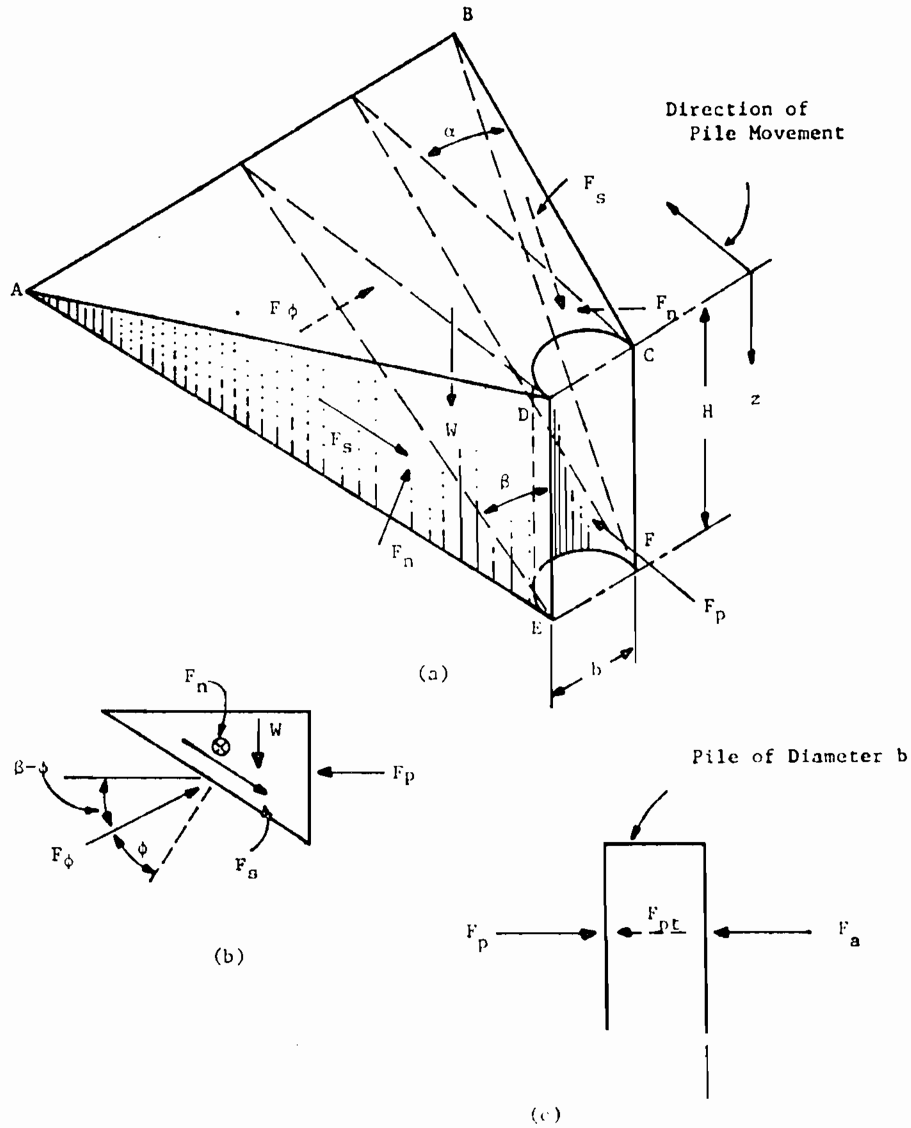

Fig. 6.6. Assumed passive wedge-type failure. (a) general shape of wedge. (b) forces on wedge (c) forces on pile (after Reese et al, 1974).

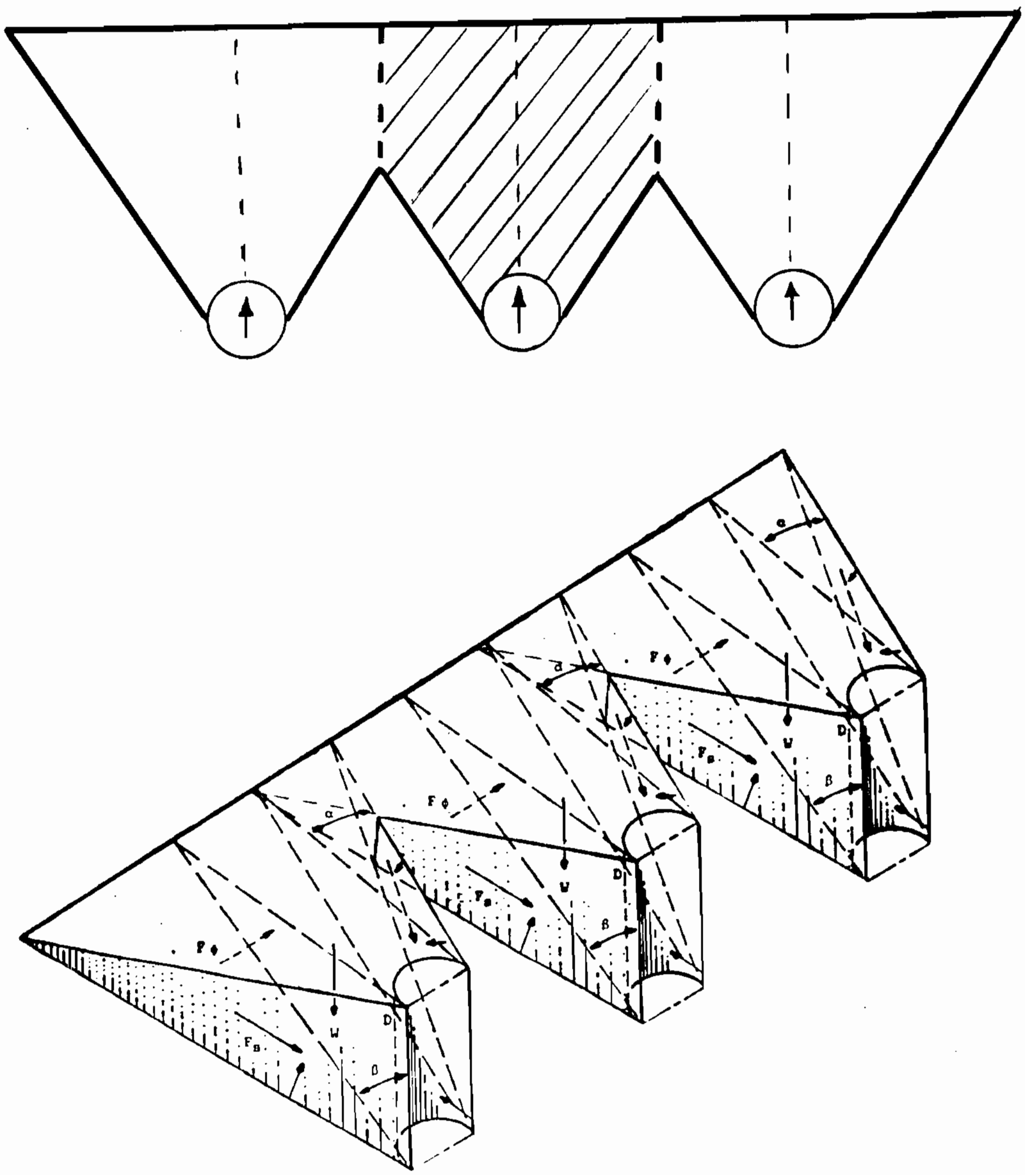

Fig. 6.7. General view of failure wedge for side-by-side piles in sand.

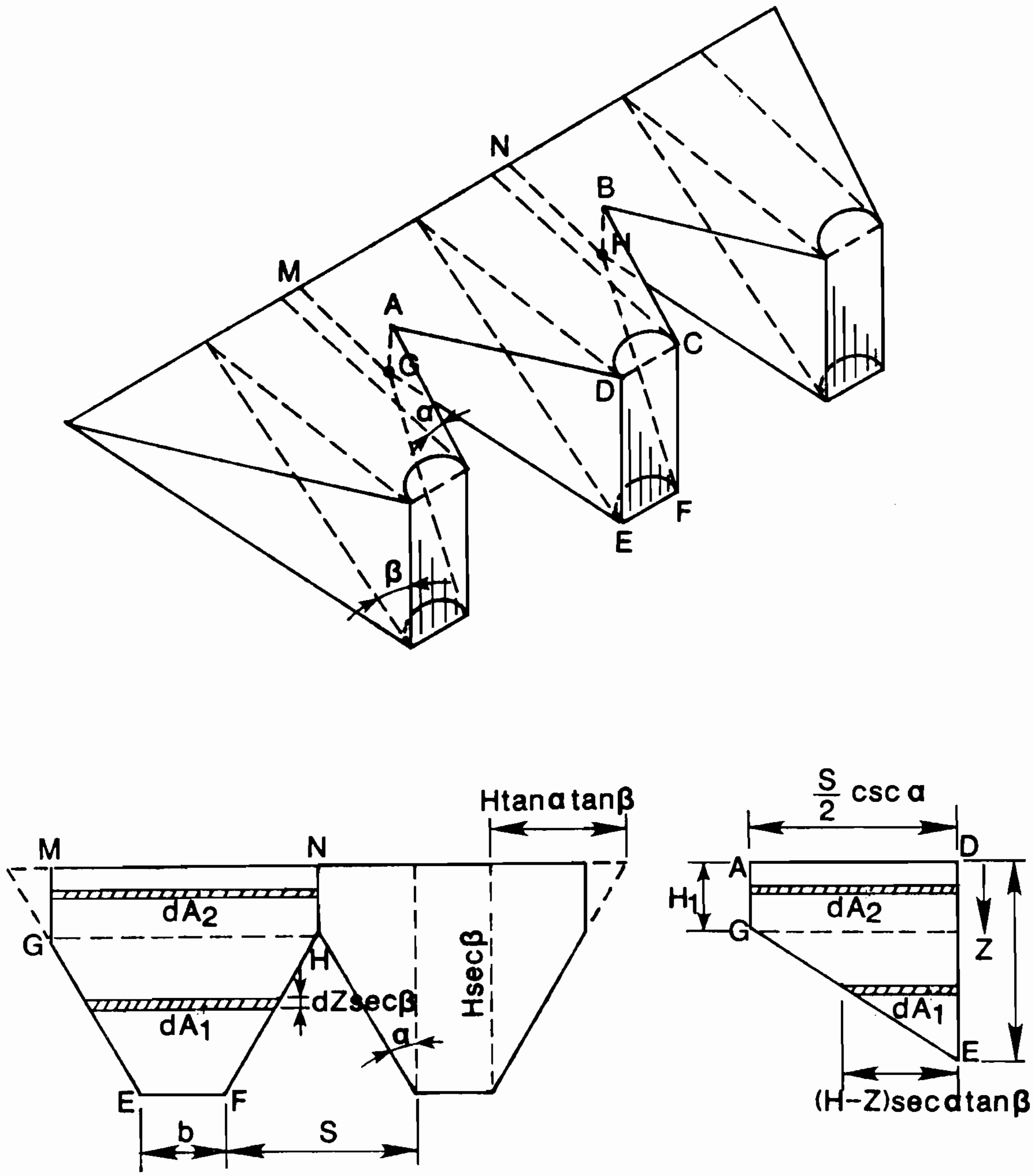

Fig. 6.8. Assumed passive wedge for piles in a row.
(a) general view (b) plane view (c) side view.

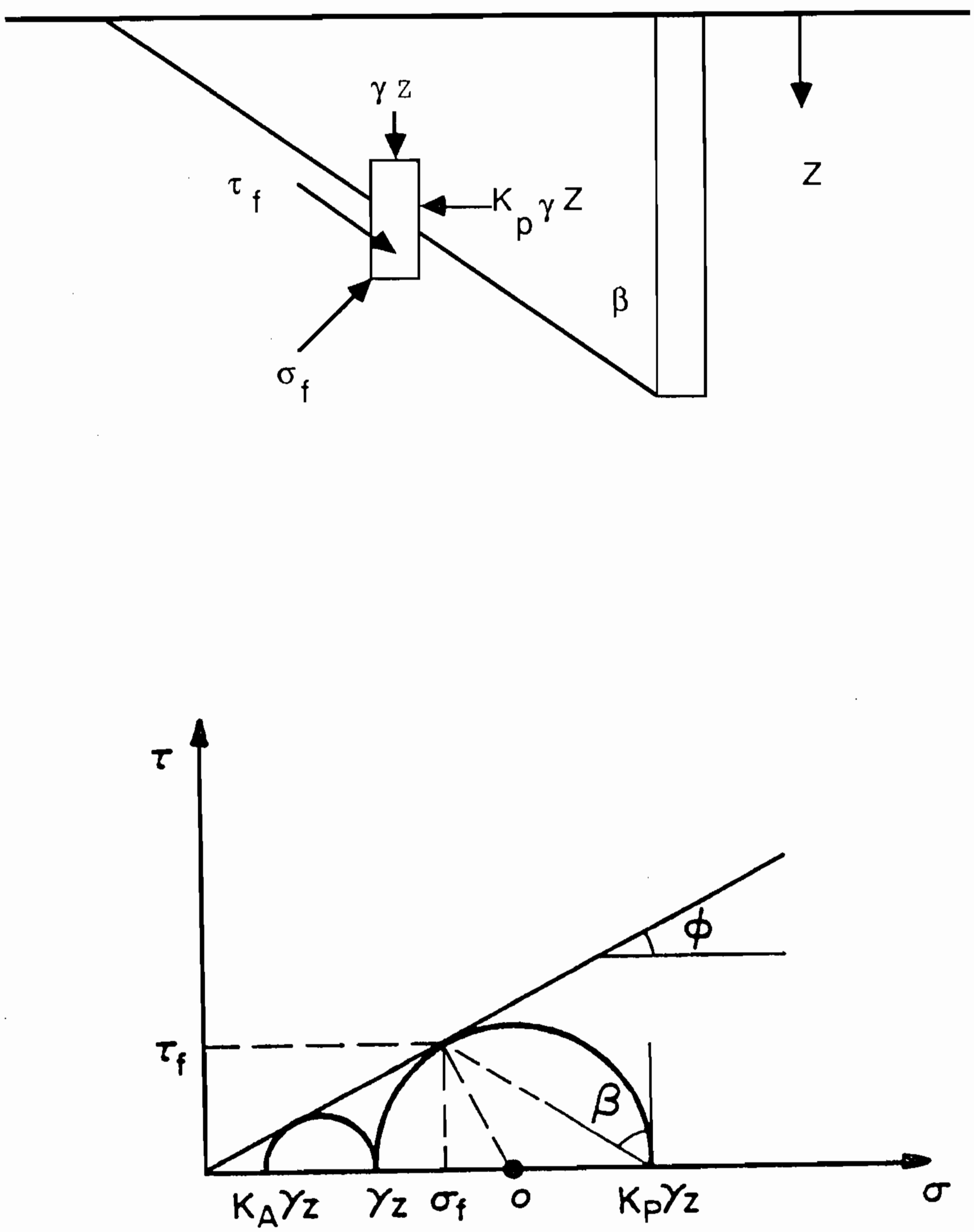

Fig. 6.9. Mohr-Coulomb diagram.

$$K_p = \tan^2 (\pi/4 + \phi/2)$$

The components of the stresses at the base of the soil wedge to resist the horizontal movement of the pile, σ_h and τ_h, are given by:

$$\sigma_h = \sigma_f \cos\beta \tag{6.7}$$

$$\tau_h = \tau_f \sin\beta \tag{6.8}$$

The average zone of failure for each pile is provided by the area of EFGHMN in Fig. 6.8. Thus, the force from the soil resisting the movement of the pile can be calculated from the following equation for the plane EFGHMN

$$F_s = \int \sigma_h \, dA + \int \tau_h \, dA \tag{6.9}$$

where the integration is carried out over the area indicated in Fig. 6.8. Substituting Eq. 6.5, 6.6, 6.7, and 6.8 into Eq. 6.9 results in:

$$\begin{aligned} F_s = & \int_{H_1}^{H} \sigma_f \cos\beta dA_1 + \int_0^{H_1} \sigma_f \cos\beta dA_2 + \int_{H_1}^{H} \tau_f \sin\beta dA_1 + \int_0^{H_1} \tau_f \sin\beta dA_2 \\ = & \int_{H_1}^{H} [\frac{1}{2} (K_p\gamma Z + \gamma Z) - \frac{1}{2} (K_p\gamma Z - \gamma Z) \sin\phi] \\ & [b + 2\tan\alpha\tan\beta (H - Z)] dZ + \int_0^{H_1} [\frac{1}{2} (K_p\gamma Z + \\ & + \gamma Z) - \frac{1}{2} (K_p\gamma Z - \gamma Z) \sin\phi] (b + S) dZ + \\ & \int_{H_1}^{H} [\frac{1}{2} (K_p\gamma Z - \gamma Z) \cos\phi] [b + 2\tan\alpha\tan\beta (H - \\ & Z)] \tan\beta dZ + \int_0^{H_1} [\frac{1}{2} (K_p\gamma Z - \gamma Z) \cos\phi\tan\beta] \\ & (b + S) dZ \end{aligned} \tag{6.10}$$

in which H_1 is equal to $H - (S/2) \cot\alpha\cot\beta$ and is indicated in Fig. 6.8. Let $K_1 = 2\tan\alpha\tan\beta$, $K_2 = K_p + 1$, $K_3 = 1-K_p$ and $K_4 = K_p-1$, then the above expression can be simplified as

$$F_s = \int_{H_1}^{H} \left(\frac{1}{2}\gamma K_2 + \frac{1}{2}\gamma K_3 \sin\phi \right) [(b + K_1 H) Z - K_1 Z^2] \, dZ$$
$$+ \int_{H_1}^{H} \frac{1}{2}\gamma K_4 \cos\phi) \tan\beta \, [(b + K_1 H) Z - K_1 Z^2] \, dZ +$$
$$\int_0^{H_1} (b + S) \left(\frac{1}{2} \gamma K_2 Z + \frac{1}{2} \gamma K_3 Z \right) dZ + \int_0^{H_1}$$
$$(b + S) \left(\frac{1}{2} K_4 \cos\phi \tan\beta \right) dZ \qquad (6.11)$$

Integrating each term and combining together, the force from the plane EFGHMN is

$$F_s = [(1/2) \gamma b (H^2 - H_1^2) + (1/6) \gamma K_1 (H^3 - H_1^3) -$$
$$(1/2) \gamma K_1 H_1^2 (H - H_1) + (1/2) \gamma (b + S) H_1^2]$$
$$[(1/2) K_p (1 - \sin\phi + \cos\phi \tan\beta) + (1/2)$$
$$(1 + \sin\phi - \cos\phi \tan\beta)] \qquad (6.12)$$

The angle β is generally taken as $45^o+\phi/2$, then $-\sin\phi+\cos\phi\tan\beta = 1.0$. Thus, Eq. 6.12 can be further simplified as

$$F_s = (1/2) \gamma K_p b (H^2 - H_1^2) + (1/6) \gamma K_p K_1 (H^3 - H_1^3)$$
$$- (1/4) \gamma K_p K_1 H_1^2 (S \cot\alpha \cot\beta) + (1/2) \gamma K_p H_1^2$$
$$(b + S) \qquad (6.13)$$

The forces on the plane EDAG and FCBH now need to be considered. Plan and elevation views of the side of the wedge are shown in Fig. 6.8. The vertical stress is given by γz and the horizontal stress is given by $K_o\gamma z$, where K_o is a coefficient of lateral earth pressure corresponding to the earth pressure at rest. The failure stresses are given by

$$\sigma_f = K_o \gamma Z \qquad (6.14)$$
$$\tau_f = K_o \gamma Z \tan\phi \qquad (6.15)$$

It can be seen in Fig.6.6 that the stresses resisting the horizontal component of the soil movement in the wedge are:

$$\sigma_h = -\sigma_f \sin\alpha \tag{6.16}$$

$$\tau_h = \tau_f \cos\alpha \tag{6.17}$$

The sum of the horizontal forces on the side planes can now be determined from

$$F_h = 2\int_0^H \sigma_h \, dA + 2\int_0^H \tau_h \, dA \tag{6.18}$$

Substituting values from Eqs. 6.14, 6.15, 6.16, and 6.17 into Eq. 6.18 results in

$$F_h = 2\int_{H_1}^{H} - K_o\gamma Z\sin\alpha \, dA_1 + 2\int_0^{H_1} - K_o\gamma Z\sin\alpha \, dA_2 + 2\int_{H_1}^{H} K_o\gamma Z\tan\phi\cos\alpha \, dA_1 + 2\int_0^{H_1} K_o\gamma Z\tan\phi\cos\alpha \, dA_2 \tag{6.19}$$

Integrating and simplifying results in

$$F_h = (1/3)\,\gamma K_o\tan\beta\,(\tan\phi - \tan\alpha)\,[\,H^3 - (3HH_1^2 - 2H_1^3)\,] + (1/2)\,\gamma K_o S\,(\tan\phi\cot\alpha - 1)\,H_1^2 \tag{6.20}$$

The active forces behind the piles can be established by

$$F_a = (1/2)\,K_a\gamma b H^2 \tag{6.21}$$

where $K_a = \tan^2(45^\circ - \phi/2)$. Finally, the ultimate resistance of the soil can now be calculated from

$$F_p = F_s + F_h - F_a \tag{6.22}$$

Appropriate expressions from Eqs. 6.13, 6.20 and 6.21 are combined to result in Eq. 6.23

$$F_p = (1/2)\,K_p\gamma b\,(H^2 - H_1^2) + (1/6)\,K_pK_1\gamma\,(H^3 - H_1^3) - (1/4)\,K_pK_1\gamma\,(S\cot\alpha\cot\beta)\,H_1^2 + (1/2)\,K_p\gamma\,(b + S)\,H_1^2 + (1/3)\,K_o\gamma\tan\beta\,(\tan\phi - \tan\alpha)$$

$$(H^3 - 3HH_1^2 + 2H_1^3) + (1/2) K_o\gamma S (\tan\phi\cot\alpha - 1)$$

$$H_1^2 - (1/2) K_a\gamma bH^2 \qquad (6.23)$$

Differentiating Eq. 6.23 with respect to depth, the ultimate soil resistance per unit length of each pile can be found

$$P_u = K_p\gamma b (H - H_1) + (1/2) K_pK_1\gamma (H^2 - H_1^2)$$

$$- (1/2)K_pK_1\gamma S H_1\cot\alpha\cot\beta + K_p\gamma H_1 (b + S) + K_o\gamma\tan\beta$$

$$(\tan\phi - \tan\alpha)(H- H_1)^2 + K_o\gamma SH_1 (\tan\phi\cot\alpha - 1) -$$

$$K_a\gamma bH \qquad (6.24)$$

The ultimate resistance of a single pile is

$$P_u = K_p\gamma bH + (1/2) K_pK_1\gamma H^2 + K_o\gamma\tan\beta (\tan\phi - \tan\alpha) H^2$$

$$- K_a\gamma bH \qquad (6.25)$$

A variable representing the spacing between piles was introduced in the above equation. The variation of the soil resistance versus the pile spacing for a typical example is shown in Fig. 6.10. As may be seen, the soil resistance for zero pile spacing is about one-half that for a single pile. Two features are shown in this expression. The first one is that if the piles contact each other, the ultimate resistance from Eq. 6.24 is equal to the value of the Rankine passive earth-pressure minus the active earth-pressure on a continuous retaining wall. The second feature in this equation is that there is no shadowing-effect if the spacing, S, between piles is larger than $2H\tan\alpha\tan\beta$ where H, α, β are defined as before.

It is apparent that Eq. 6.25 for a single pile should be employed in the computation when pile spacing is larger than the value suggested above.

Ultimate soil resistance in cohesive soil (ϕ=0). The soil model for computing the ultimate resistance on a single pile for wedge-type failure in clay was derived by Reese in 1958.

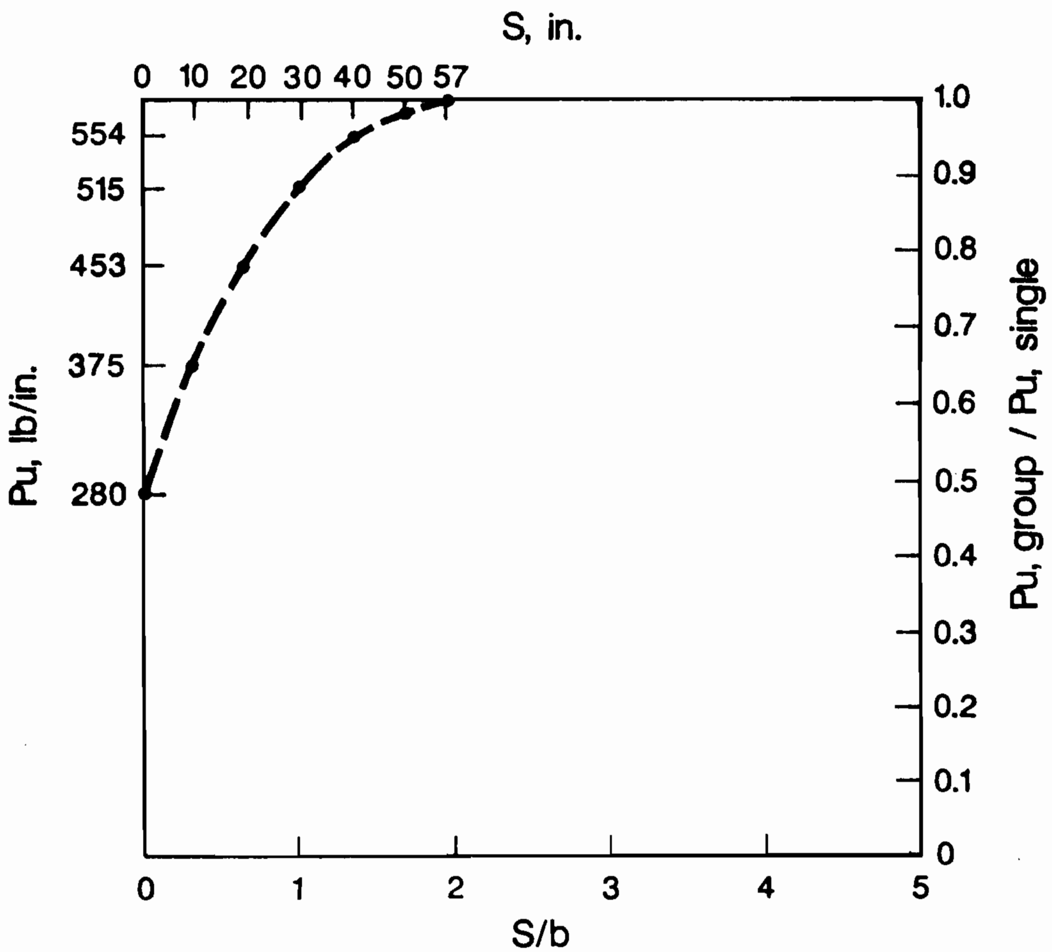

Fig. 6.10. Example study of ultimate soil resistance in sand (diameter = 30 in.).

Figure 6.11 shows a free body of a wedge at failure for a single pile in a clay deposit. The forces acting on the wedge are determined as follows: F_1 is the body force; F_2 is the shear force on plane ABEF; F_6 is the normal force on plane ABEF; F_3 is the shear force on plane ACE; F_4 is the shear force on plane BDF; F_5 is the shear force on plane CDFE; and F_7 is the normal force on plane CDFE. There are normal forces acting on plane ACE and BDF, but they are assumed to have no effect in this problem. The wedge is assumed to move along plane ABFE, and the shear forces act in a direction opposite to the movement.

It is assumed that the full shear strength, c, of the soil is developed on planes ACE, BDF, and ABFE, and that only a part of the shear resistance, Kc, is developed on plane CDFE. Based on these assumptions, the following equations can be written for the forces:

$$F_1 = 0.5\gamma bH^2\tan\theta,$$
$$F_2 = cbH\sec\theta,$$
$$F_3 = 0.5cH^2\tan\theta,$$
$$F_4 = 0.5cH^2\tan\theta, \text{and,}$$
$$F_5 = KcbH.$$

Summing forces in the vertical direction yields:

$$F_6 = 0.5\gamma bH^2\sec\theta + KcbH\csc\theta + cbH\csc\theta + ch^2$$

Summing the forces in the horizontal direction yields:

$$F_7 = (1/2)\gamma bH^2 + KcbH\cot\theta + cbH\,(\cot\theta+\tan\theta) + cH^2(\sin\theta\,\tan\theta + \cos\theta)$$

The soil resistance against a single pile can be obtained by taking the derivative of F_7 with respect to depth. Thus,

$$P_u = \gamma bH + Kcb\cot\theta + cb(\cot\theta+\tan\theta) + 2cH(\sin\theta\,\tan\theta + \cos\theta) \qquad (6.26)$$

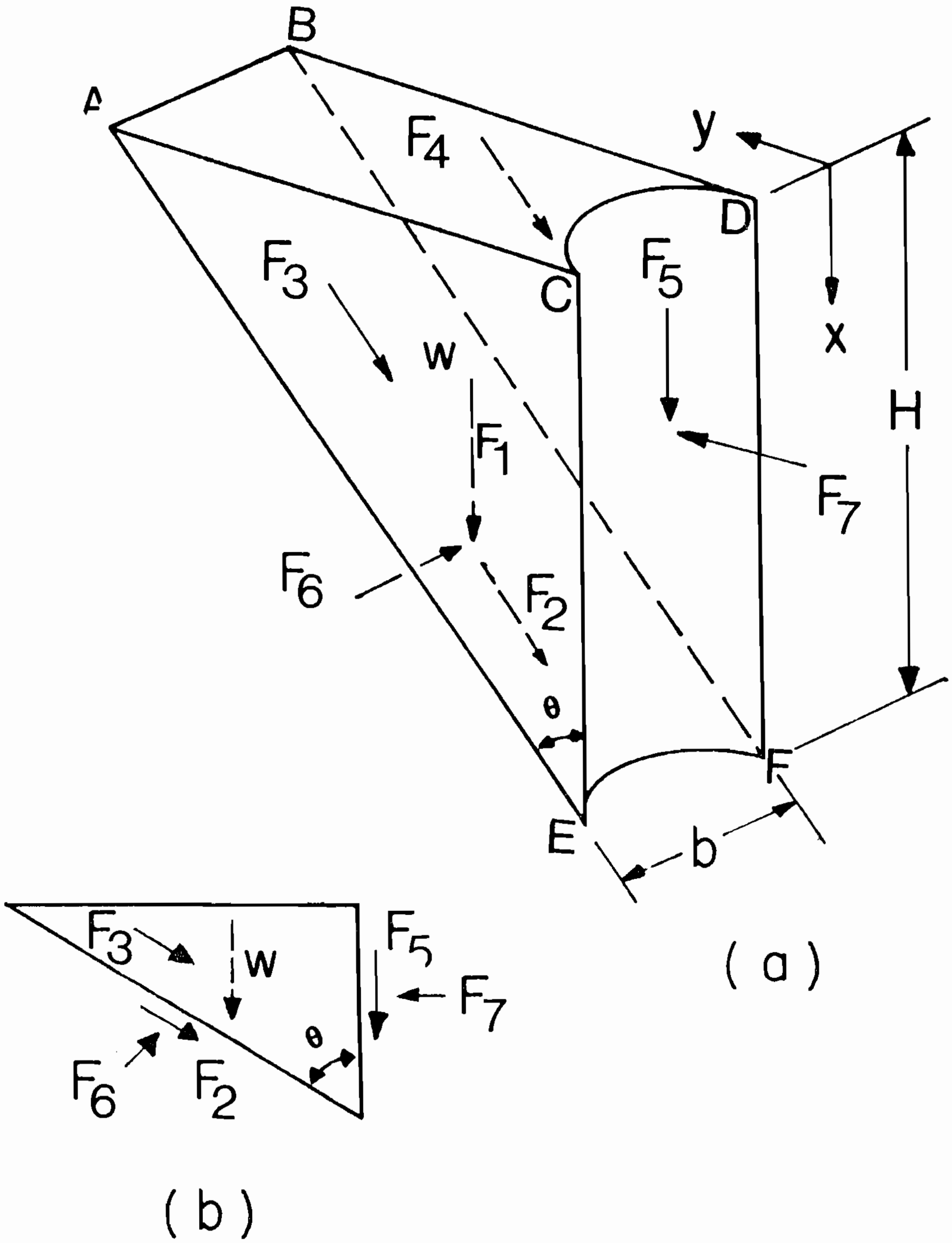

Fig. 6.11. Assumed passive wedge-type failure for clay. (a) shape of wedge (b) forces acting on wedge (after Reese, 1958).

If the value of θ is assumed to be 45° and K is assumed to be zero, then

$$P_u = 2cb + \gamma bH + 2.83cH \quad (6.27)$$

When piles are in a row, the development of the side shears F_3 and F_4 for each pile depend on the resistance offered by the interval zone BDFIGH between two piles (Fig. 6.12). If the spacing is large enough for the block BDFIGH to resist the shear forces developed on each side of this block due to the deformation of the soil block in front of each pile, the soil resistance can be obtained as a single pile without the consideration of interference. But if the resistance from zone BDFIGH is less than the shear forces from F_3 and F_4, the soil block BDFIGH will move together with the nearby block as a whole and the shear-failure planes on each side of the blocks will no longer exist.

The mechanism of failure has been verified by laboratory experiments that will be discussed in detail in Chapter 7. Generally, two kinds of failure have been observed in the laboratory tests. For piles with a large spacing, say 2 diameters, the soil in front of piles deformed individually without any shadowing-effect as shown in Fig. 6.13. However, when pile spacing decreased to one-fourth of the pile diameter, the soils in front of piles move together and there is a separation between the front soil and the back soil adjacent to piles. This phenomenon supports the previous considerations.

Obviously, the resisting force from zone BDFIGH has three components, the body force F_1 from zone BDFIGH, the shear force F_2 on plane BGIF, and the resistant force on plane DHIF. Therefore, based on the previous assumptions made for a single pile, the following results for piles in a row are obtained:

If $\quad F_{3,ACE} + F_{4,BDF} < F_{1,BGIF} + F_{2,BGIF} + F_{5,DHIF}$

$$(\text{e.g. } cH^2 < (\sqrt{2}/4)\,\gamma SH^2 + \sqrt{2}\,cSH + (\sqrt{2}/2)\,cSH$$

then

$$P_u = 2cb + \gamma bH + 2.83cH \quad (6.28)$$

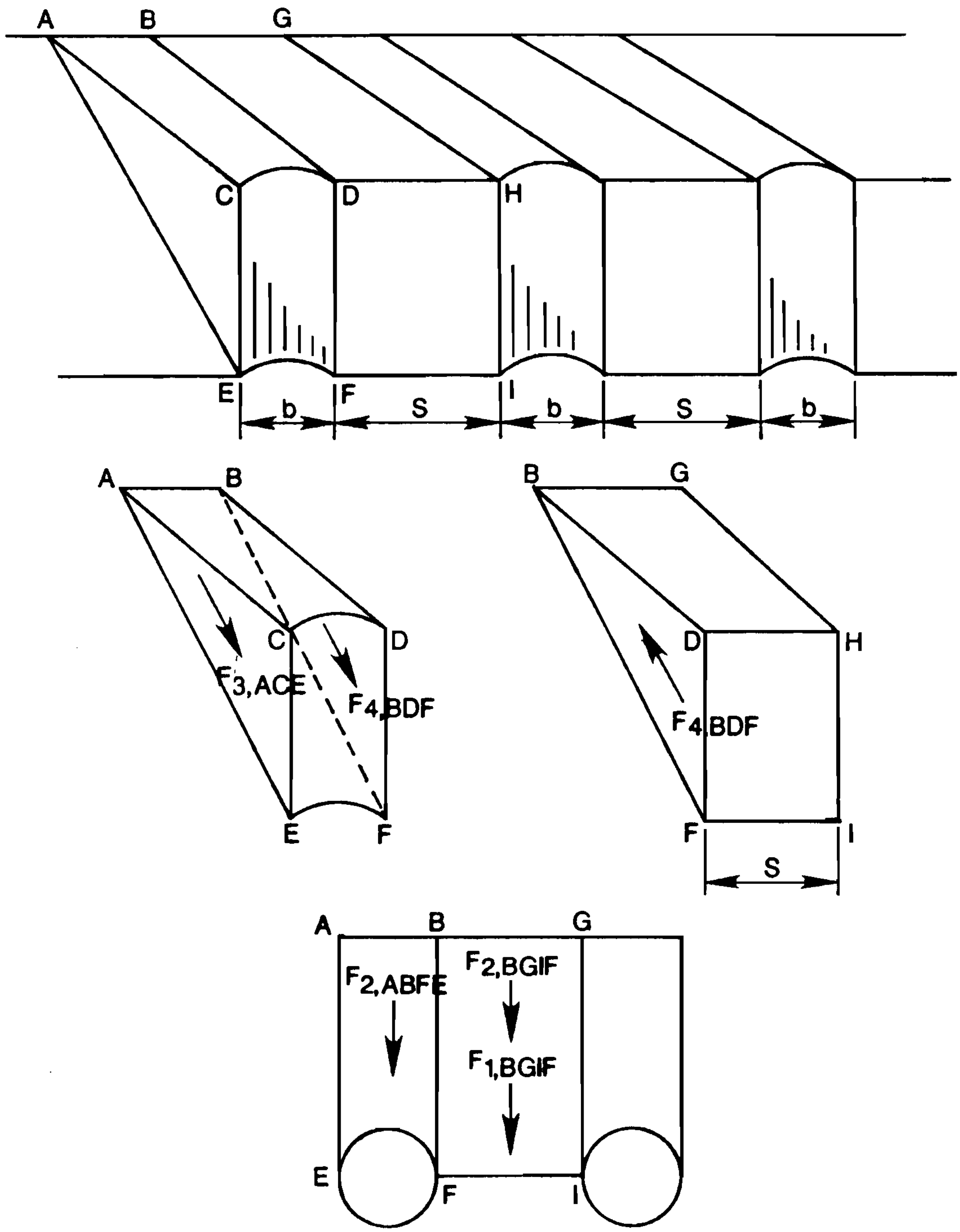

Fig. 6.12. Passive wedge failure in clay for piles in a row.

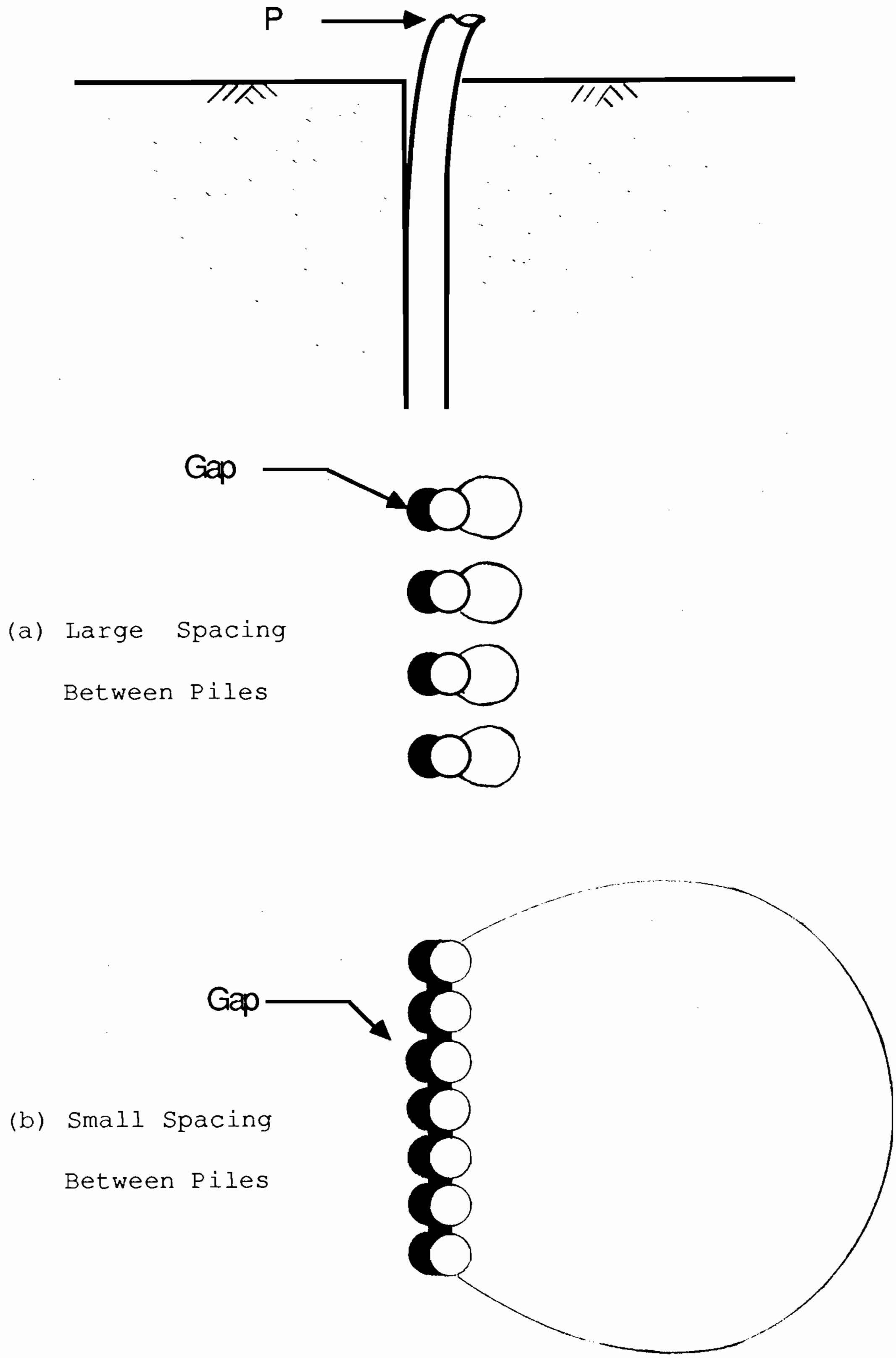

Fig. 6.13. Soil deformation and gaps observed in the experimental study.

If $F_{3,ACE} + F_{4,BDF} > F_{1,BGIF} + F_{2,BGIF}$

then

$$P_u = 2c\ (b+S) + \gamma\ (b + S)\ H + cS \qquad (6.29)$$

The critical spacing which changes the single-pile behavior to group pile behavior is determined from the following expressions:

$$S_{cr} = \frac{2.828cH}{\gamma H + 6c} \qquad (6.30)$$

or

$$\frac{S_{cr}}{H} = \frac{\frac{2.828c}{\gamma H}}{\frac{6c}{\gamma H} + 1}$$

A plot of S_{cr}/H versus $c/\gamma H$ (see Fig. 6.14) becomes asymptotic to 0.471 and the critical spacing is a function of the ratio of $c/\gamma H$.

If the spacing is zero and the pile diameter is taken as unitity, Eq. 6.29 has the following form.

$$P_u = 2c + \gamma H \qquad (6.31)$$

It is not surprising that Eq. 6.31 is the passive earth-pressure on a continuous wall embedded in cohesive soil with $\phi = 0$. Active earth pressures are ignored in the analyses presented herein, because, for the relatively shallow depths of interest, active earth pressures in cohesive soils are usually negative. Thus, it seems reasonable to neglect these forces due to tensile failure and separation of the pile from the soil in the area of interest. The total resistance force P_u on a pile with different spacing for a typical case is presented in Fig. 6.15. Again, the P_u at zero spacing is approximately equal to one-half that for a single pile.

Flow-Around Failure

Single pile reaction. A plan view of soil movement near a single pile at several diameters below the ground surface is shown in Fig. 6.16. The potential failure surfaces that are shown are

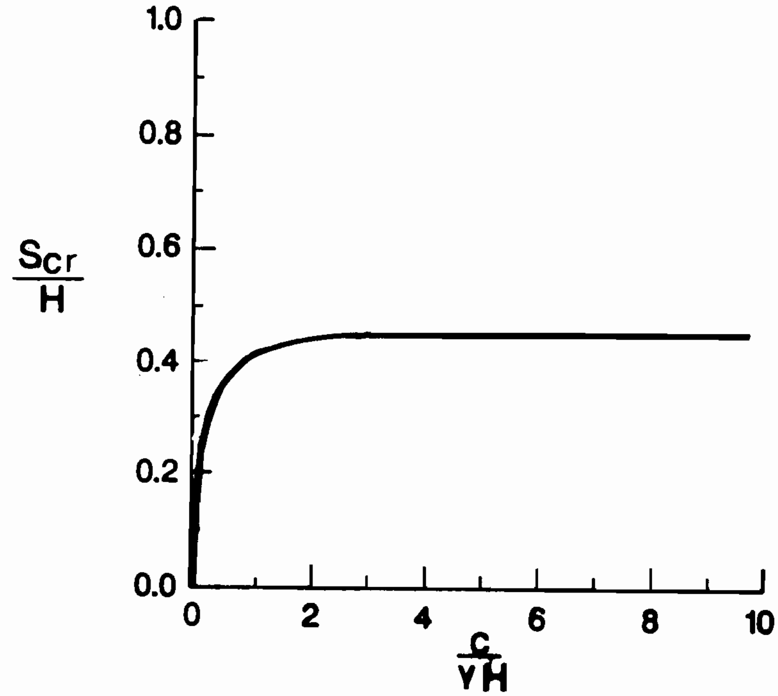

Fig. 6.14. A plot of S_{cr}/H versus $c/\gamma H$.

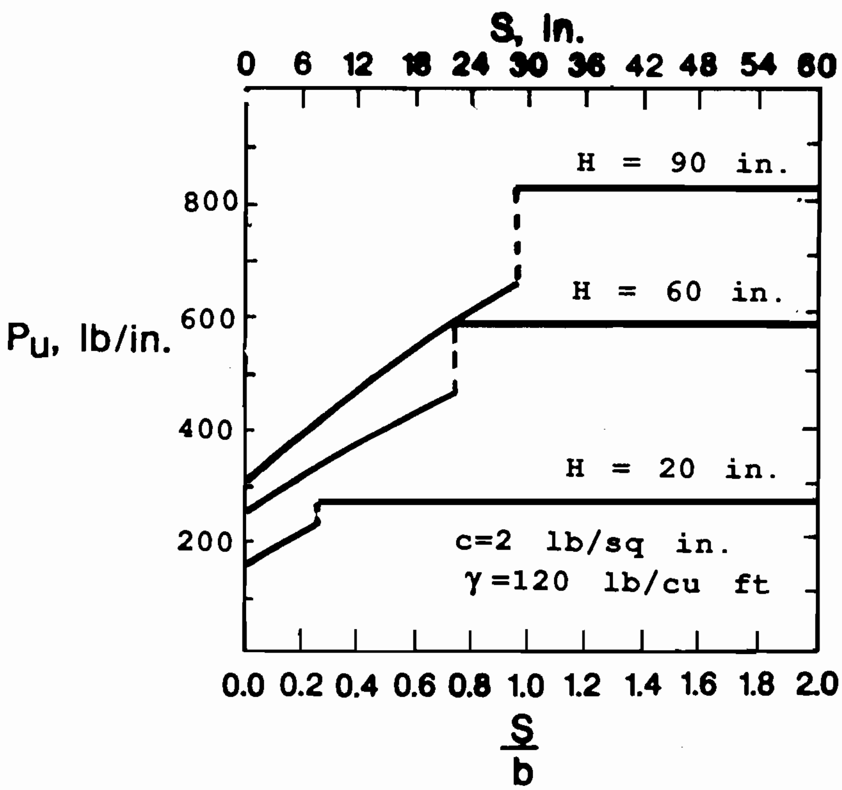

Fig. 6.15. Example study of ultimate soil resistance in clay (diameter = 30 in.).

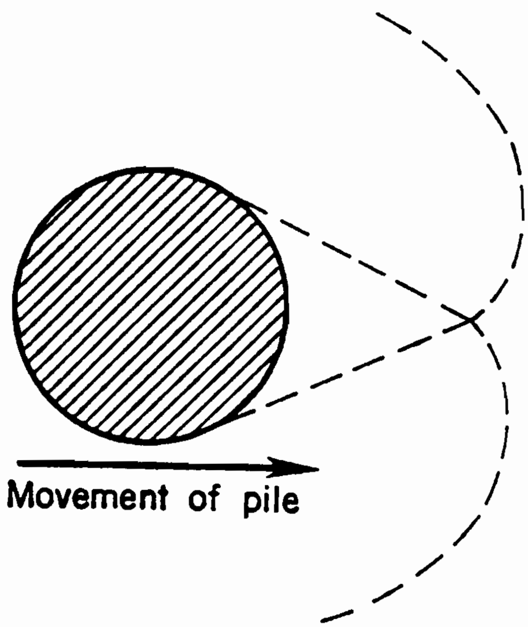

Fig. 6.16. Potential failure surfaces generated by pile at several diameters below ground surface (after Reese, 1984).

indicative of plane-strain failure. While the ultimate resistance can not be determined precisely, elementary concepts are used to develop approximate expressions for current p-y criteria. The concepts of the block soil-model proposed by Reese (1958) in studying the flow-around failure in clay are illustrated in Fig. 6.17. If it is assumed that blocks 1,2,4 and 5 fail by shear and that block 3 develops resistance by sliding; the stress conditions are represented by Fig. 6.17b. By examining a free body of a section of the pile, Fig. 6.17c, one can conclude that

$$P_u = 11cb \qquad (6.32)$$

In p-y criteria, the soil model for computing the ultimate resistance in sand at some distance below the ground surface is shown in Fig. 6.18. The stress σ_1 at the back of the pile must be equal to or larger than the minimum active earth pressure; if not, the soil could fail by slumping. This assumption is based on two-dimensional behavior and is subjected to some uncertainty. However, this assumption should be adequate for present purposes. Assuming the states of stresses shown in Fig. 6.18b, the ultimate soil resistance for horizontal flow around the pile is:

$$p_u = K_a \gamma bH\ (\tan^8\beta - 1\ ) + K_o \gamma bH \tan\phi \tan^4\beta \qquad (6.33)$$

Equations 6.32 and 6.33 are approximate, but they serve a useful purpose in indicating the form, if not the magnitude of the ultimate soil resistance.

Plastic-deformation model for piles in a row. Ito et al (1975) developed a method to estimate the ultimate lateral force acting on a row of piles that are utilized to prevent the failure of an earth slope. The fundamental consideration of soil deformation in this method is restricted to the plane-strain condition. The resistance was obtained from the movement of the soil mass against the piles, as shown in Fig. 6.19. Two sliding surfaces are assumed to occur along the lines AEB and A'E'B', in which the lines EB and E'B' make an angle $(\pi/4+\phi/2\ )$ with the x-axis. The soil becomes plastic only in zone AEBA'E'B', where the Mohr-Coulomb yield criterion is applied. The ultimate resisting

(a)

(b)

(c)

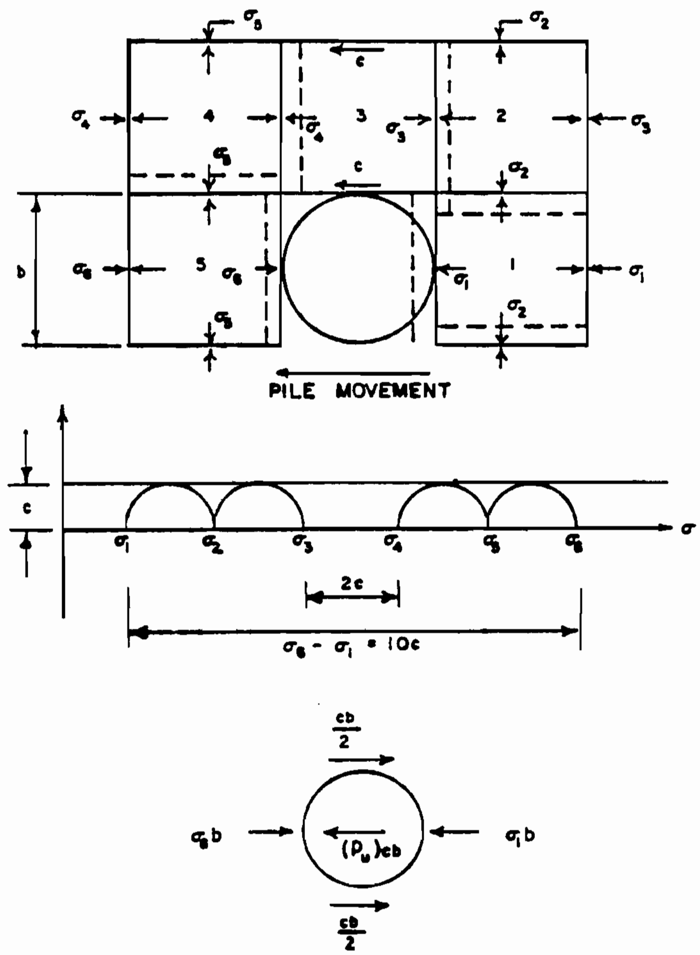

Fig. 6.17. Assumed lateral flow-around type of failure for clay. (a) Section through Pile (b) Mohr-Coulomb diagram (c) Forces acting on Pile (after Reese, 1984).

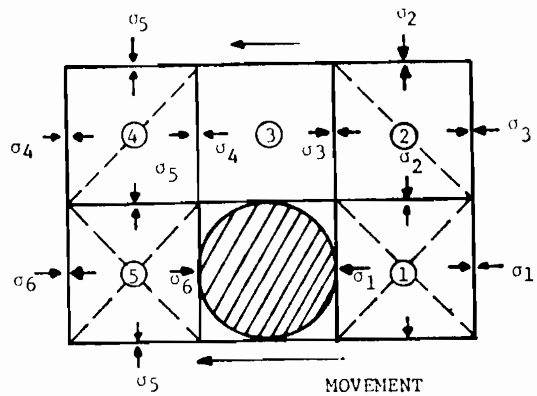

(a)

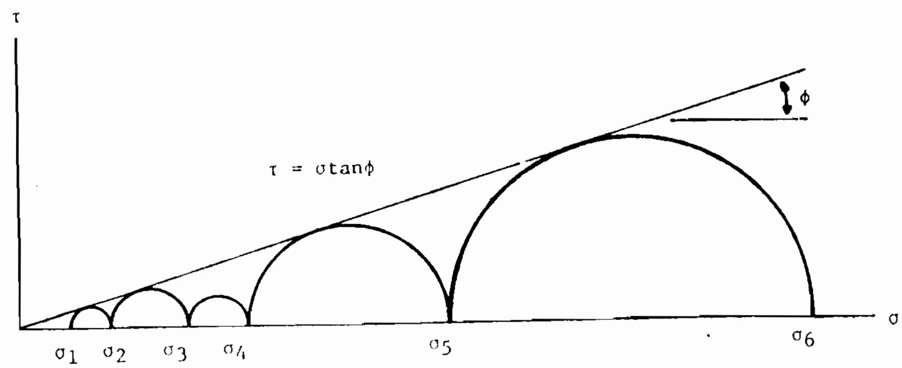

(b)

Fig. 6.18. Assumed mode of soil failure by lateral flow around the pile. (a) section through the pile (b) Mohr-Coulomb diagram representing states of stress of soil flowing around a pile.

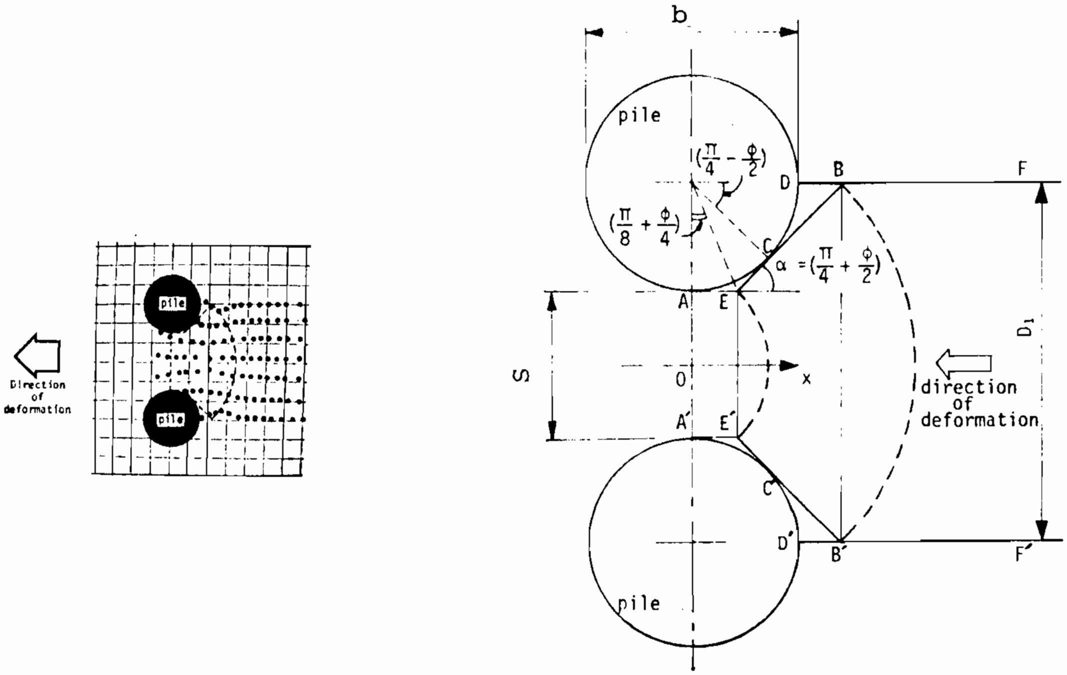

Fig. 6.19. Equilibrium state of soil between two closely-spaced piles (after Ito et al, 1975).

force is obtained by integrating the failure shear stresses along the sliding surfaces. Ito et al have made several crude assumptions to simplify the complicated state of stresses in the medium. The integration is carried out by beginning with the small element in zone EBB'E and then extending to zone AEE'A. A complex formula has been derived by Ito et al as shown in Eq. 6.34. The detailed derivation can be found from the cited reference.

$$P_z = cD_1 \left(\frac{D_1}{S}\right)^G \left[\frac{1}{N_\phi \tan\phi}\left(EXP(C_1) - 2N_\phi^{1/2}\tan\phi - 1\right) + \frac{C_2}{G}\right] - c\left[D_1 \frac{C_2}{G} - 2SN_\phi^{-1/2}\right] + \frac{\gamma Z}{N_\phi}\left[D_1 \left(\frac{D_1}{S}\right)^G EXP(C_1) - S\right] \qquad (6.34)$$

where

$G = N_\phi^{1/2}\tan\phi + N_\phi - 1$,

$C_1 = N_\phi \tan\phi \tan(\pi/8 + \phi/4)$,

$C_2 = 2\tan\phi + 2N_\phi^{1/2} + N_\phi^{-1/2}$,

$N_\phi = \tan(\pi/4 + \phi/4)$,

D_1 = center to center interval between piles in a row,

S = clear interval between piles,

c = cohesion of soil,

Φ = frictional angle of soil,

γ = unit weight of soil, and

Z = an arbitrary depth from the ground surface.

To verify these equations, Ito et al conducted a series of laboratory experiments. In their experimental model, the soil was forced to move against the piles that were fixed in position for a given spacing. The measured results are presented in Fig. 6.20. According to the comparison between the measured and predicted values, the value computed from Eq. 6.34 did not agree with the measured ultimate force acting on the piles. Generally, the computed P_z is only about 60% of the measured ultimate force.

Ito et al explained that the soil is not a rigid-perfectly plastic material and the discrepancy may result from some improper

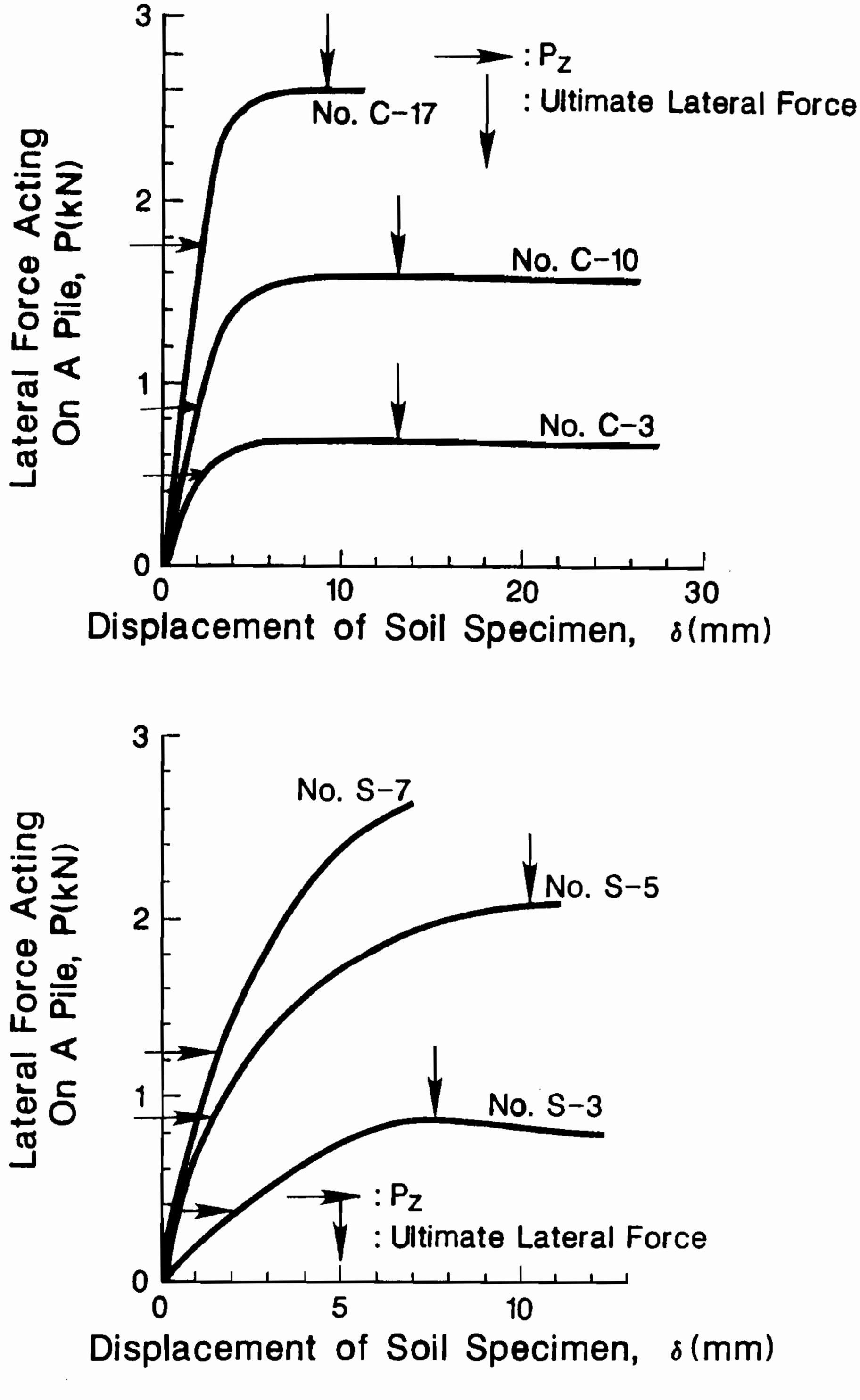

Fig. 6.20. Relation between lateral force acting on a pile and soil movement (after Ito et al, 1982).

assumptions made in the analysis. They believed that Pz probably represents a state of stress where soils begin to yield. At yield, Pz is only about 60% of the ultimate resistance. Therefore, a modification factor 1.6 needs to be introduced in Eq. 6.34 to compute the ultimate soil resistance.

$$P_u = 1.6 \times P_z$$

where

P_z = soil resistance at yield

P_u = ultimate soil resistance

The predicted results from Ito et al's formula for various spacings have been plotted in Fig. 6.21 and Fig. 6.22 In each figure, the ultimate soil resistance of a single pile from p-y criteria is indicated by a horizontal line. When S is large (for a single pile), the results from Ito's predictions are much less than those from p-y criteria. It is understandable that the rupture surfaces for widely spaced piles correspond to the effect of individual piles against soil. Ito's plastic deformation model can only represent the possible failure conditions for closely spaced piles, in which the individual effects are overshadowed by group action.

On the other hand, if the interspace between the piles becomes zero the forces on piles become infinite using Ito's equation. It is obvious that this result does not correspond to a real situation in a three-dimensional medium.

Discussion of results from slip-line theory. Ito et al made several crude assumptions to simplify the states-of-stress in the plastic-failure region. However, the theory of the plastic flow of rigid, perfectly-plastic materials under plane-strain conditions is well established in the technical literature (Sokolovskii, 1950; Hill, 1954). The state of stress conditions at failure can be solved using the theory of slip lines. The extrusion of metal in the forming process is similar to the problems discussed here and the slip-line theory has been successfully applied in that area for more than 20 years. A brief

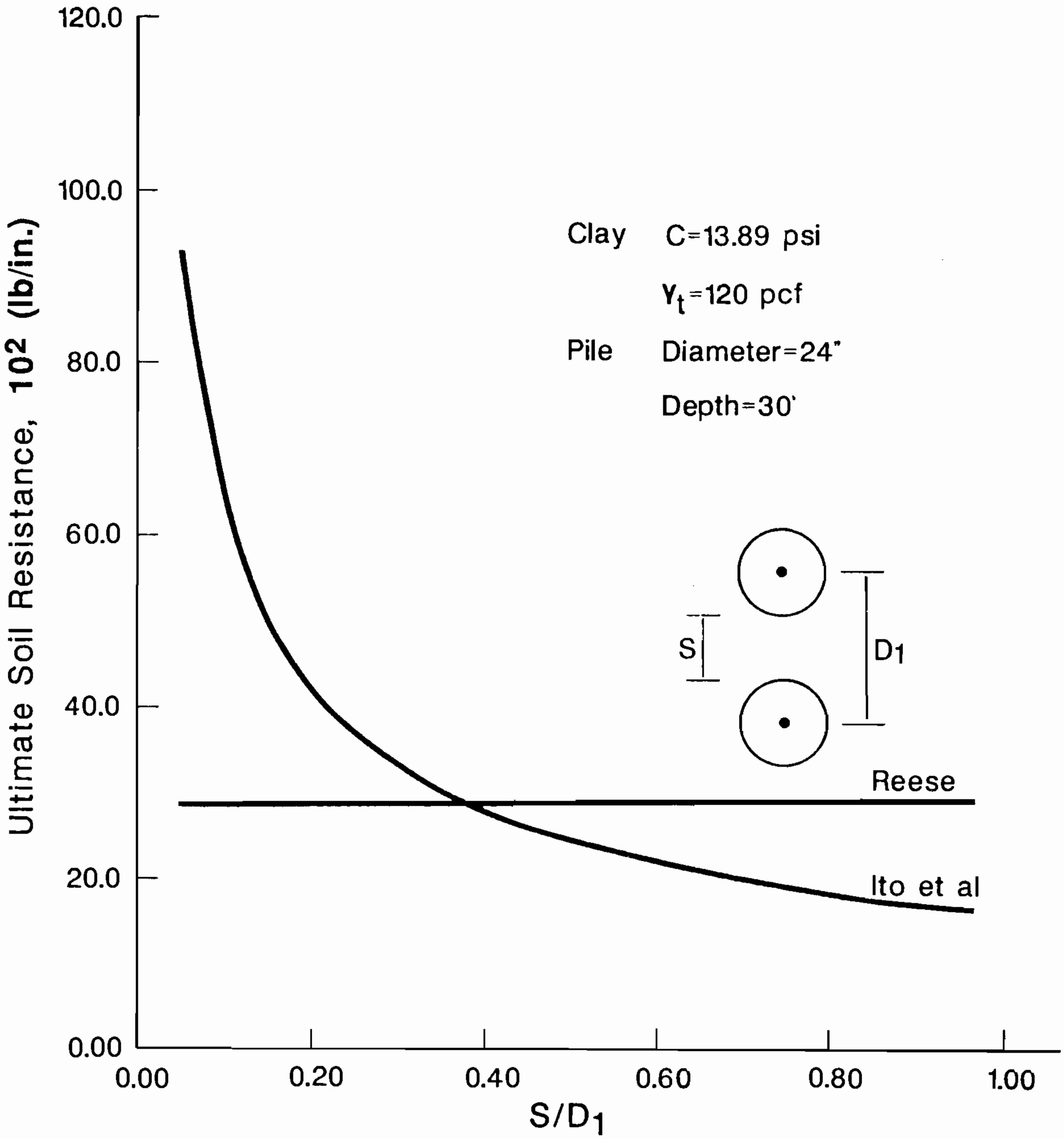

Fig. 6.21. Comparison of ultimate soil resistances from Ito et al's equation and Reese's equation in clay.

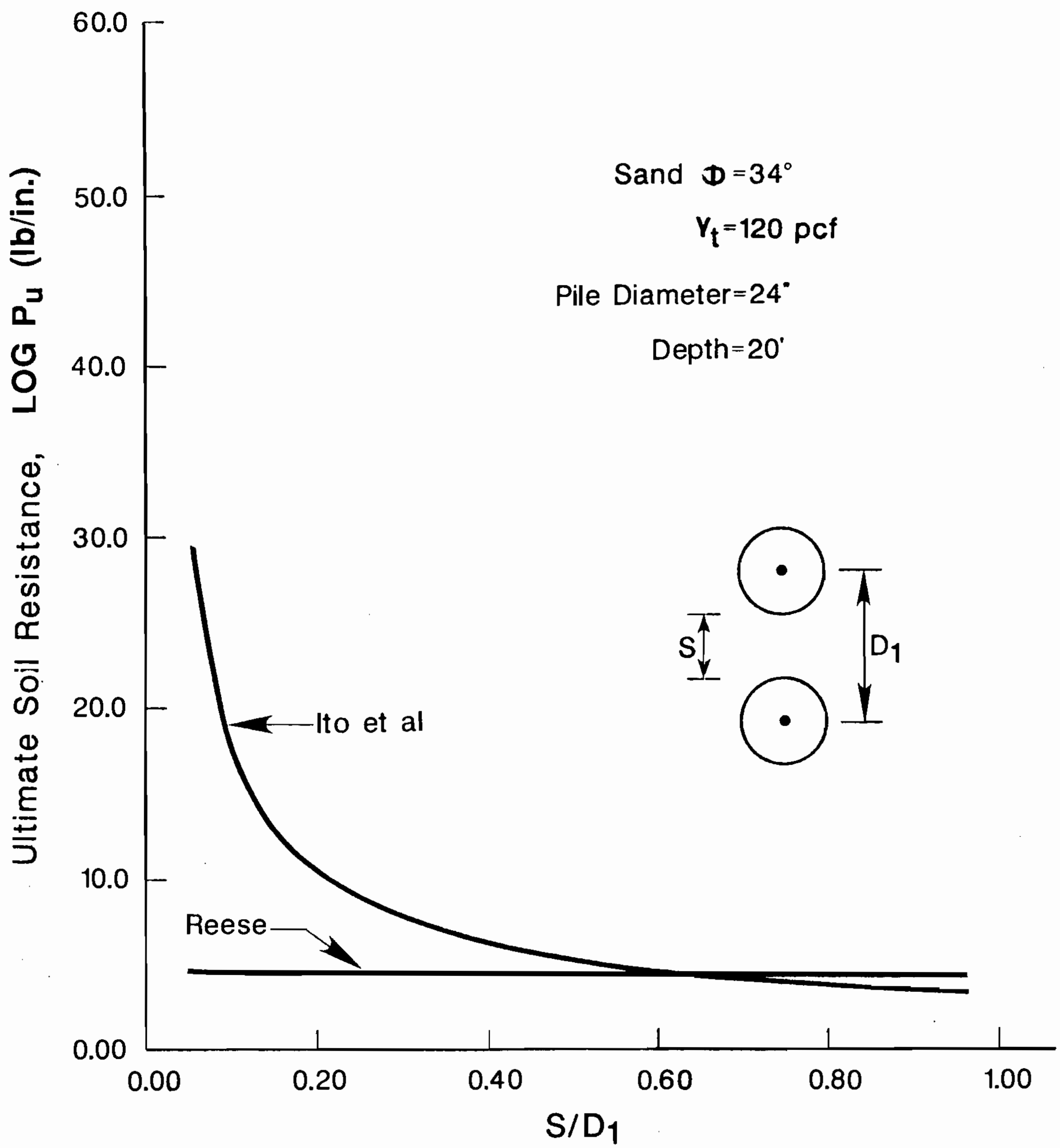

Fig. 6.22. Comparison of ultimate soil resistances from Ito et al's equation and Reese's equation in sand.

discussion of this theory from the viewpoints of soil mechanics will be presented in Appendix B.

Broms (1964) made the first presentation of the ultimate soil resistance computed from the slip-line theory for the plain strain condition, as shown in Fig. 6.23. The results from Broms' paper have been verified to be correct in the course of this study. Based on the early thinking of Broms', the study reported herein has been extended to the computation of the ultimate soil resistance for piles in a row.

If the pile section is assumed to be square for simplicity, the clear spacing between two piles should be larger than 1.414D to avoid the interference of plastic deformations from one pile to the next as shown in Fig. 6.24a. Once the pile spacing becomes less than this value, the failure regions of individual piles will converge (Fig. 6.24b). This phenomenon is very similar to the piercing problem with a flat die that was studied by Hill (1954) and Johnson (1982). The surface of the wall of the plate was assumed to be smooth and the slip-line field, as well as the die pressure versus the reduction of the width of piercing area, are shown in Fig. 6.25. Broms (1983) believed resistance increased as the spacing between piles decreased and presented a simple equation to compute the soil resistance (Fig. 6.26).

$$P_u = 5.14c + \frac{2\alpha c D_1}{S} + \sigma_h \tag{6.35}$$

where

c = undrained shear strength,

S = clear spacing between piles,

D_1 = center to center spacing,

σ_h = earth pressure acting on the line AA',

α = friction coefficient.

Randolph and Houlsby (1984) presented an exact analytical solution for the flow of cohesive soil (ϕ=0) around a circular pile. If friction, f_s, at the pile-soil interface is allowed and the friction is assumed to be less than or equal to the shear strength of soil, then the ultimate soil resistance per unit length of pile is given by

SLIP FIELD PATTERN	SURFACE	ULTIMATE LATERAL RESISTANCE, q_{ult}/c
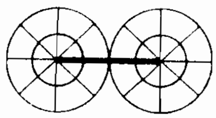	ROUGH	12.56
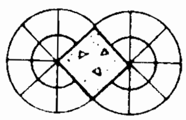	ROUGH	11.42
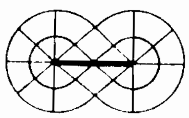	SMOOTH	11.42
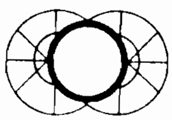	SMOOTH	9.14
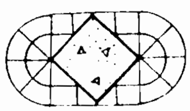	SMOOTH	8.28

Fig. 6.23. Ultimate lateral resistance from slip-line theory (after Broms, 1964).

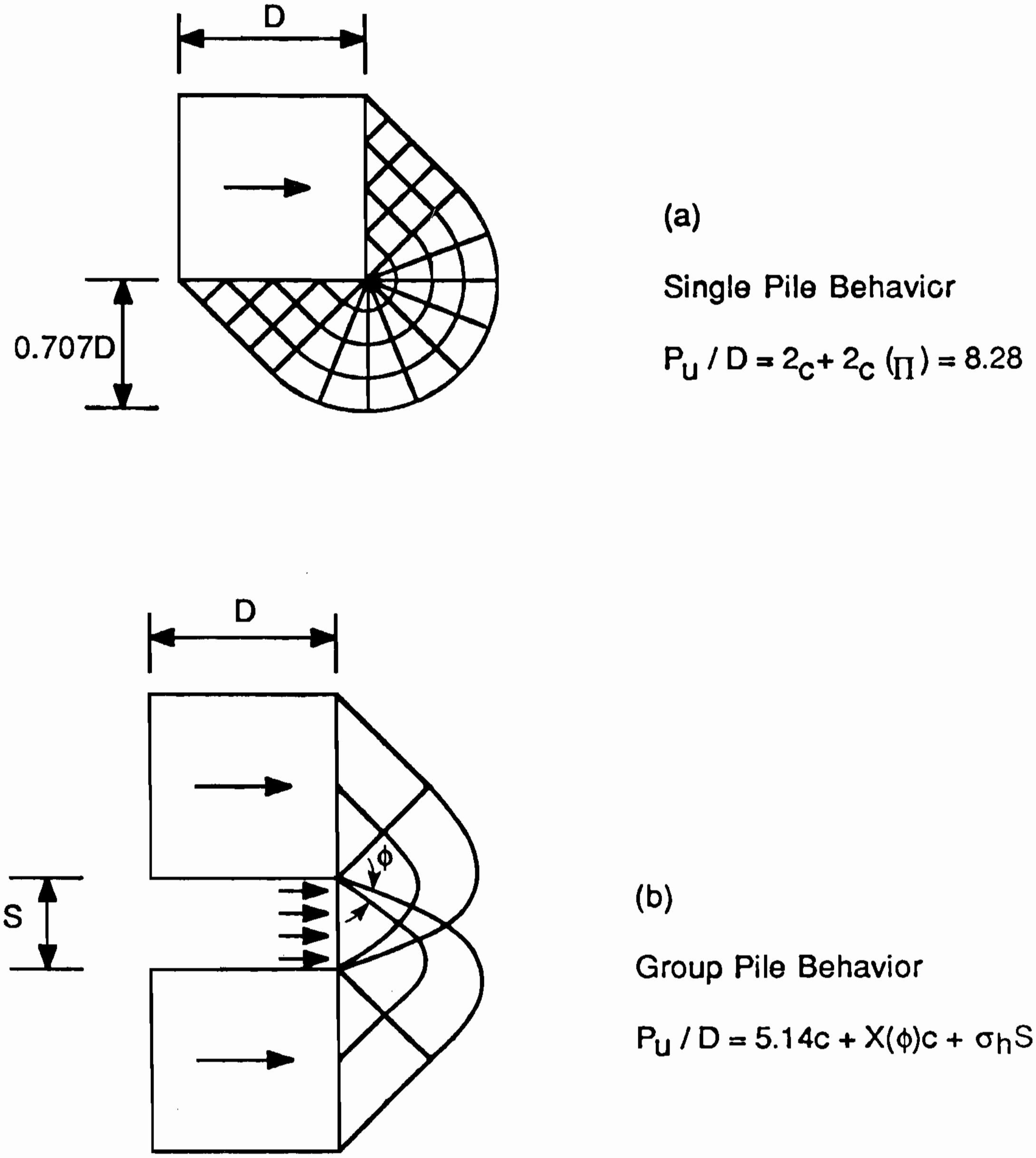

Fig. 6.24. Slip-line field for square-section piles.

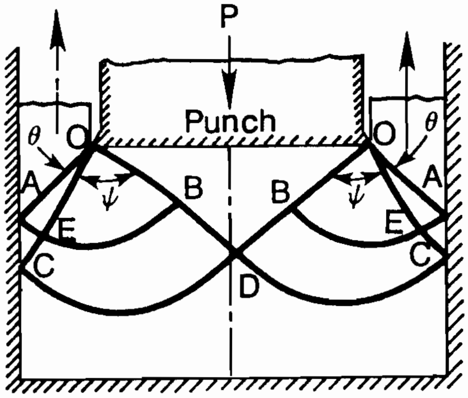

Symmetrical piercing
reduction > 50%.

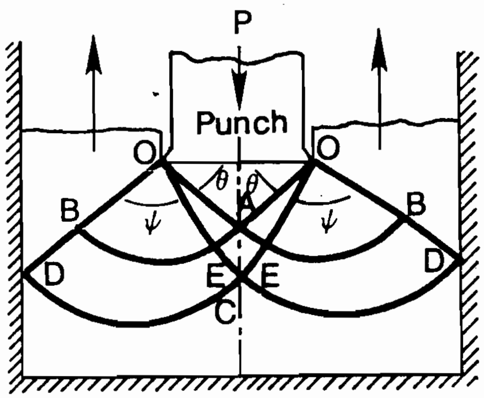

Symmetrical piercing
reduction < 50%

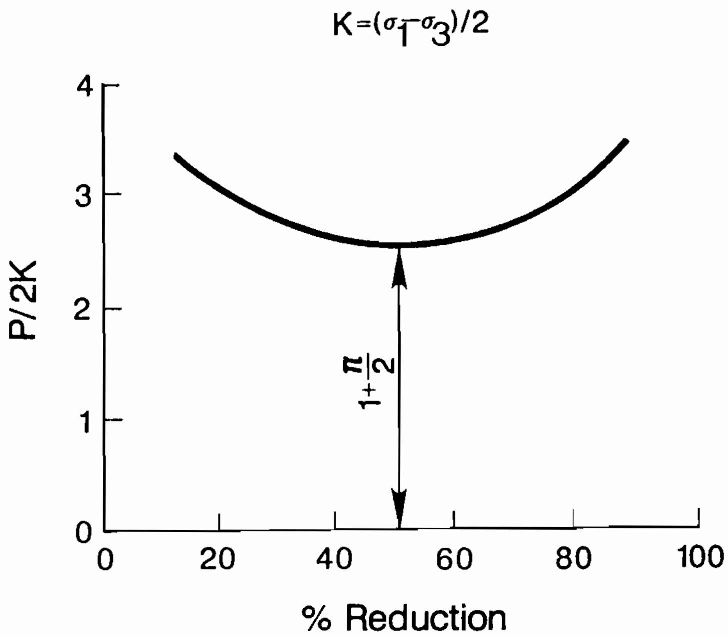

Fig. 6.25. Relation between die-pressure and reduction in thickness in piercing (after Hill, 1954; Johnson, 1982).

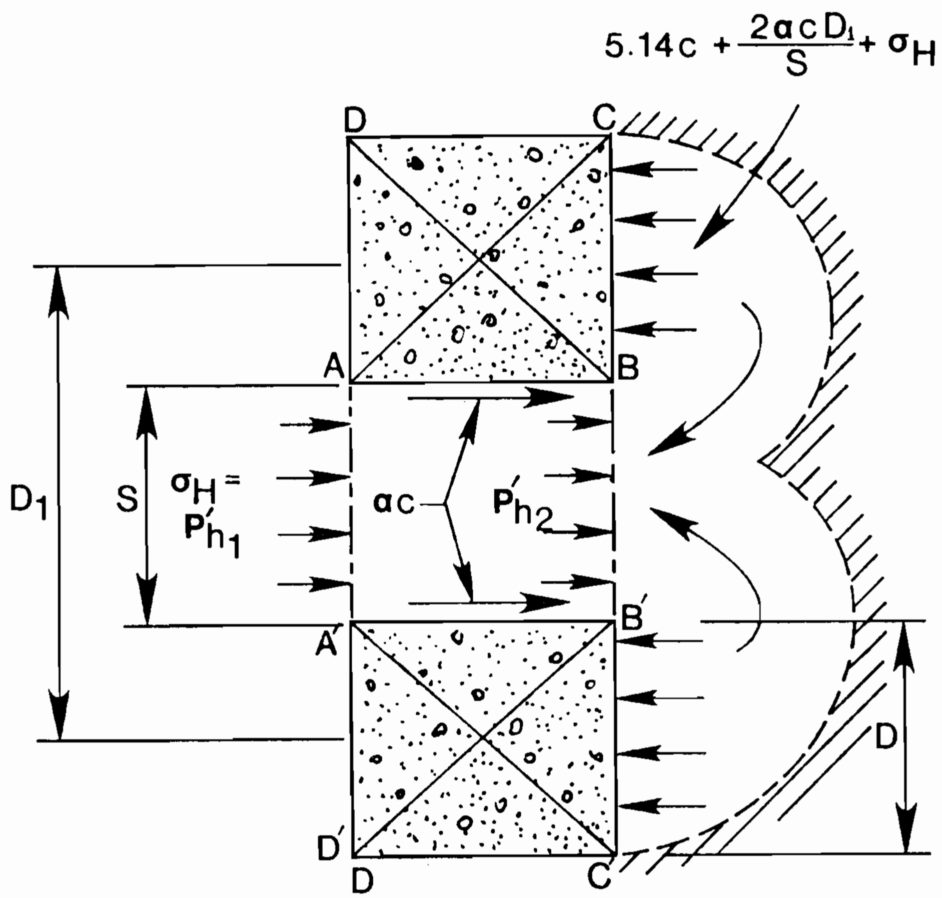

Fig. 6.26. Plan view of a pile group in clay and lateral pressures (after Broms, 1984).

$$P_u = cb\ [\ \pi + 2\omega + 4\cos(\pi/4 - \omega/4)\ (\ 1.414 + \sin(\pi/4 - \omega/4)\ )\ ] \qquad (6.36)$$

where $\omega = \sin^{-1}(f_s/c)$ and b is the pile diameter. The variation of ultimate resistance with friction ratio f_s/c is shown in Fig. 6.27. The value of P_u varied from 9.14cb for a perfectly smooth pile, up to 11.94cb for a perfectly rough pile. Figure 6.27 also show the slip line fields of piles with and without the surface friction. Reese's block model for flow around failure has the value of 10cb, if side friction is not considered; that is believed to be a good approximation.

As mentioned earlier, when two piles that are spaced closely are forced to move laterally, the soils near the piles may be forced to flow through the space. This mechanism is very similar to metal in the forming process. A numerical method from Samanta (1970) was employed in obtaining a solution for the flow of material between two cylinders and a typical slip-line field for a narrow spacing is shown in Fig. 6.28. Results from the slip-line method for various pile spacing are compared with Ito's experimental results in Fig. 6.29. The numerical model cannot give precise results because difficulties occur in the convergence between the stress field and the velocity field, especially at larger spacings. The method is successful for the metal-forming process in which the spacing is relatively very small. Furthermore, the failure planes change significantly at larger spacing due to individual effects. The present model is not adequate for those cases.

Under certain conditions, soil flowing through the spacing between piles is only one possible mechanism for failure. As mentioned earlier, it is unrealistic for equations to yield an infinite soil resistance when the pile spacing becomes zero. Because the problem being solved is three-dimensional, the whole row of piles needs to be treated as a continuous wall. Soil near the piles seems to flow plasticly from the front to the back of the contiguous piles, as shown in Fig. 6.30a. The associated slip-line field for this plastic deformation is presented in

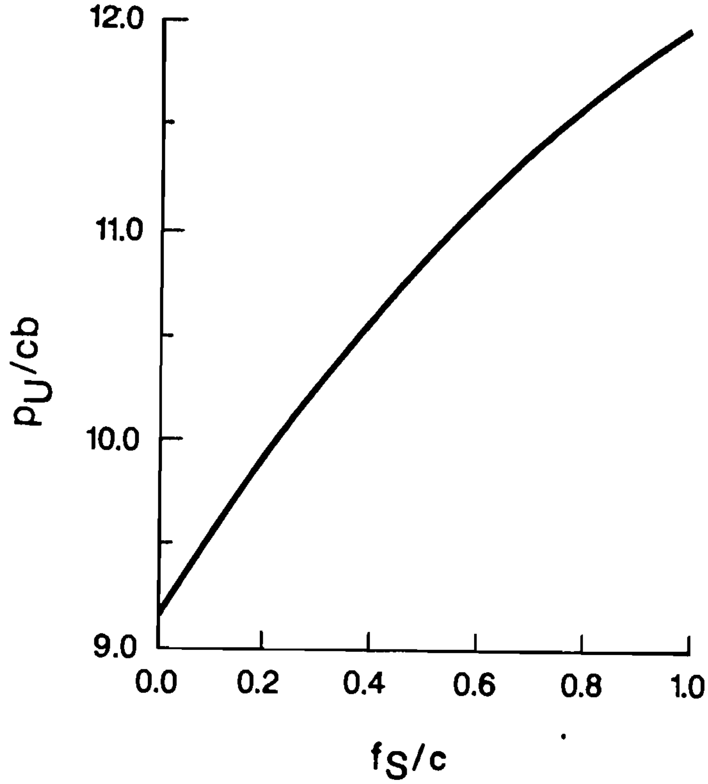

Variation of limiting force with friction ratio

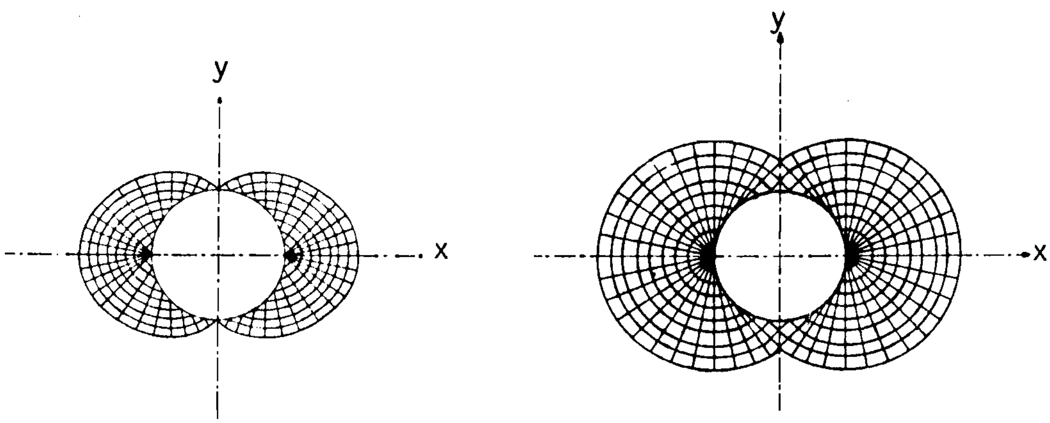

Fig. 6.27. The ultimate soil resistance on a circular pile for flow around failure based on the slip-line theory (from Randolph and Houlsby, 1984).

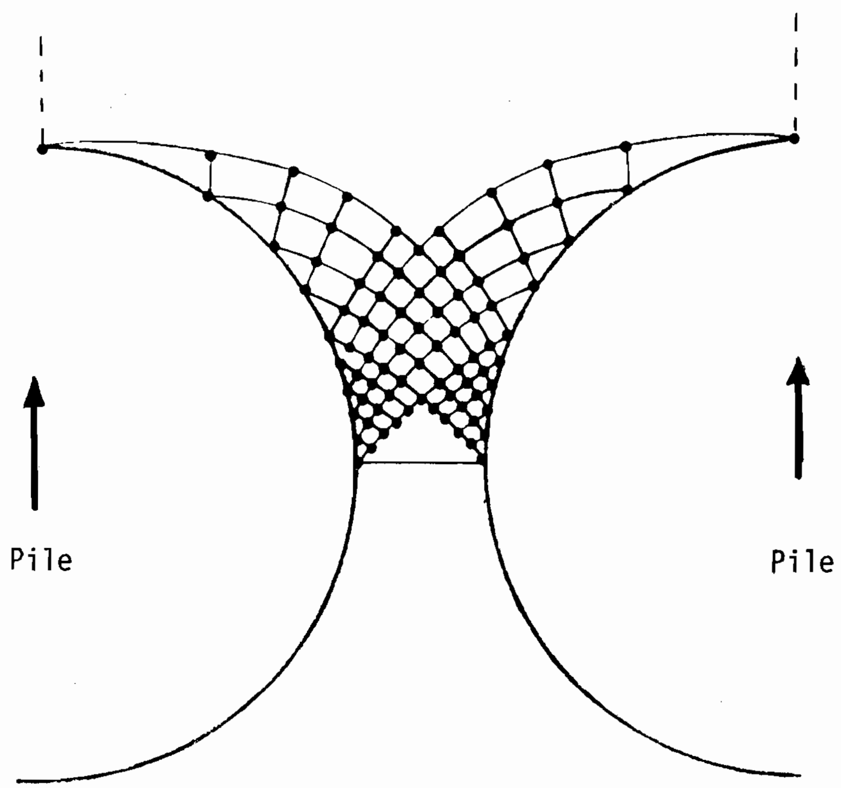

Fig. 6.28. Slip-line field between two side-by-side piles.

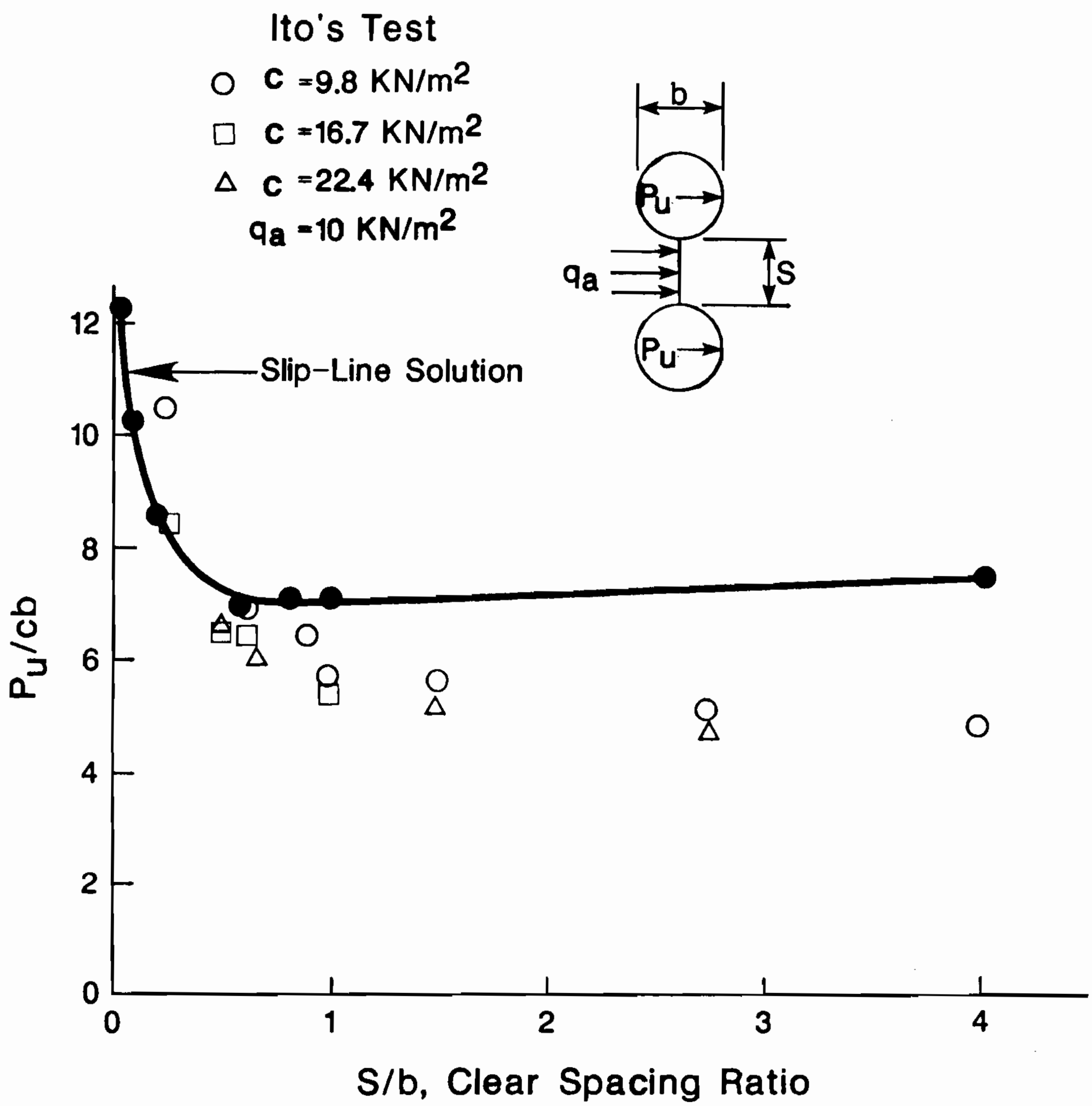

Fig. 6.29. Comparison between theoretical data and test results.

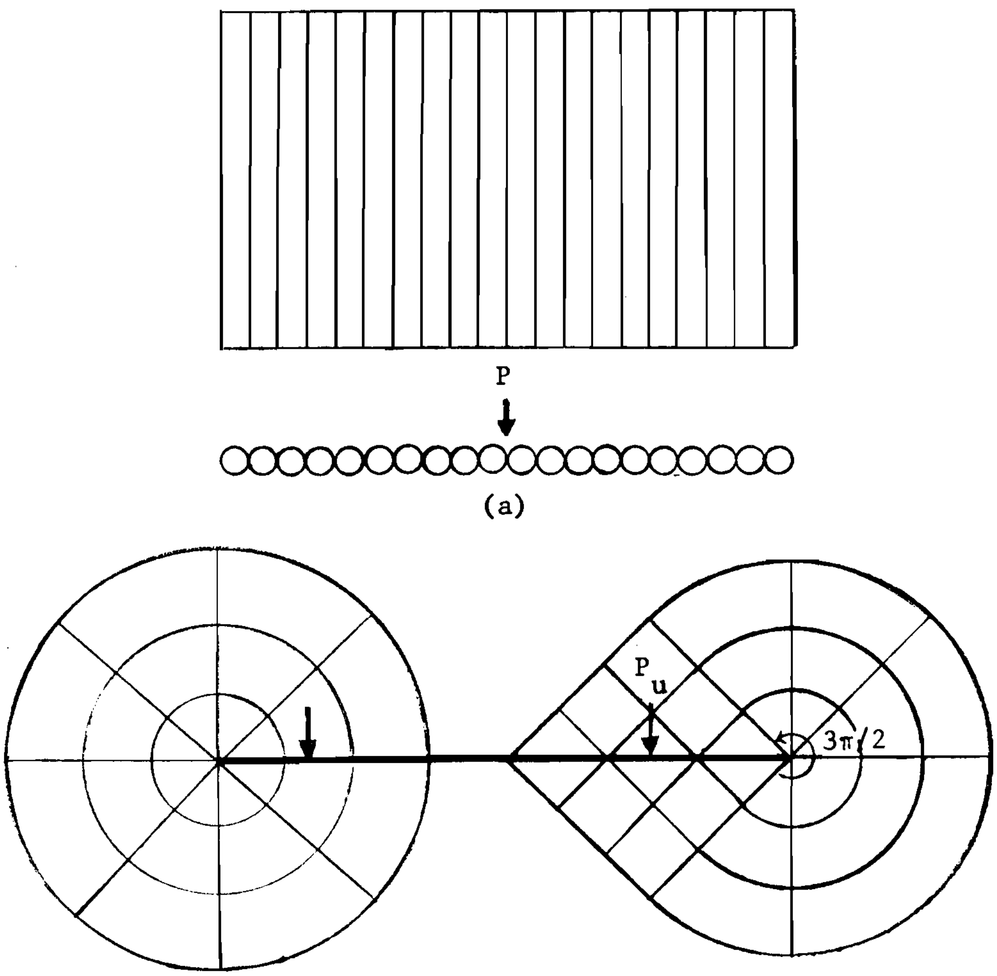

(b) with surface friction

$P_u = 4(\pi)cb = 12.56cb$

(c) without surface friction

$P_u = \{2c+2c(\frac{3\pi}{2})\}b = 11.42cb$

Fig. 6.30. Failure mechanism for piles in a continuous wall.

Figure 6.30b. The ultimate resistance on each pile is 11.42cb, assuming no friction on the pile surface and 12.56cb when assuming friction on the pile surface.

The plastic flow discussed above is limited to the planes that are perpendicular to the pile axis. However, a pile embedded in the soil is actually a three-dimentional problem. Johnson and Hillier (1963) considered a partially embedded wall that was loaded by a transverse force and presented the associated plastic flow in a vertical plane (Fig.6.31). For short, rigid drilled shafts used as a retaining structure, this is another possible failure condition. The ultimate soil resistance that is computed, based on this slip-line field, is 11.42cb for no friction on the pile surface and 12.56cb for friction on the pile surface, the same as the case shown in Fig.6.30.

When applying the slip-line method to problems of flow-around failure, the failure criterion for undrained clay results in two families of shear lines. Since the maximum and minimum shear directions at a point are orthogonal to each other, the two families of slip lines form an orthogonal set. In a more general case of soil satisfying the Coulomb failure condition, two families of shear lines are obtained as shown in Fig. 6.32. However, these two sets of curves are not orthogonal to each other and one family of curves is termed as the Rankine active state and the other is termed as the Rankine passive state (Fig. 6.32). The theory of slip-lines can be employed to solve the same plane-strain problems but the slip-line field must be associated with their failure states. The active and passive states may both occur in a single system, as illustrated in Fig. 6.33 for a bearing capacity analysis. Many studies of the slip-line theory for granular materials has been done in the area of soil mechanics. These developments can provide useful information for the analysis of flow-type failure in sand.

Broms suggested a similar model to the one previously shown for computing the ultimate resistance for piles in cohesionless soil (Fig. 6.34). The ultimate lateral resistance P_u can be calculated from

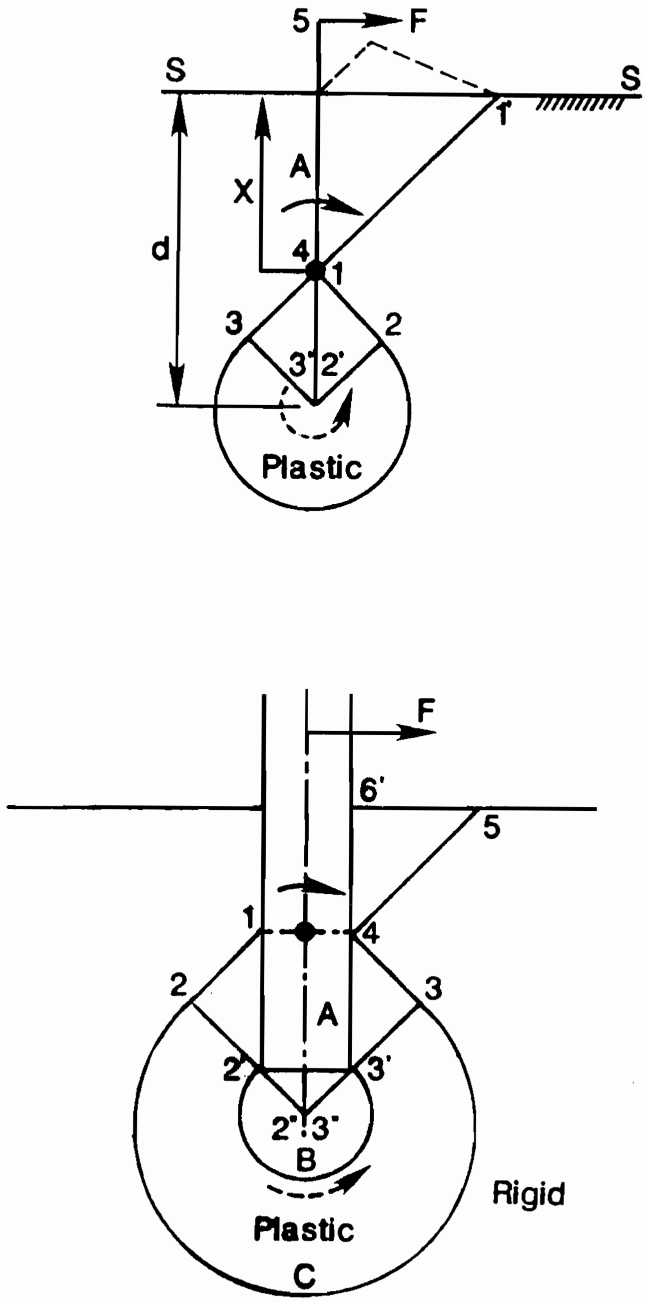

Fig. 6.31. Failure mechanism for partially embedded wall loaded by a transverse force (after Johnson and Hillier, 1963).

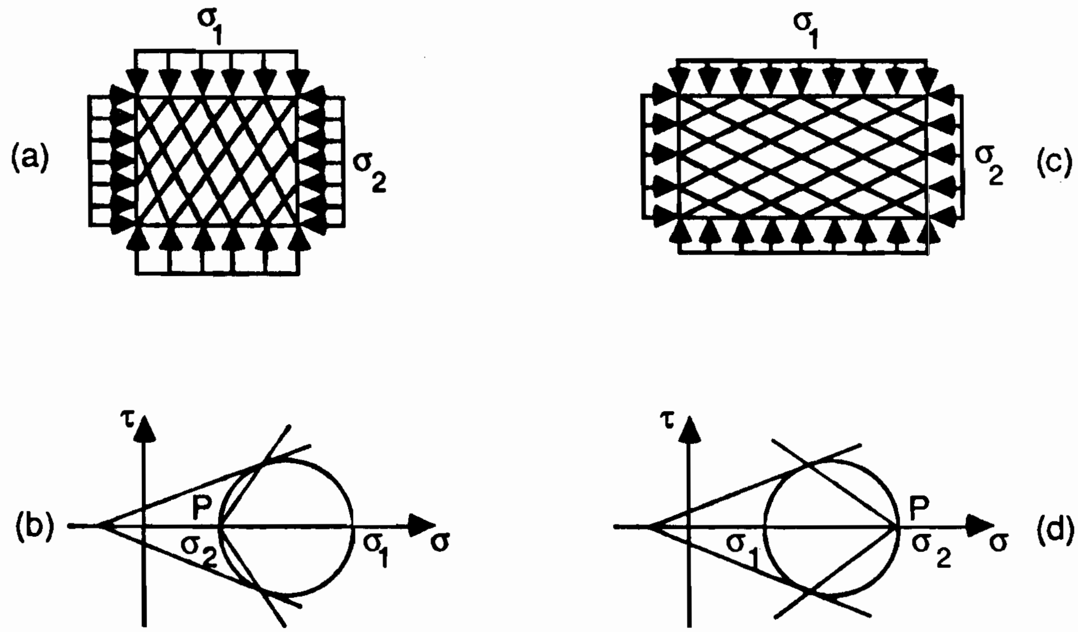

Fig. 6.32. Slip-lines associated with active and passive states.

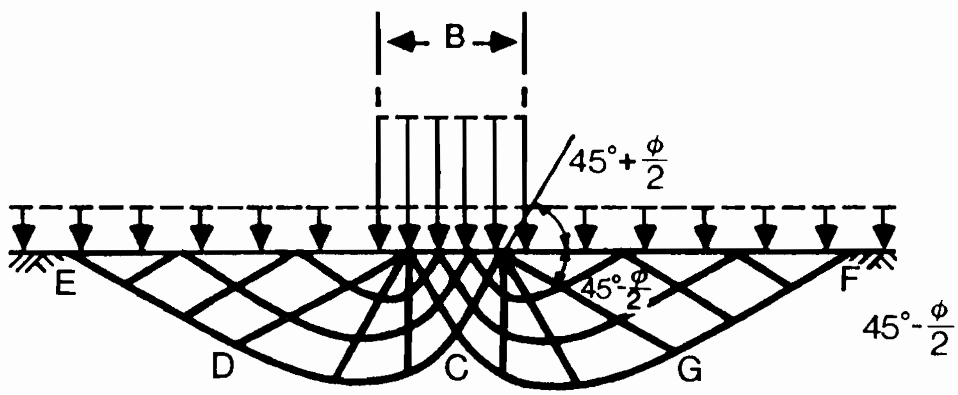

Fig. 6.33. Failure under a shallow strip footing with a smooth base.

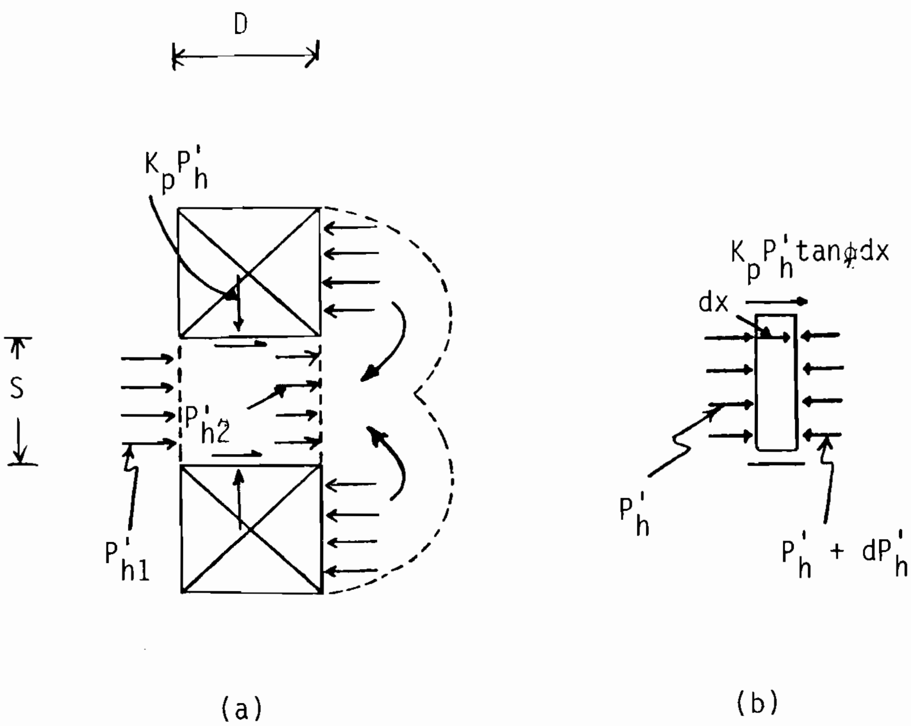

Fig. 6.34. Lateral resistance of pile group in sand (after Broms, 1984).

$$P_u = P_{h2}' N_q \qquad (6.37)$$

where N_q is the bearing capacity factor with respect to the effective confining pressure P_{h2}'.

The confining pressure P_{h2}' is affected by the friction resistance along the sides of the two piles. By integrating the friction force on the side wall, the confining pressure P_{h2}' can be given as

$$P_{h2}' = K_o \gamma H \, EXP \, (2DK_p \tan\phi / S) \qquad (6.38)$$

Finally, by substituting Eq.6.38 into Eq.6.37, the ultimate lateral resistance can be expressed as a function of the clear spacing

$$P_u = K_o \gamma H \, EXP \, (2DK_p \tan\phi / S) \, N_q \qquad (6.39)$$

The bearing capacity factor N_q is assumed not to vary in the above equation. However, the effect of adjacent footings on the bearing capacity coefficient N_q has been reported by several authors (Myslivec and Kysola, 1968; Khadilkarand and Varma,1977; Pula and Rybak, 1981). The bearing capacity coefficient N_q increases with the decrease in spacing between two footings. The influence on N_q for foundations in sands with various spacings is obtained from Pula and Rybak (1981) and presented in Fig. 6.35. It is obvious that substituting N_q* in Fig. 6.35 with N_q in Eq. 6.39 may result in a more reasonable prediction for the ultimate soil resistance.

It has been recognized that there are two possible failure conditions when piles are close to each other; one failure occurs in the plane perpendicular to the pile axis, the other failure occurs in the vertical plane. The slip-line fields for these two cases are presented in Fig. 6.36 and Fig. 6.37, repectively. Although the failure planes are in different phases, the ultimate soil resistance based on the slip-line theory is expected to have the same expression as:

$$P_u = K_o \gamma Hb \, EXP(3\pi \tan\phi) \, \tan^2(45^\circ + \phi/2) \qquad (6.40)$$

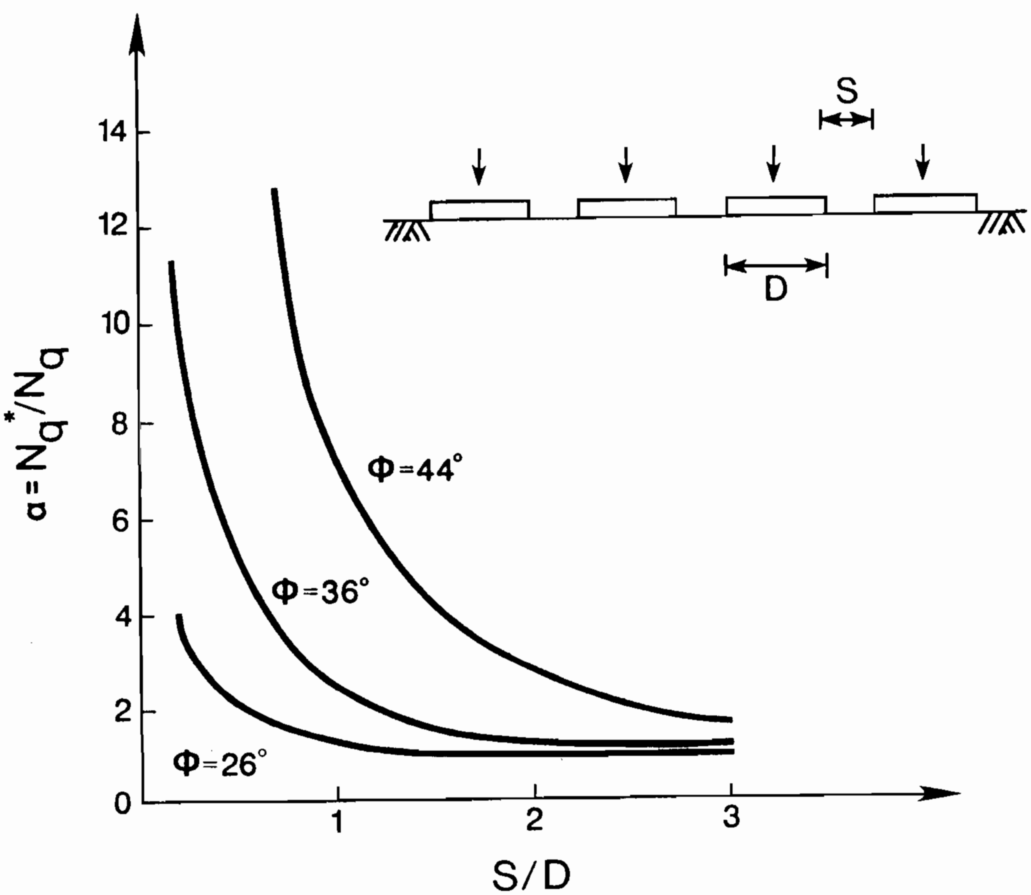

Fig. 6.35. The influence of spacing bearing capacity factor N_q.

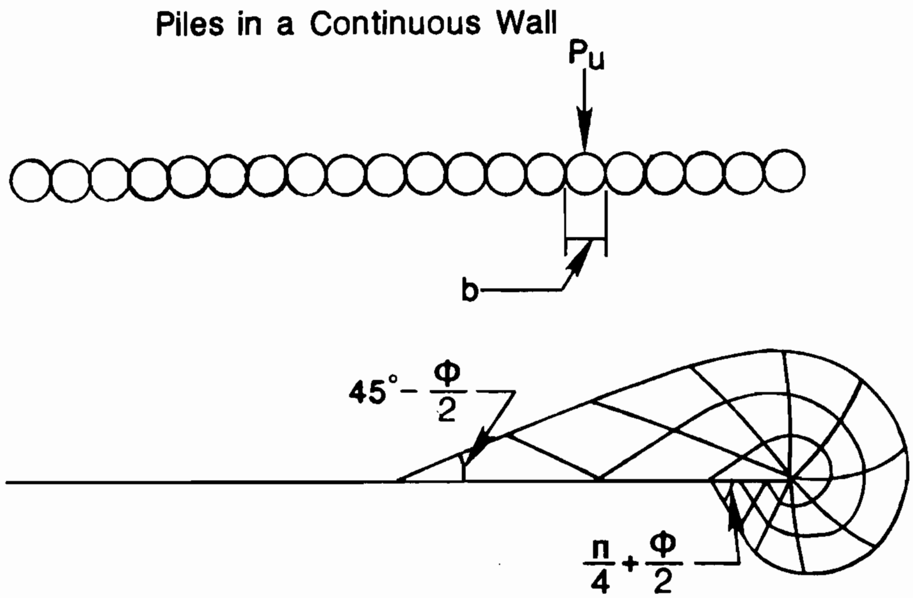

$$P_u = K_o \gamma H b \ \text{EXP}(3\pi \tan\phi) \ \tan^2(45^\circ + \phi/2)$$

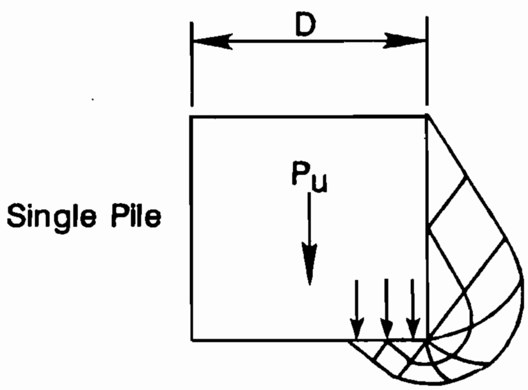

$$P_u = K_o \gamma H D \ \text{EXP}(2\pi \tan\phi) \ \tan^2(45^\circ + \phi/2)$$

Fig. 6.36. Failure mechanism for piles in sand.

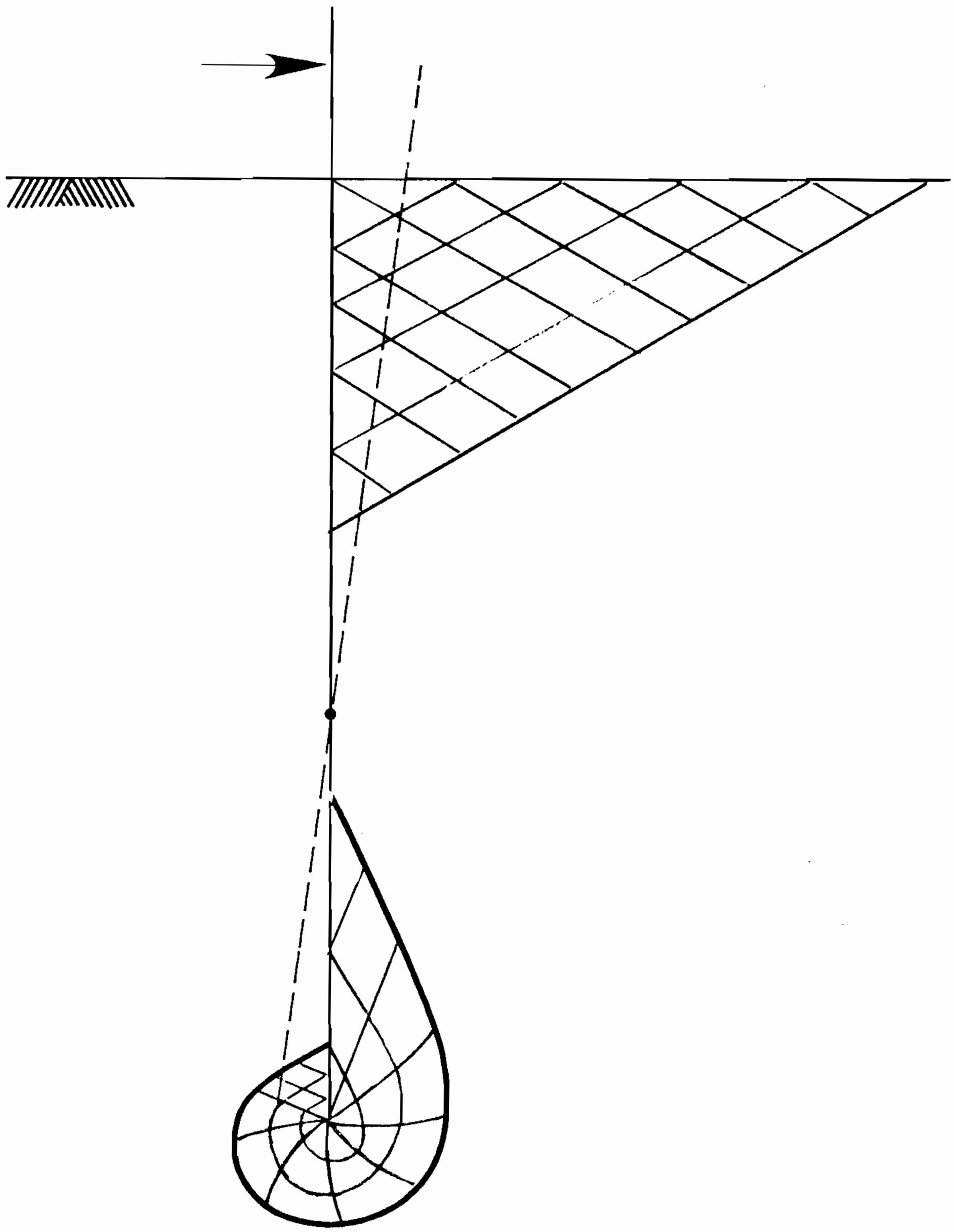

Fig. 6.37. Failure mechanism in a vertical plane of a continuous wall embedded in sand.

Discussion of results from finite-element method

General remarks. In earlier development of finite-element methods many authors have concentrated on linear applications. However, nonlinearities arise in engineering situations from several sources and the need for nonlinear analysis has expedited the advancement of this method. Today, the finite element method is accepted as a powerful technique for the numerical solution of many large-strain plasticity problems. Because the finite element method appears well-suited to the analysis of problems involving material with nonlinear properties, Yegian and Wright (1973) pioneered the use of the method in developing p-y relationships. Thompson (1978) continued the research of Yegian and Wright and took into account many sophisticated factors such as the separation of the soil on the back side of a pile during displacement, and achieved a highly satisfactory result.

The use of p-y curves is based on the Winkler assumption that each p-y curve employed at a specific depth along the length of the pile is independent of pile displacement and soil reactions at points above and below. This assumption reduces the problem from a three-dimensional to a two-dimensional one. Plane-strain-deformation conditions employed in the two-dimensional finite-element model are applicable to the study of flow-around failures. The finite element method provides another means of approaching the problem of computing the ultimate soil resistance under plain-strain conditions. A computer code originally developed by Owen and Hinton (1976) for handling large-strain and elasto-plastic materials was modified and employed in the analyses reported herein.

Finite-element mesh and the outer boundary. A complete cross section at several diameters below the ground surface for plain-strain analysis is presented in Fig. 6.38. Yegian and Wright (1973) pointed out the advantage of the boundaries of symmetry and antisymmetry that exist in the cross section (Fig.6.38). The use of these boundaries can save substantial amounts of computational time and effort. Therefore, the finite element mesh for single-pile problems was constructed only in one-fourth of the influence

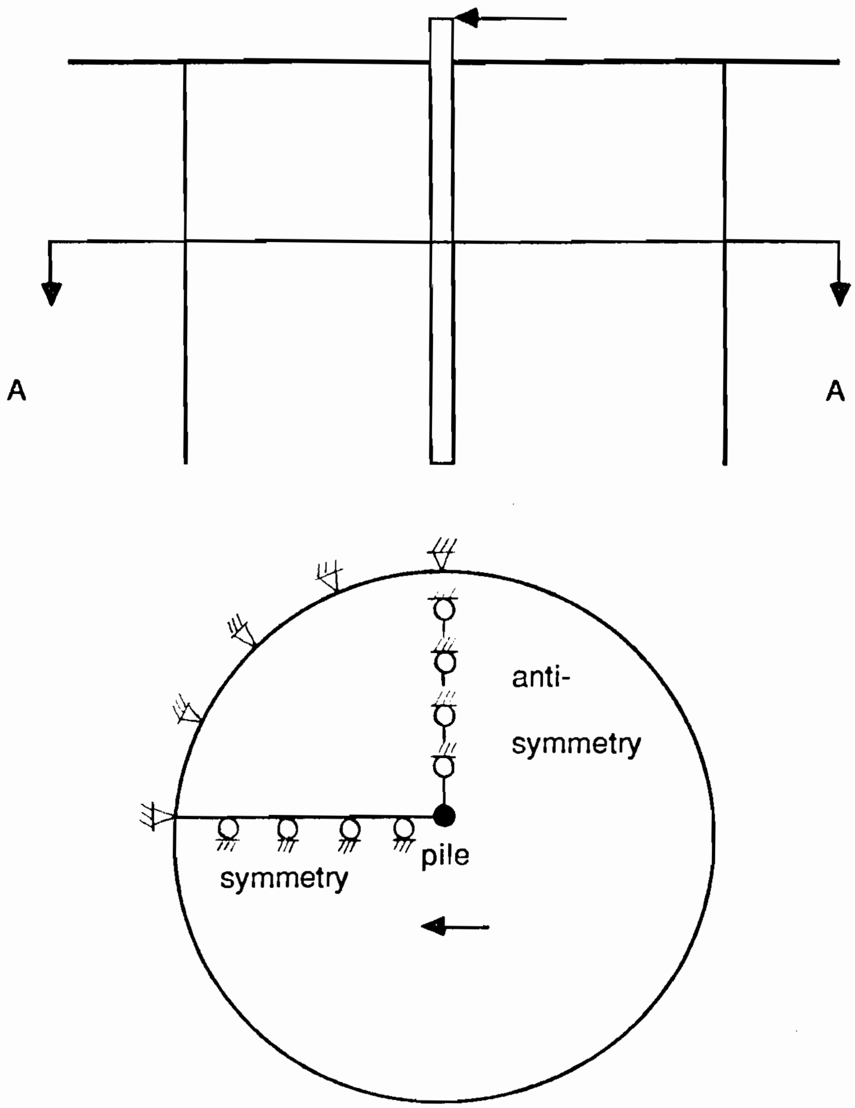

Fig. 6.38. Soil-pile cross-section showing symmetry and antisymmetry boundaries.

zone and is illustrated schematically in Fig. 6.39. The distribution of stress and strain in the one-fourth of the influence zone are presented in Fig. 6.40 to Fig. 6.42. As may be seen, the results reasonably present the behavior in that region. Eight-noded quadratic, serendipity elements were selected and were expected to give better results than the four-noded, linear, quadrilateral elements used in the nonlinear analysis. The relative size and number of elements in the finite mesh were determined on the basis of past studies. In general, it is desirable to use small elements near the pile due to the large gradient in stress which occurs. With increasing distance away from the pile the gradient in stress decreases and larger elements can be used.

For piles in a group, it is interesting to study the effect of close spacing on the soil resistance in the local region. Due to the symmetrical boundaries in the plane section that are similar to the case of a single pile, the finite element mesh can be limited, as shown in Fig. 6.43, in order to save computer time.

Soil model. The accuracy of the finite element model depends on use of the correct model to formulate the nonlinear stress-strain behavior of the soil. A hyperbolic-plastic stress-strain relationship (Fig. 6.44) has been used to describe the behavior of the soil in many finite-element studies in geotechnical engineering. The use of a hyperbolic expression for the stress-strain curve for soil was initially proposed by Konder (1963) and further developed by Duncan and Chang (1972). Methods have been proposed by which laboratory stress-strain data can be reduced to the form of a hyperbola and serve an input to the finite element analysis.

In this study, the finite-element method was expected to provide some insight with regard to the effect of closely spaced piles. To make a proper comparison between this method and slip-line theory, the soil model used in the finite-element studies had to be similar to that for rigid, perfectly-plastic material. Therefore, no strain-hardening was assumed for the soil and the elastic range in the stress-strain curves was kept small enough to

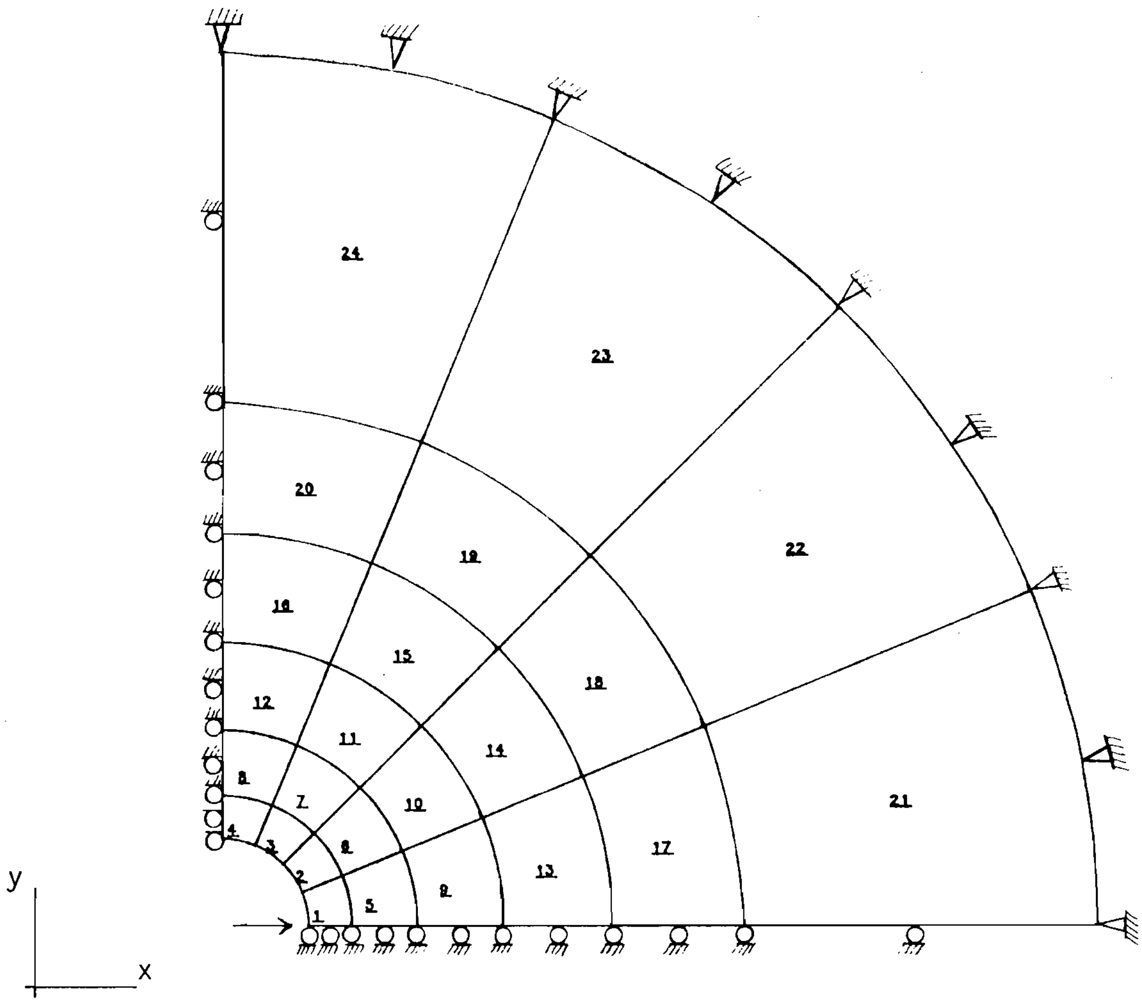

PILES IN A ROW

Fig. 6.39. One-fourth of the influence zone for a single pile.

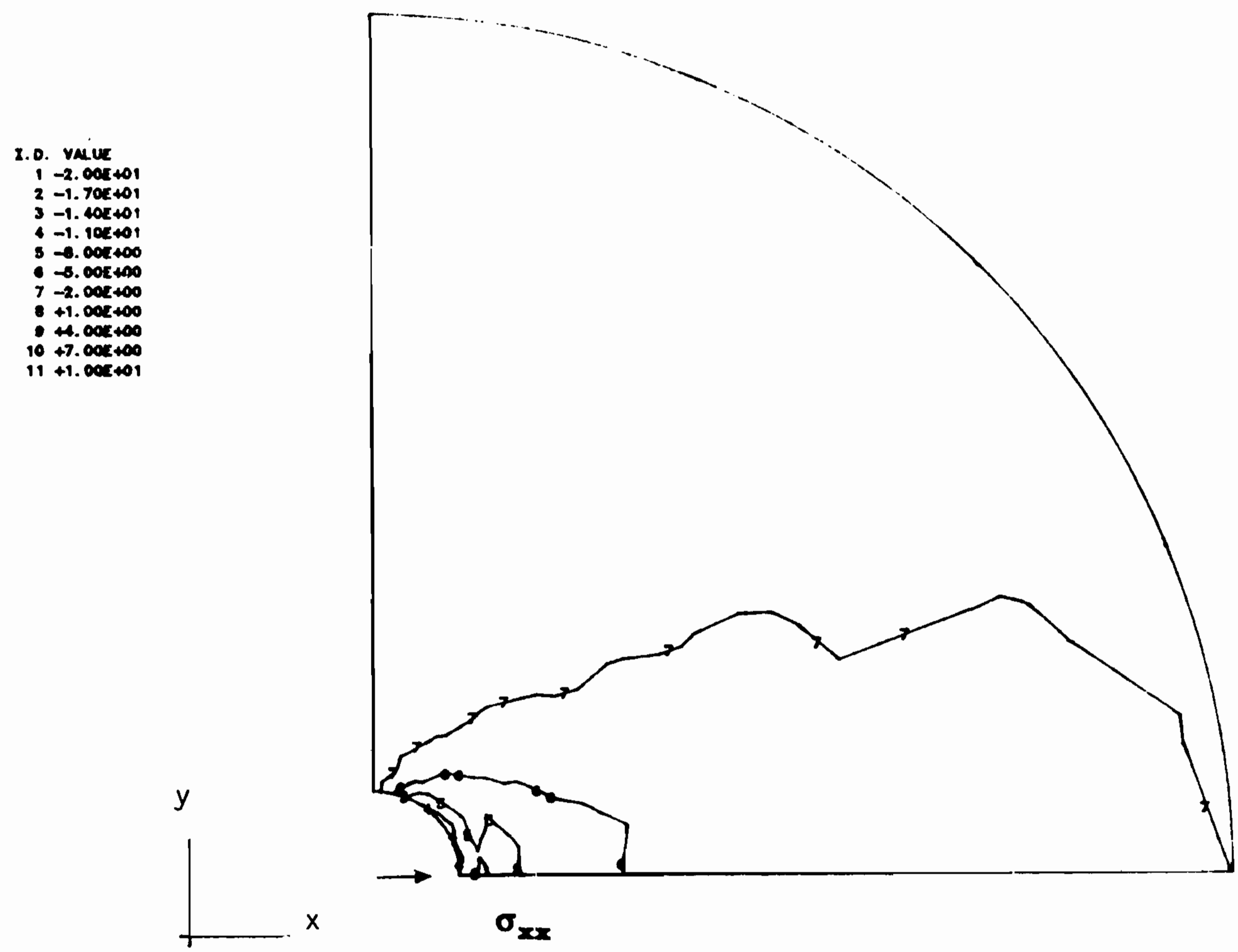

Fig. 6.40. Normal stress distribution for single pile analysis using one-fourth of the influence zone.

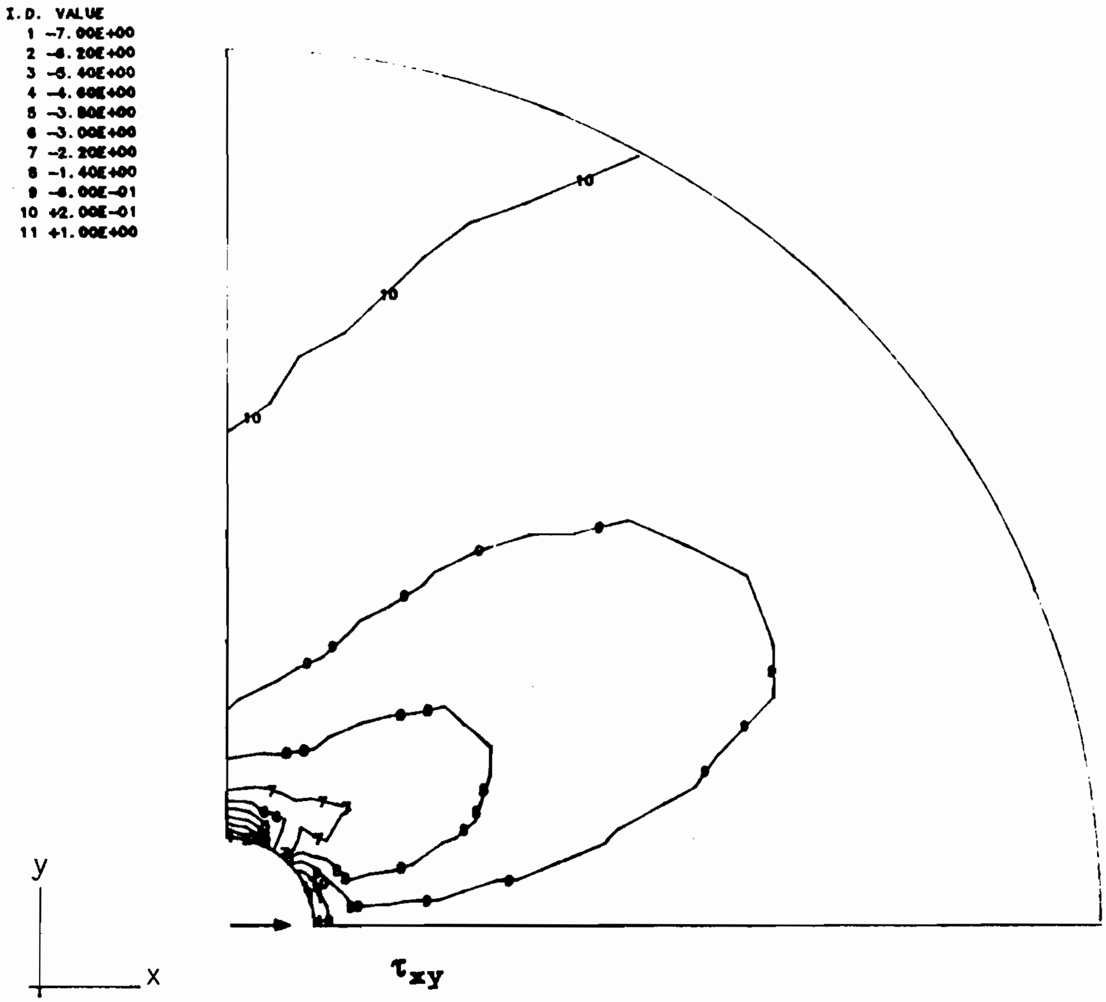

Fig. 6.41. Shear stress distribution for single pile analysis using one-fourth of the influence zone.

solid lines - displaced mesh
dash lines - original mesh

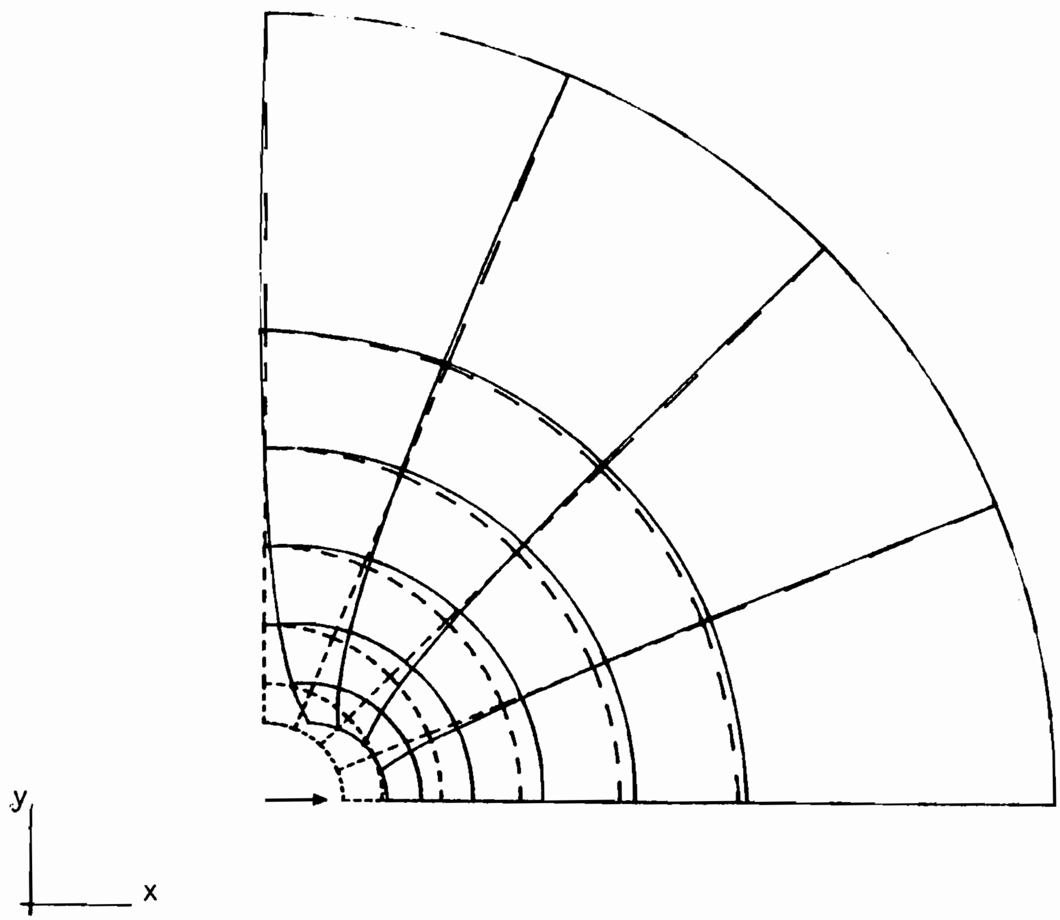

Fig. 6.42. Deformation of a single pile analysis using one-fourth of the influence zone.

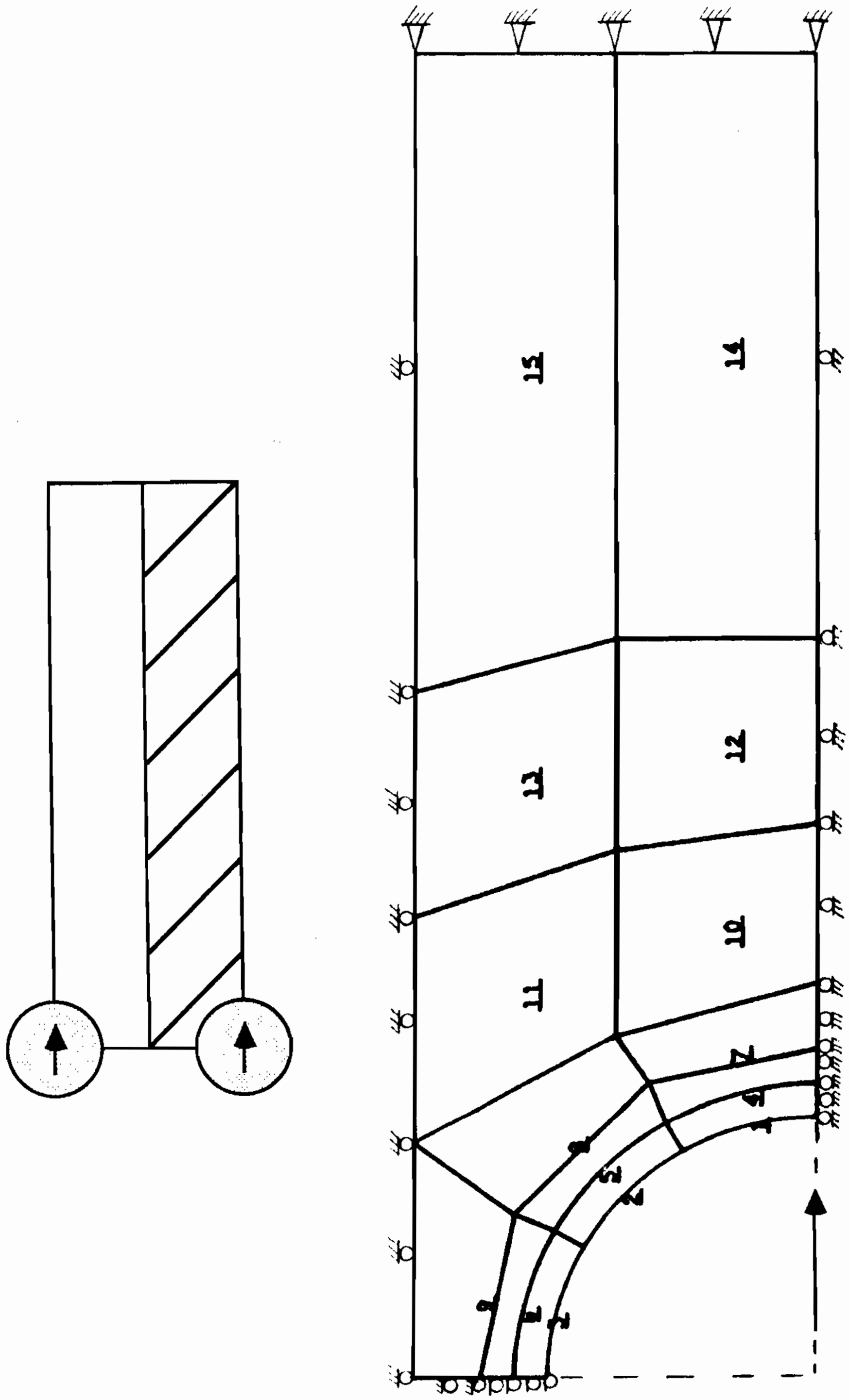

Fig. 6.43. The finite element meshes for the study of side-by-side piles.

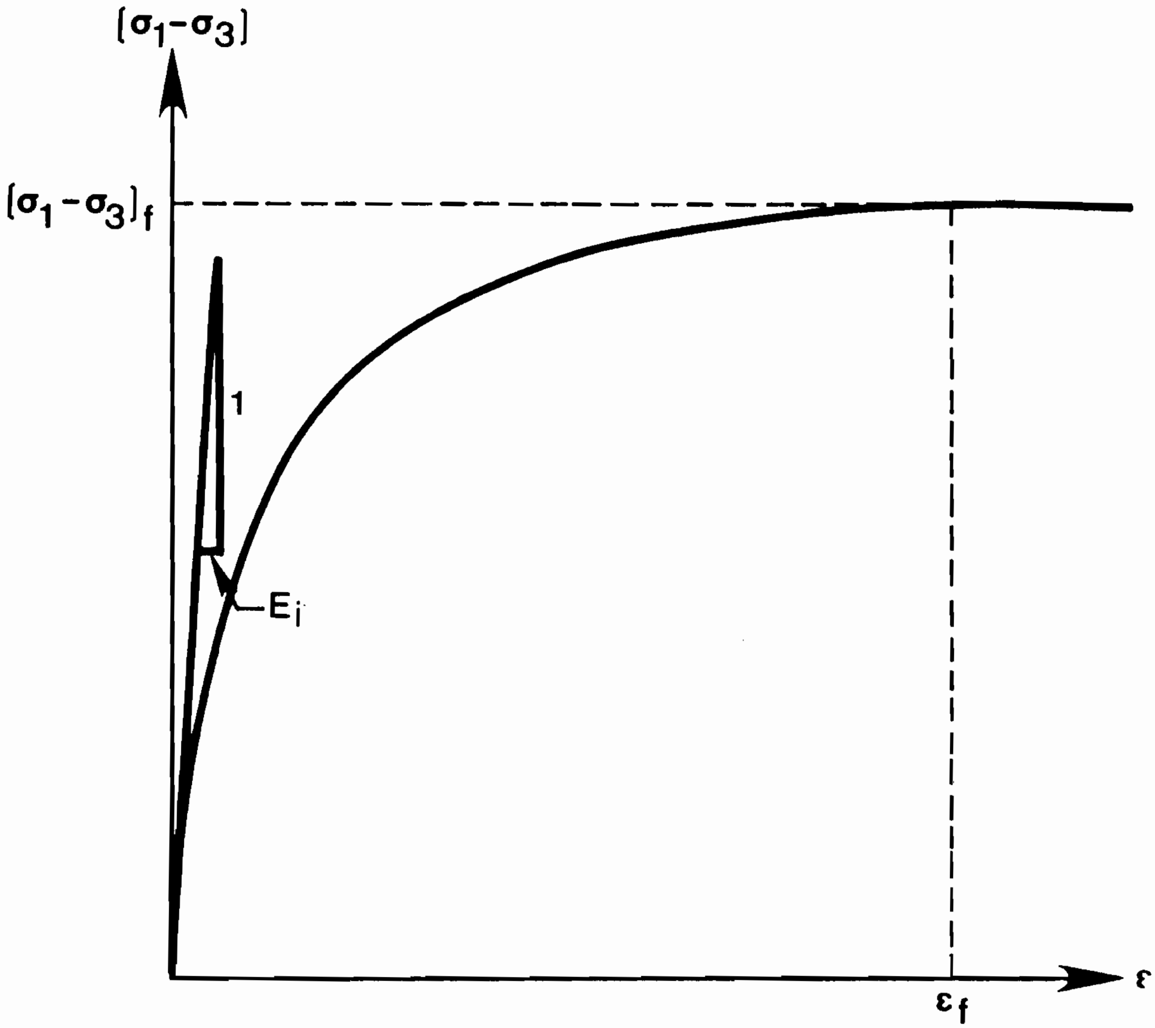

Fig. 6.44. Hyperbolic stress-strain relationship.

avoid any difficulty in the convergence. This simplified elasto-plastic soil model was used for every analysis.

Results of Finite-Element Analyses

The computation of soil resistance by the finite element method was accomplished by specifying an equal displacement to the nodal points at the pile surface and then computing the reaction forces from the surrounding medium at those nodal points. No separation of the soil from the pile is assumed in the analyses. Thus, the total resisting force on a pile section is obtained by summing the nodal forces at the circumference of the entire pile section. The increment of displacement that describes the boundary condition at the pile surface should be selected properly in order to ensure convergence. The results from the finite-element studies are shown in Fig. 6.45. As may be seen, the ultimate soil resistance for a single pile is a little higher than the theoretical value (9.14cb) from slip-line theory. This discrepancy may result from the assumption in slip-line theory of a rigid- plastic model with exclusion of any reaction from elastic deformation. The other possible reasons are that the mesh size in the finite-element analyses is not fine enough and that the distance between the outer boundary and the center of the pile is not large enough.

However, an important finding is that a significant increase of the ultimate soil resistance occurs at a spacing ratio of less that 0.5. This finding is consistent with the result from slip-line theory. The dramatically increased resistance makes it difficult for the local soil to flow through the interval between the two piles; thus, the failure mechanism developed by the motion of the global system mentioned in the previous section seems to prevail in these situations. The deformation of the soil medium in the interval due to the movement of piles is shown in Fig. 6.46. As may be seen, the soil tends to flow through the interspace between two piles under plane-strain condition. The distribution of normal stress and shear stress near the piles are presented in Fig 6.47 and Fig. 6.48, respectively. The stress

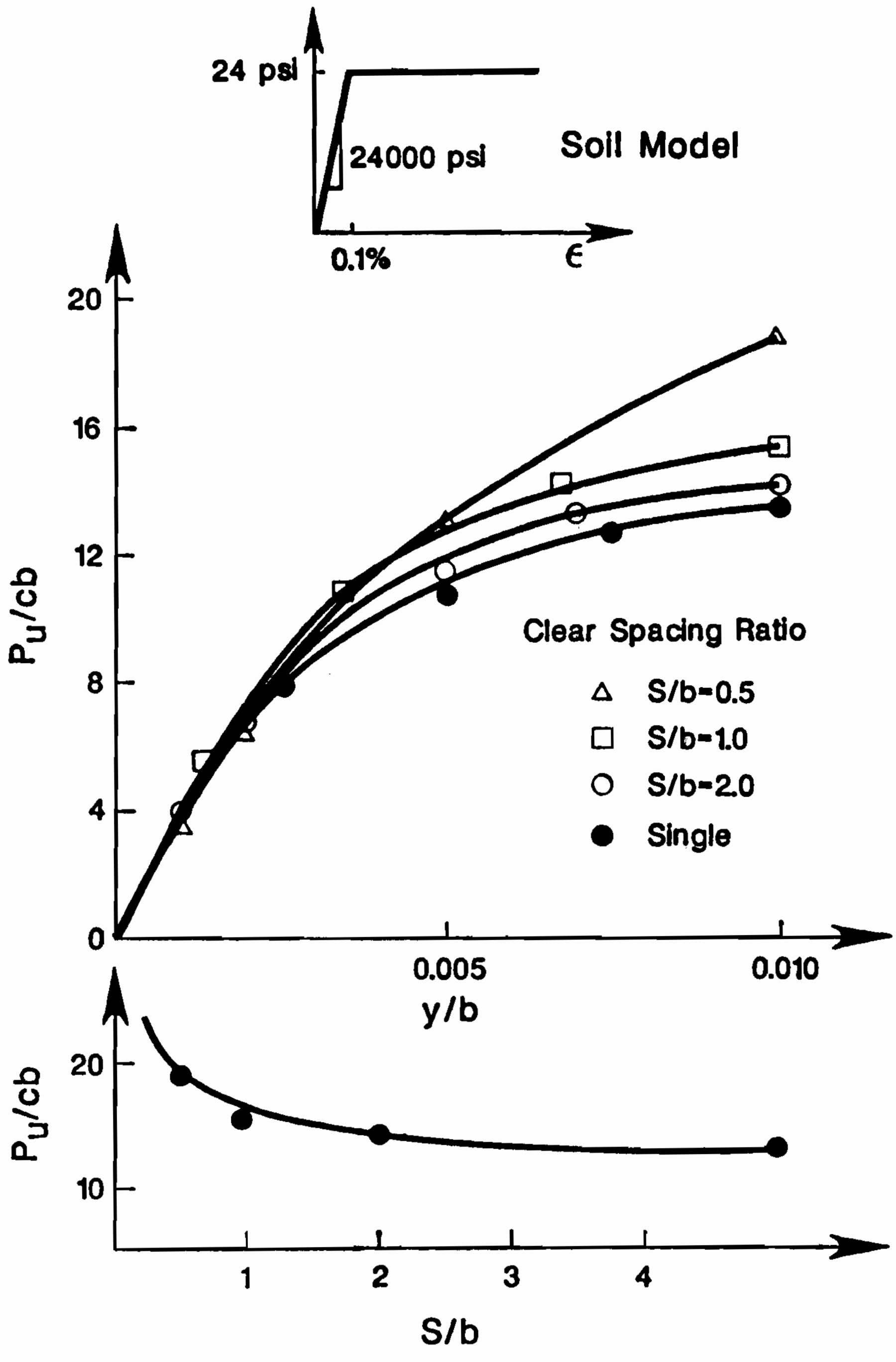

Fig. 6.45. Results from FEM analysis.

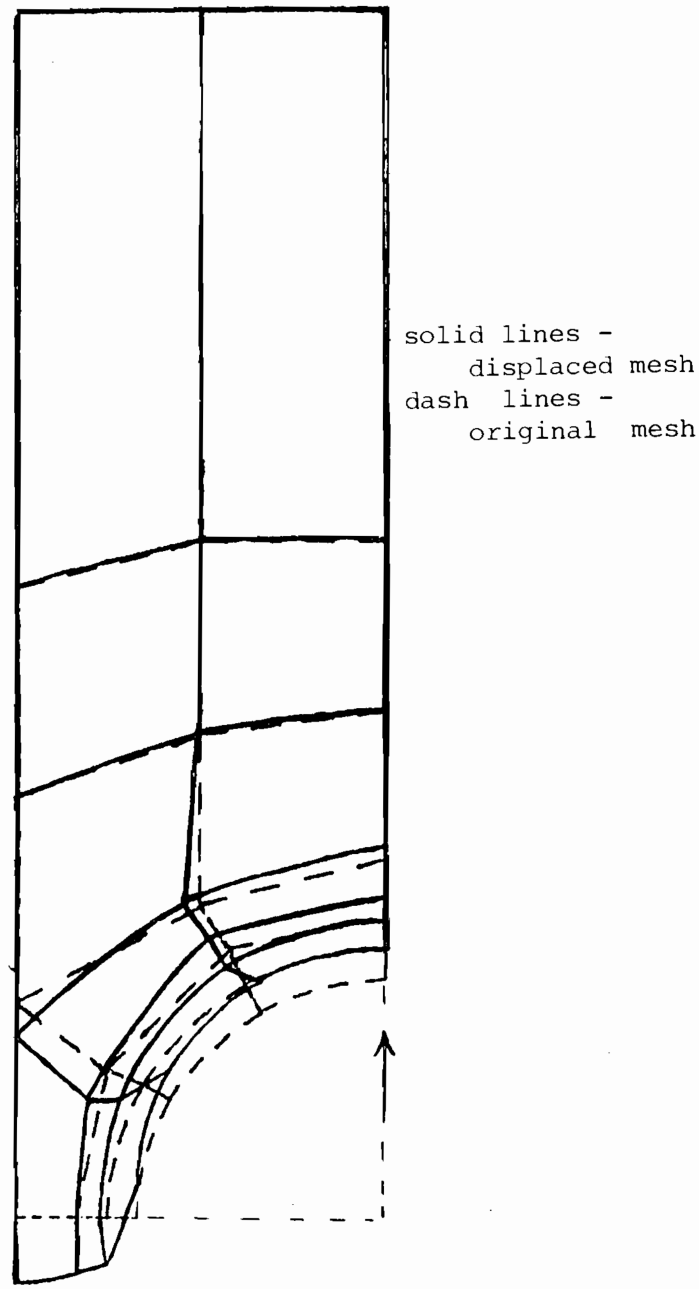

Fig. 6.46. Soil deformation between two piles.

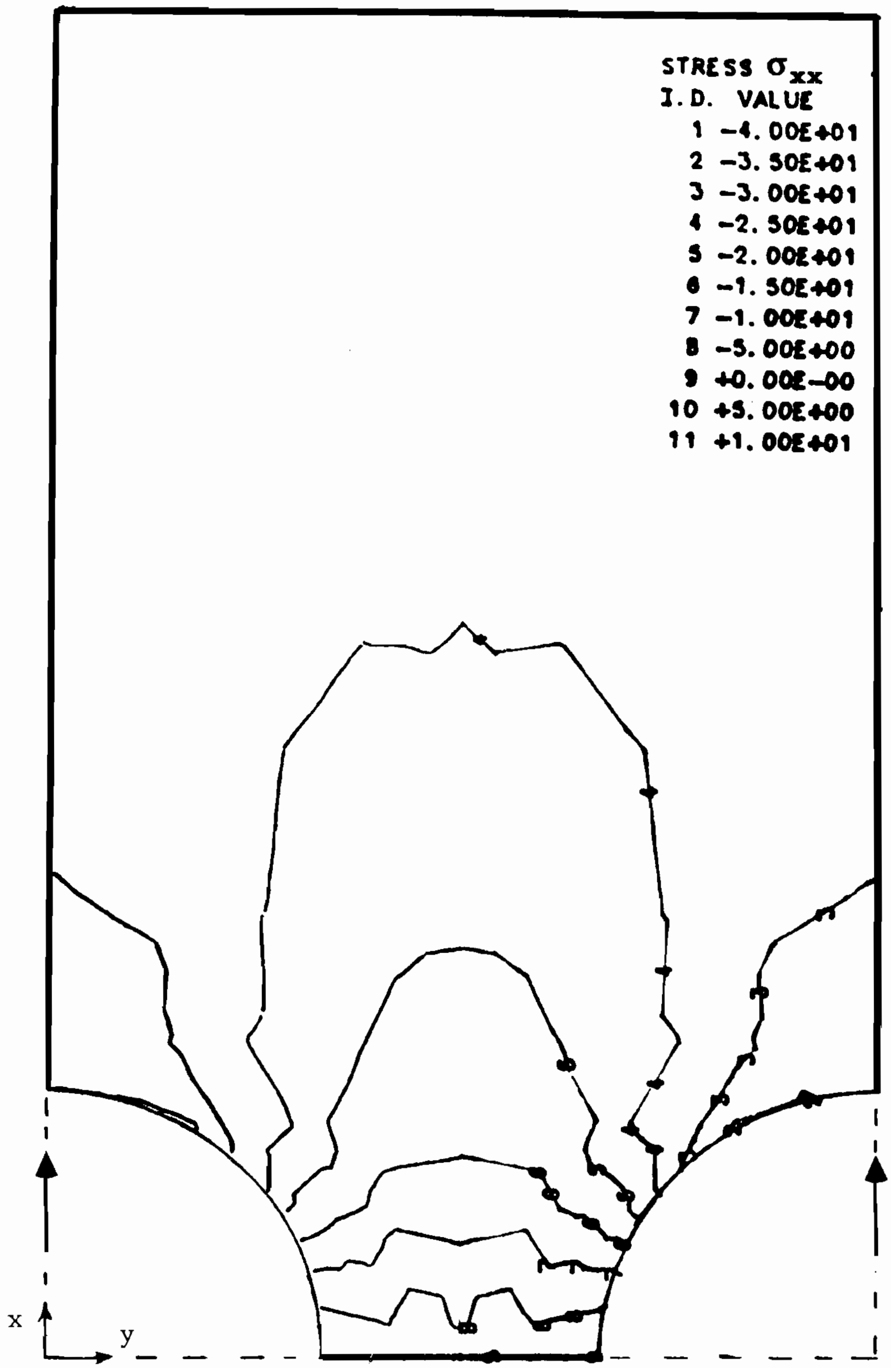

Fig. 6.47. Normal stress distribution between two piles.

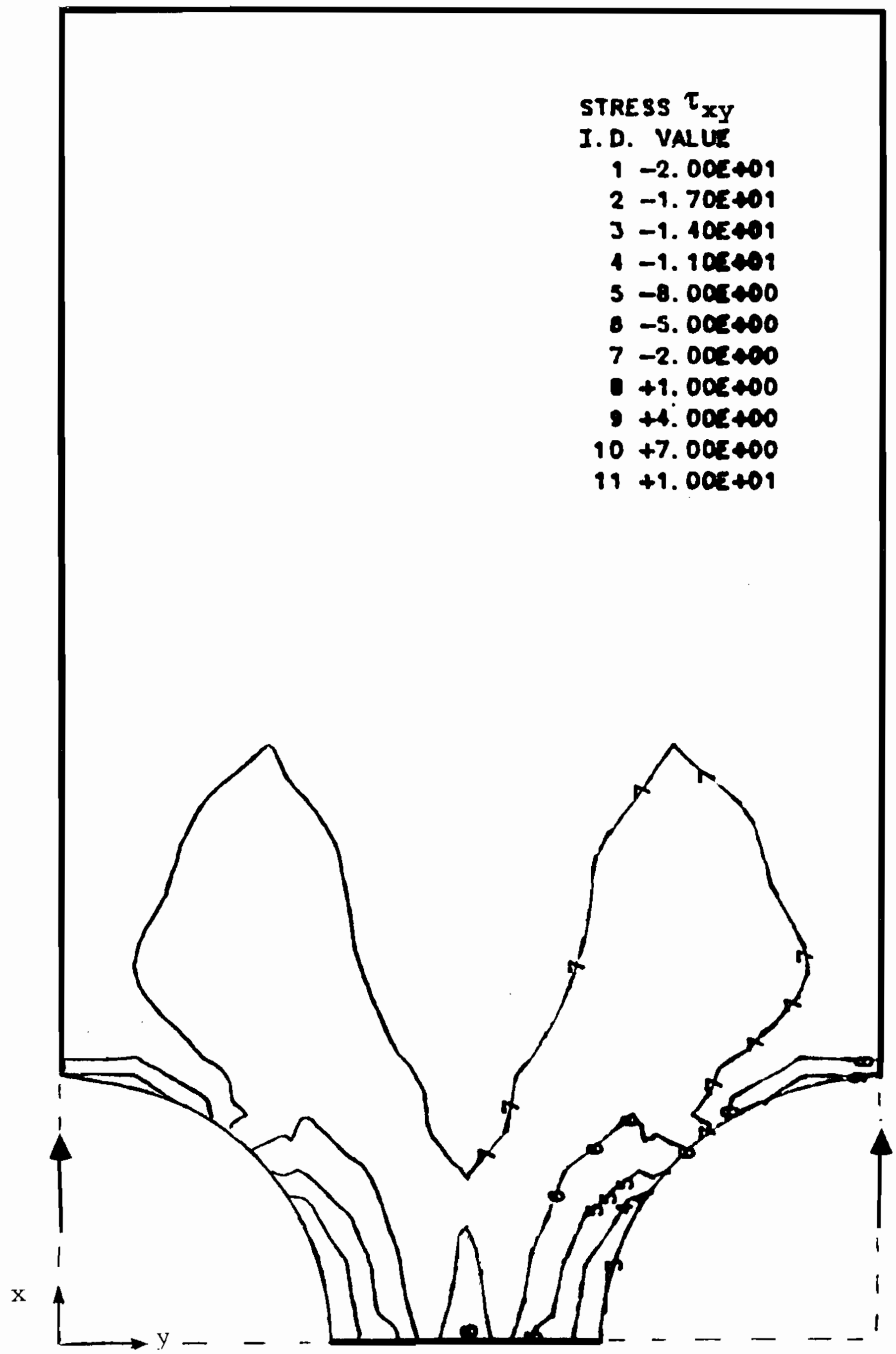

Fig. 6.48. Shear stress distribution between two piles.

contours clearly indicate the influence of one pile on another in a row.

As discussed earlier, the finite element study was not aimed at providing a powerful analytical tool for this topic. The method is not adequate for many practical problems because of its complexity and the uncertainty of soil properties. But, it does give good results for the problems of concern from the aspect of theoretical considerations.

Recommended equation for computing ultimate soil resistance at several diameters below the ground surface. In general, in the analysis of laterally loaded piles the soil resistance at several pile diameters below the ground surface has less influence than that near the ground surface. Thus, computing soil resistance for plain-strain failure is not as crucial as for the wedge-type failure. To avoid complicated computation in the design procedures, a group factor α_g is recommended for introduction into the current p-y criteria for computing the ultimate soil resistance at several diameters below the ground surface.

From the above discussion, if the clear spacing is greater than three diameters there is a negligible effect from adjacent piles on soil resistance. Both the slip-line method and the finite-element analysis show an increased soil resistance for piles with a small spacing under the plain-strain condition. However, once the piles are in contact as a continuous wall, the failure mechanism based on the consideration of a global system seems to be more critical than that of plastic flow through the local spacing. The failure based on the consideration of a continuous wall has an ultimate soil resistance of 11.42cb described earlier if the friction on the pile surface is not taken into account. This ultimate soil resistance is close to the value of 9.14cb for single piles under the condition of flow-around failure.

The global-system failure may also occur for a group of piles with a small spacing S, if the arching effects prevent the soil from passing through the interspace. Then the soil resistance on each pile becomes

$$P_u = 11.42c\ (\ b + S\ ) \qquad (6.41)$$

It is not clear about the possible value of spacing S to cause the global system reacting as a continuous wall, but the previous studies have shown the soil resistance increases dramatically when the pile spacing becomes less than 0.25 diameters. Therefore, an approximate expression for the ultimate soil resistance and the group factor α_g are recommended in Fig. 6.49.

For cohesionless soils, the ultimate soil resistance from Eq.6.39 is believed to serve as a good approximation. The ultimate soil resistance computed from Eq. 6.39 for piles with large spacing is consistent with the result from p-y criteria for a single pile in sand. If the friction on the pile surface does not vary with the spacing, the modification factor α can be expressed as

$$\alpha_g = \frac{Nq^*}{Nq} \qquad (6.42)$$

However, the failure based on the consideration of a continuous wall is the most critical condition for piles next to each other; therefore, the α_g-factor for this case, referring to Fig. 6.36, would be

$$\alpha_g = e^{\pi \tan\phi} \qquad (6.43)$$

For simplicity, the values from Eq. 6.42 and Eq. 6.43 are recommended for modifying the ultimate soil resistance for the plane-strain conditions for closely spaced piles (Fig. 6.50).

GROUP EFFECTS FROM ELASTIC BEHAVIOR

As mentioned at the beginning of this chapter, a hybrid method was adopted to take into account the effects of pile groups in this study. The equations for computing the ultimate soil resistance have been described in the previous sections. The group effect due to the elastic response is another important

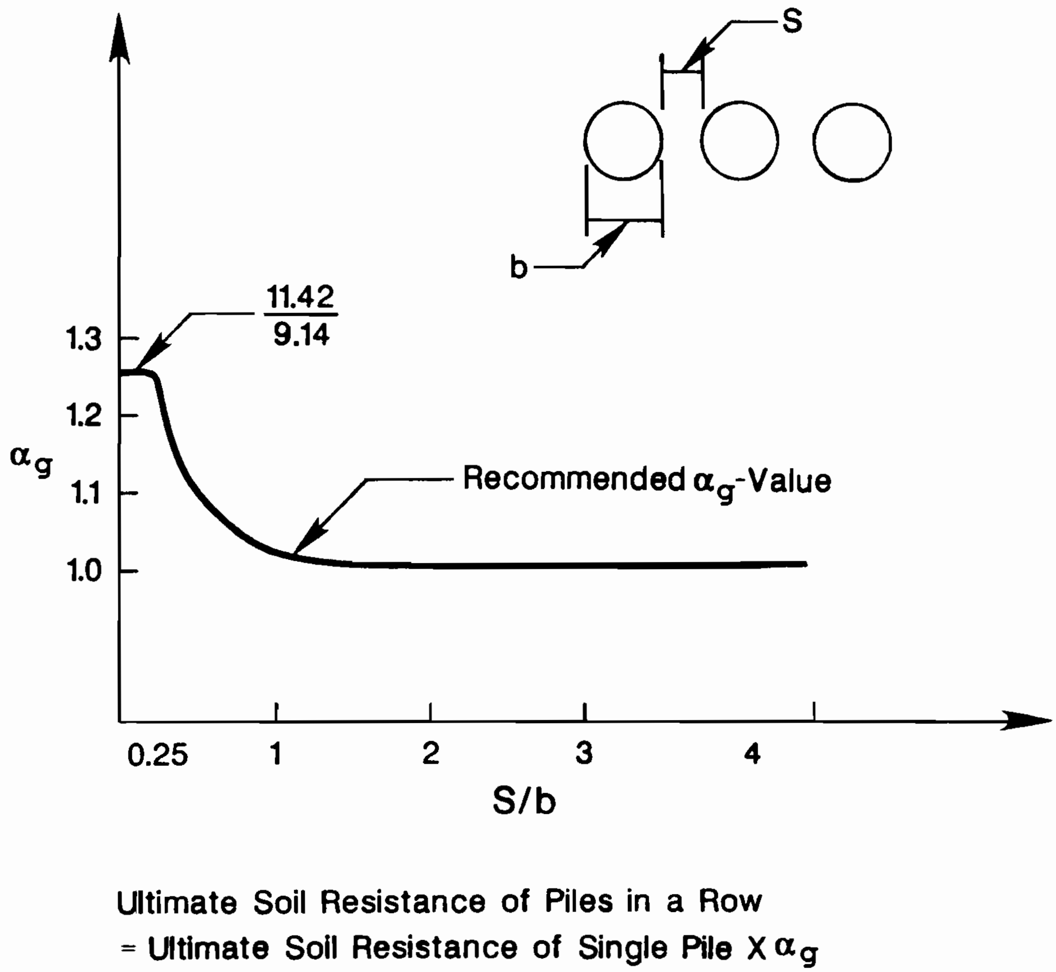

Fig. 6.49. Recommended α_g-factor for piles in a row in a clay layer.

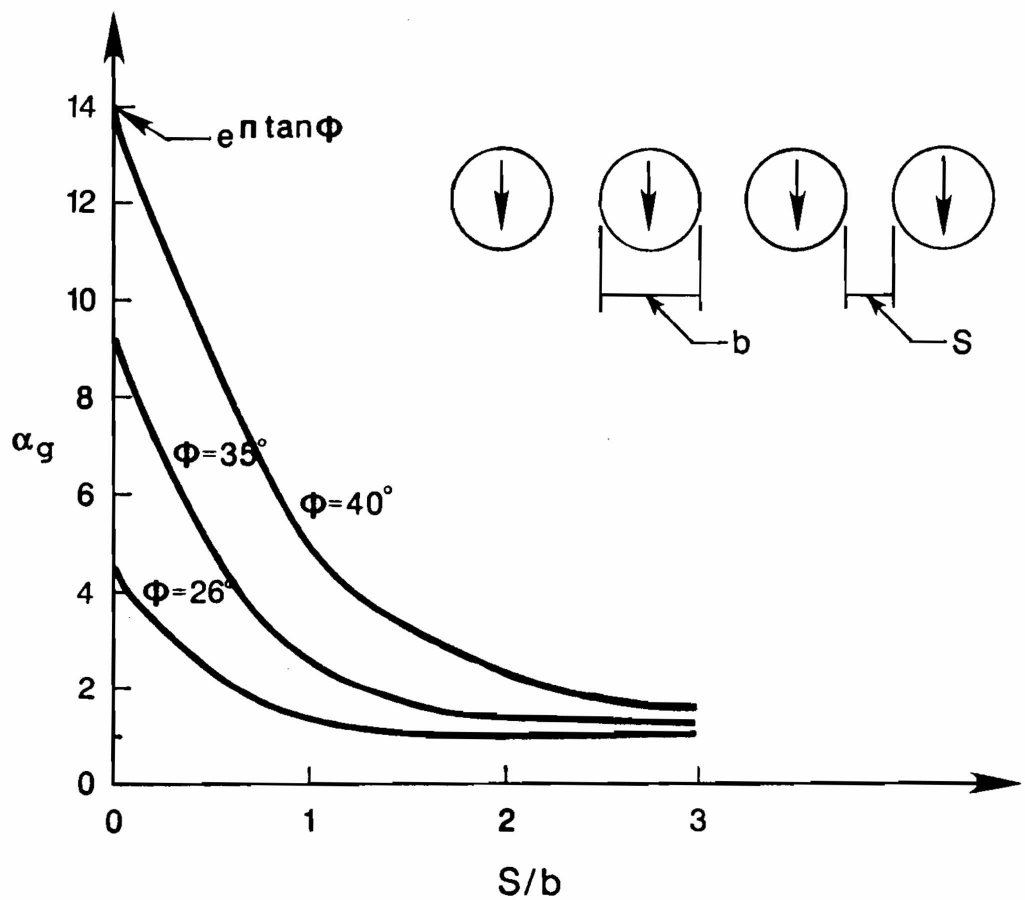

Fig. 6.50. Recommended α_g-factor for piles in a row in sand.

component that needs to be included in developing p-y curves for drilled-shaft retaining walls.

General Remarks Based on Elastic Stress Distribution

The effect of pile spacing on the interference of stresses may be evaluated theoretically using the distribution of stresses beneath a loaded area. The distribution of compressive stress in an elastic half-space for an uniform strip loading at the ground surface, calculated using the Boussinesq equation is shown in Fig. 6.51. If the mutual interference can be ignored when the compressive stresses are less than 10% of the applied surface pressure, the approximate limits on pile spacing can be established by referring to Fig. 6.51. Generally speaking, the effects of group action disappear at a pile spacing of about 8b (b is the width of the loaded area) in the direction parallel to the load and 3b in the direction normal to the load.

The elastic stress-distribution discussed above is limited to plane-strain condition. However, piles loaded by lateral forces are actually three-dimensional in space. To make a realistic study of the interaction between piles and soils, a three dimensional continuum-model is needed. Because of the complexity involved in the full three-dimensional analysis, a hybrid finite-element method is often employed for a footing or a pile in linearly elastic or visco-elastic media of infinite extent (Waas, 1972). In this approach, the soil profile is discretized in two-dimensional horizontal layers. A non-axisymmetric pile displacement pattern is represented by an equivalent Fourier series about the axis for each sublayer. The displacements are assumed to vary linearly within each layer, but have the exact analytical variation in the circumferential and radial directions. The three-dimensional nature of the problem is preserved because the three degrees of freedom associated with each ring (or named nodal circle). In each thin layer, a closed-form solution is used to solve for components of stress and strain and reduces the computation by a great amount. A computer code ELPILE, based on this method, was developed for this study, to compute the stress and strain in the surrounding medium due to pile deflection.

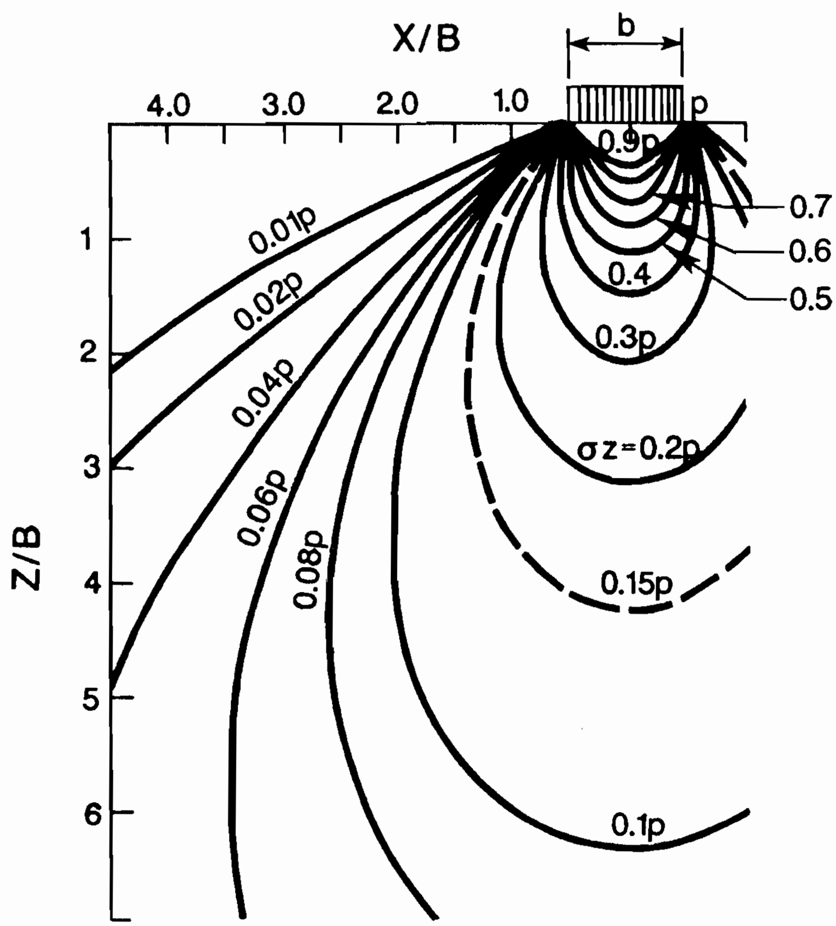

Fig. 6.51. Isobars of vertical normal stresses due to a strip load.

For piles in a group, stress and strain in the medium are obtained simply by the superposition of the components of stress and strain from individual piles. Although, the model is not truly three dimensional, it does consider the interactions between piles and soils from every direction. The distribution of the stress and strain in soil in front of a group of piles was studied with the method. The deflection curve along the length of the pile (Fig. 6.52) was assumed to be the same for each pile and the deflection corresponding to each sublayer was input as the displacement boundary. There are total of 9 piles standing in a row and the clear spacing between piles varied from 3-pile diameters to zero for the case studies.

The γ_{max} (maximum shear strain) of one diameter away from the center pile in the direction of pile movement was plotted versus depth as shown in Fig. 6.53. It is apparent in the figure that pile spacing larger than 2 diameters has negligible group-effects. However, the influence of nearby piles became important when the spacing between piles was small.

Figure 6.54 presents the stress distribution in a horizontal plane about one diameter below the ground surface. The difference between the single pile and piles in a row is obvious. The stress is distributed uniformly at a distance of about one diameter from the pile surface.

Mindlin's Equation

The displacement of a particular point within the soil mass is influenced by loads at other points in the same medium. The soil near the drilled shaft has significant amount of displacement because of the elastic reaction of piles in a group. The movement of the soil must be considered in the proposed p-y criteria in order to predict the correct soil resistance.

The mathematical algorithm for computing the elastic deformation is contributed by Mindlin (1936), who developed expressions for the vertical and radial displacements of a point within a semi-infinite elastic mass due to point loads within the medium (Fig. 6.55). A lateral displacement due to the horizontal

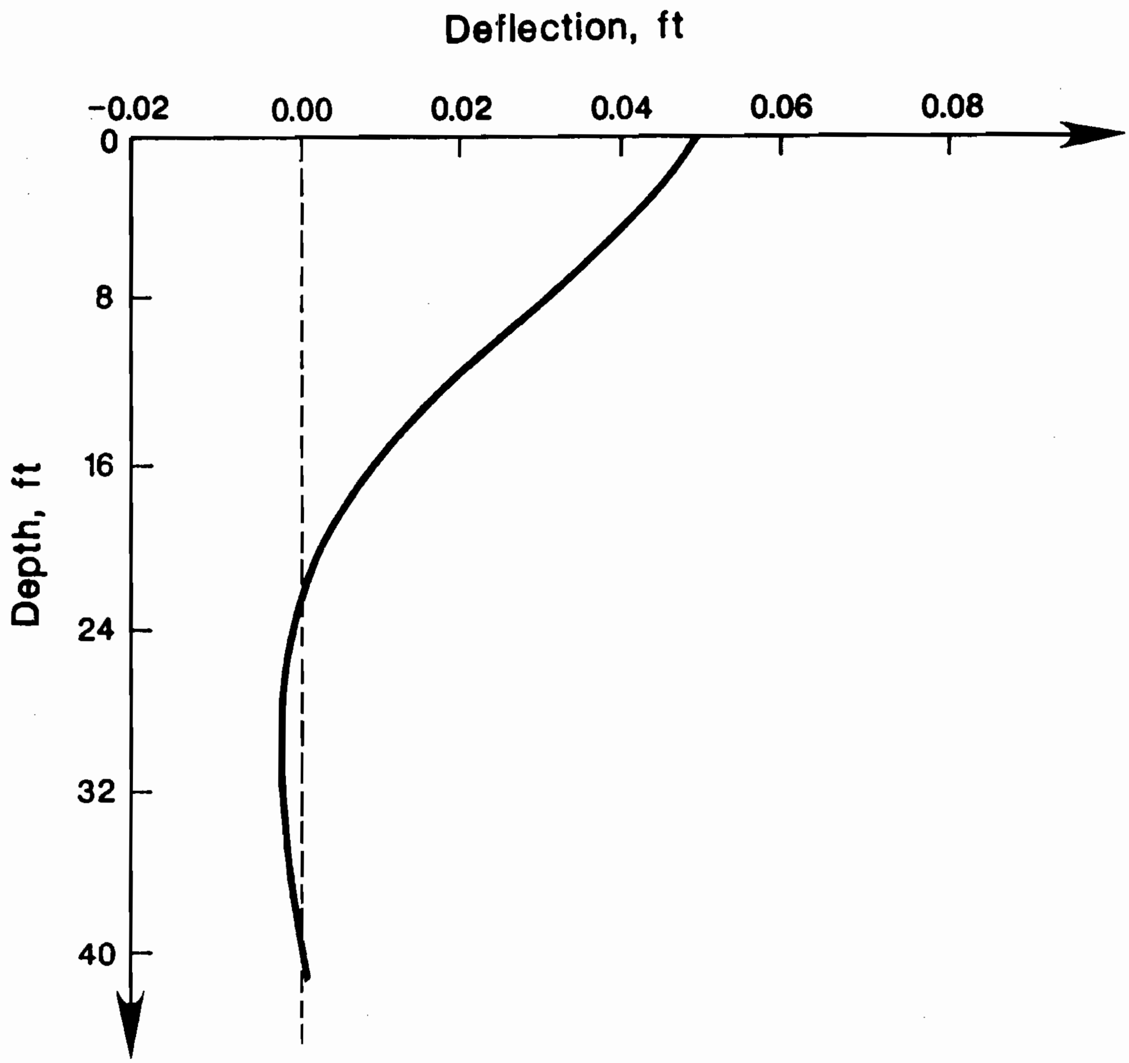

Fig. 6.52. The lateral deflection of piles for studying the elastic group-effect.

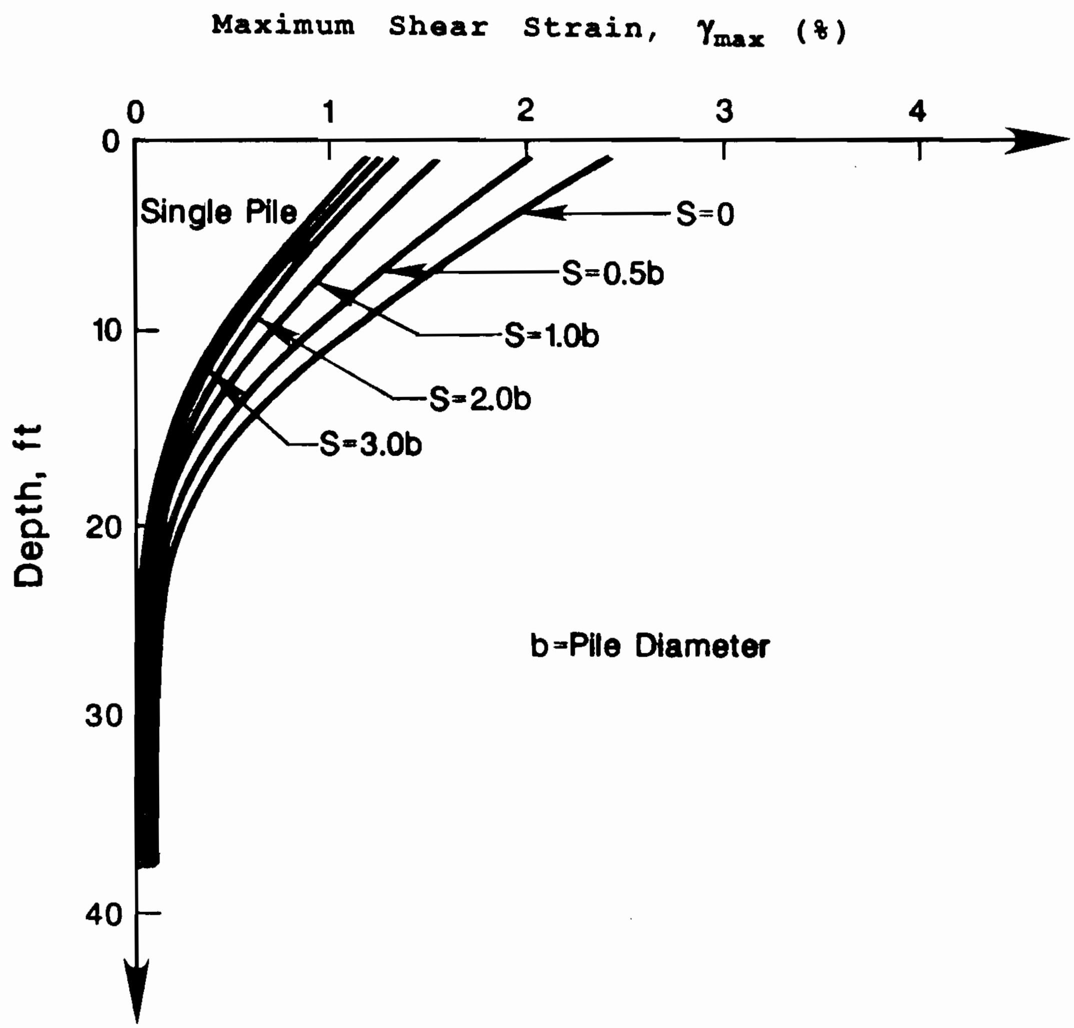

Fig. 6.53. Maximum shear strain along the pile length for different pile spacings.

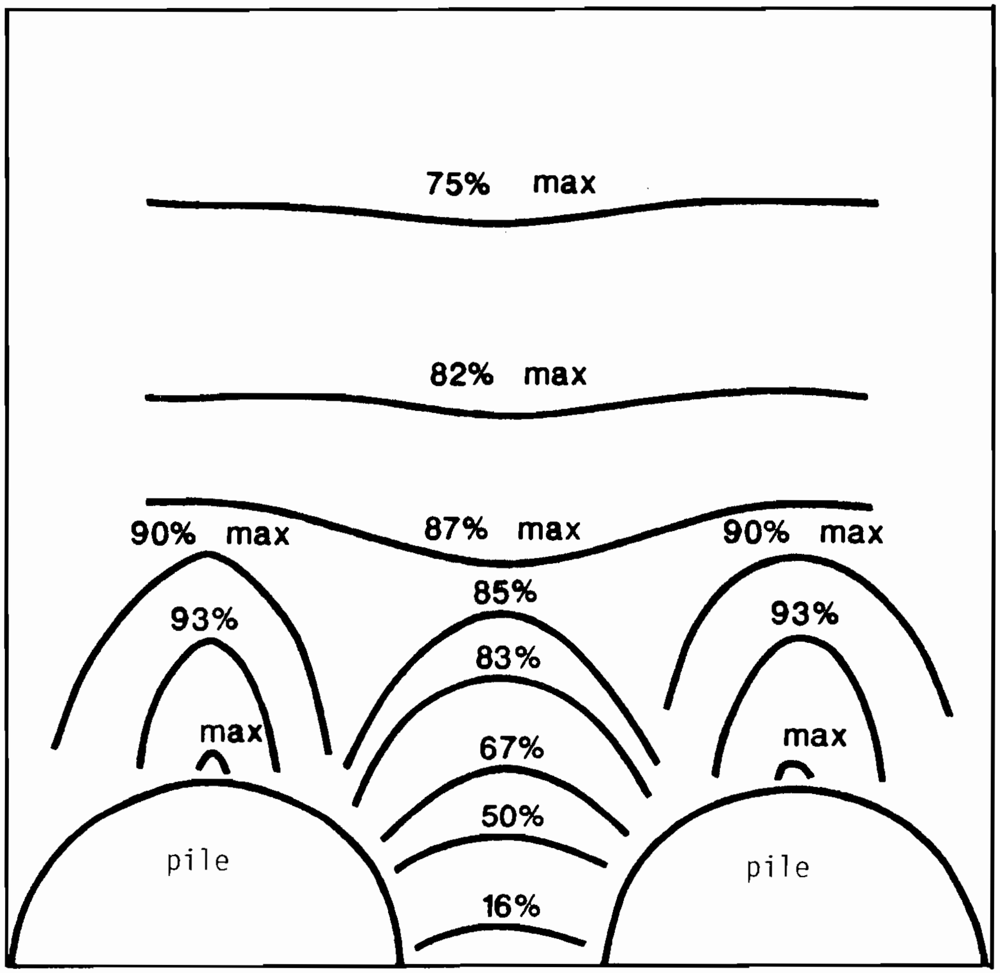

Fig. 6.54. Contours of the normal stresses in plane at one diameter below the ground surface.

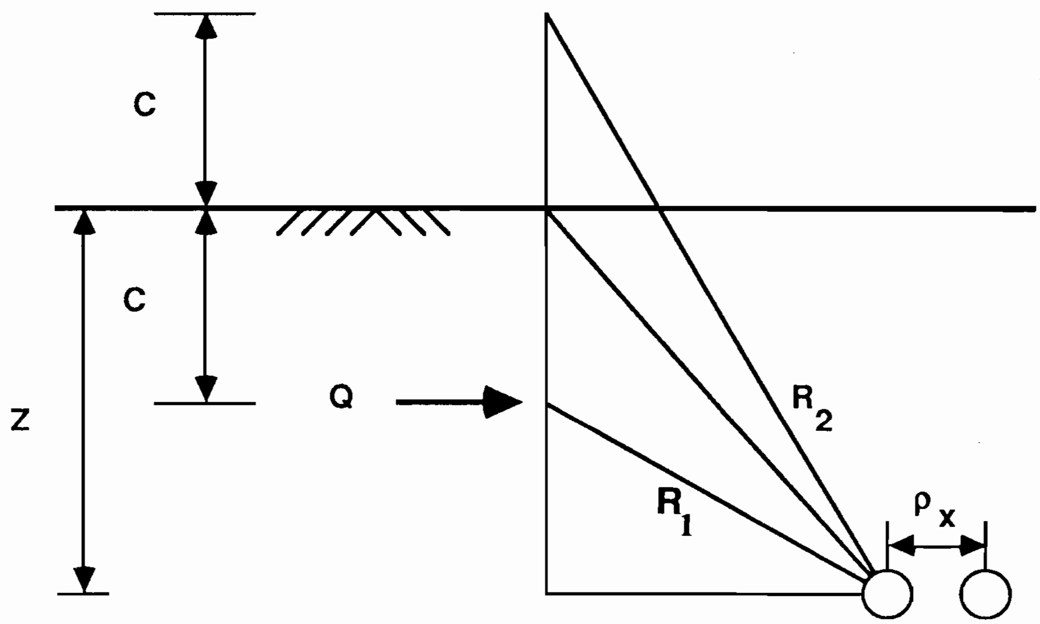

Fig. 6.55. Mindlin equation for horizontal displacement due to a point load.

point Q acting beneath the surface of a semi-infinite elastic mass is

$$\rho_x = \frac{Q}{16\pi G \, (1- \upsilon)} [\frac{3 - 4\upsilon}{R_1} + \frac{1}{R_2} + \frac{x2}{R_1{}^3} + \frac{(3 - 4\upsilon) \, x^2}{R_2{}^3} + \frac{2CZ}{R_2{}^3} \, (1- \frac{3x^2}{R_2{}^2}) + \frac{4 \, (1 - \upsilon) \, (1 - 2\upsilon)}{R_2 + Z + C} \, (1 - \frac{x^2}{R_2 \, (R_2 + Z + C)}) \tag{6.44}$$

where

G = shear modulus of the elastic mass, and
υ = poisson's ratio of the elastic mass.

The additional deflections of soils around the n-th drilled shaft due to the loads against the m-th drilled shaft in the system (Fig. 6.56) can then be computed from Eq. 6.44. It is assumed that uniform horizontal pressures on each discrete element of the m-th drilled shaft were replaced by equivalent point loads acting at the center of the element and that the drilled shafts have the same properties as the surrounding soil. Because there is no drilled shafts parallel to the direction of loads in drilled-shaft walls, Eq.6.44 can be simplified to

$$\Delta d^{ni}_{mj} = \frac{Q^{mj}}{16\pi G \, (1- \upsilon)} [\frac{3 - 4\upsilon}{R_1} + \frac{1}{R_2} + \frac{2CZ}{R_2{}^3} + \frac{4 \, (1 - \upsilon) \, (1 - 2\upsilon)}{R_2 + Z + C}] \tag{6.45}$$

The Procedures of Analysis

It is found above that there is essentially no influence of one drilled shaft on another, providing the spacing normal to the direction of loading is at least 3 diameters. Based on this consideration, the computation of elastic group-effect is limited to drilled shafts that have a center to center distance of three diameters or less.

The mathematical equation for summing up those additional displacement is expressed as

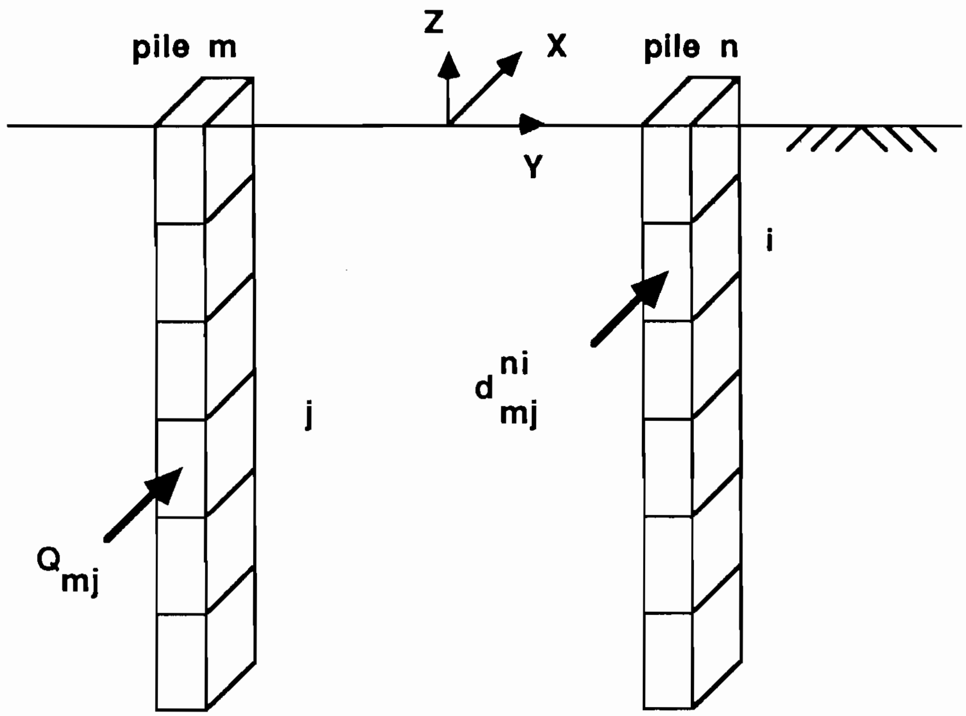

Fig. 6.56. Elastic displacement on pile n due to load Q on pile m.

$$\Delta D_{mj}^{ni} = \sum_{\substack{m=1 \\ m \neq n}}^{M} \sum_{j=1}^{K} \Delta d_{mj}^{ni} \qquad (6.46)$$

where

M = the total number of drilled shafts in the influence zone of group effects,

K = the total number of increments on each drilled shaft,

Δd_{mj}^{ni} = the displacement at node i of drilled shaft n due to the pressure on the node j of drilled shaft m, computed from Mindlin equation, and

ΔD_{mj}^{ni} = the total elastic displacement at node i of drilled shaft n due to the group reaction.

The step-by-step procedures for the computation scheme are:

(1) At the end of each iteration of deflection computation, distributed pressures on every increment of drilled shafts, which are included in the group reaction, are computed and converted to an equivalent lump force acting at the center of the element.

(2) The additional displacement at the i-th node of a denoted drilled shaft n is computed from Eq. 6.46.

(3) Modify the p-y curve at node i by adding the displacement obtained from step 2.

(4) Use the deflection of drilled shaft computed from step 1 and obtain the new resistance p from the modified p-y curves. Solve the difference equation with the new obtained soil resistance P.

(5) Repeat step 1 to step 4 until the solution converges.

In developing curves giving soil resistance (p) as a function of pile deflection (y), the different boundary surfaces at the front and the back of the drilled-shaft wall should be taken into account. In general, the p-y curves developed for piles under a plane surface are symmetric on each side as indicated in Fig. 3.4.

However, due to the different ground levels at the front and at the back of the wall, the p-y curves have become unsymmetric about the vertical axis as shown in Fig. 6.57. The additional soil deflection that results from the elastic group-effects of nearby piles also offsets the p-y curves to a certain amount. The computer code developed for this study is capable of handling these unsymmetric soil-resistance curves.

To observe the potential influence from the elastic group-reaction, a case of a row of drilled shafts embedded in sand with zero clear spacing was studied. The deflection at the head for varied lateral loads is about 30% higher than those without group influence (Fig. 6.58). For a loading of 20 kips at the top of a drilled shaft, these additional deflections are plotted along the length of drilled shafts in Fig. 6.59.

It is interesting to note that the added displacement is in the same direction as the applied load for almost all points along the pile. The maximum influence occurs at points near the ground surface and gradually decreases towards the tip of the drilled shaft.

SUMMARY

This chapter describes the analytical procedures for developing p-y curves for drilled-shaft retaining walls. The hybrid method was employed in this study to take into account the effects of pile groups this study. The equations used to compute the ultimate soil resistance for the wedge-type failure were derived based on the limit-equilibrium analysis. The flow-around failure, based both on the slip-line method and the finite-element analysis, were used to develop the recommended equations. Group effects from the elastic reaction are included in the p-y relationship. The Mindlin equation provides a simplified means of calculating the additional deflection due to the interaction of piles in a group.

The procedures of modification of p-y curves for a drilled-shaft wall can be summarized as follows.

1. Compute the ultimate soil resistance for a wedge-type failure per unit length of the drilled shaft in sand. Use

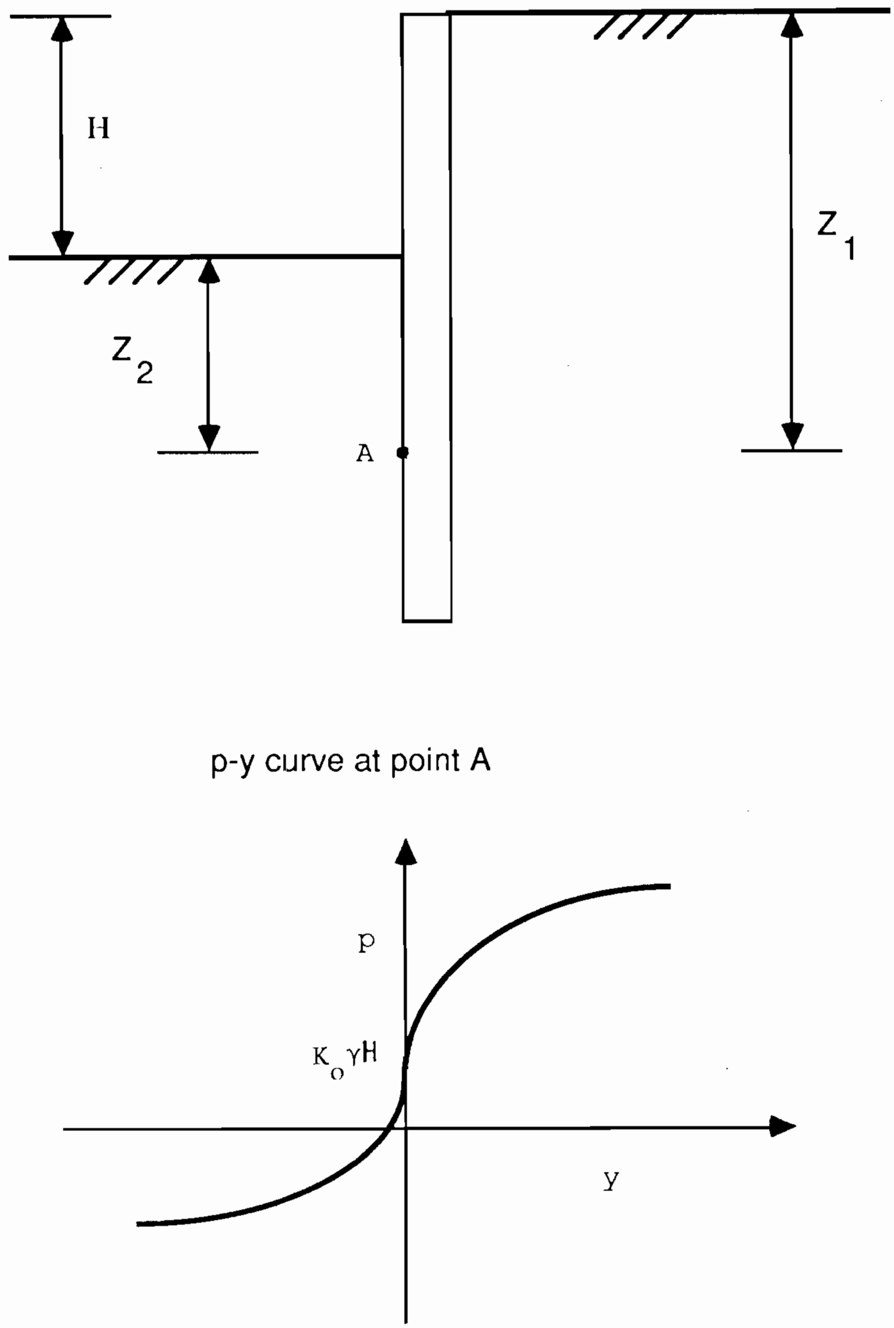

Fig. 6.57. The unsymmetric p-y curve on drilled-shaft walls.

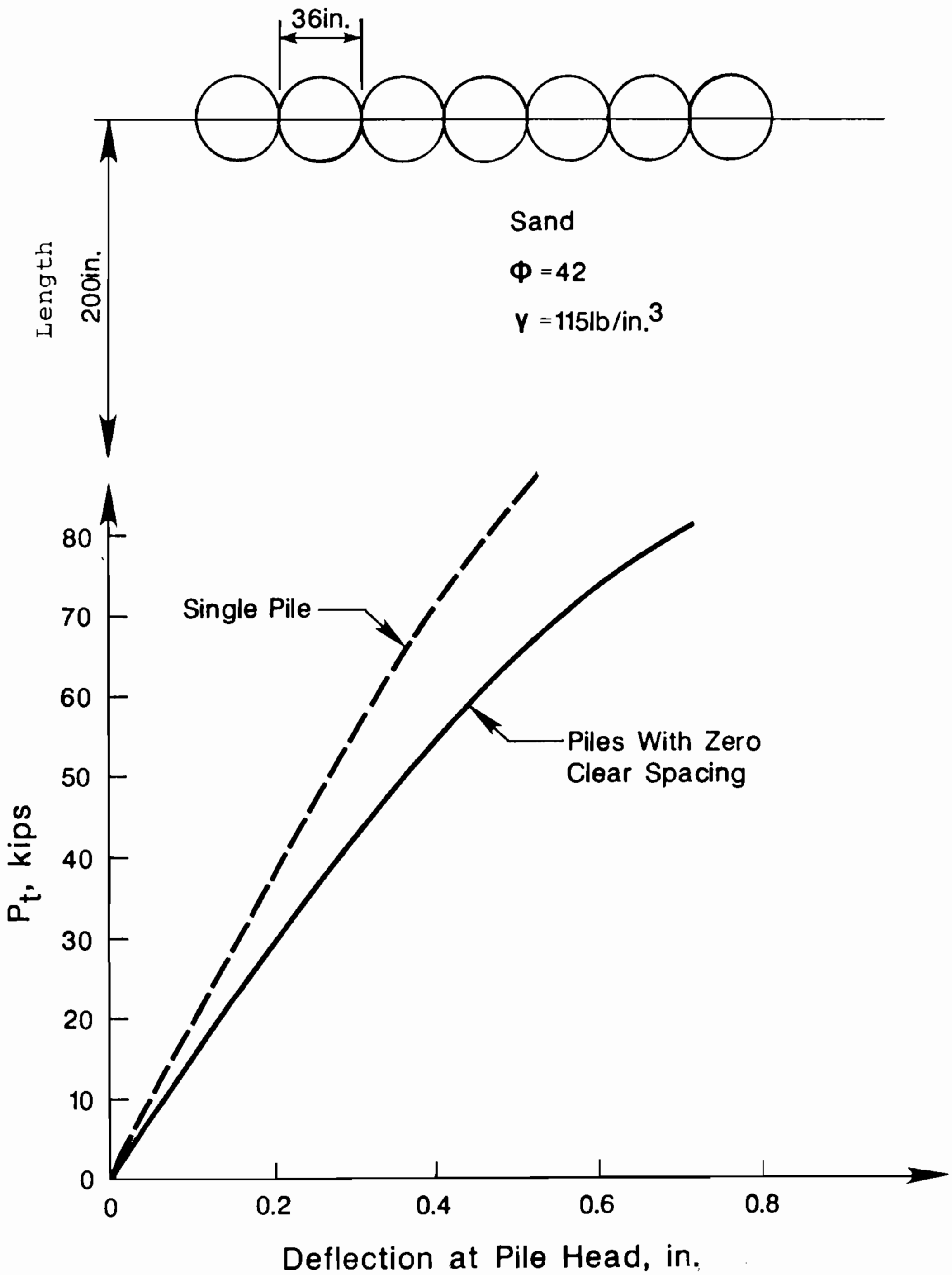

Fig. 6.58. Influence of elastic group effect on load-deflection curves.

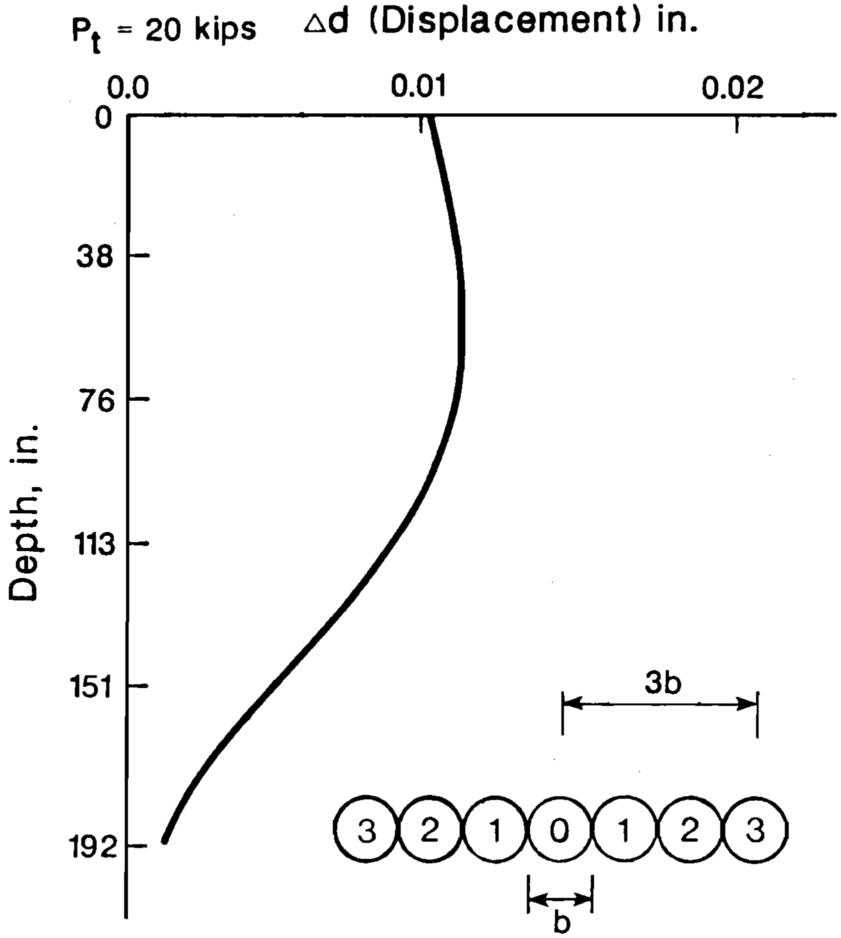

Fig. 6.59. Additional displacement due to the elastic group effect.

Eq. 6.24 to include the shadowing effect if the clear spacing is less than $2H\tan\alpha\tan\beta$. Use Eq. 6.25, recommended by Reese (1984) for single piles, to compute the ultimate soil resistance if the clear spacing is larger than $2H\tan\alpha\tan\beta$.

2. Compute the ultimate soil resistance for a wedge-type failure per unit length of the drilled shaft in clay from Eqs. 6.28 and 6.29. Use Eq. 6.29 to take into account the shadowing effect if the clear spacing is smaller than the value recommended by Eq. 6.30; otherwise, use Eq. 6.28 for the ultimate soil resistance in clay.
3. Compute the ultimate soil resistance of flow-around failure using equations (Eqs.6.32 and 6.33) developed for single piles. To account for the shadowing effect, modify the ultimate soil resistance of single piles by the α_g-factor, that is recommended in Fig. 6.49 for clay and in Fig. 6.50 for sand.
4. Select the smaller value of ultimate soil resistance between the wedge-type failure and flow-around failure.
5. Construct the p-y curve in the same manner as for single piles by following the criteria recommended by Reese (1984) after the ultimate soil resistance has been selected.
6. Take into account the elastic-group effect using the Mindlin equation. The soil movement due to the elastic reaction can be ignored if the clear spacing between two drilled shafts is larger than 2 diameters. The elastic movement of soil at a particular depth can be computed internally in the computer program, PYWALL.
7. The p-y curve for drilled-shaft retaining walls is completed after adding the elastic soil movement from step 6 to the curve obtained from step 5.

The proposed p-y criteria for drilled shafts in a row, that have the group effects taken into account, are believed to be a rational method for use in the analysis of soil-structure-interaction problems.

CHAPTER 7. TESTING OF SMALL-SCALE PILES UNDER LATERAL LOADING

INTRODUCTION

It was felt that experimental work was needed to verify and supplement the theoretical predictions made by this study. Full-scale tests in the field are expensive and often not possible due to economic considerations. Because soil behavior is strongly dependent on stress level, scale effects must be considered when model tests are used to predict prototype behavior. By taking into account scale effects in the small-scale-model tests in the laboratory, useful quantitative results can be easily obtained to improve prediction methods that are based primarily on theoretical considerations.

The main purpose of this experimental program was to provide information about the validity of the prediction of soil resistance on side-by-side piles, as discussed in the previous chapter. The tests used cohesive and cohesionless soils. The model piles used for this test were 1-in.-diameter aluminum tubes. A preliminary analytical study of the proposed pile was made to determine an adequate length of embedment with at least two zero-deflection points along a pile (Swan, Wright, and Reese 1986). The results of this study are shown in Figs. 7.1 and 7.2. Based on this study, the model pile was required to have the wall thickness of 0.035 in. for the proper range of the flexural rigidity, and 24 in. for the embedded length. To limit the effects of the size of the container on the results from tests, pile deflection and load were measured on only the center piles in a transverse row. The behavior of a single, isolated pile with the same pile-head conditions in the same soil was also measured. Therefore, a direct comparison could be made of the response of an isolated pile and for one pile in a closely-spaced group. A wooden bin, 15

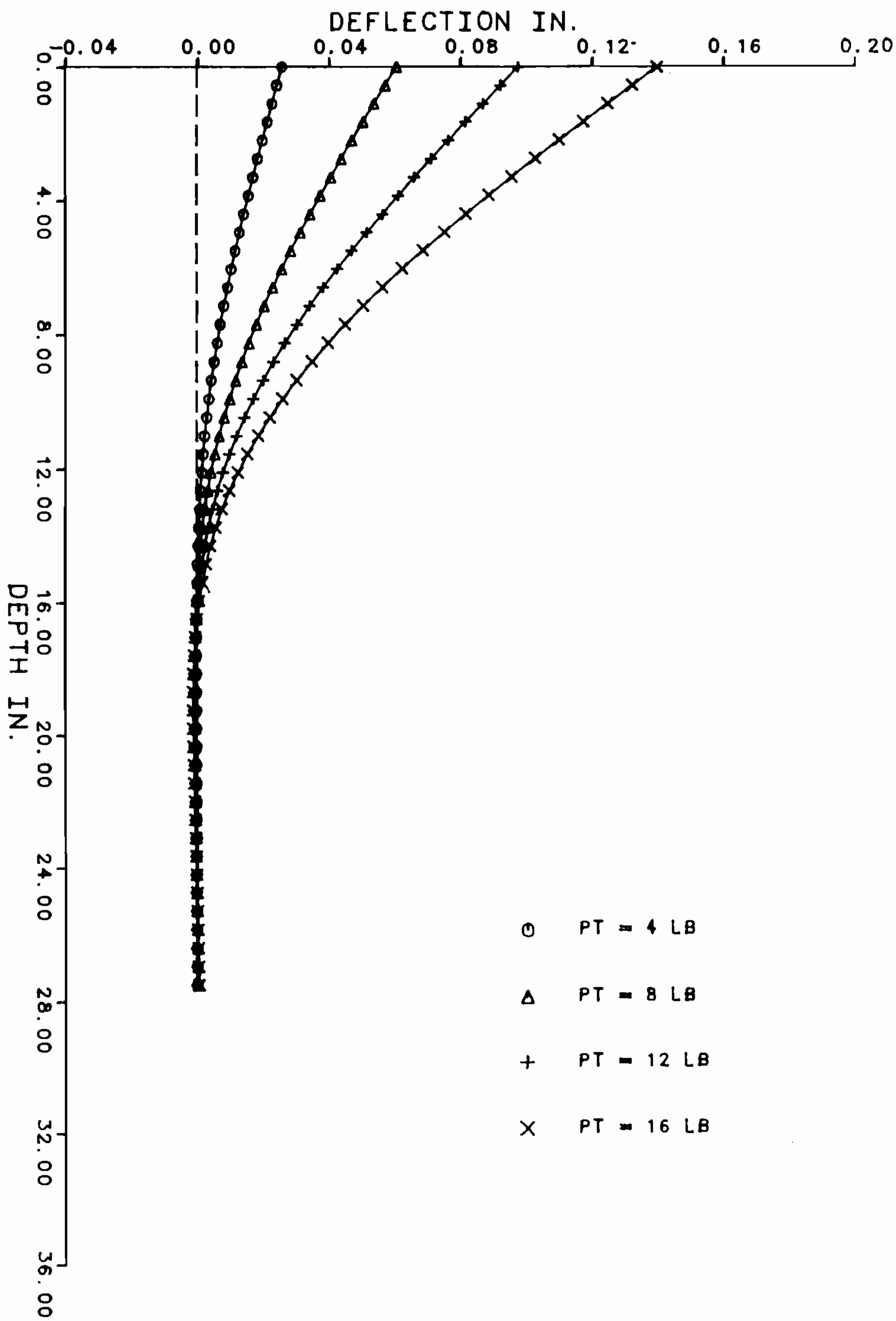

Fig. 7.1. Preliminary study for the piles embedded in sand.

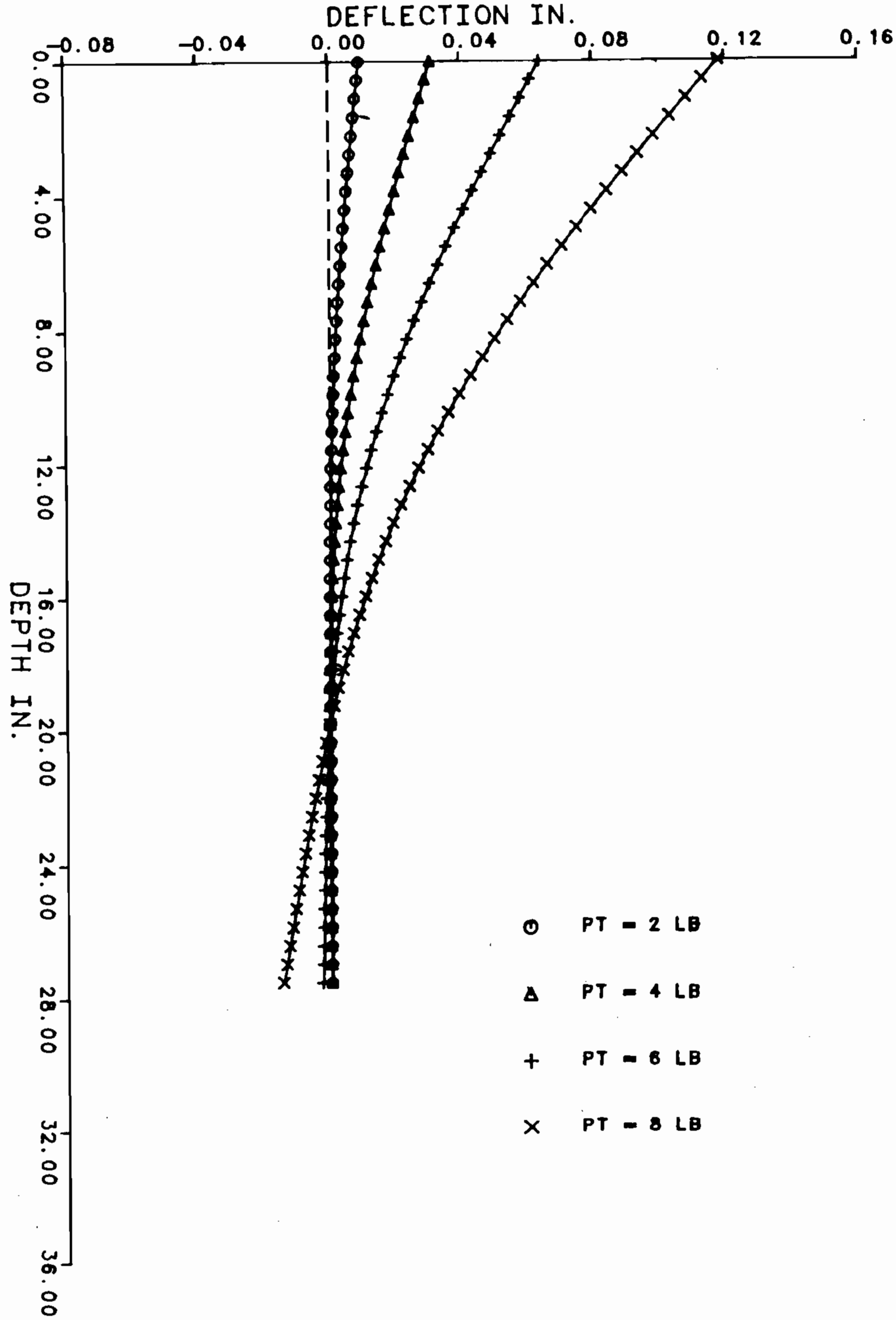

Fig. 7.2. Preliminary study for the piles embedded in soft clay.

in. wide by 36 in. deep by 48 in. long, was built to contain the pile group and also a single pile. The inside wall of the bin was covered by a plastic membrane to prevent the soil from drying. The clear spacing between side-by-side piles was selected to be 0, 0.25, 0.5, 1.0, 2.0, and 3.0 diameters for each case. The loadings were static and short-term. A photograph of test arrangement is shown in Fig. 7.3.

It was recognized that the sides of the bin would probably influence the behavior of nearby piles; therefore, it was decided to place the test pile completely across the bin but to use the measurements from only the center piles.

TEST SETUP

Selection of Soil

The cohesive soil for the test was made from pulverized fire clay, obtained from the Elgin Butler Brick Co., Austin, Texas. The dried fire clay was packaged in 50-lb bags and most of the particles passed a #100 sieve. The clay is greyish in color and the moisture content at room temperature was about 3%. The liquid limit was 53 and the plastic limit was 20. The classification using the Unified Classification System is CH, a high plasticity clay.

The cohesionless soil used in the tests was washed mortar sand, which was classified as SP by the Unified Soil Classification System. A gradation curve for this sand is shown in Fig. 7.4. The sand has a mean grain diameter, D_{50}, of 0.55 mm and a uniformity coefficient, C_u, of 1.70. The specific gravity of this sand is 2.67 and the moisture content at room temperature was about 0.3%.

Placement of Soils and Piles

Uniformity of soil properties was the basic requirement for the placement of soils in the test container. The dried clay provided by the manufacturer, was mixed to several different water contents, and it was found that a high water content provided more uniform properties and good workability. Therefore, a moisture content of 45% for the clay was selected for all tests. One bag of

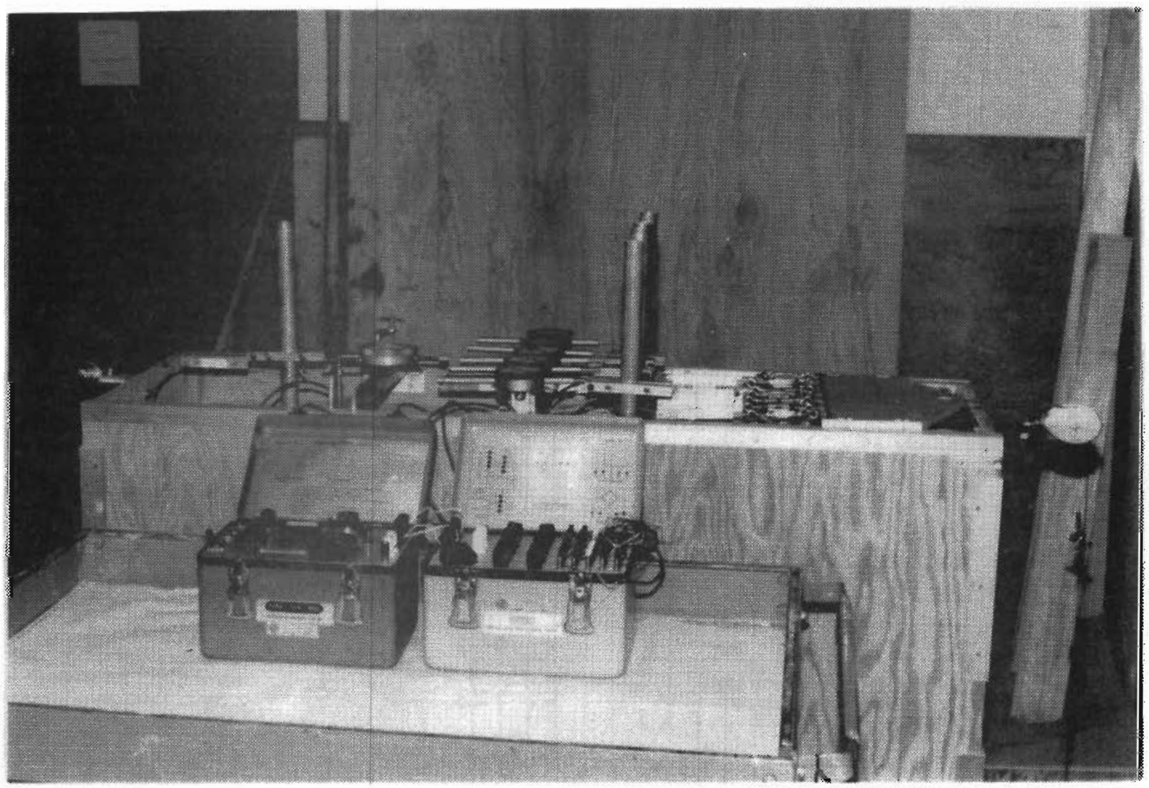

Fig. 7.3. Photograph of the test facility.

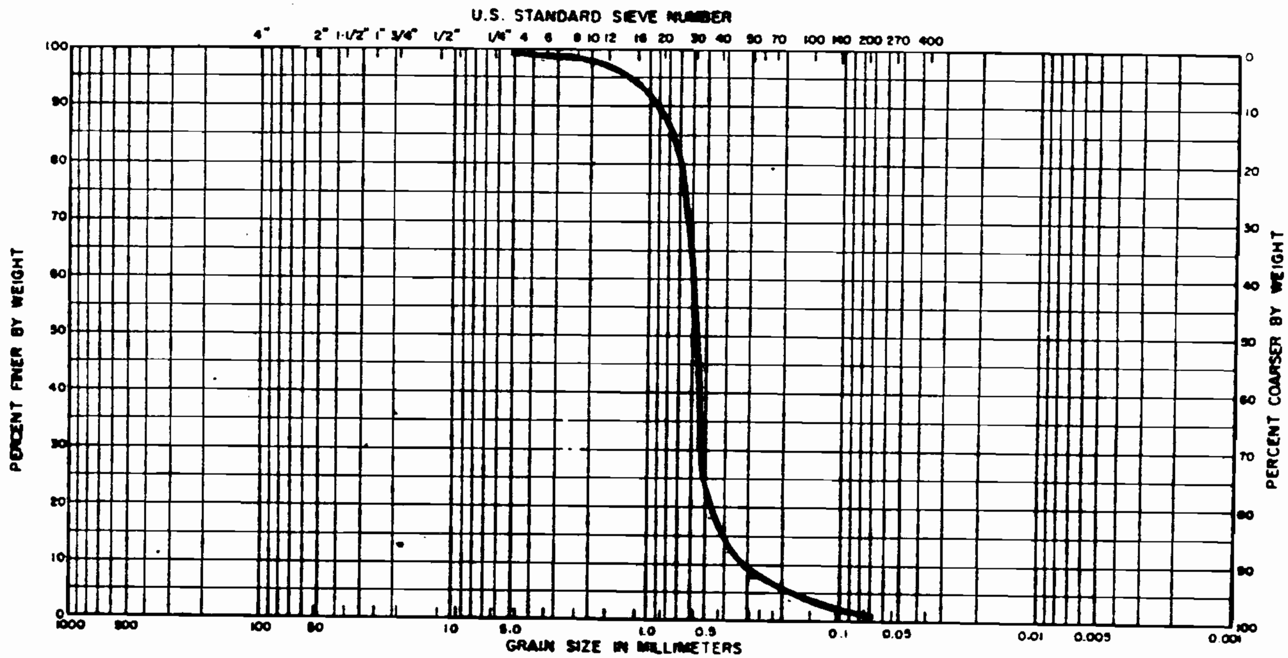

Fig. 7.4. The gradation curve of washed mortar sand

soil and the proportional amount of water were placed in a small container and mixed thoroughly using shovels. It took 20 to 30 minutes to mix one bag of clay. The clay was then placed into the test bin layer by layer. The surface of the soil was leveled and a plastic sheet was placed on the surface to prevent drying.

Five guides (Fig. 7.5) were built to help in placing the piles. Each guide had two levers of plates into which holes were drilled to give the model piles the desired spacing. Using a guide, the piles were pushed slowly into the soil. Because the clay in the container was remolded, the placing of a thin-walled tube is believed not to affect the soil properties by any great amount. After one set of tests was completed, the soil in the disturbed area was replaced by clay with the same physical properties and covered by a plastic membrane for about 24 hours before the next set of tests were begun.

Two soil densities were selected for tests using cohesionless soils. The first set of tests was conducted on piles in sand with a low density. The dried sand was filled uniformly into the soil container without compaction. It was decided that the best procedure for the tests in cohesionless soil was to place the soil around the piles rather than to drive them into place. After sand had been placed in the bin to the level of the tips of the piles, the piles were positioned in a guide and placement of soil continued until the required height was reached. Each batch of sand was weighed before it was placed into the container. The dry density of sand was calculated to range from 85 to 87 lb/cu ft.

The second group of tests in cohesionless soils was conducted in dense sand. The soil was placed in six-inch layers and each layer was compacted by use of a concrete vibrator that penetrated the sand about 6 inches. The vibrator was inserted into each layer at 90 different locations in the plan of the tank and vibrated 10 seconds at each location. The dry density of compacted sand was measured to be about 98 to 101 lb/cu foot.

Measurement of Soil Strength

The clay prepared for the tests had a high moisture content and low shear strength. The shear strength was measured using the

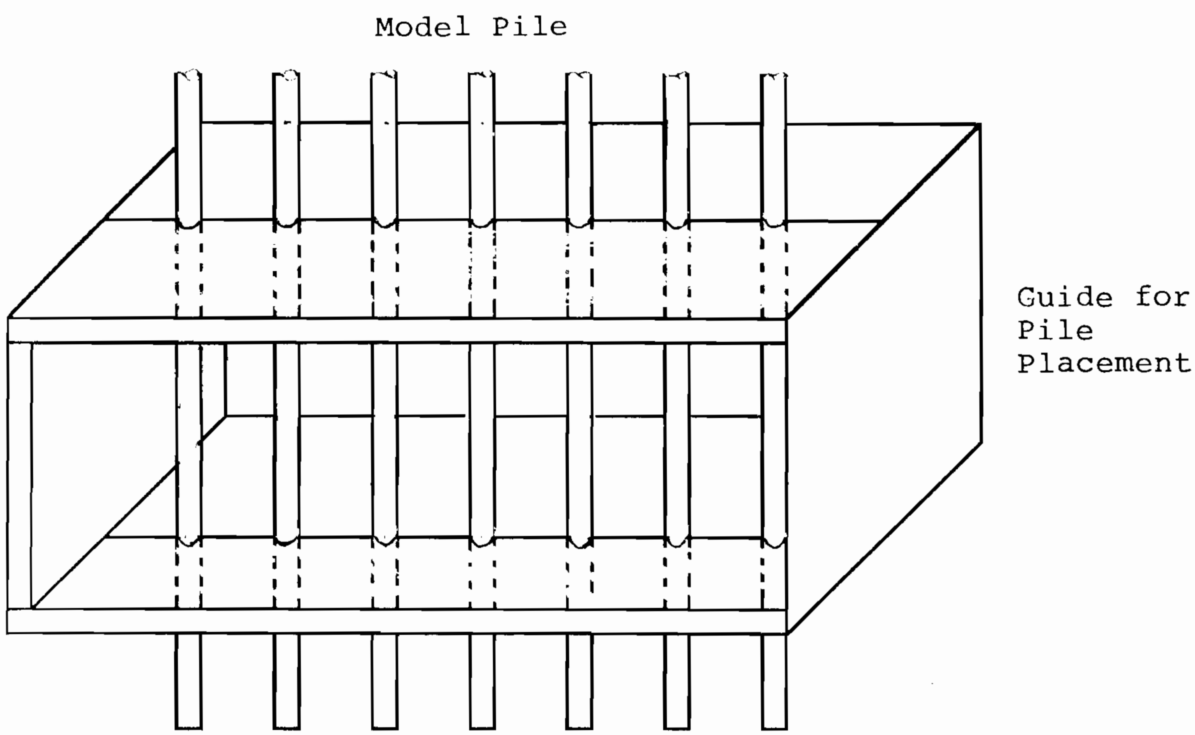

Fig. 7.5. The sketch of guides for the placement of piles

vane-shear test, a widely used method to estimate the undrained shear strength of very soft clay. A miniature vane was mounted on the top of the tank to measure the strength with depth. The vane size was 1/2 in.-diameter and 1/2 in.-length. Several 5/32 in.-diameter rods were prepared to allow testing at different depths. When using the vane, a hole was drilled to a desired depth and the vane was carefully pushed into the soil. For the greater depths, a tube was inserted into the pre-bored hole to prevent soil collapse.

The torque during the testing was obtained from a calibrated torque spring. The shear strength was calculated using:

$$S_u = \frac{T}{\pi\left(\frac{d^2h}{2} + \frac{d^3}{6}\right)} \tag{7.1}$$

where

S_u = undrained shear strength from vane-shear test,

T = maximum torque,

d = diameter of vane blades, and

h = height of vane blades.

The shear strength was measured at four locations in the container. The shear strength and moisture content are both plotted in Figure 7.6. The average shear strength was approximately 0.8 lb/ sq in. near the top and 1.1 lb/sq in. near the bottom of the container. The water content was about 46%.

To measure the stress-strain characteristics of the clay, Q-type triaxial tests were conducted. The soil was placed in a mold and then extruded to form a 1.5-in.-diameter by 3.0-in.-long specimen. Three specimens were tested and the undrained strengths ranged from 0.3 to 0.5 lb/sq in. As could be expected, the strength is lower from triaxial tests than from vane tests but it is believed that the stress-strain curve, as shown in Fig. 7.7, is reasonably representative.

The angle of internal friction ϕ for dry sand is difficult to measure because of difficulty in sampling. However, ϕ can be obtained by developing the correlation between ϕ and the relative

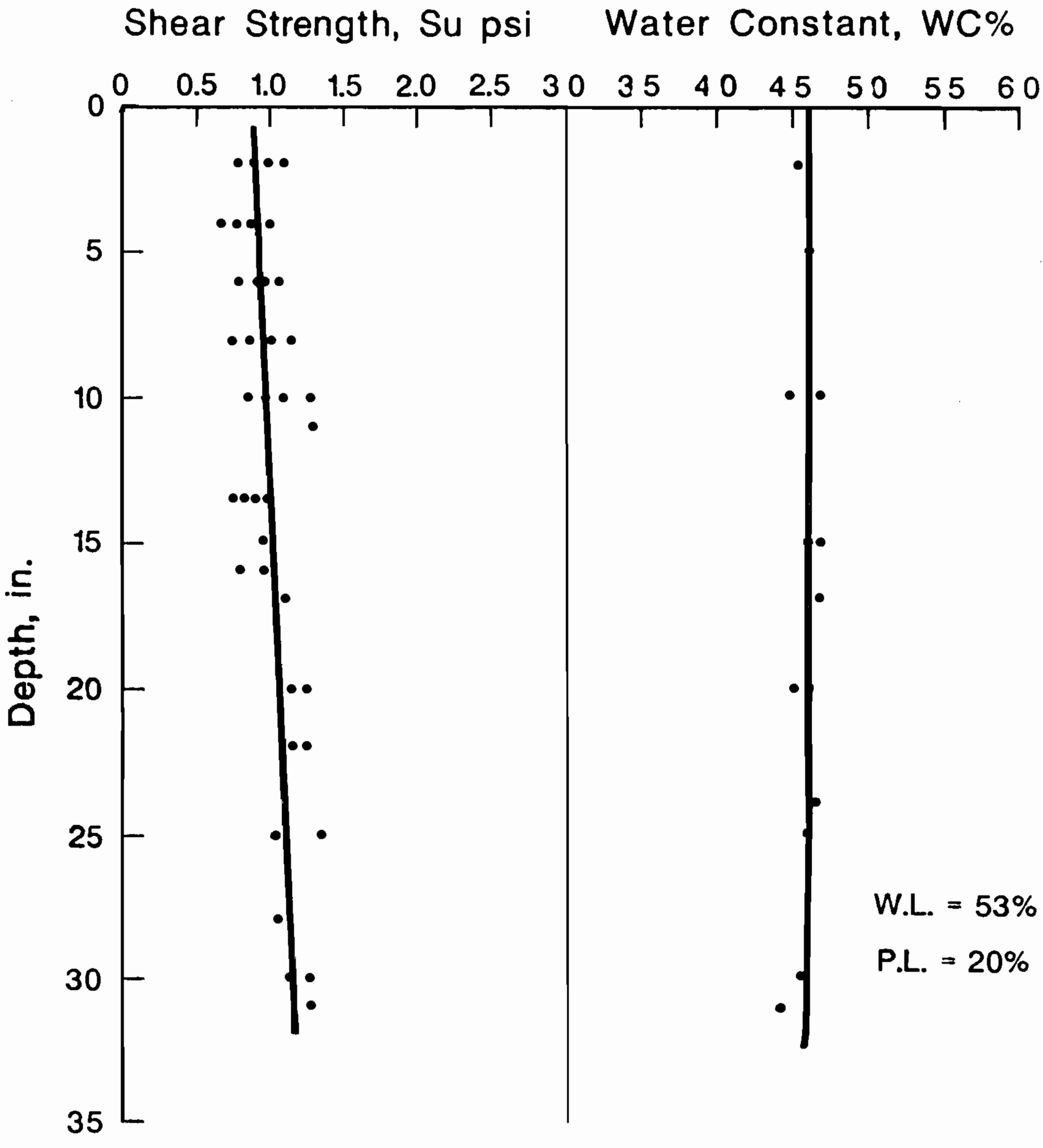

Fig. 7.6. The strength and moisture content profile in the soil tank.

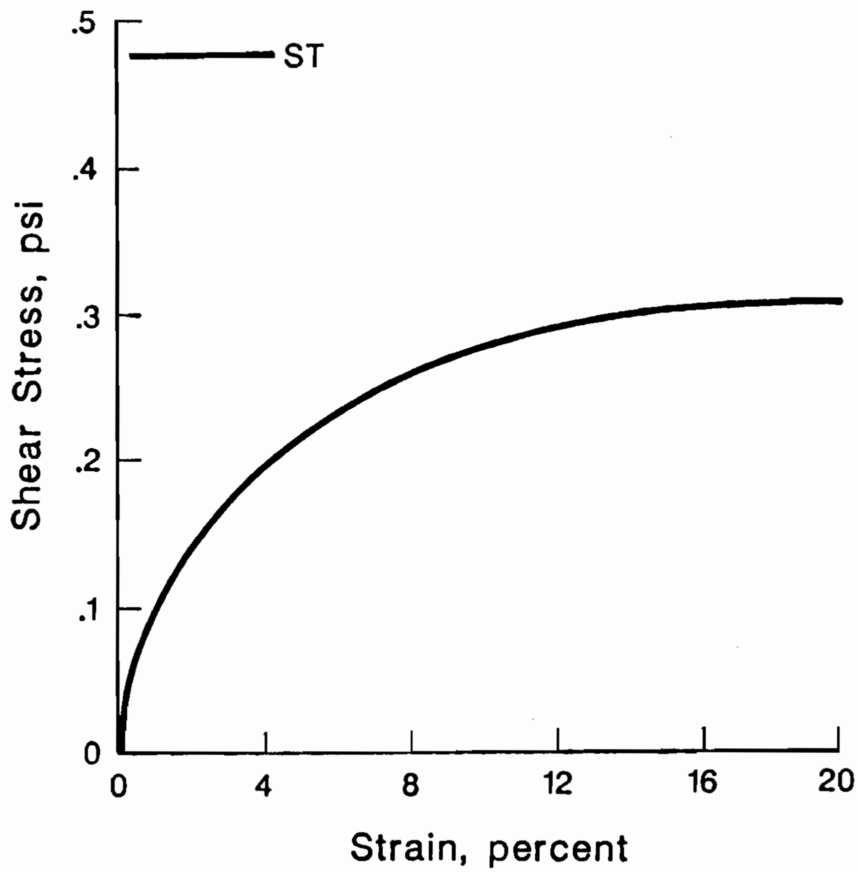

Fig. 7.7. The stress-strain characteristic of soft clay.

density for the sand used in the testing. The variation of ϕ with relative density of the same kind of sand was measured by Rix (1983) and is shown in Figure 7.8. The internal friction angle of dense sand was estimated to be about 40° and that of loose sand is about 34° using this figure.

Test Equipment

From a preliminary study, a maximum load for the pile-group tests was estimated to be as high as 400 lbs. An aircraft cable with 1000 lbs of tensile capacity was used to apply the load using dead wieghts. The wall passed across a pulley that was fixed to the end of the bin and attached to a rigid, metal wagon with 5 smooth bearings that was designed to transmit the load to the individual piles. The load was applied at the geometric center line of the plate. Thus, the wagon moved uniformly and allowed an equal deflection of each pile. The maximum load on individual piles was about 50 lbs. The connection between each pile included a load cell and a turnbuckle for adjustment of the length of the connection. A photograph of the test set-up is shown in Figure 7.9.

Load cells. Strain gauges were used to construct the load cells. The guages were type No. EA-06-250TG-350, Micro-Measurements Group, with a 1/4-inch gauge length. The strain gauge data provided by the manufacturer are listed below:

TABLE 7.1. STRAIN GAUGE DATA

Resistance	350.0 + 0.2% ohms
Gage factor at 75° F	2.06
Gage factor tolerance	0.5%

Aluminum plate, 4 in. long, 1/2 in. wide, and 1/16 in. thick, was selected for the load cell because it gave an appropriated strain under the small load. A full-bridge was used, as shown in Fig 7.10, to measure the strain in the plate. The advantages of a full-bridge system are the elimination of variation in output due

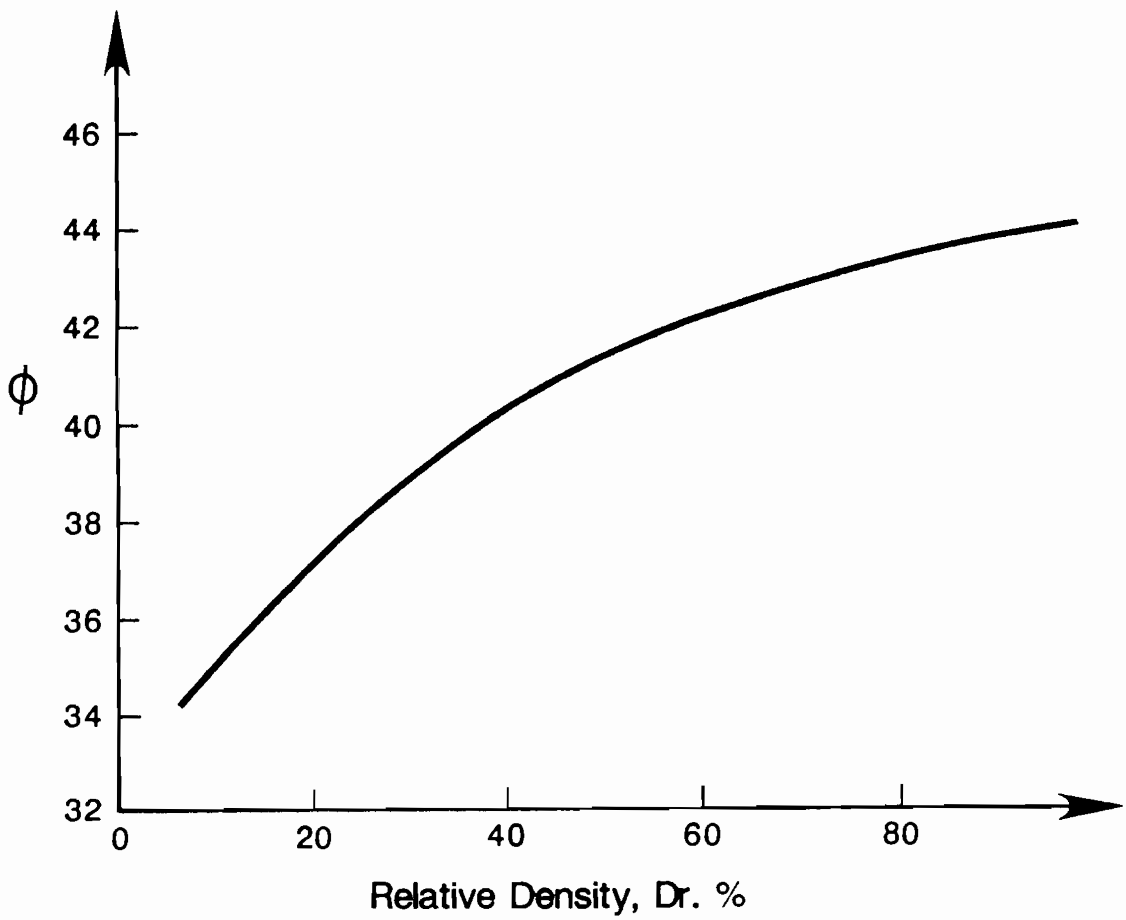

Fig. 7.8. The variation of internal friction angle and the relative density (after Rix, 1983).

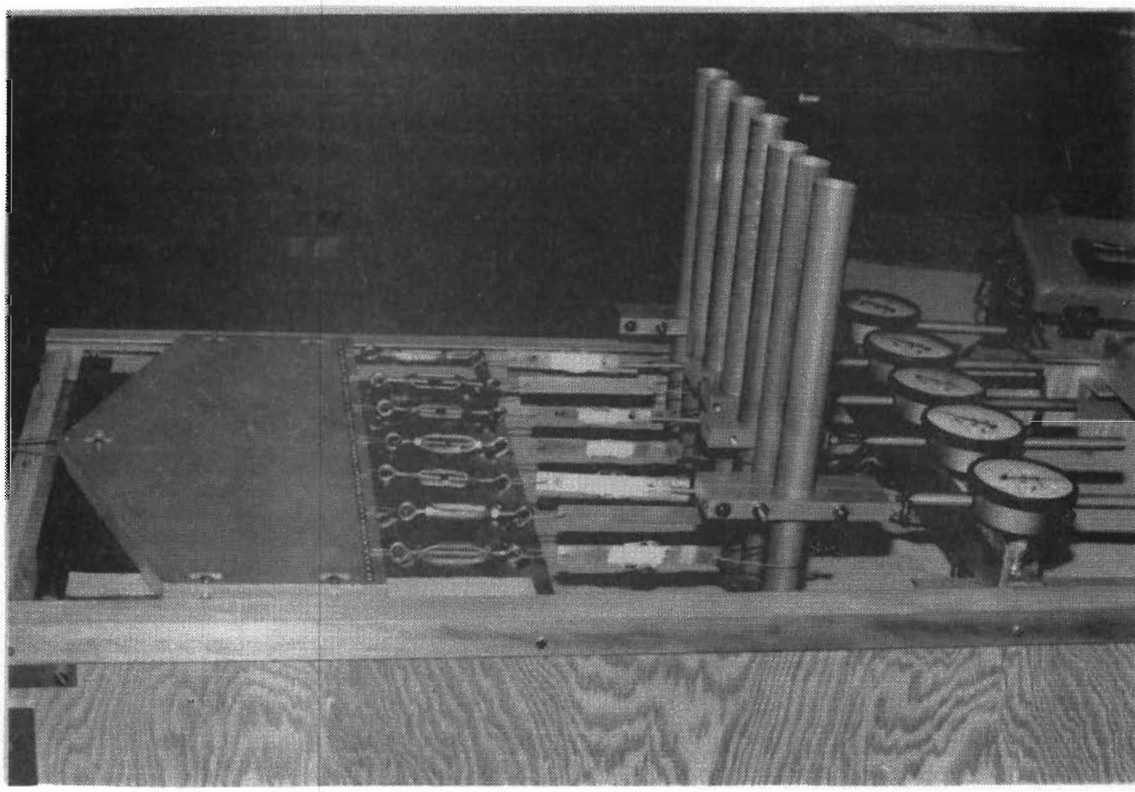

Fig. 7.9. The detailed photograph of the loading system.

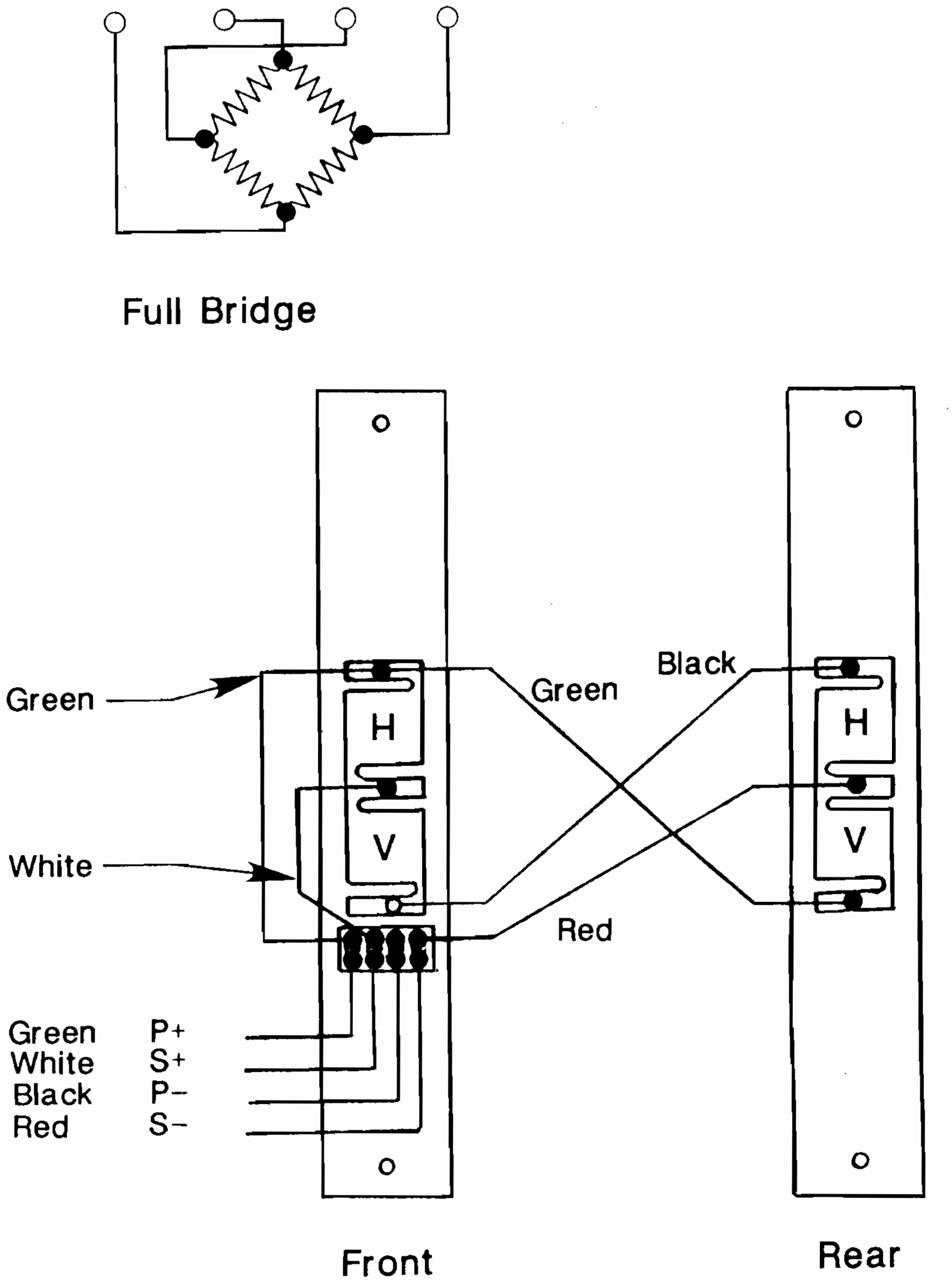

Fig. 7.10. The design of full bridge for load cells.

to temperature and greater sensitivity than a half-bridge system. The manufacturer's instructions were carefully followed in attaching the strain gauges to the plates. A suitable coating was applied after gauge installation to protect the gauges. Each load cell was calibrated up to a maximum load that was about 60 pounds.

Dial indicator. The horizontal deflection of the piles was measured using dial gauges with a sensitivity of 0.001 inch. The dial gauges were mounted on a cross beam placed at 3 inches above the surface of the soil. Each dial indicator was adjusted so that it was lined up and activated by a flat surface affixed to each pile.

Test Procedures

With the pile group and a single pile in place in the selected soil, the pile length above the soil surface was measured to ensure the penetration was the same for each pile. For the pile-group test, loads were applied by using dead weights. If the deflections of piles due to the seating load were different, the space between the wagon and the piles was adjusted by use of the turnbuckles until relatively uniform deflections were obtained for each pile in the group. For the isolated pile, a steel wire across a pulley transfered the weight on the loading platform to a load cell, then to the pile. After the loading system was set up, the electrical conductors from each load cell were connected to a switch-and-balance unit. The strain was read by a Vishay strain indicator.

In all tests, a constant load was applied in several increments until deflections seemed to be accelerating with time or until the deflection was at 15% to 20% of the pile diameter. The increment of loading was about 2 lb. per pile. Readings were taken after the deflection reached a constant or stable value. For cohesionless soil, it took only a second or two to get a constant dial reading after the load was applied. For clays, it took 5 to 10 seconds for deflection to become stable value, depending on the magnitude of the load. Because the experiment was aimed at determining short term behavior, any long-term effects due to the consolidation or creep were excluded during the testing.

TEST RESULTS

Pile Tests in Clay

A total of 6 tests on side-by-side groups of piles in soft clay were conducted in the laboratory. Figure 7.11 shows the results of the lateral force and corresponding pile deflection at a point about 3.5 in. above the soil surface for a single pile from the group. The results show the consistency of measurements. Therefore, the soil conditions for each test were assumed to be similar.

In the pile-group tests, the load-deflection curve for the piles in the center region were measured. The complete data can be found in Appendix C. The load-deflection curve for a single pile, obtained for the same soil conditions, is also presented in the Appendix for comparison. Although the data contained some scatter; in general, the soil resistance per pile decreases as the pile spacing decreases. If the load-deflection curve for a pile in the geometric center of the group represents as a typical result for the specified spacing, then the test results for group of piles with different spacings can be plotted together for comparison as in Fig. 7.12. As seen in the figure, the load increases for a given deflection as the spacing is increased to a point where there is two diameters of clear space between the piles.

Reese (1984) has pointed out that the failure of a laterally loaded pile can result from excessive deflection or from excessive stress in the pile material. If the pile is defined as "short", it will have one point of zero deflection (its tip will deflect) and excessive deflection will probably control. If the pile is "long", there will usually be two or more points of zero deflection and stress in the pile material will probably control. The pile penetration selected in this test program is not short; therefore, stress in the pile material would control the failure or collapse load. For purposes of comparing the load on a pile as a function of pile spacing, it was decided to define the failure load or ultimate load as that corresponding to a pile deflection

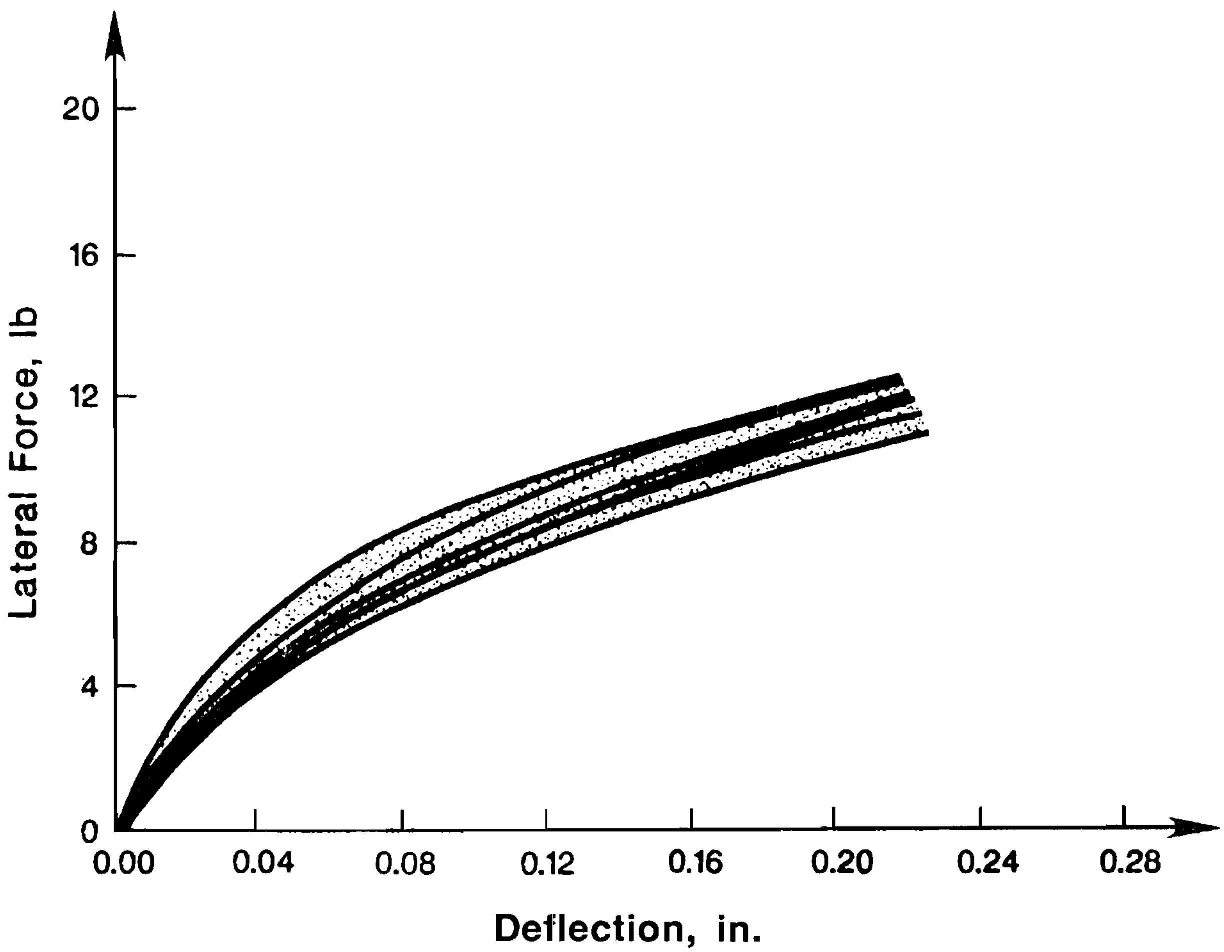

Fig. 7.11. Load-deflection curves of single piles from different tests in soft clay.

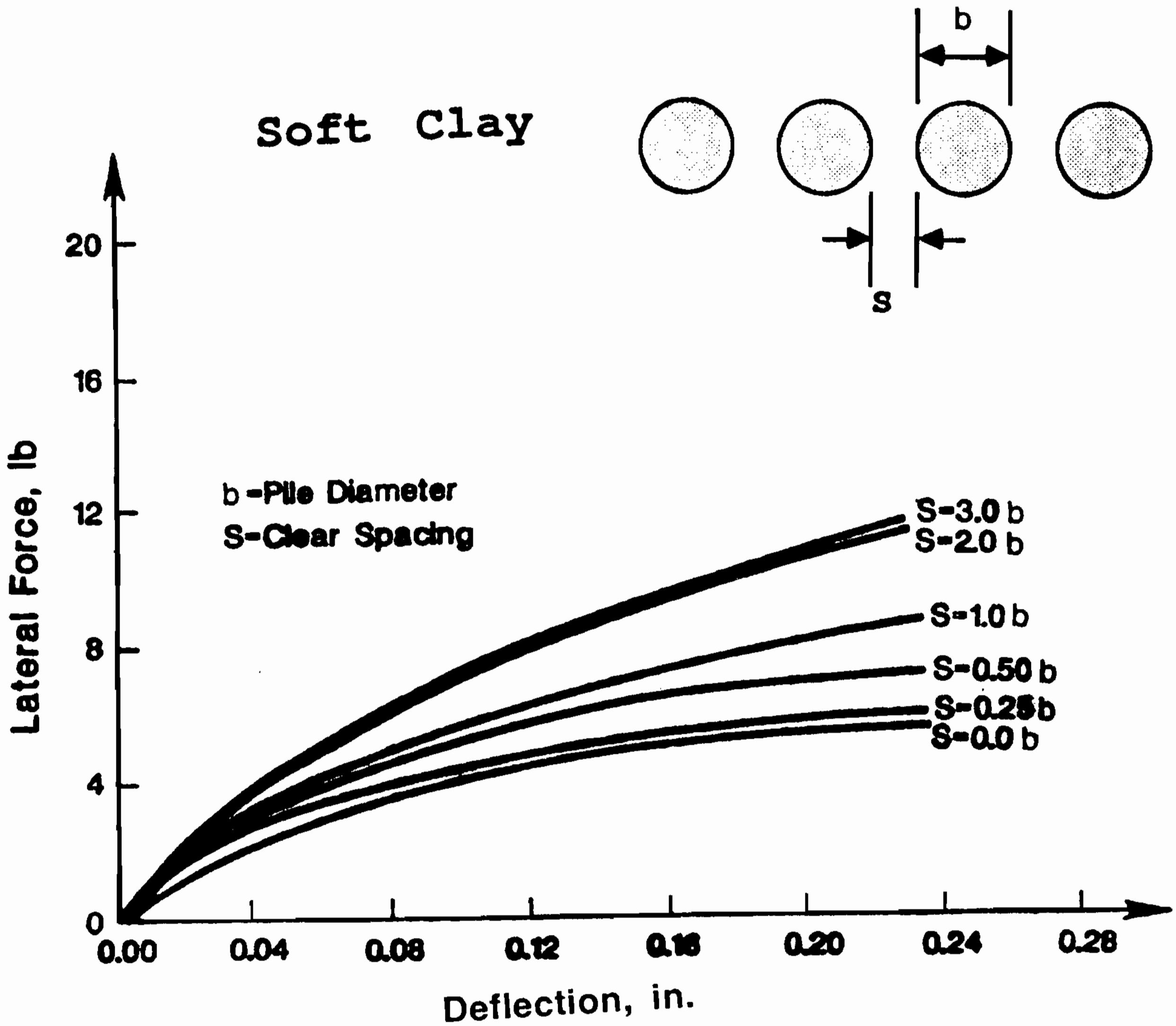

Fig. 7.12. Load-deflection curves for the center pile from the group with spacing varied, tests in soft clay.

of 20% of the pile diameter. Thus, the relationship between the ultimate load and pile spacing, shown in Fig. 7.13, was obtained for piles in soft clay. As shown in the figure, soil resistance decreases rapidly when the pile spacing is less than two pile diameters. Clear spacings of two diameters or more are sufficient for developing capacities that approach those for isolated piles. The ultimate load ratio is usually defined as the ultimate load for a pile in the group divided by the ultimate load for a single pile. The lowest value of the ultimate load ratio shown in Fig. 7.13 is about 0.5 for piles without any clear spacing.

Comparison of Results for Piles in Soft Clay with Results from Literature

Several studies have been made to investigate the efficiencies of side-by-side piles under lateral loading. Cox, Dixon, and Murphy (1984) conducted lateral-load tests on 1-in.-diameter piles in very soft clay in side-by-side and in-line groups. Although the soil properties and the boundary conditions for the piles in the Cox tests were quite different from this study, a general comparison between the results is of interest.

The soil used by Cox et al was Wilcox clay, which contains 85% to 90% kaolinite. The Atterberg limits were 61 for the liquid limit and 21 for the plastic limit. The dried and sieved particles of clay were mixed with water and then placed in a steel container that had dimensions of 25 in. × 25 in. × 23 inches. The soil had a uniform moisture content of approximately 59% and a shear strength of 0.29 psi, as determined by a miniature vane.

Strain bars were used as the transducers for measuring load in individual piles. The pile penetrations of 4, 6, and 8 diameters were selected in the tests for side-by-side groups. The clear spacings were selected as 0.5, 1, 2, 3, and 5 pile diameters and the number of piles in a group was limited to 3 or 5 piles. The pile group was assembled in a frame in which each pile was fixed in the desired position. The group tests were run at a rate of horizontal movement of 0.038 in./min. The readings were recorded using a digital data-acquisition system. Most group tests were run for a total horizontal travel of approximately 0.29

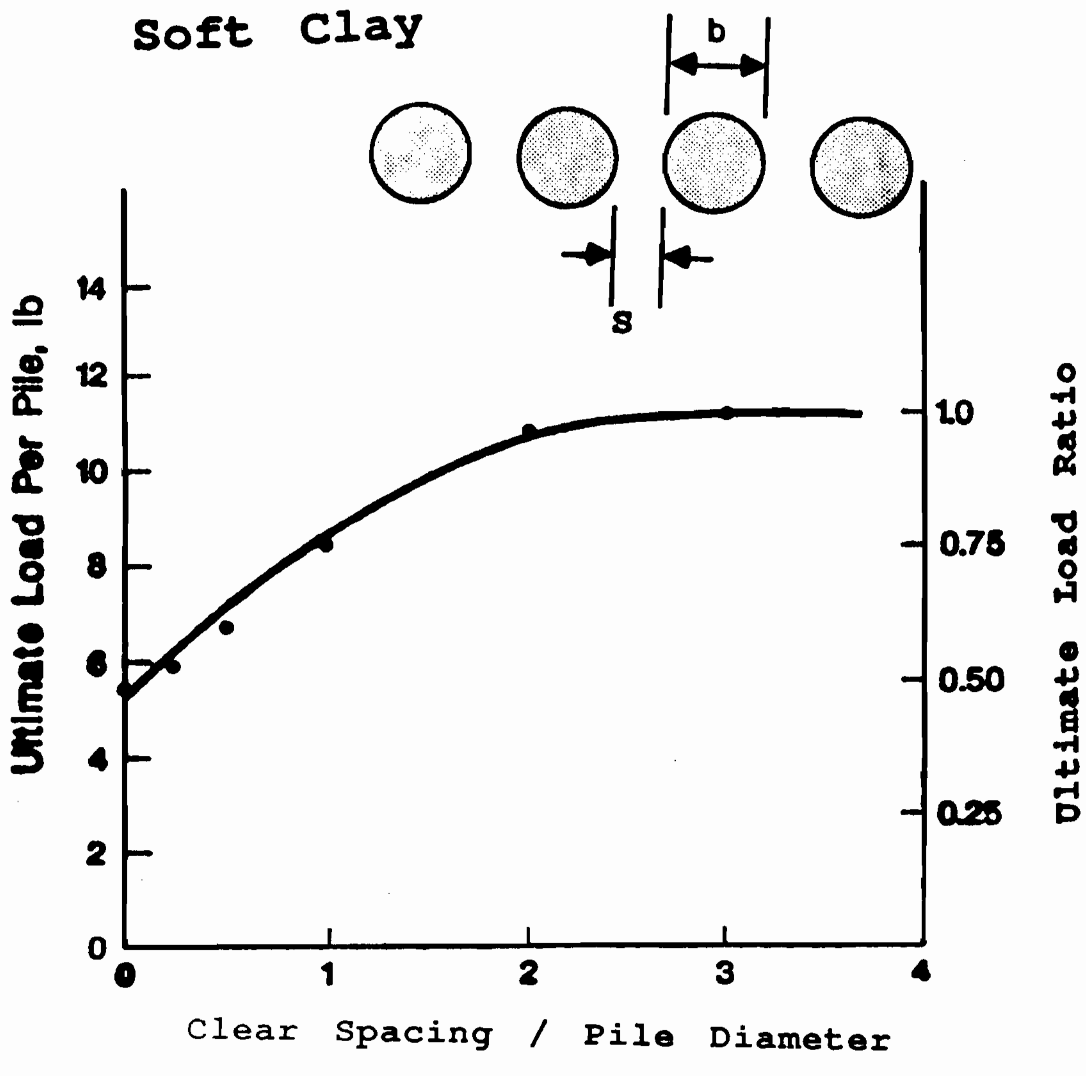

Fig. 7.13. Ultimate load per pile from pile-group tests in soft clay with various pile spacings.

in. This amount of travel was sufficient to develop the ultimate resistance of pile groups for the short penetration.

Cox et al found a remarkably uniform distribution of the total load to each pile in the groups. The load-deflection curves for side-by-side three-pile groups in the Wilcox clay with eight-diameter penetration are presented in Fig. 7.14. As may be seen, the ultimate soil resistance is well-defined because of the short penetration. The results indicate that the ultimate soil resistance was reached if pile deflection at the mudline is larger than 10% of pile diameter. The average ultimate load ratio versus the clear pile spacings from all tests, including those for experiments described herein, are shown in Fig. 7.15. The ultimate load ratio of groups with three piles at four-diameter penetration and 0.5-diameter clear spacing was 0.76 in the Cox tests. The tests performed in this research for the same pile spacing but with 10 piles in a group give an ultimate load ratio of about 0.62. The high ratio of about 0.99 for three piles at eight-diameter penetration with a clear spacing of three diameters agrees well with the test results obtained in the experiments in this study.

Generally speaking, the measured data from the two different experiments provide valuable information for understanding the behavior of groups of side-by-side piles in soft clay.

Pile Tests in Sand

There are two sets of data from tests described herein of piles in sand. The results for pile groups tested in loose sand will be discussed first; then the results from tests in dense sand will be discussed. The results of tests of single piles in loose sand which accompanied the tests on pile groups are plotted in Fig. 7.16. The scatter in these curves is relatively small and the soil conditions for each test are believed to be close to the same. The ultimate load corresponding to the pile deflection of 0.2 diameter at the loading point is about 10 pounds.

The results from tests of side-by-side groups are shown in Appendix C. There is some scatter in the data; however, the influence of pile spacing can be found. The load-deflection

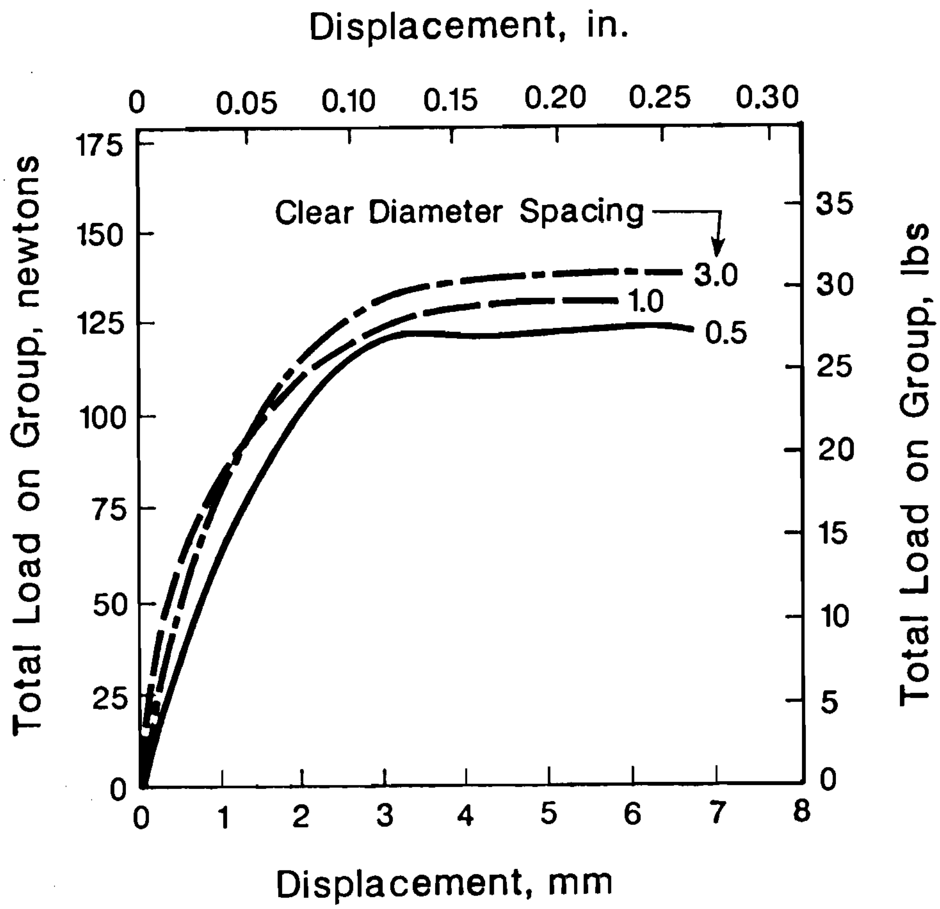

Fig. 7.14. Load-deflection curves for side-by-side three-pile groups in clay with eight-diameter penetration (after Cox et al, 1984).

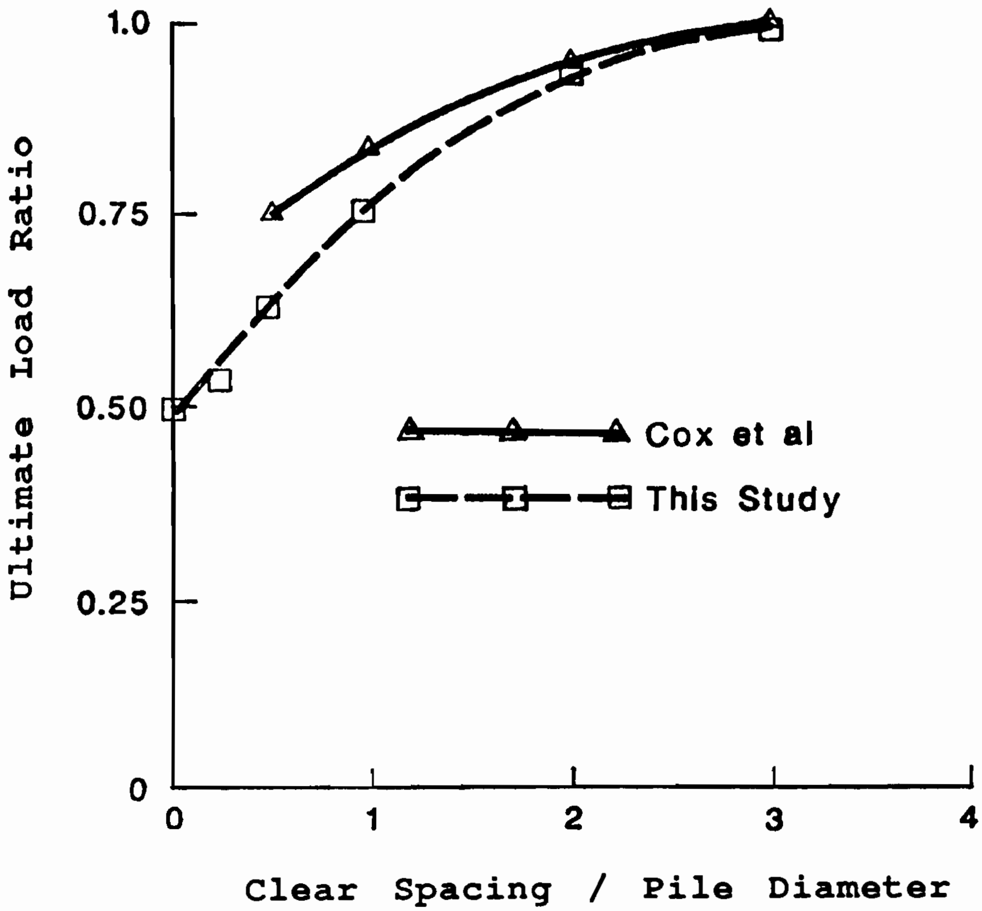

Fig. 7.15. The average ultimate load ratio from available test results for piles in clay.

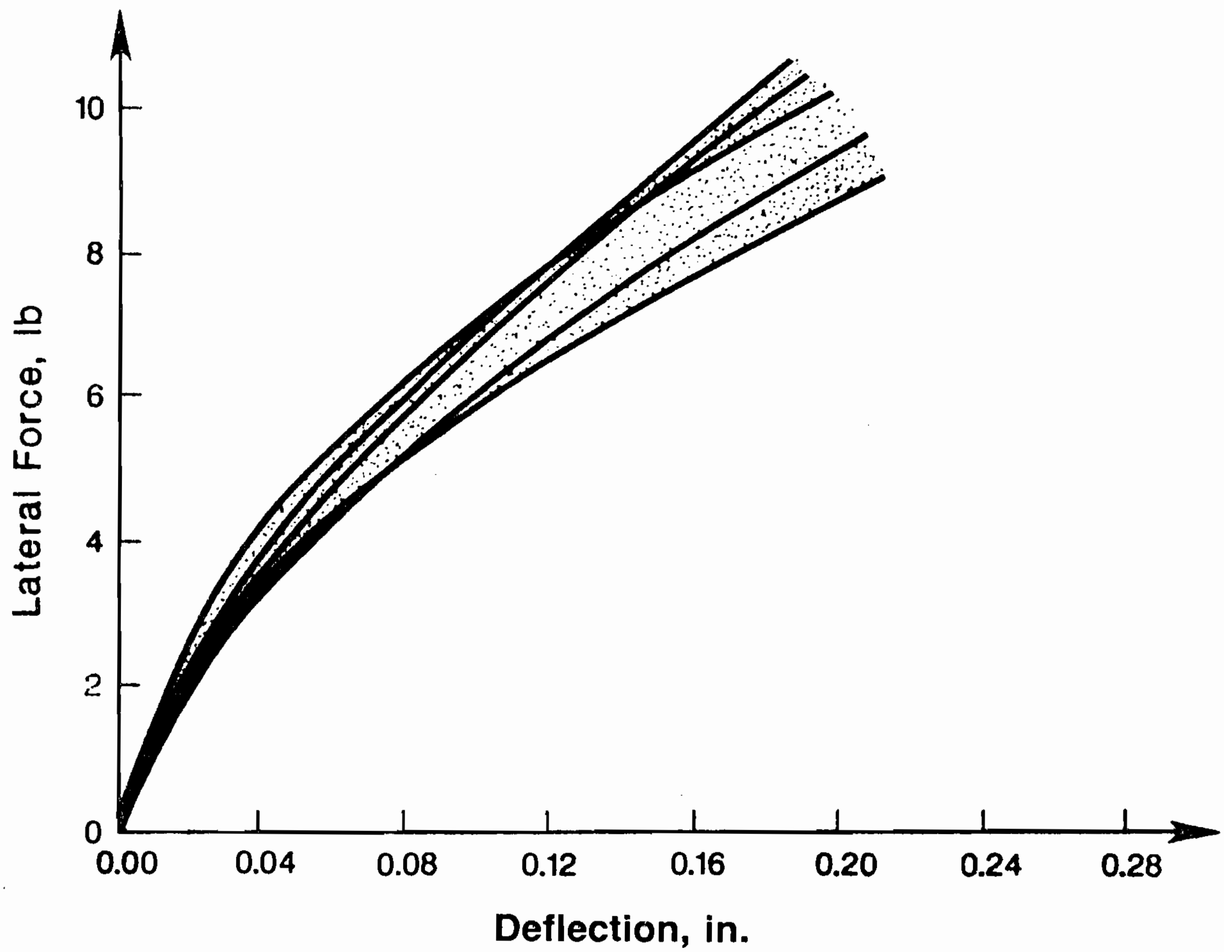

Fig. 7.16. Load-deflection curves for single piles from different tests in loose sand.

curve for the center pile for each test was plotted, as shown in Fig. 7.17. It can be seen that the soil resistance was reduced when the pile spacing was less than one diameter. The ultimate soil resistance, corresponding to a pile deflection of 0.2 in., was plotted as a function of pile spacing, as shown in Fig. 7.18. The ultimate load ratio for piles without interspaces is as low as 0.54, a value similar to that found for the test in soft clay.

The results of tests of single piles in dense sand which accompanied the tests of pile groups are presented in Fig. 7.19. The scatter in these curves is relatively small and it is believed that the vibrator densified the sand rather consistently. The data for the pile-group tests for dense sand can be found in Appendix C. The load-deflection curves for the center pile in the pile-group tests are presented in Fig. 7.20. It is apparent that soil resistance decreases with pile spacing with the results for a clear spacing of two and three diameters being very close to each other. Most measurements for tests in dense sand were stopped at a measured pile deflection of about 0.15 in. The load at this deflection was plotted versus the pile spacing and is shown in Fig. 7.21. The ultimate load ratio is relatively low for pile spacing less than 0.5 diameters and becomes unity at a spacing of about two diameters. These results for dense sand are consistent with those shown for loose sand.

Results for Piles in Sand from Literature

Most published results from model tests on groups of laterally loaded piles in sand have been for 2 X 2 or 3 X 3 pile groups. Studies available for side-by-side groups are sparse. Prakash (1961) performed one test on side-by-side piles in his study on the behavior of pile groups. Aluminum model piles with 0.5 in.-diameter were driven 21 in. into a dense sand. The clear spacing was 2 diameters between side-by-side piles. The load-deflection curves for piles in the group and for a single pile are shown in Fig. 7.22. This test indicates that the group effect is insignificant for side-by-side piles if pile spacing is greater than 2 or 3 pile diameters.

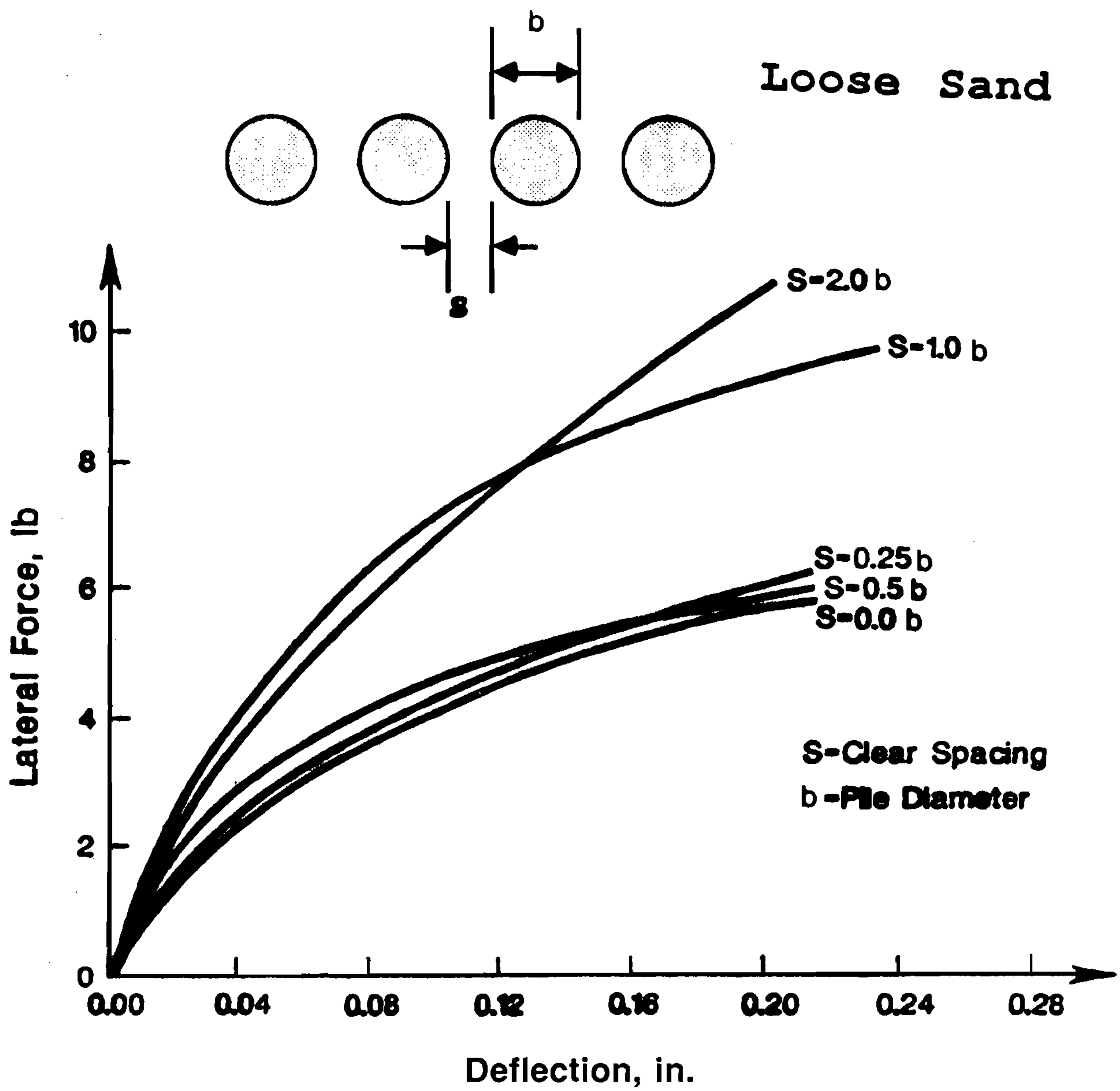

Fig. 7.17. Load-deflection curves for the center pile from the group with spacing varied, tests in loose sand.

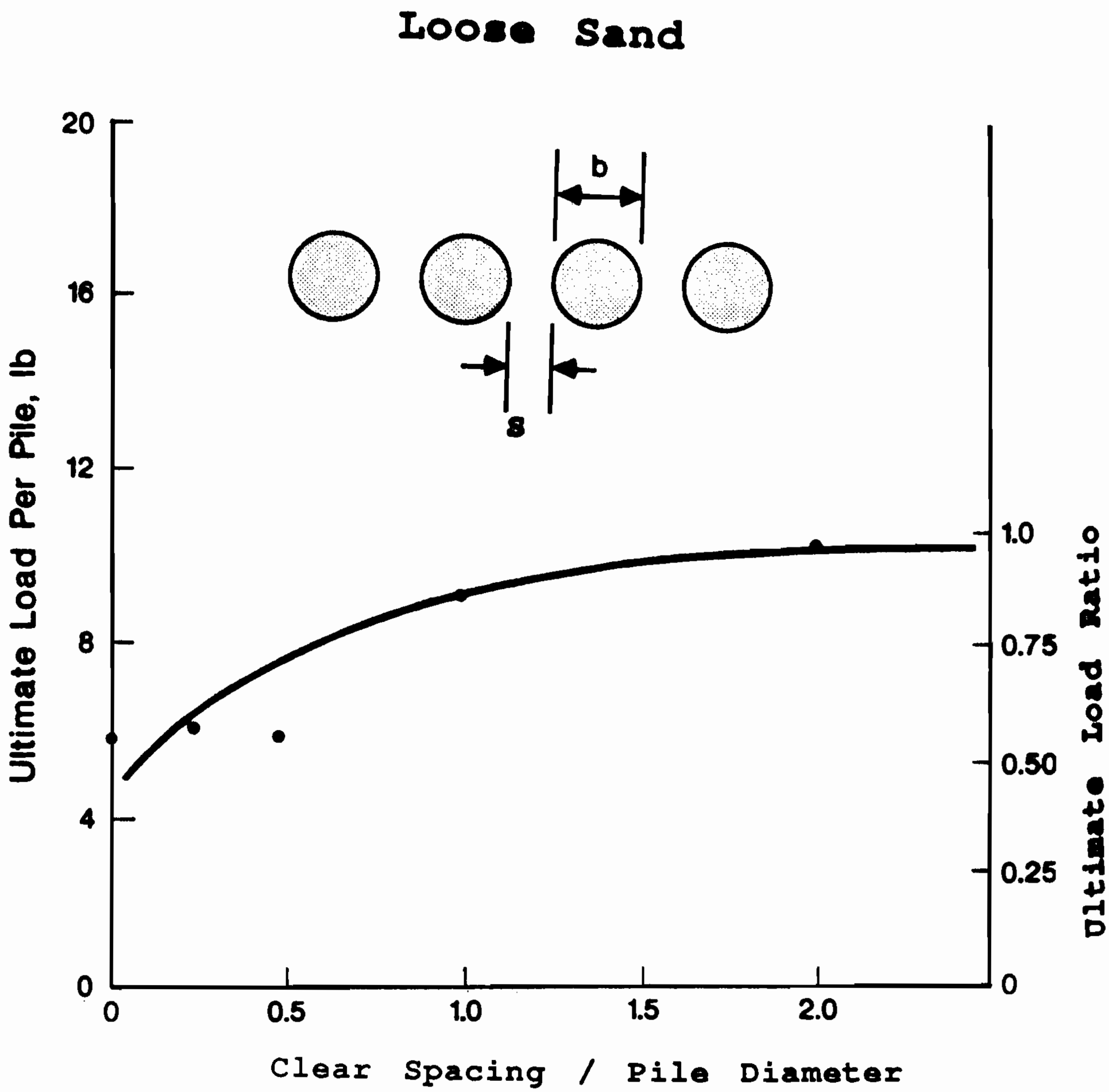

Fig. 7.18. Ultimate load per pile from pile-group tests with various pile spacing in loose sand.

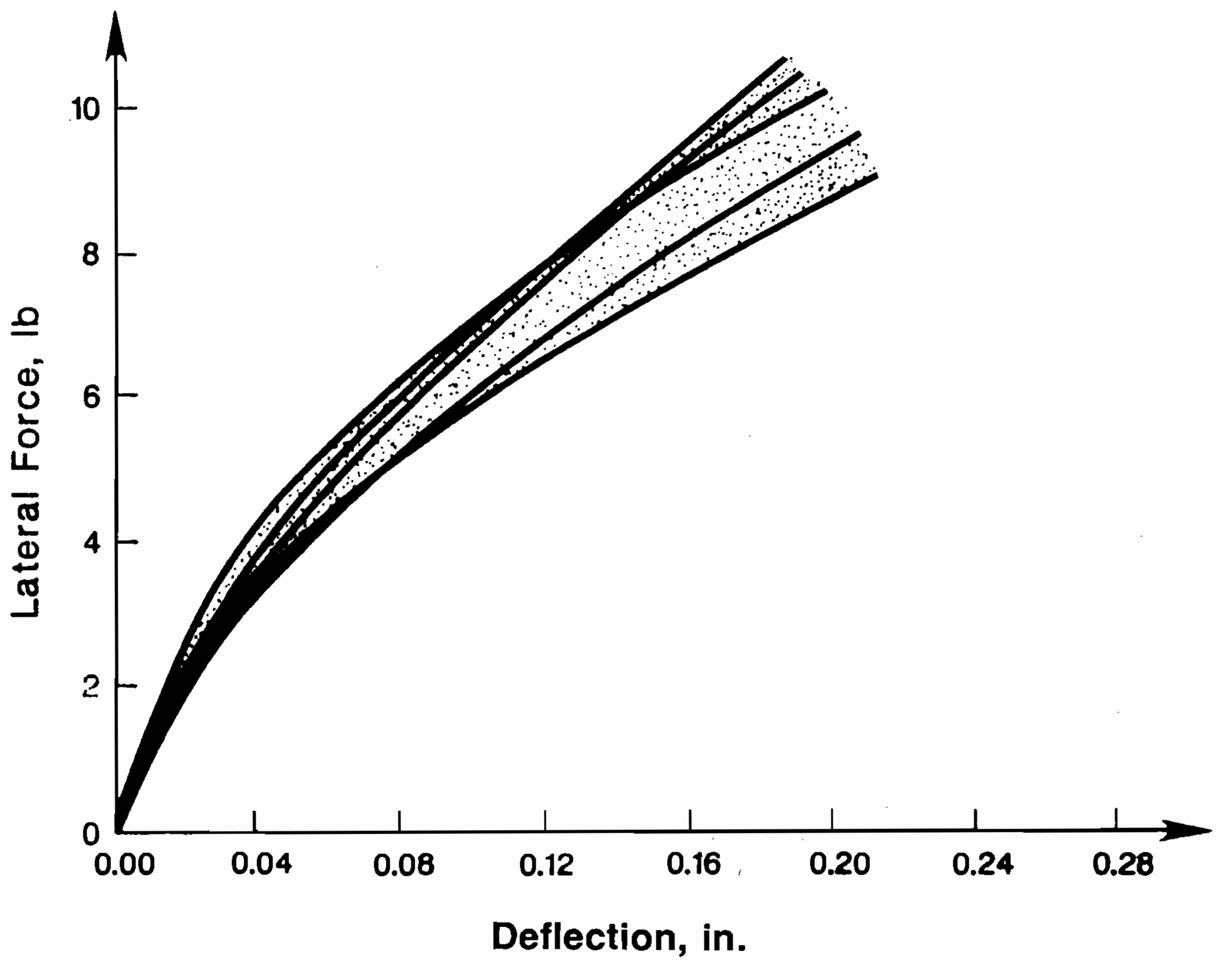

Fig. 7.19. Load-deflection curves of single piles from different tests in dense sand.

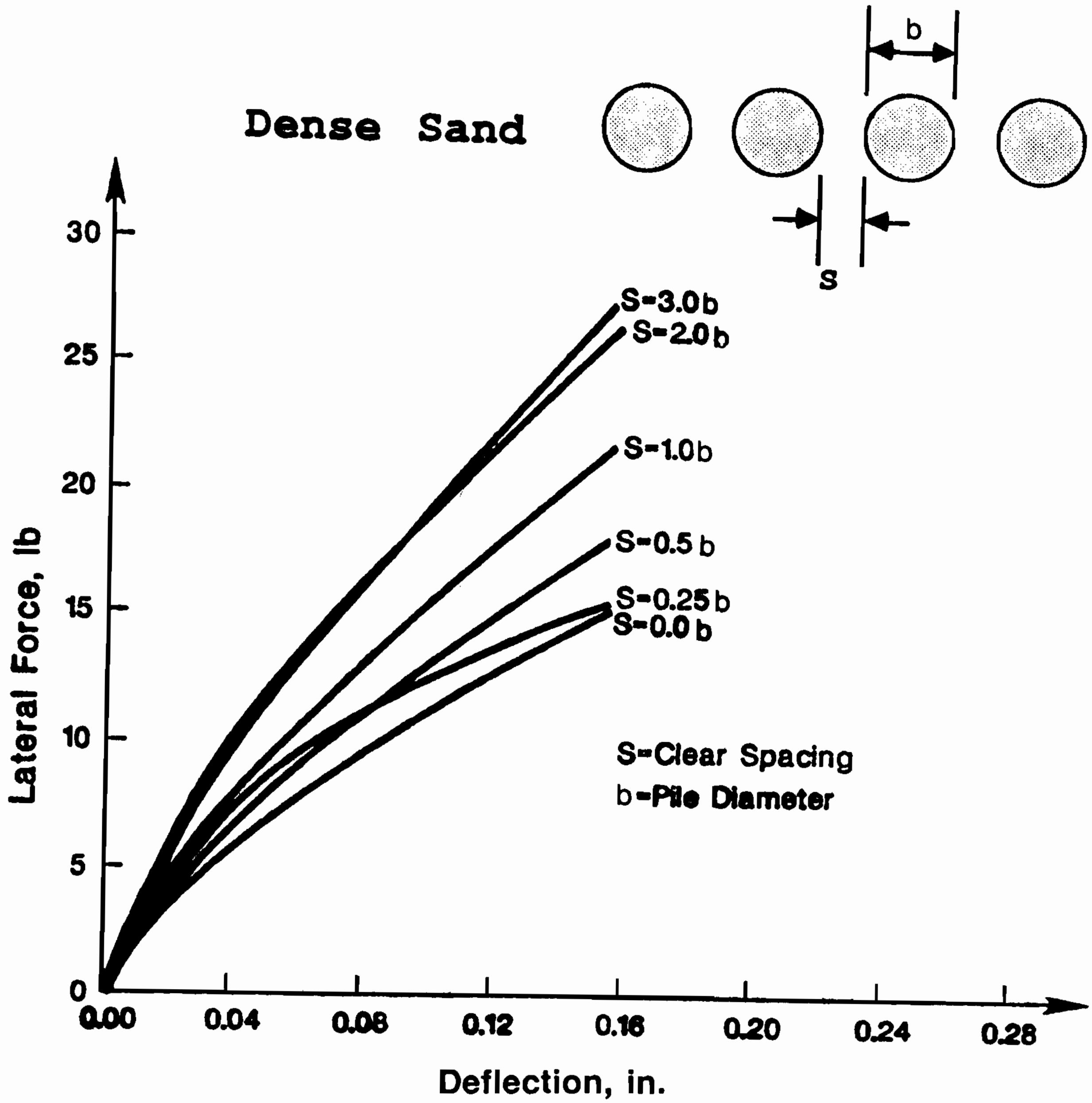

Fig. 7.20. Load-deflection curves for the center pile from the group with spacing varied, tests in dense sand.

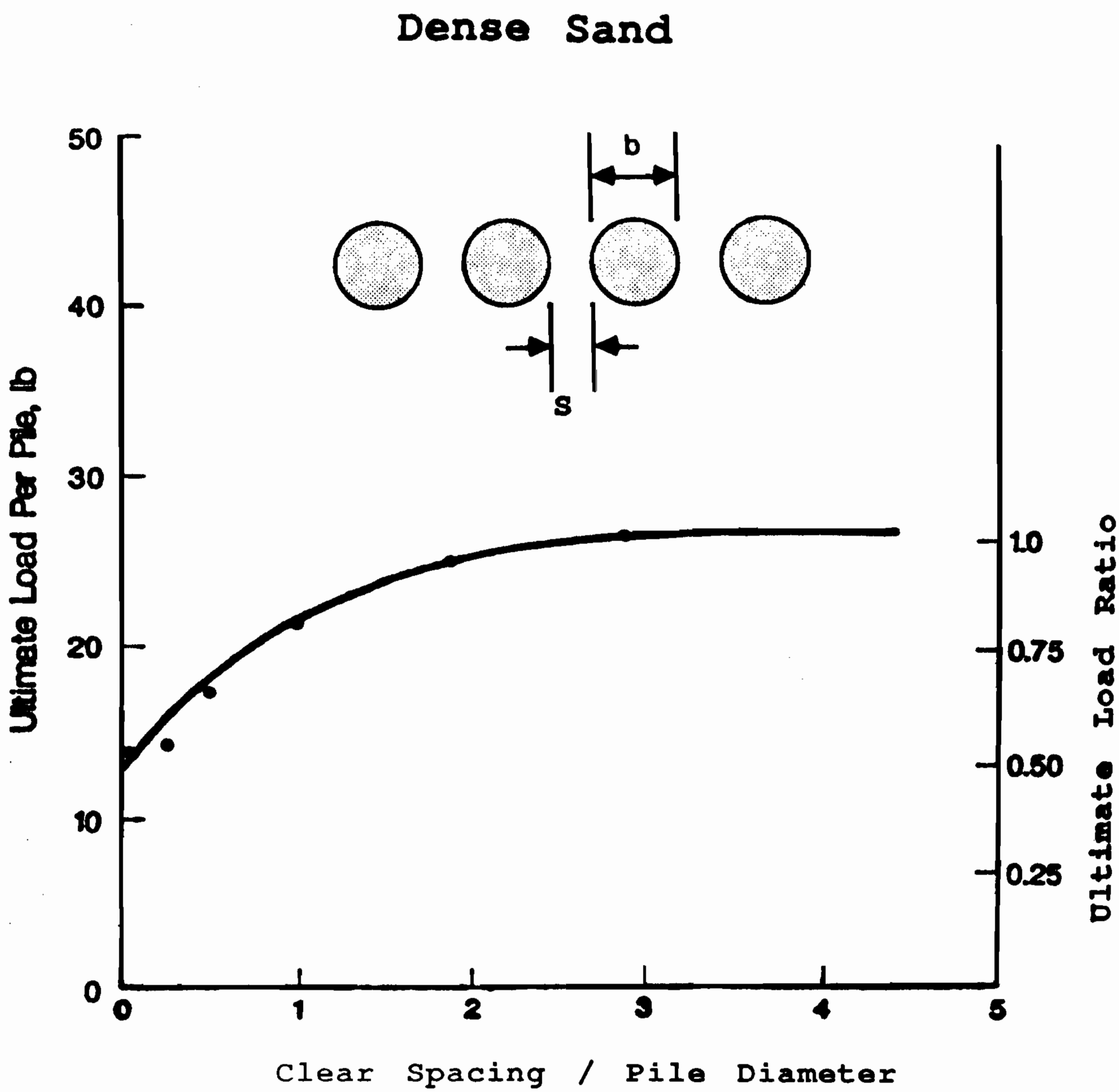

Fig. 7.21. Ultimate load per pile from pile-group tests with various pile spacings in dense sand.

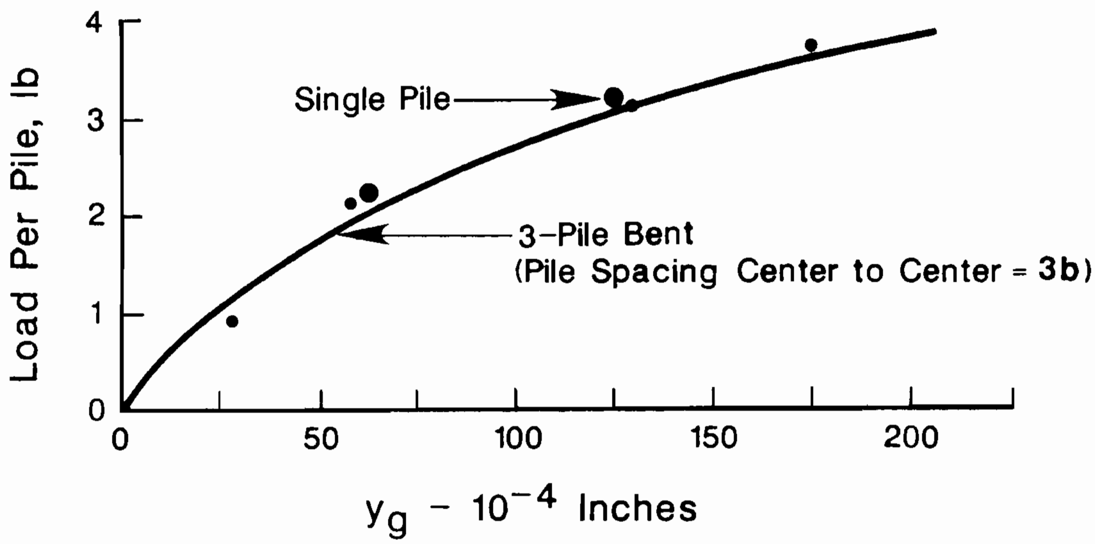

Fig. 7.22. Load-deflection curves for side-by-side piles in dense sand (after Prakash, 1968).

COMPARISON BETWEEN MEASURED AND PREDICTED RESULTS

The performance of each case that has been studied experimentally was predicted using the proposed p-y criteria for piles in a row. A computer program was written to handle all mathematical operations. The input data, including pile geometry, pile and soil properties, and pile loading are consistent with data from the tests.

The predicted and measured load-deflection curves for single piles in soft clay are shown in Fig. 7.23. In general, the undrained shear strength measured by the vane-shear test is higher than that from the conventional tests such as triaxial UU tests or unconfined compression tests because the rate of loading is higher for the vane test. Dennis and Olson (1982) reported that triaxial shear strength is only 70% of values from insitu vane tests. Therefore, it was decided to reduce the shear strength employed in the analysis to 0.6 lb/sq in. at the soil surface and to 0.8 lb/sq in. near the bottom of the piles. As shown in Fig. 7.6, the shear strength averaged about 1.0 lb/sq in. from the vane tests. Using the modified shear strength, Fig. 7.23 shows that there are no significant differences between the measured and predicted load-deflection curves. Comparisons made for pile groups with the different pile spacings are presented in Fig. 7.24 to Fig. 7.29. The clear-spacing ratio shown in the figures is defined as the clear spacing, S, divided by the pile diameter, b. The predicted results are a little higher than the measured results if pile spacings are larger than 0.5 pile diameters. However, good agreement can be found for cases with pile spacing less than 0.5 diameters. It seems that the p-y curves established in this study for piles in a row in clay are acceptable.

The comparison between the measured and predicted results for a single pile in dense sand is shown in Fig. 7.30. The agreement is impressive. For pile groups, the predicted load-deflecion curves show good to excellent agreement with the measured results (Fig. 7.31 to Fig. 7.36). This implies that the proposed p-y criteria for either single piles or side-by-side piles in dense sand can be used for design.

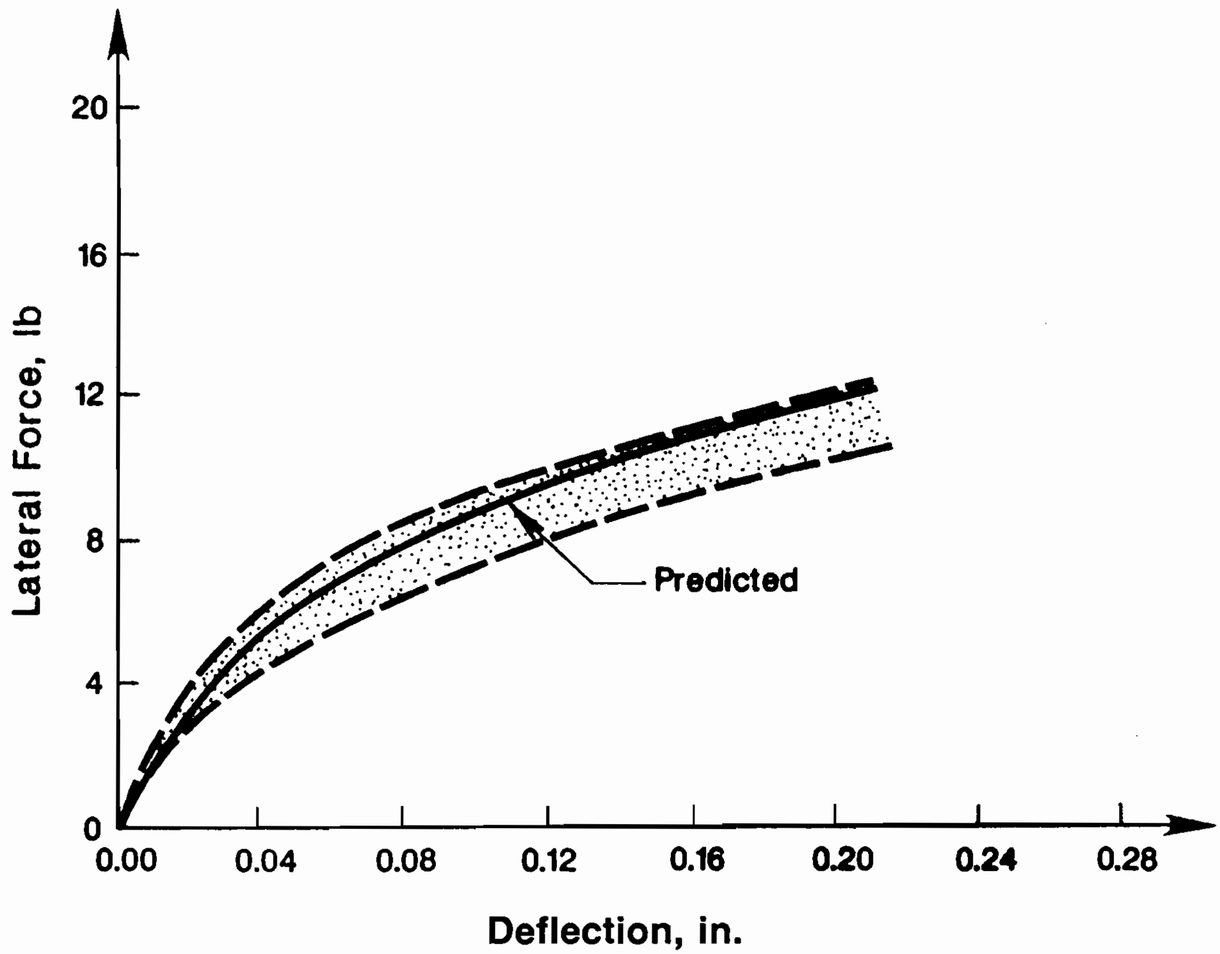

Fig. 7.23. The predicted and measured results for a single pile in soft clay.

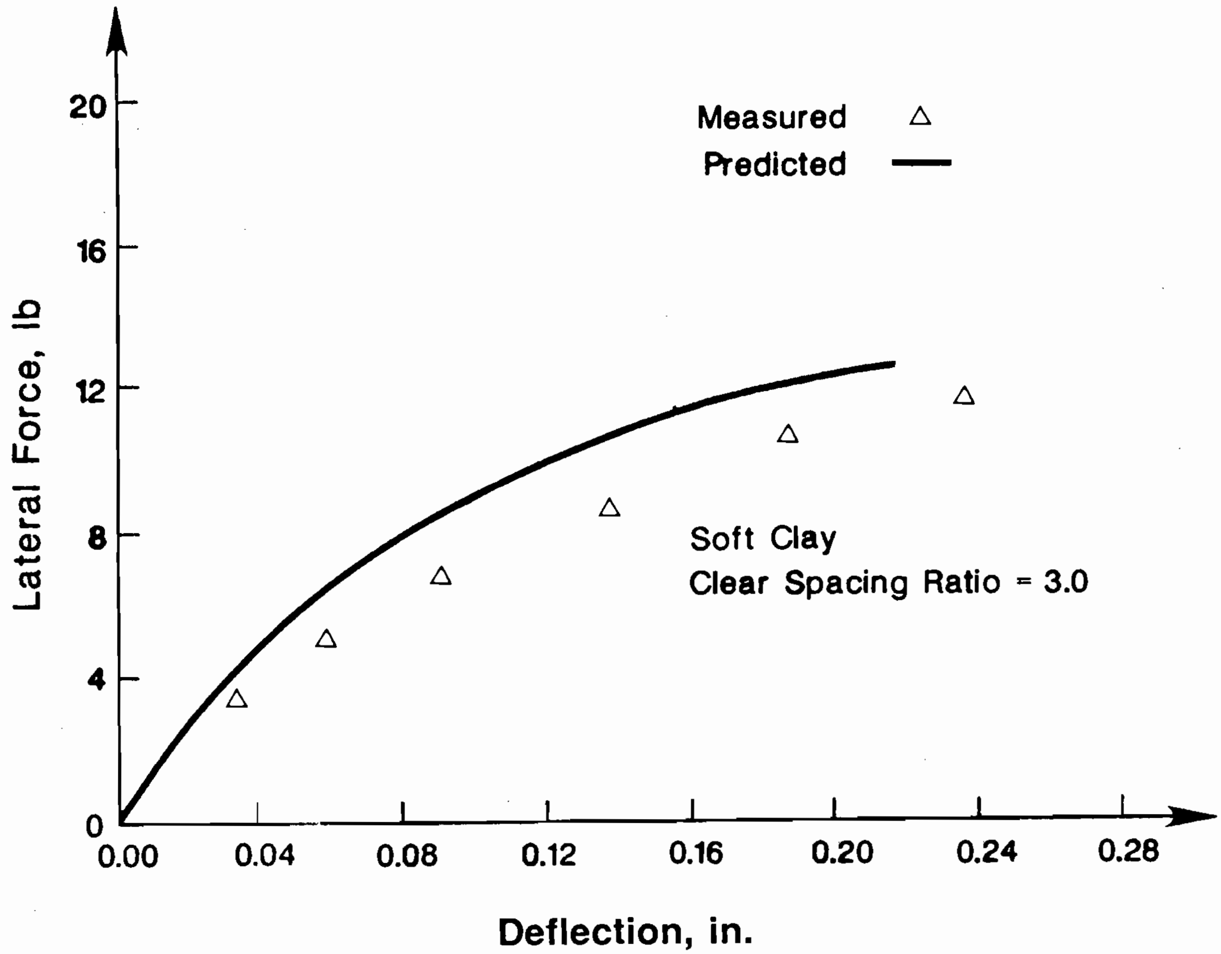

Fig. 7.24. The predicted and measured results for a pile in a pile group with 3-diameter clear spacing in soft clay.

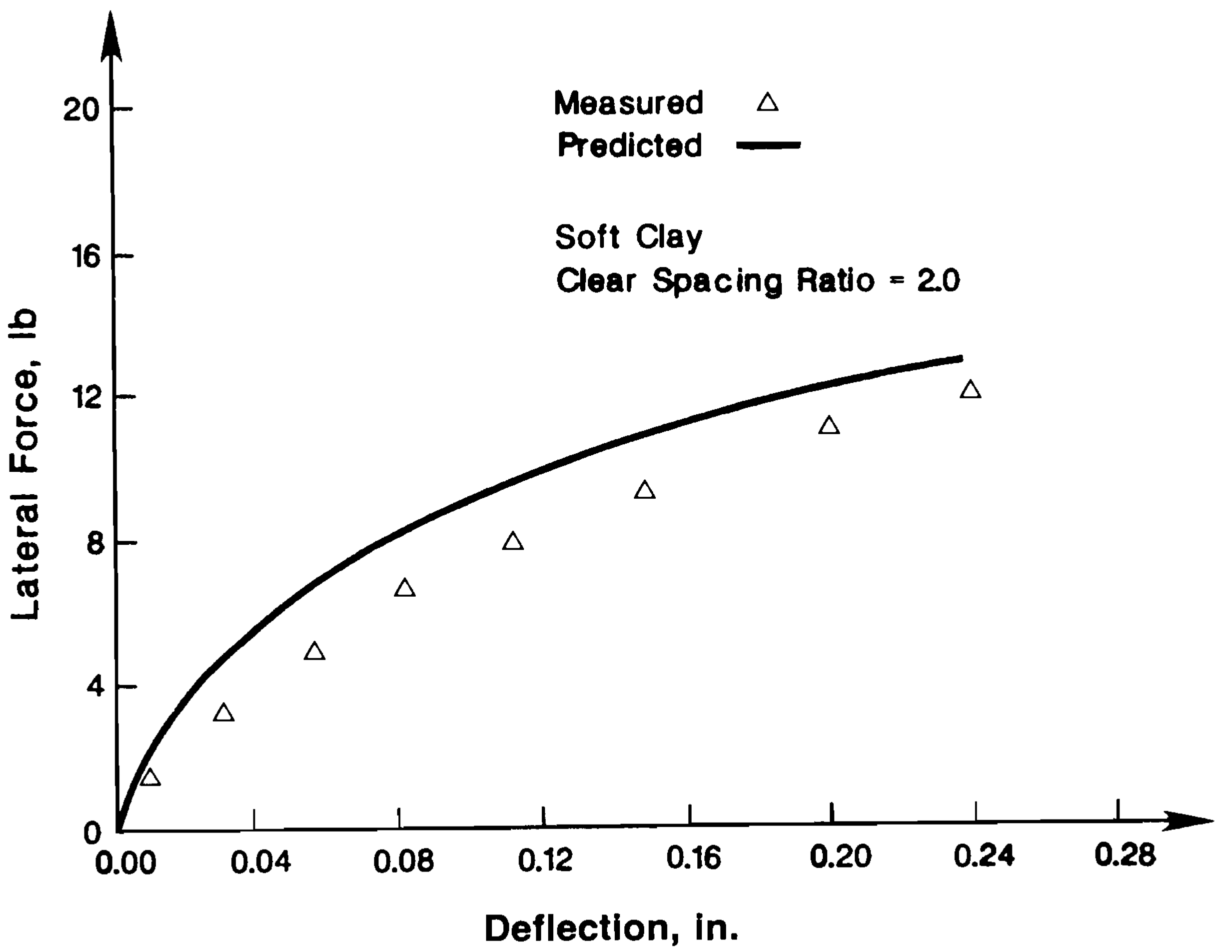

Fig. 7.25. The predicted and measured results for a pile in a pile group with 2-diameter clear spacing in soft clay.

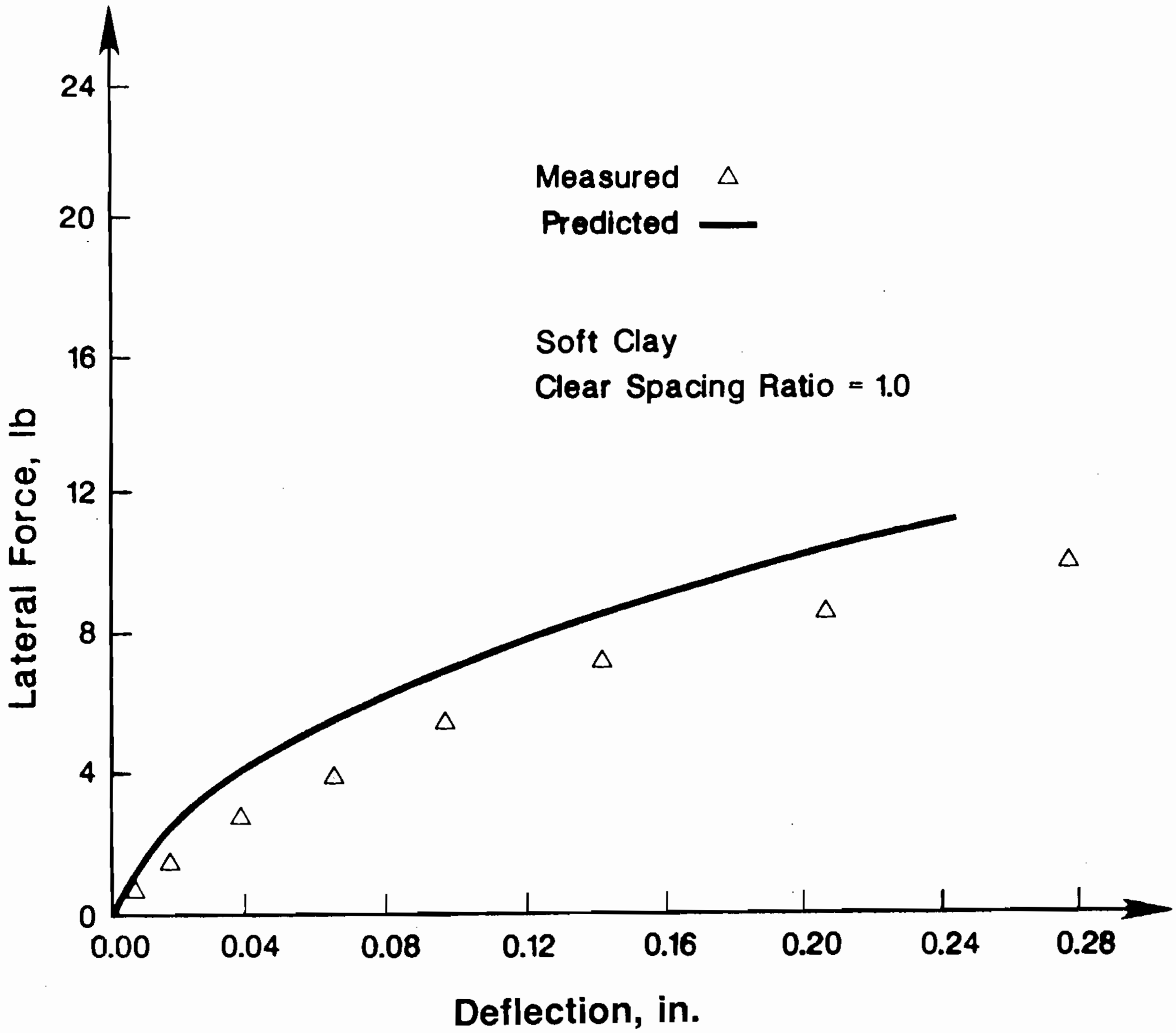

Fig. 7.26. The predicted and measured results for a pile in a pile group with 1-diameter clear spacing in soft clay.

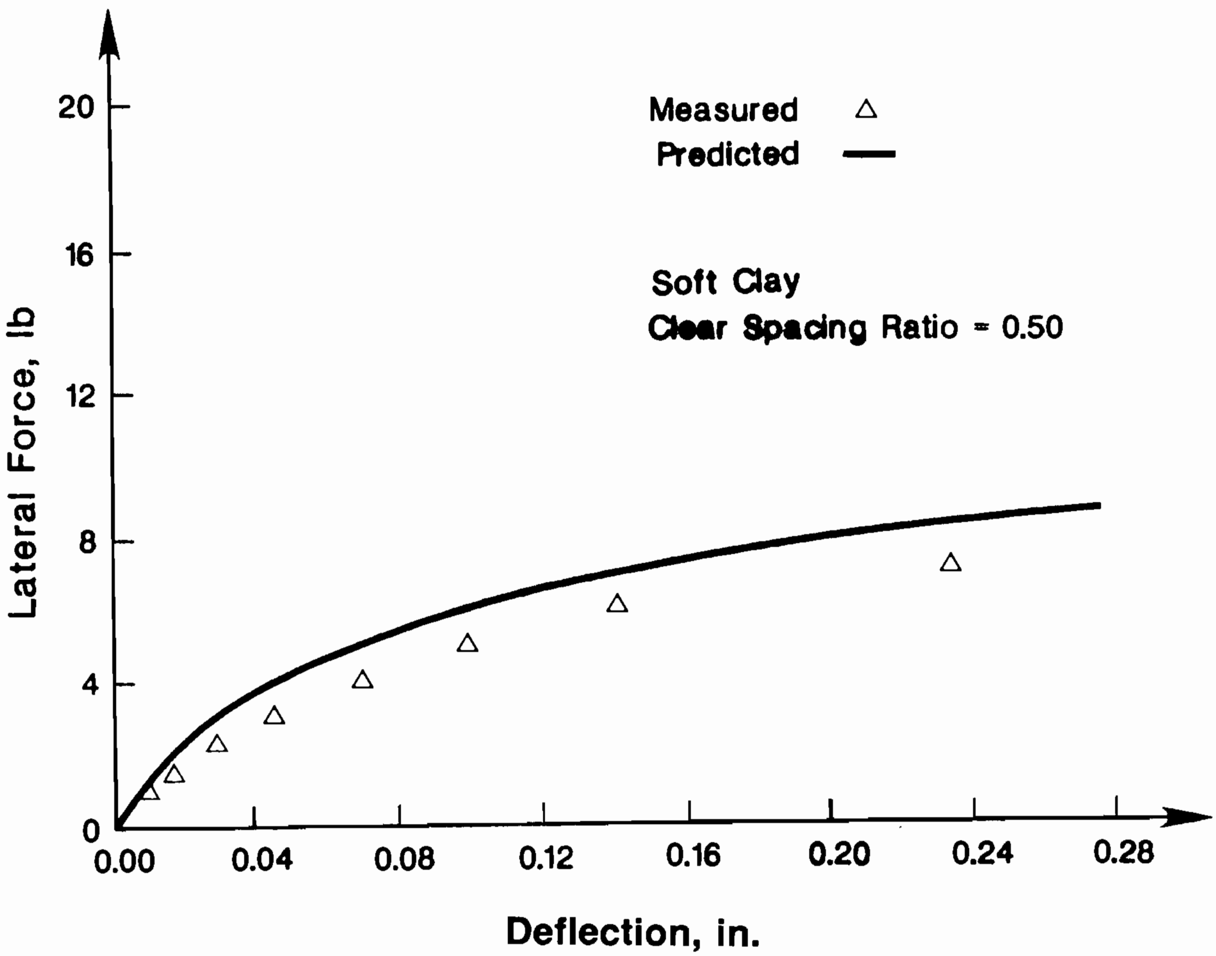

Fig. 7.27. The predicted and measured results for a pile in a pile group with 0.5-diameter clear spacing in soft clay.

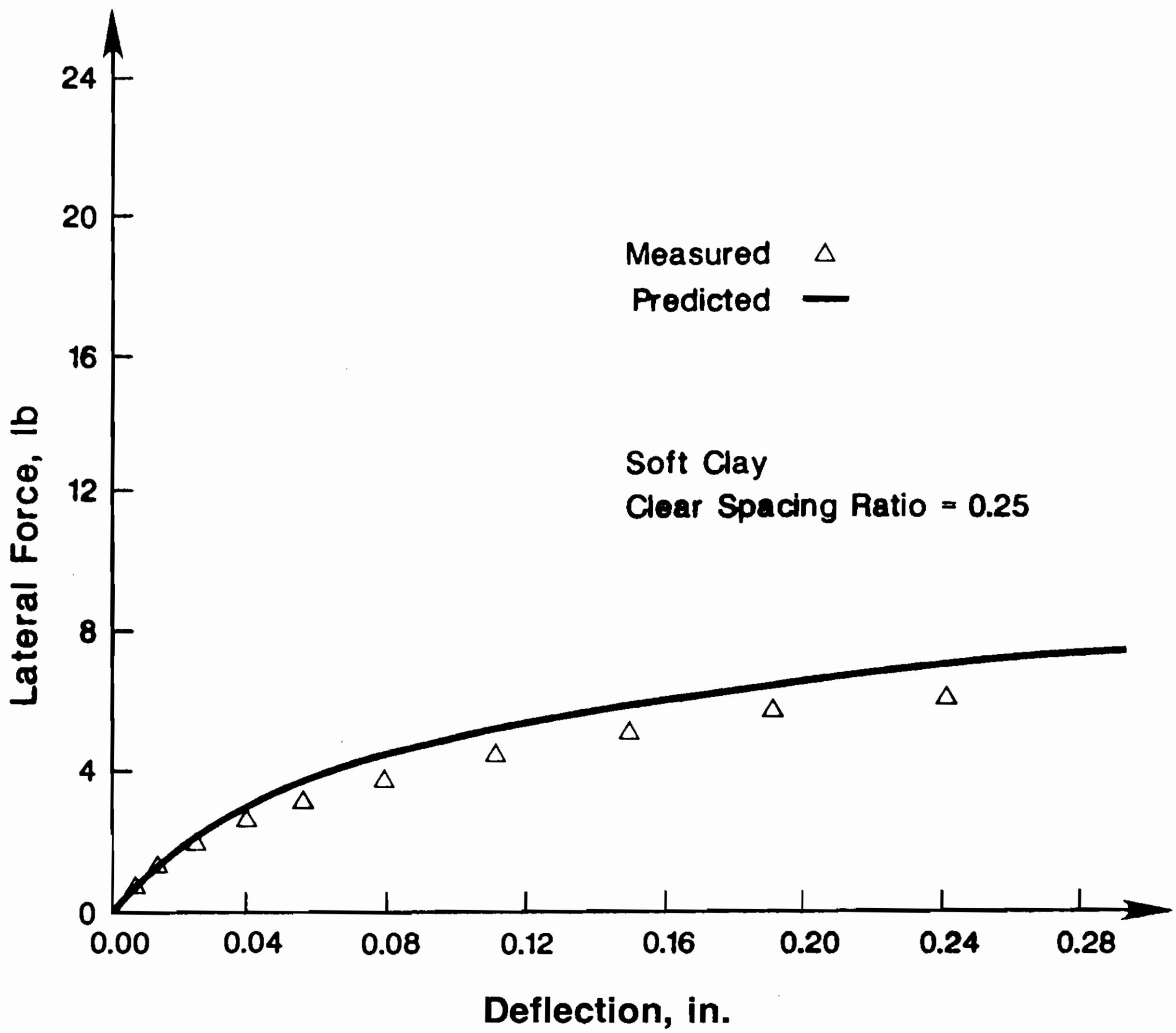

Fig. 7.28. The predicted and measured results for a pile in a pile group with 0.25-diameter clear spacing in soft clay.

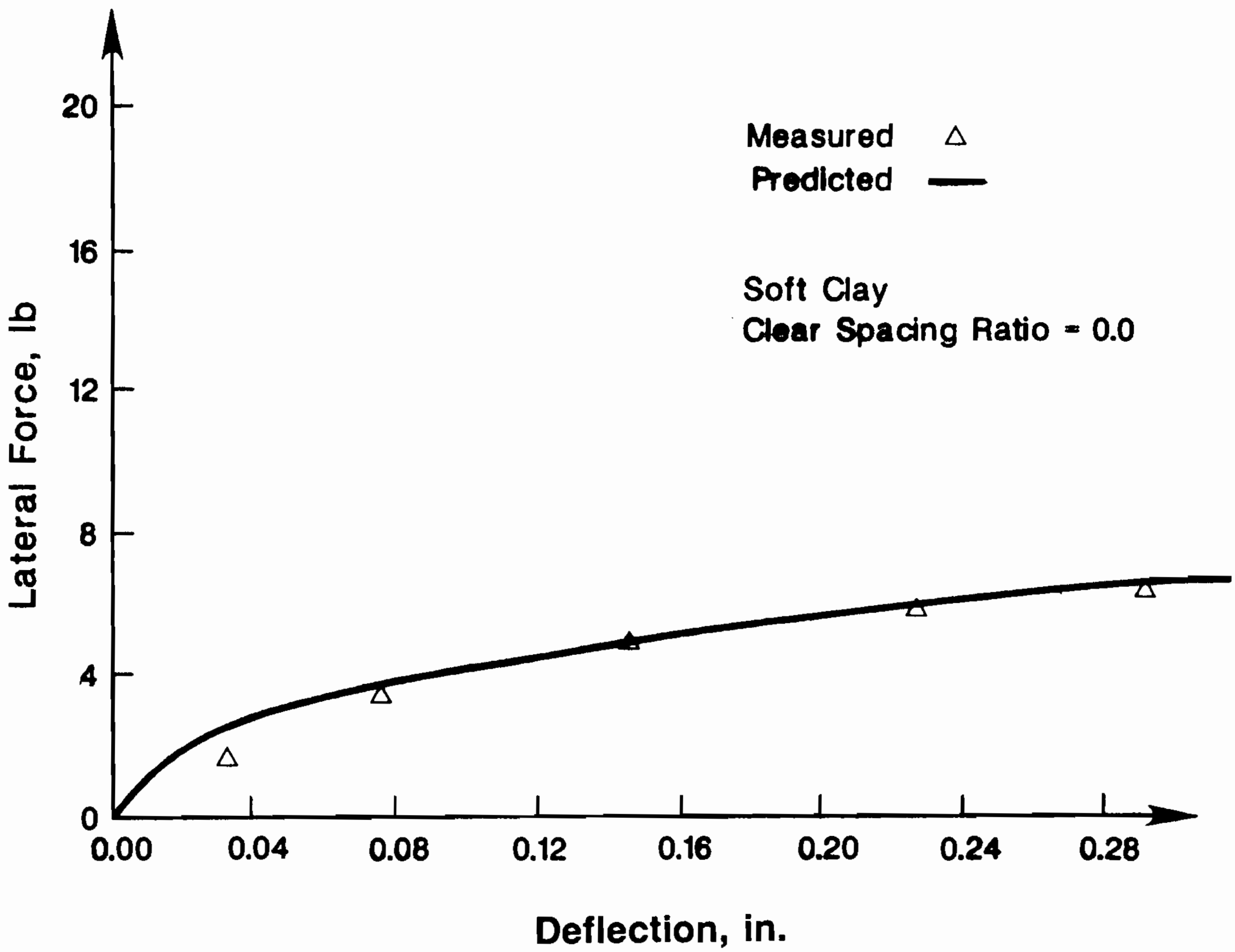

Fig. 7.29. The predicted and measured results for a pile in a pile group with zero clear spacing in soft clay.

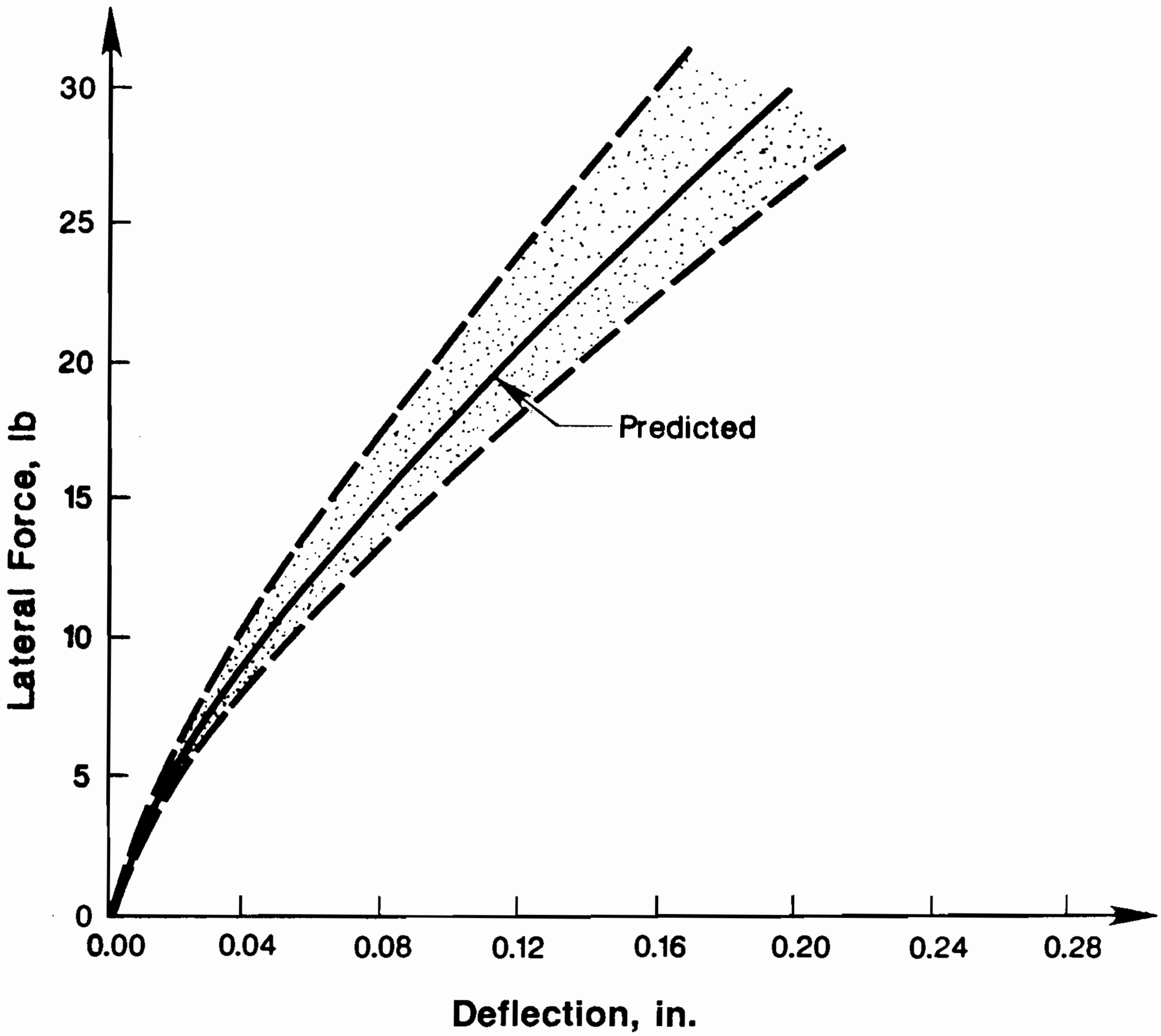

Fig. 7.30. The predicted and measured results for a single pile in dense sand.

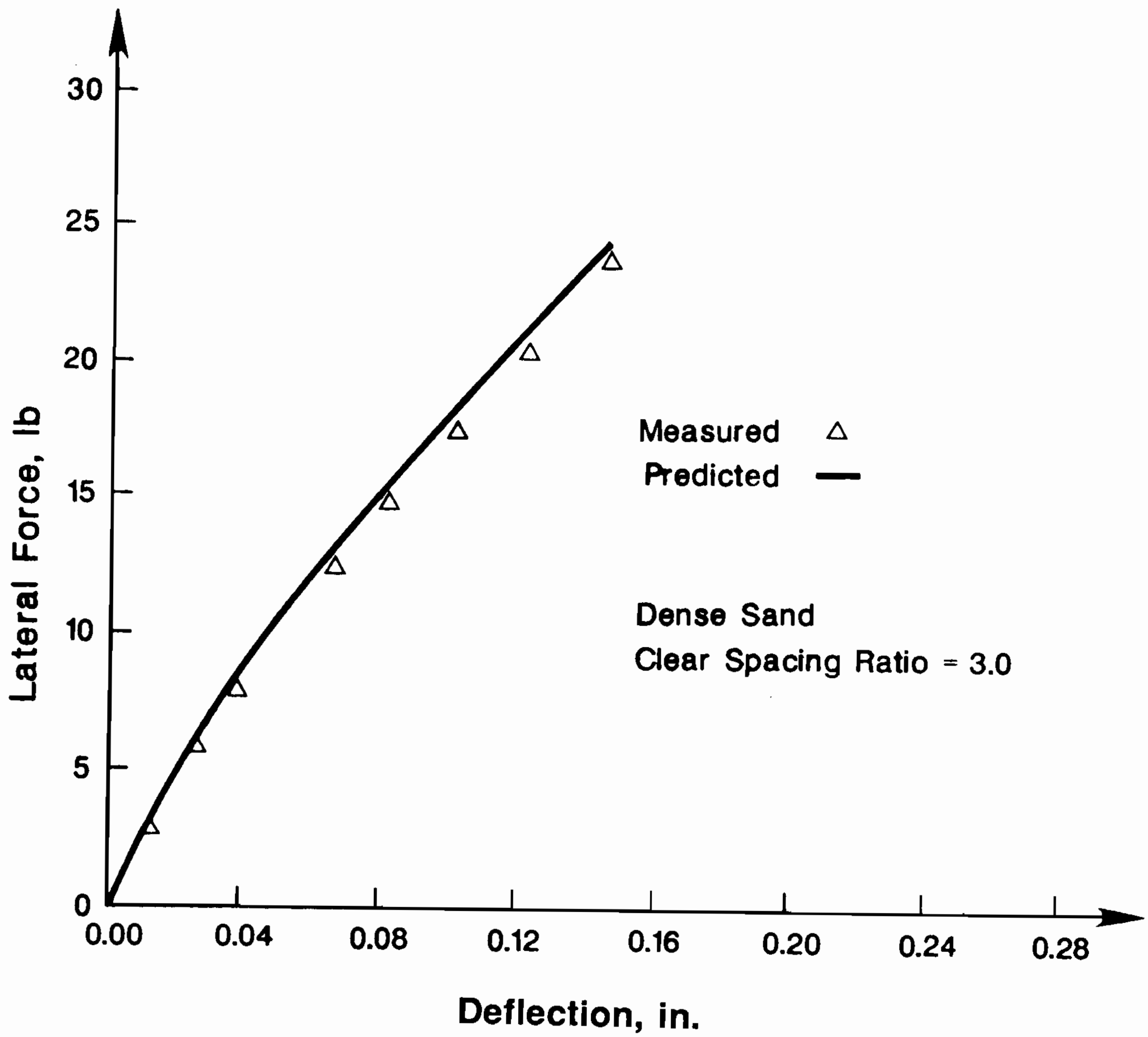

Fig. 7.31. The predicted and measured results for a pile in a pile group with 3-diameter clear spacing in dense sand.

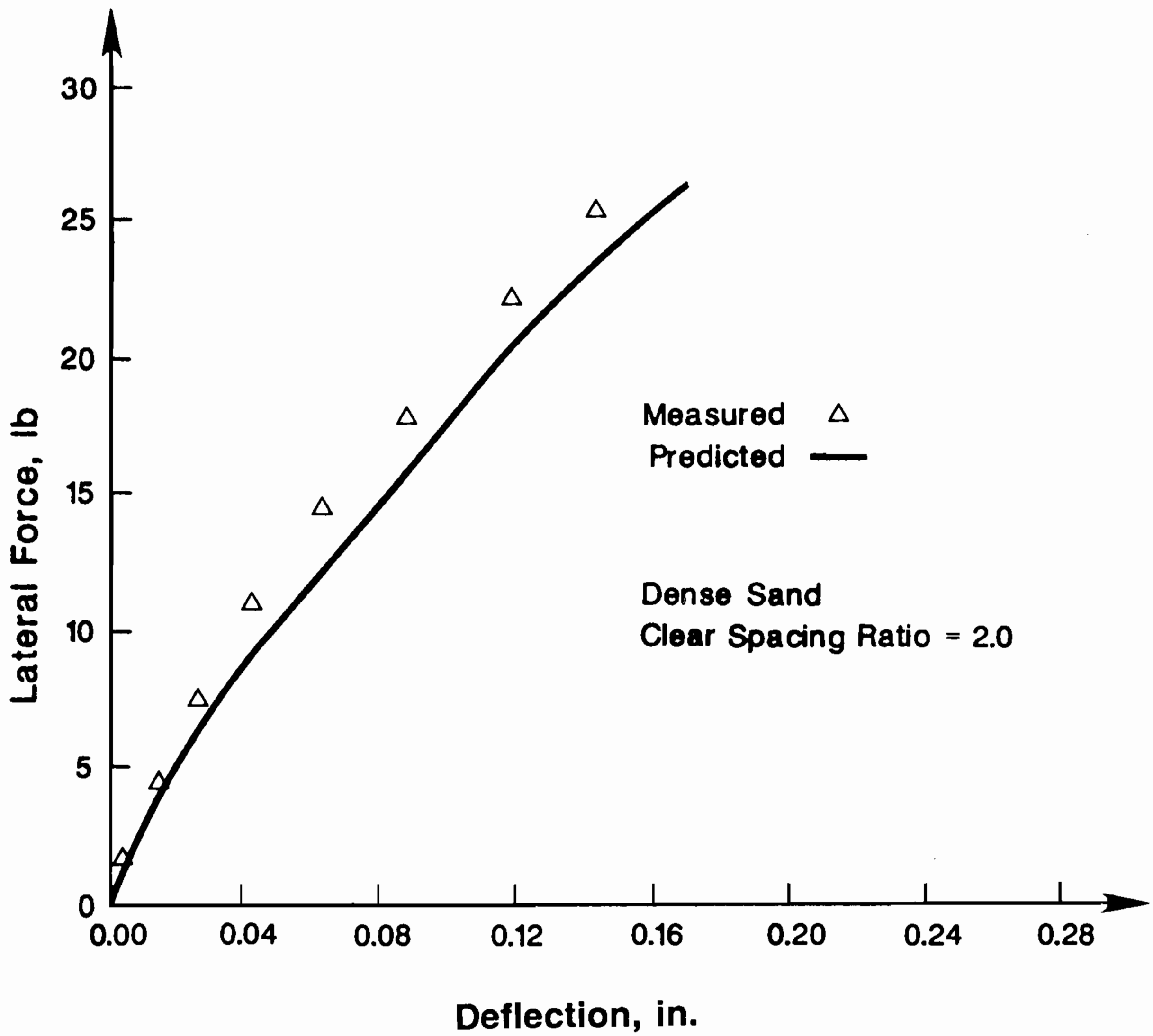

Fig. 7.32. The predicted and measured results for a pile in a pile group with 2-diameter clear spacing in dense sand.

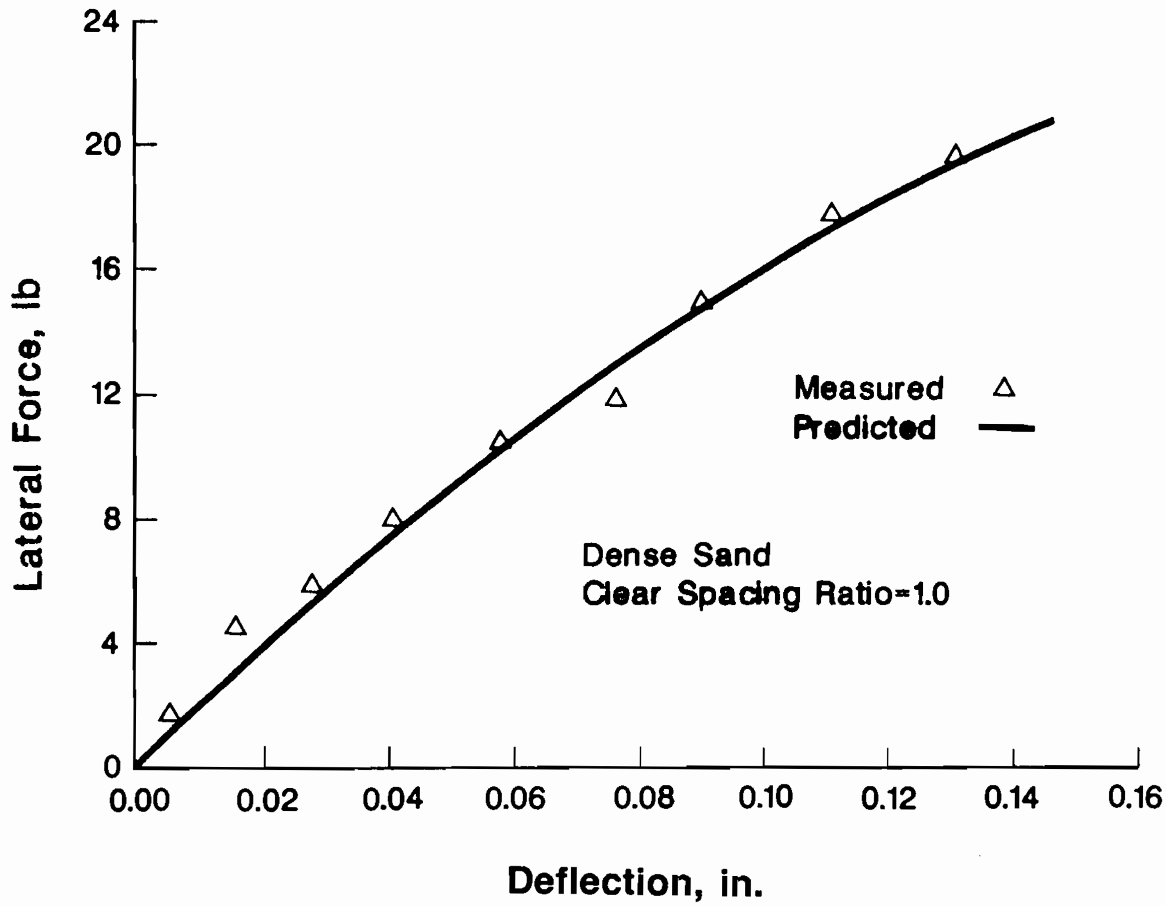

Fig. 7.33. The predicted and measured results for a pile in a pile group with 1-diameter clear spacing in dense sand.

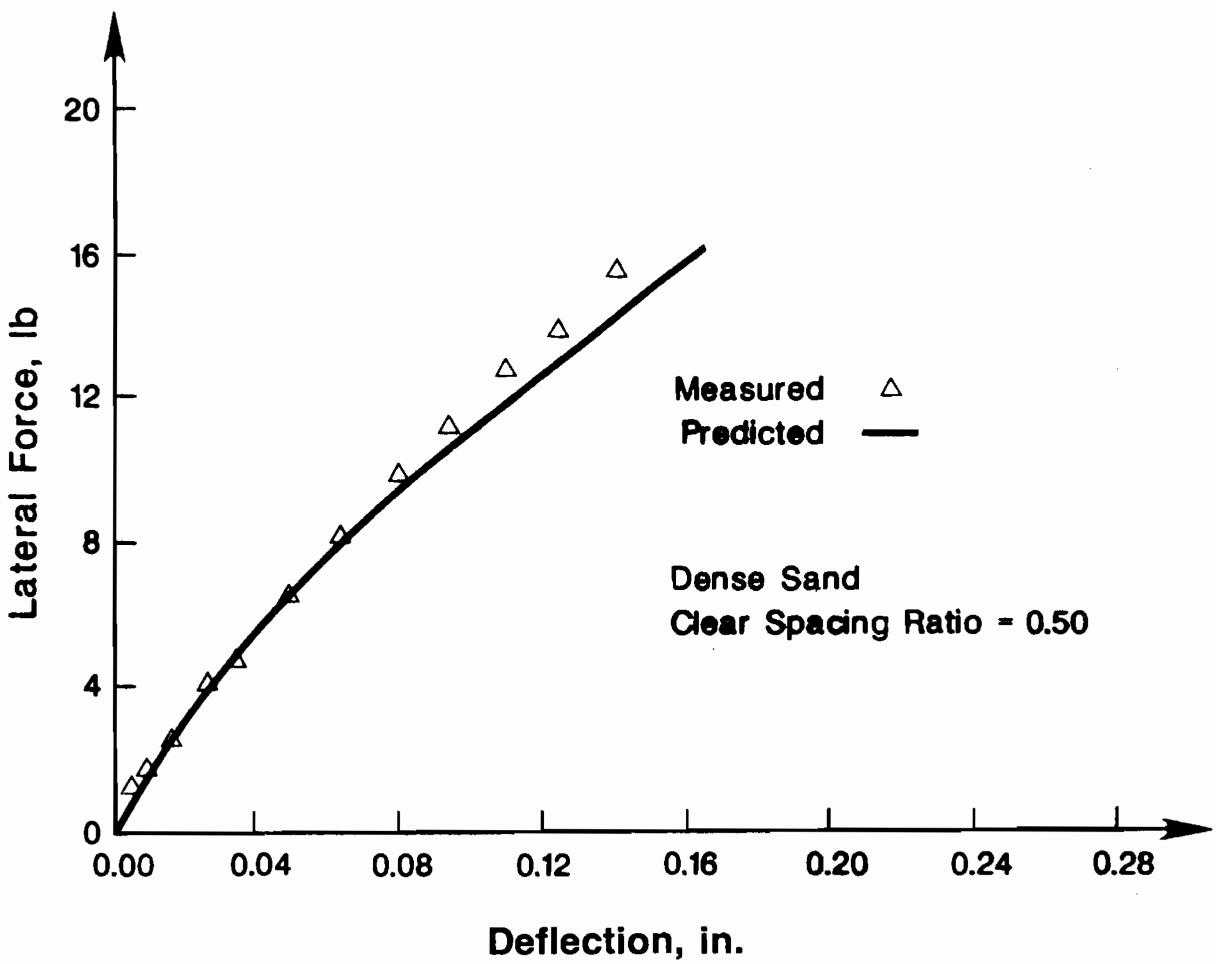

Fig. 7.34. The predicted and measured results for a pile in a pile group with 0.5-diameter clear spacing in dense sand.

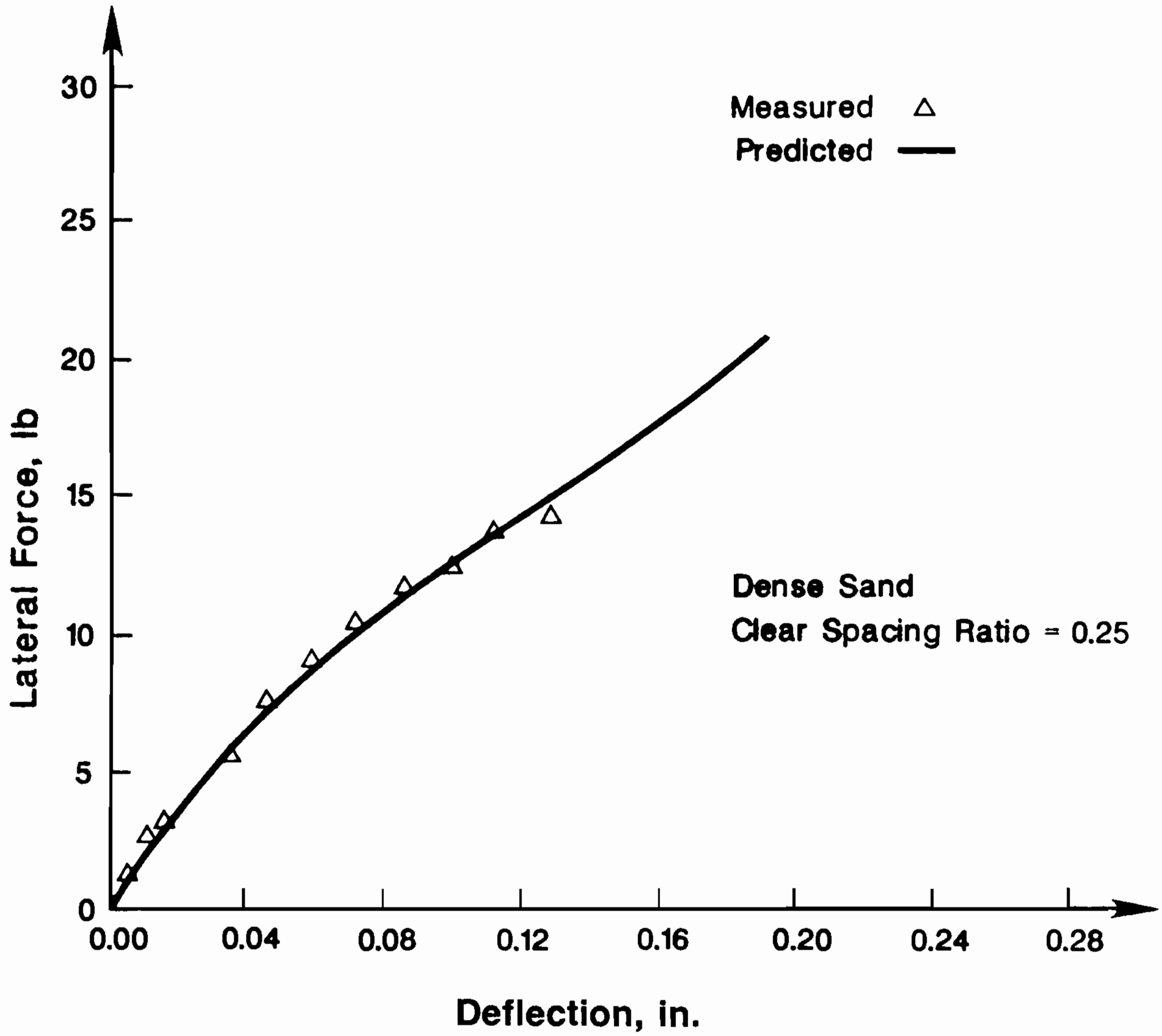

Fig. 7.35. The predicted and measured results for a pile in a pile group with 0.25-diameter clear spacing in dense sand.

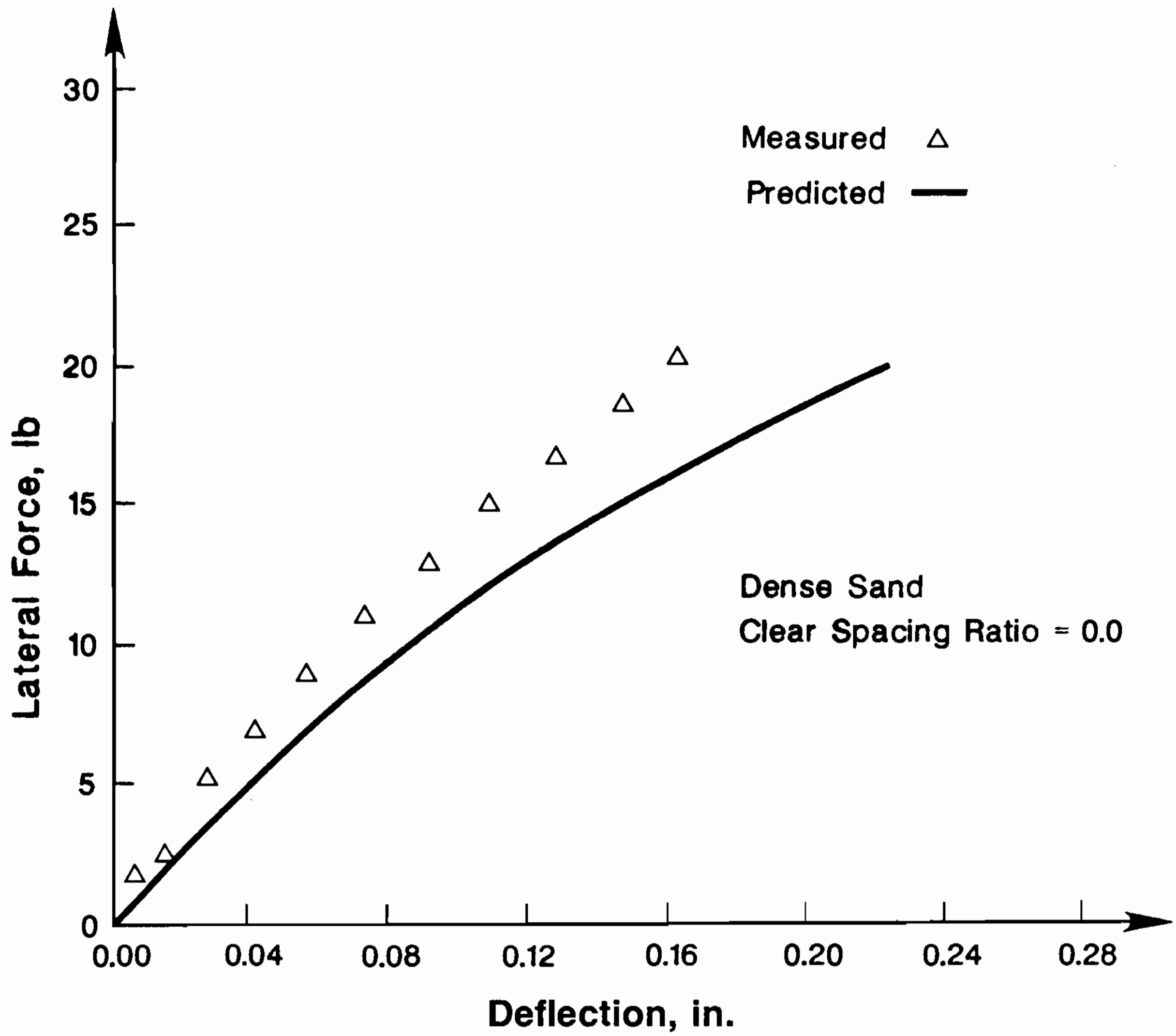

Fig. 7.36. The predicted and measured results for a pile in a pile group with zero clear spacing in dense sand.

Loose sand, in general, has a relatively unstable condition because of high void ratio. Except for a quite small amount of initial deflection, the void ratio of the soil around a pile should be reduced dramatically with increased deflection. The measured and predicted load-deflection curves for a single pile in loose sand are presented in Fig. 7.37. It appears that the predicted results are a little conservative for low-magnitude loads and unconservative for high-magnitude loads. The comparisons for pile groups are presented in Figs. 7.38 to 7.42. In general, the agreement is good at small deflections, and fair at large deflections.

SUMMARY

To verify the proposed p-y criteria for drilled-shaft retaining walls, small-scale experiments were conducted using three types of soils: soft clay, dense sand, and loose sand. The edge-to-edge spacing of the piles in terms of pile diameter were 0, 0.25, 0.50, 1.0, 2.0, and 3.0. Results were predicted from methods that have been developed from theory and results from predictions were compared with those from measurements. The agreement was good for pile groups in soft clay, fair for loose sand, and excellent for pile groups in dense sand. In addition, the measured results from this study agreed well with the results of small-scale tests on side-by-side piles reported by others.

The measurements in the laboratory and the literature survey indicated that the proposed p-y criteria, as modified to account for group effects, can be used to predict the behavior of small-sized piles with an accuracy that is fair to excellent, depending on the type of soil.

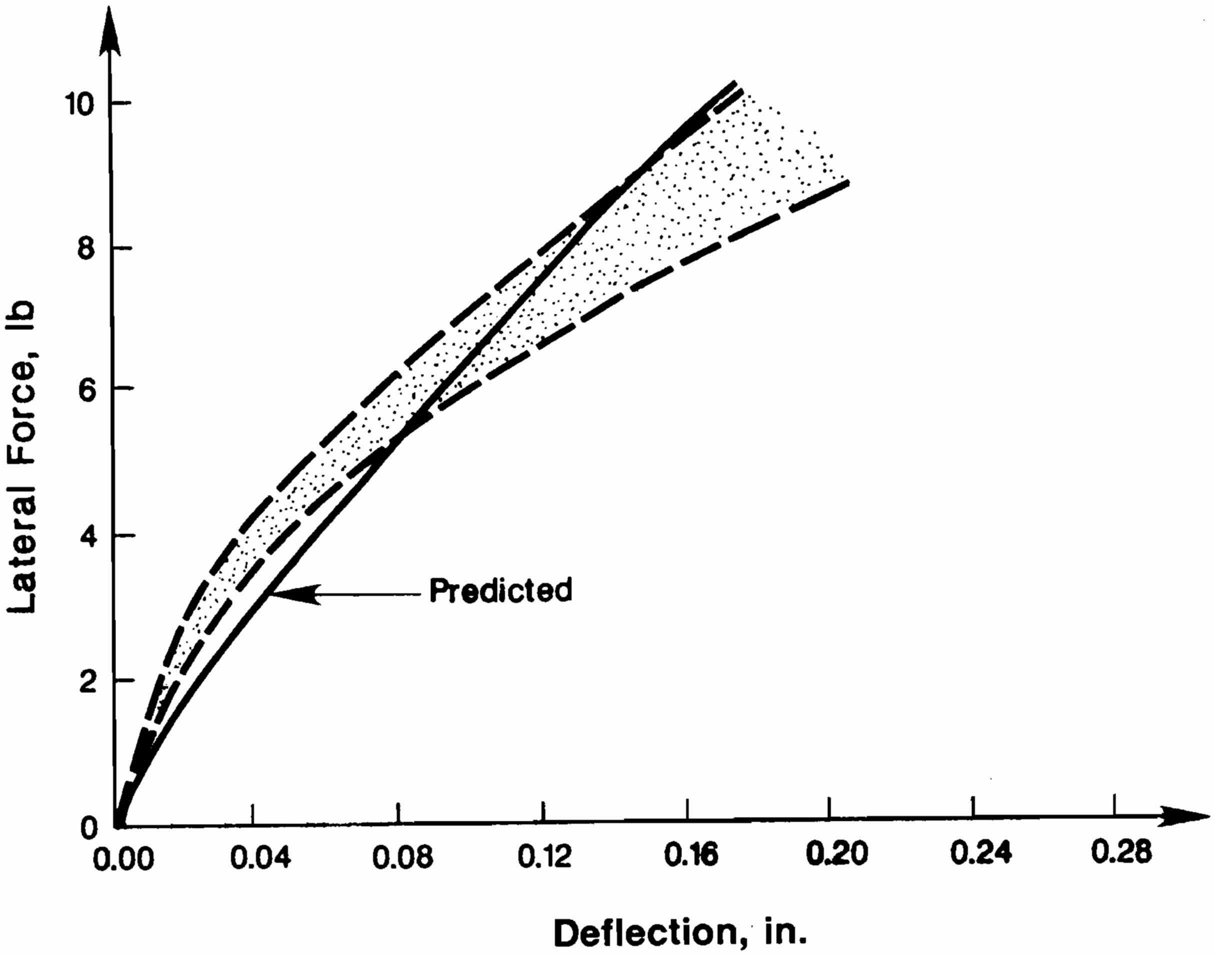

Fig. 7.37. The predicted and measured results for a single pile in loose sand.

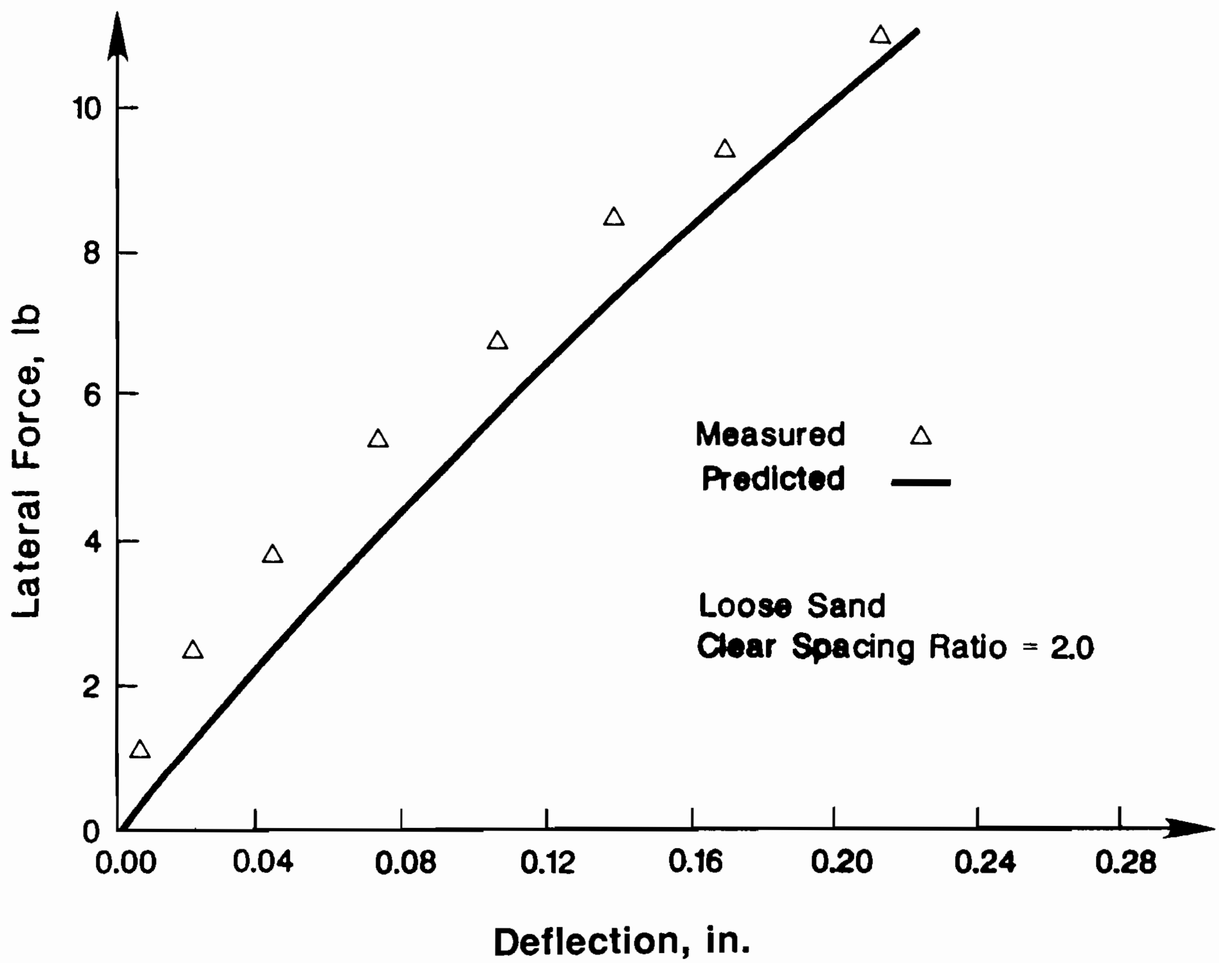

Fig. 7.38. The predicted and measured results for a pile in a pile group with 2-diameter clear spacing in loose sand.

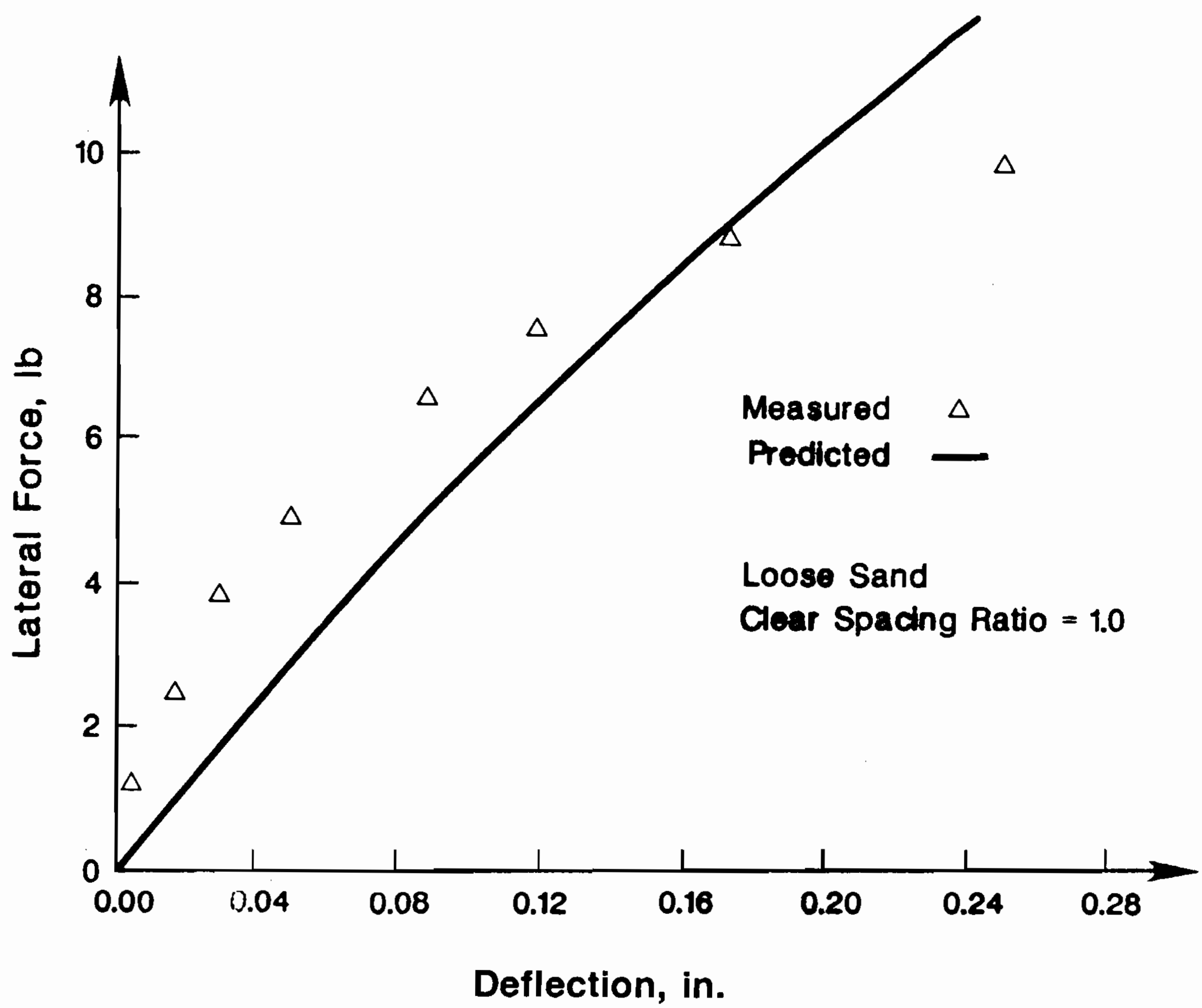

Fig. 7.39. The predicted and measured results for a pile in a pile group with 1-diameter clear spacing in loose sand.

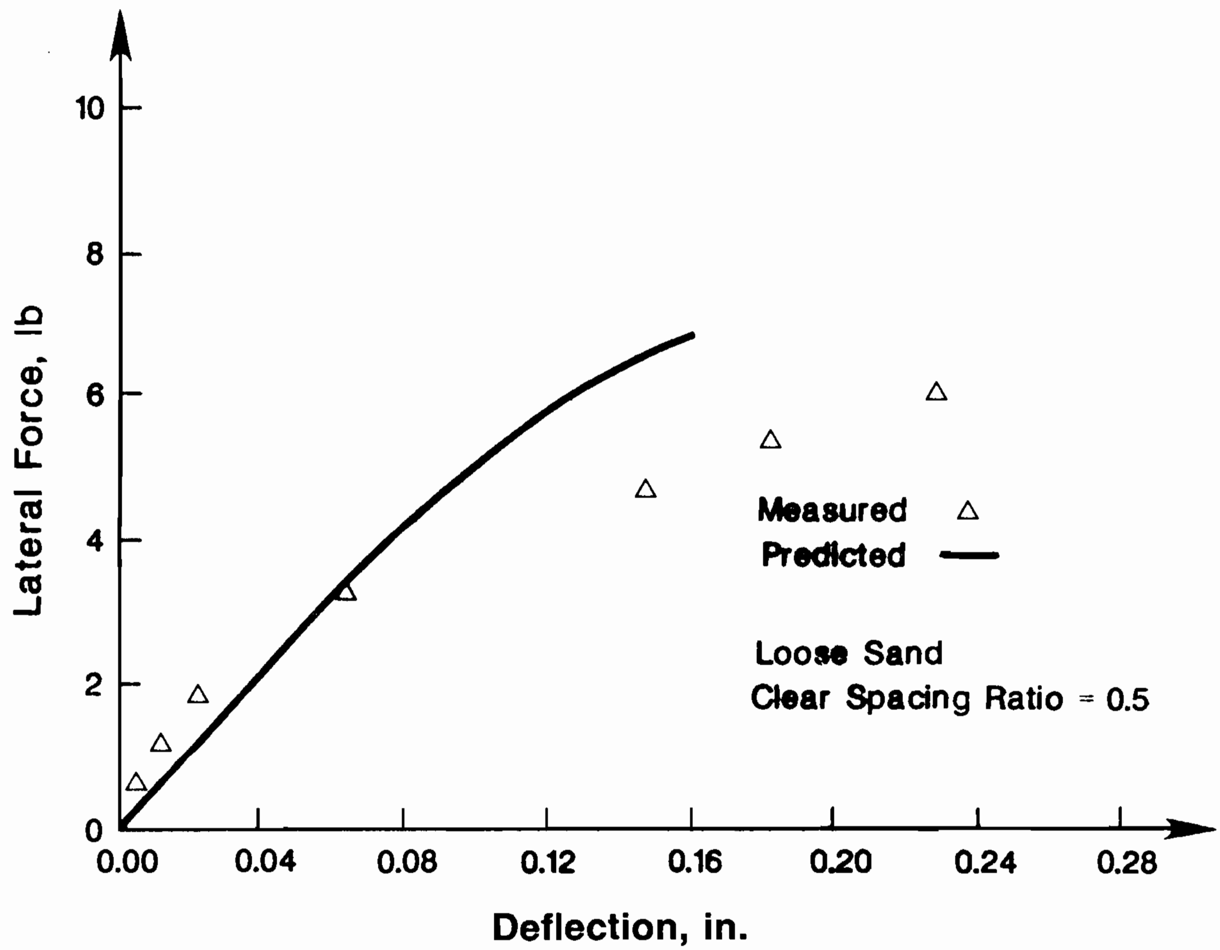

Fig. 7.40. The predicted and measured results for a pile in a pile group with 0.5-diameter clear spacing in loose sand.

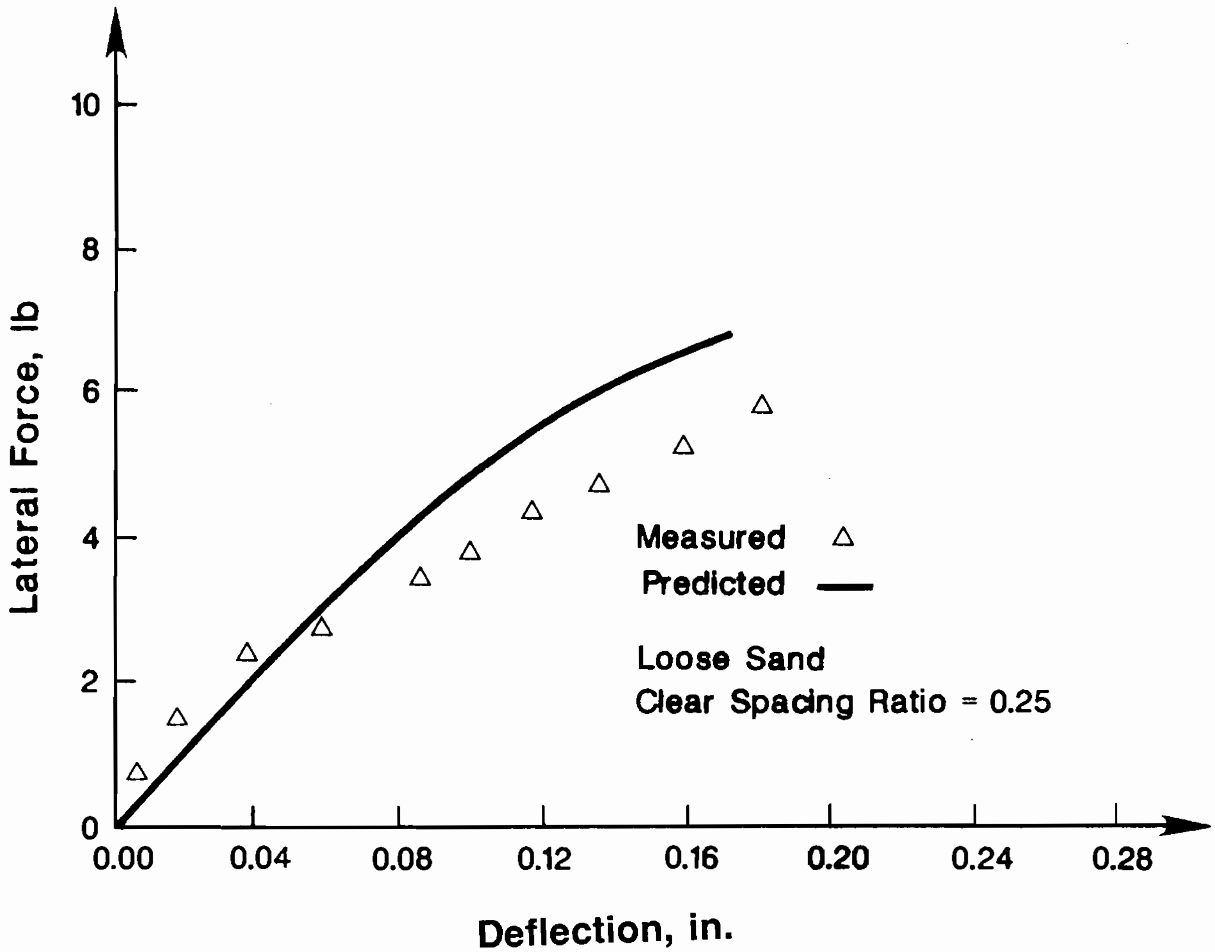

Fig. 7.41. The predicted and measured results for a pile in a pile group with 0.25-diameter clear spacing in loose sand.

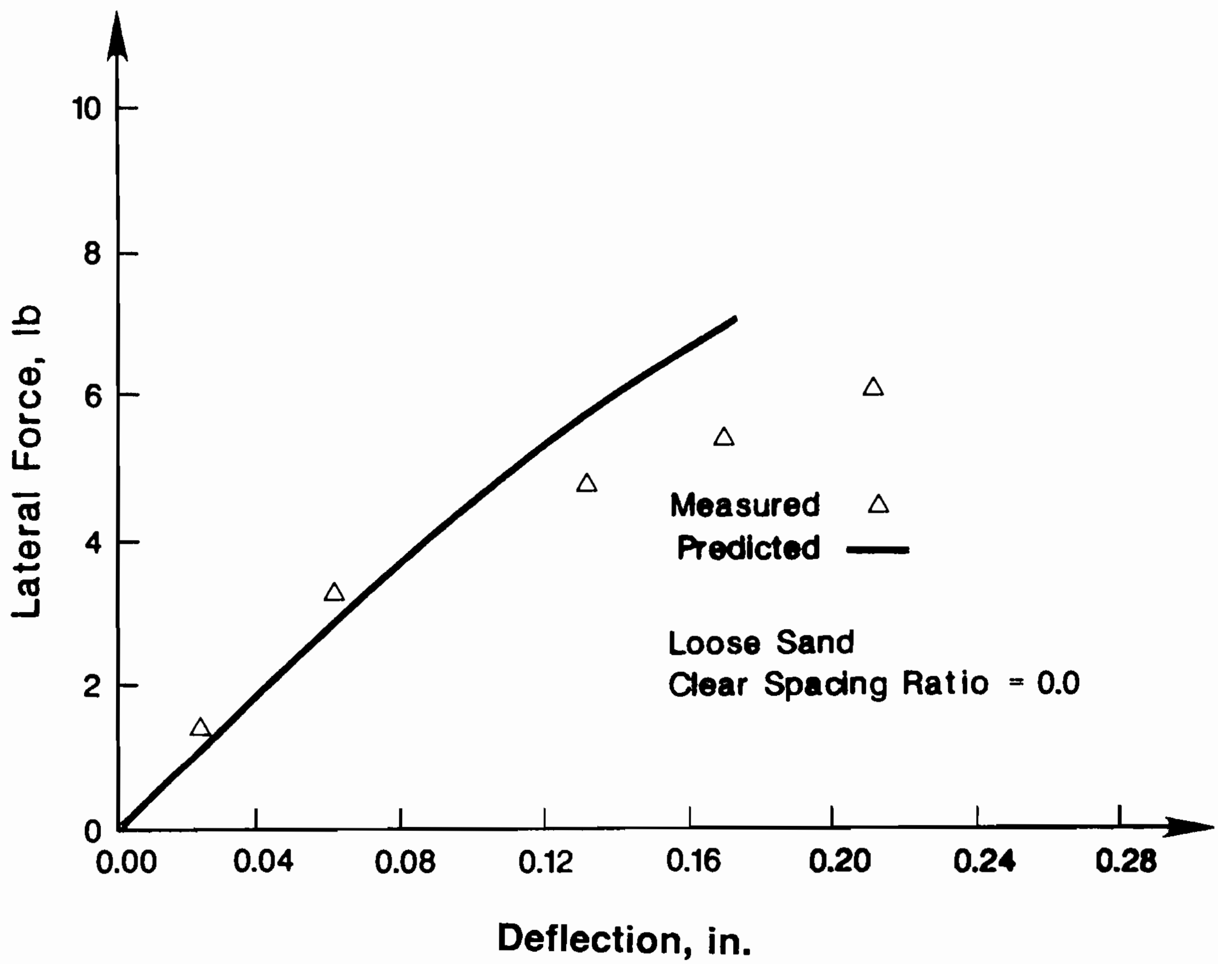

Fig. 7.42. The predicted and measured results for a pile in a pile group with zero clear spacing in loose sand.

CHAPTER 8. STUDIES OF CASE HISTORIES

INTRODUCTION

In the preceding chapter, the experimental verification of the proposed p-y criteria for drilled-shaft retaining walls was discussed. However, studies of case histories with data from field measurements are important. To facilitate the mathematical calculations, a computer program, PYWALL, for the complete analysis of drilled-shaft retaining walls was developed and is available through the University. The study of case histories presented in this chapter is for both the verification of the proposed method and for demonstration of the analytical procedure using PYWALL. To perform the analysis, it is necessary that information be available for wall dimensions, properties of the drilled shafts or piles, engineering properties of the soil, and response of the wall to loading. There are a limited number of case histories where this information is available. Only five case histories are included in this study. Three are for drilled-shaft retaining walls with close spacing of the drilled shafts. The other two are for diaphragm walls. These latter two are included because diaphragm walls are fundamentally similiar to the drilled-shaft walls with no interspaces between drilled shafts.

CASE STUDIES

Case No. 1 -- Drilled-Shaft Walls in Houston With Level Ground Surface

Williams and Shamooelian (1981) reported on a drilled-shaft retaining wall for a 24-ft deep excavation for a high-rise building in downtown Houston. The subsurface conditions consisted of 20 to 25 ft of stiff to very stiff clay and sandy clay underlain by a heterogeneous stratum of medium to dense, clayey and silty sand, sandy silt, and very stiff silty clay extending to about 70 to 75 ft in depth. The water table was at about 24 ft in depth. The retaining wall consisted of 48-in.-diameter drilled shafts, about 68 ft in length, and with a clear spacing of 12 inches. The arrangement of rebars in the drilled shafts was not given in the paper, but a gross stiffness (EI) was employed for the analysis. An inclinometer well, consisting of SINCO 3.34-in. O.D. plastic casing, was wired to the reinforcing cage for one shaft. Lateral deflections were calculated from the measured slope profile. In addition, movements at the top of the instrumented shaft were measured directly, using surveying techniques. Curves of lateral movement obtained at completion of the excavation to a depth of 24 ft and at elapsed times of, 0, 17, and 113 days are presented in Fig. 8.1.

A triangular distribution of pressure was assumed and the active earth pressure along the wall was back-calculated from the measured slope profile by Williams and Shamooelian. The earth pressure acting at the dredge level on a drilled shaft, taking into acount the spacing is about

$$
\begin{aligned}
P_a &= K_a \gamma H \ (b+S) \\
&= \gamma_e H \ (b+S) \\
&= (35)\ (24)\ (4+1) \\
&= 4200 \text{ lb/ft}
\end{aligned}
$$

This triangular pressure distribution, shown in Fig. 8.2, is the loading on the retaining wall. Subsurface soils between depths of 24 ft to 70 ft consist of stiff to very stiff overconsolidated clay mixed with layers of silty sand and sandy silt. This deposit, in general, can be treated as a clay layer with an undrained shear strength of about 1 to 2 ton/sq ft (Williams and Focht, 1978). A value of 1.5 ton/sq ft was selected for analysis. The average value of ε_{50} was assumed to be 0.005, and the submerged unit weight of the soil was 58 lb/cu ft. The input data regarding the soil and structural properties are shown in Fig. 8.2.

A comparison of measured and computed deflections of the wall for short-term loading is presented in Fig. 8.3. The agreement seems to be reasonable. The predicted values are larger than those

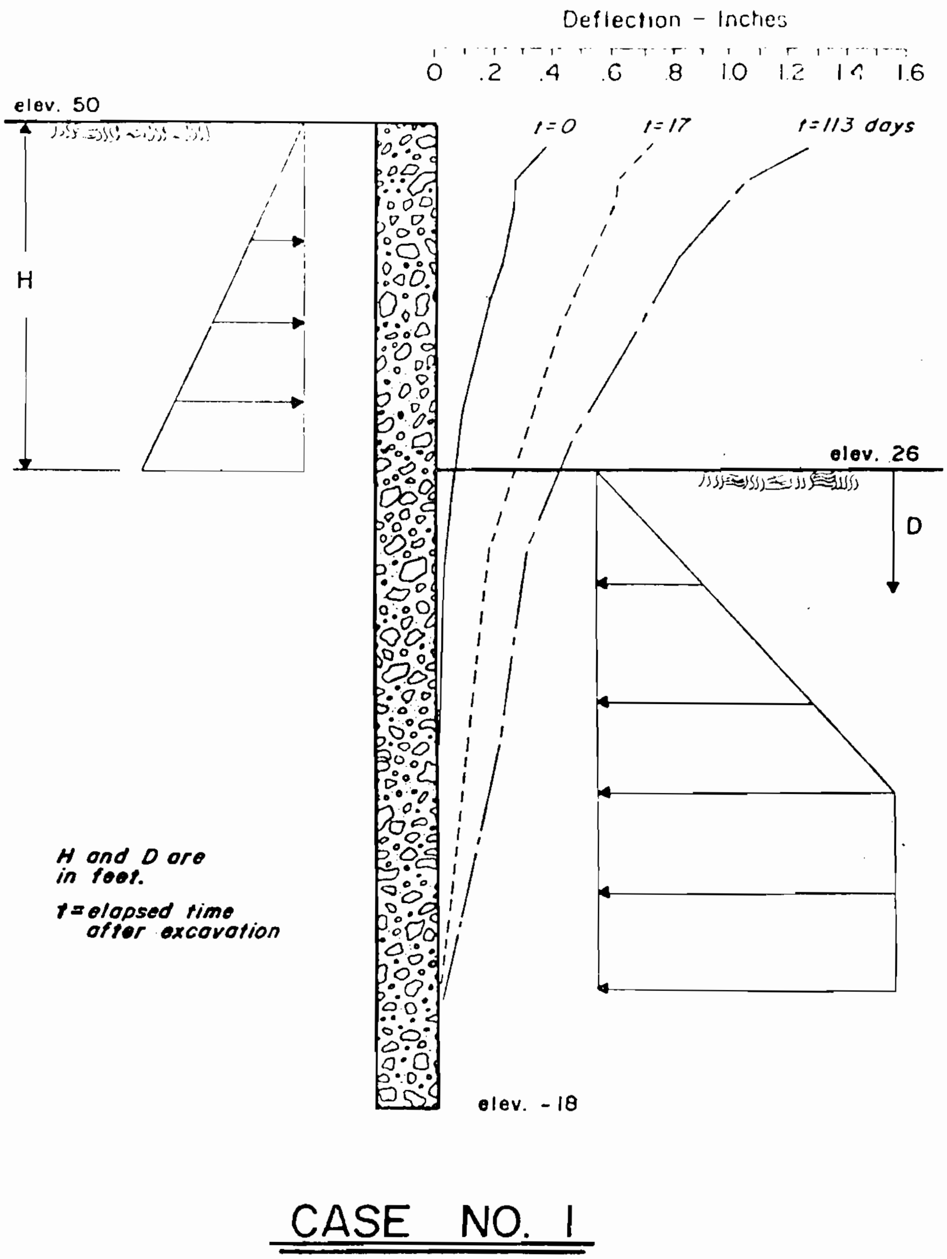

Fig. 8.1. The measured deflections for the instrumented drilled shaft at different elapsed times, Case No. 1 (after Williams and Shamooelian, 1981).

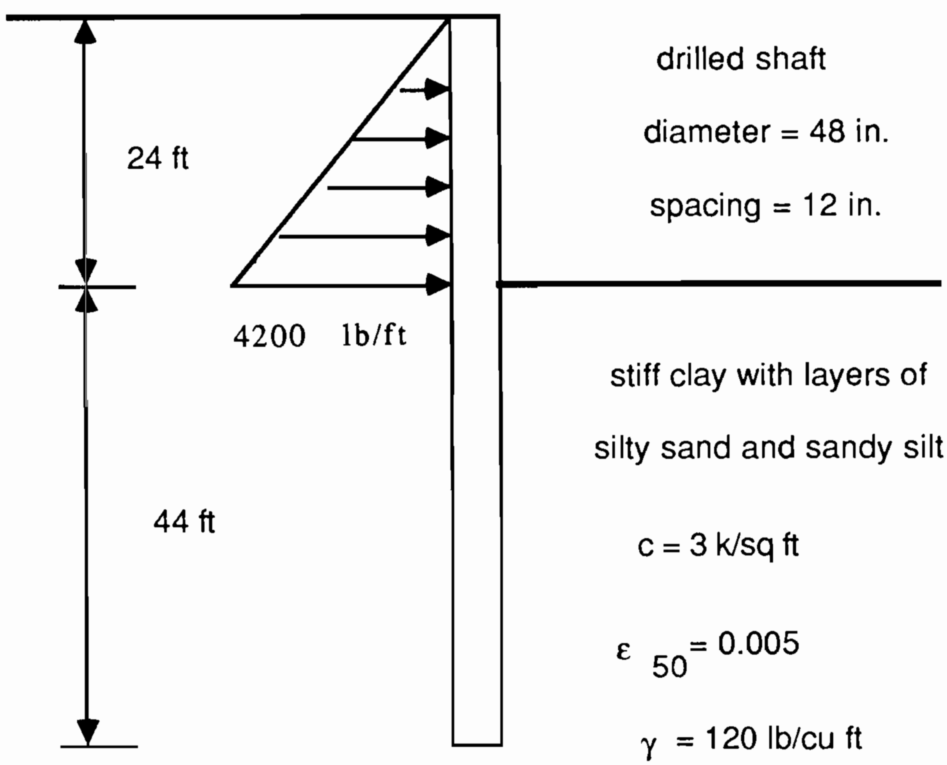

Fig. 8.2. Input parameters and earth pressure distribution along the wall, Case No. 1.

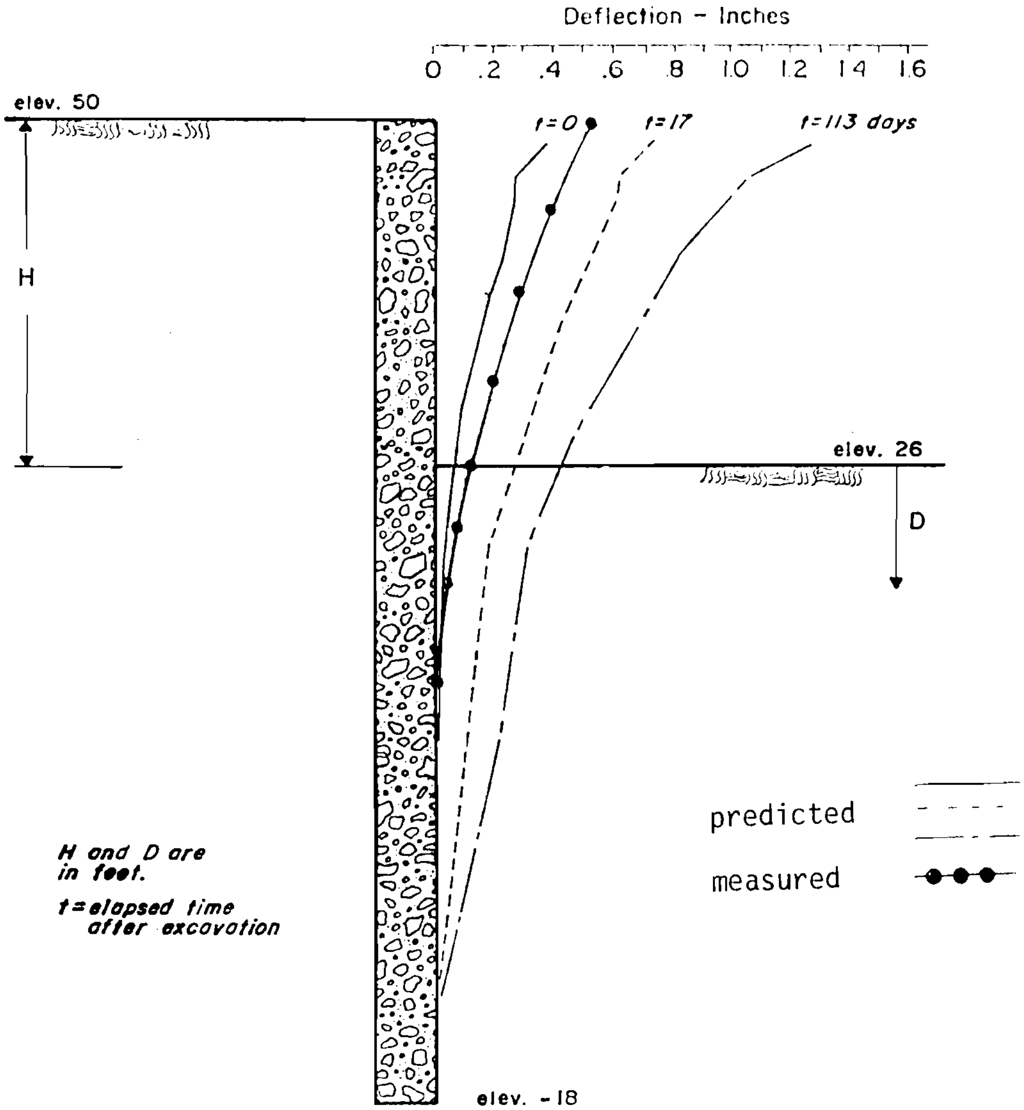

CASE NO. 1

Fig. 8.3. The comparison of measured and predicted short-term deflections on the wall, Case No. 1.

measured on the day of completion of excavation, but are significantly less than those obtained 17 days after the excavation.

The site is covered by an overconsolidated stiff clay and negative pore water pressures dissipated with time after the excavation. The active earth pressure based on a drained analysis is more critical than the undrained analysis. The earth pressure near the dredge level increases from 4200 lb/ft at completion of the excavation to about 6720 lb/ft 63 days after excavation was the completed. When the increased earth pressure is employed in the analysis, the predicted and measured deflections above the dredge level agree well as shown in Fig. 8.4. The deflections measured below the dredge level are higher than the predicted values. The soil below the dredge level may have been softened due to release of the negative pore pressure, and the soil may have been partially remolded by construction operations. Generally speaking, the predicted performance of this drilled-shaft wall is close to the field observations.

Case No. 2 -- Drilled-Shaft Walls in Houston With Transitional Slope at The Ground Surface

The second case reported by Williams and Shamooelian similar to the first one, is for a retaining wall that was installed in connection with the construction of a high rise tower in downtown Houston. An excavation with a depth of 31 ft was required for this case. Because there was sufficient area at the construction site, an upper transitional slope was cut and a shorter wall was used, as shown in Fig. 8.5. The drilled shafts were the same size and spacing as those used in Case No. 1. The subsurface conditions consisted of about 22 ft of stiff to hard clay, underlain by 40 to 50 ft of a heterogeneous stratum of medium-to-dense clayey silts and sands, silty sands, and stiff to very stiff silty clay. The groundwater level was observed at about 25 ft deep.

The monitoring system employed was similar to that used for Case No. 1. Deflections were obtained during and after excavation and in the time period between completion of the mat and construction of perimeter walls. The deflections along the

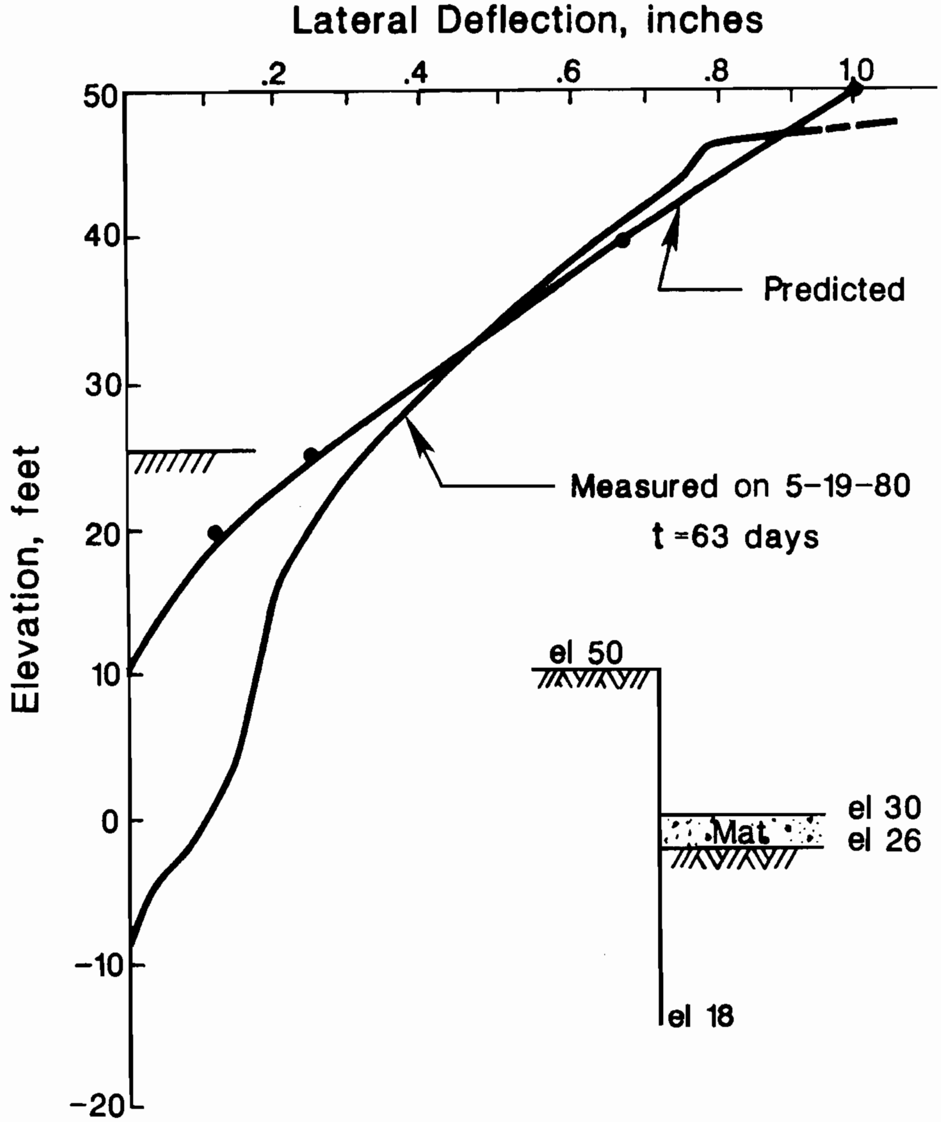

Fig. 8.4. The comparison of measured and predicted deflections on the instrumented drilled shaft after 63 days of excavation, Case No. 1.

drilled shaft were measured immediately after completion of the excavation and at 34 days after the completion. The coefficient of active earth pressure, estimated from Case No. 1, is about 0.3 based on an undrained analysis. If the ground had a plane surface, active earth pressure can be represented by a dashed line, as shown in Fig. 8.5. Because of the existing transitional slope near the ground surface, the resulting earth pressure was reduced, and can be simplified by assuming the pressure increases from zero at the top of the wall to full active pressure at the dredge level, assuming no cut (Fig.8.5). With this estimated distribution of pressure, the deflection of the wall was predicted by the analytical model and compared with the measured values as shown in Fig. 8.6. As may be seen, the agreement with the initial measurements is excellent. The predicted moment and shear diagrams for one drilled shaft are presented in Fig. 8.7 and 8.8, respectively. Based on the predictions of bending moment and shear by the computer, the drilled shaft can be designed with considerable confidence.

Case No. 3 -- Dunton Green Retaining Wall

The third case that involved drilled shafts for retaining systems is the Dunton Green retaining wall in London, reported by Garrett and Barnes, (1984). The subsurface conditions consisted of heavily overconsolidated Gault clay, which is known as a highly expansive clay. The weathered Gault clay was typically encountered at between the depths of approximately 4 m to 10 m below the original ground surface. The unweathered Gault clay was generally located at 11 m below the original ground surface. The Gault clay had a liquid limit of about 75 and a plastic limit of 28. These plasticity indices correspond to a clay of high plasticity. The moisture content is about 35% to 40% near the ground surface and decreased with depth to values near the plastic limit in the unweathered Gault clay. The moisture content in the near-surface layers, however, varies with rainfall and temperature throughout the year.

The undrained shear strength determined by conventional laboratory tests is highly variable (Fig. 8.9). One reason for

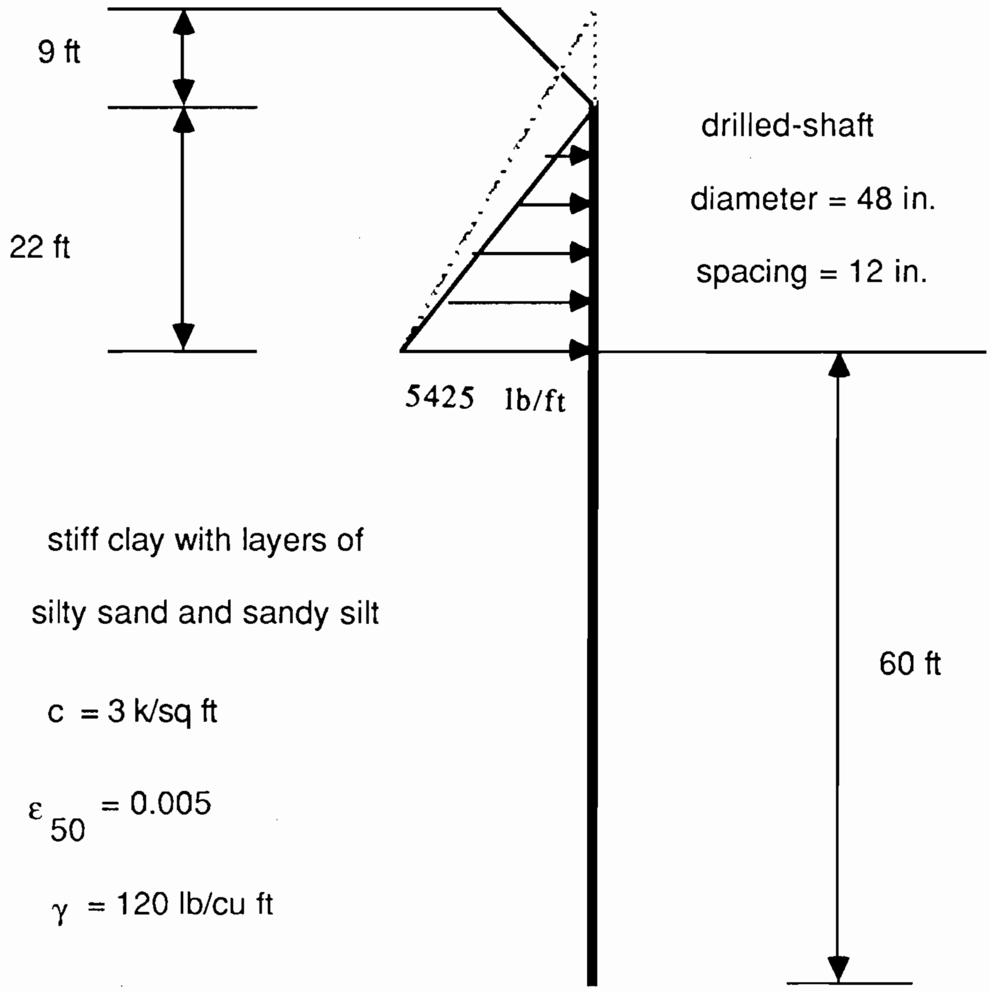

Fig. 8.5. Input parameters and earth pressure distribution on the wall, Case No. 2.

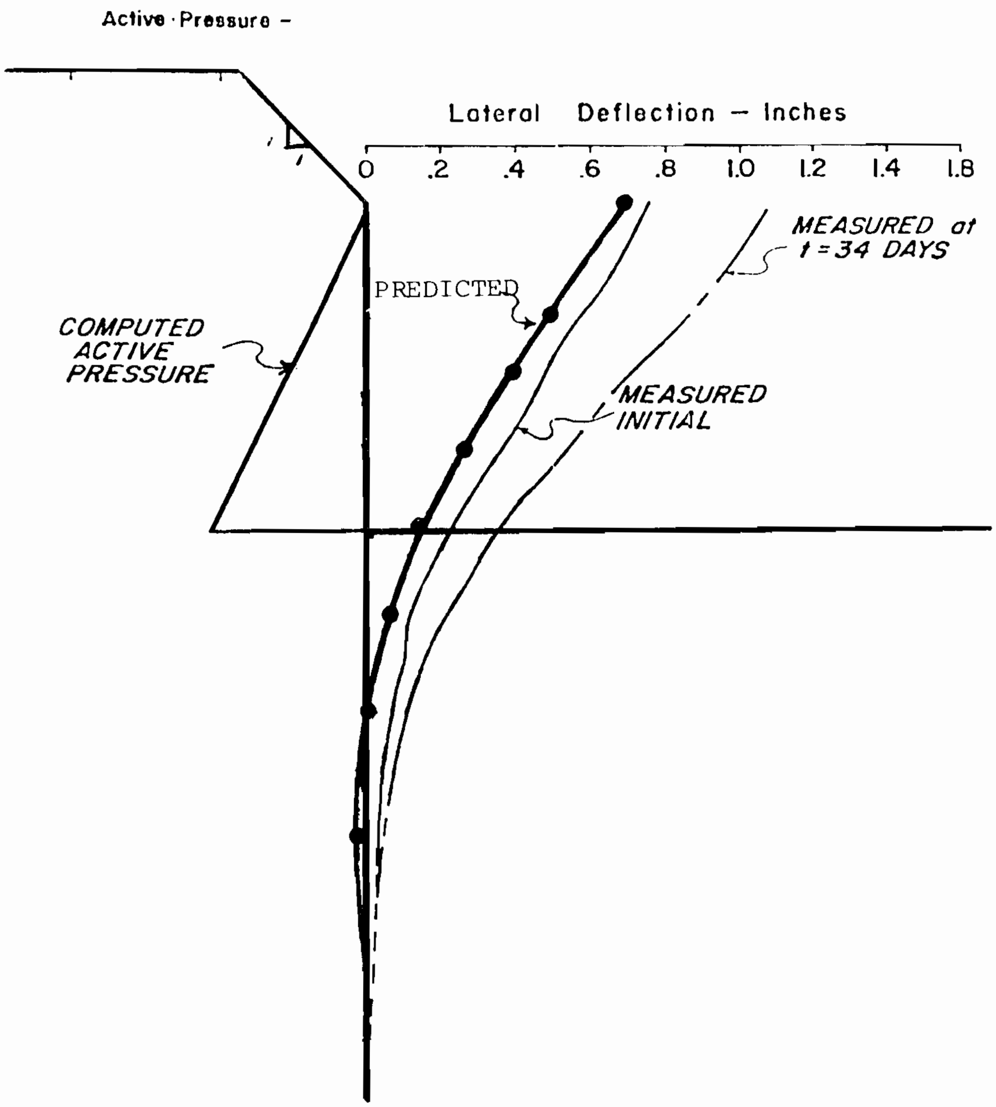

Fig. 8.6. The comparison of measured and predicted short-term deflections on the wall, Case No. 2.

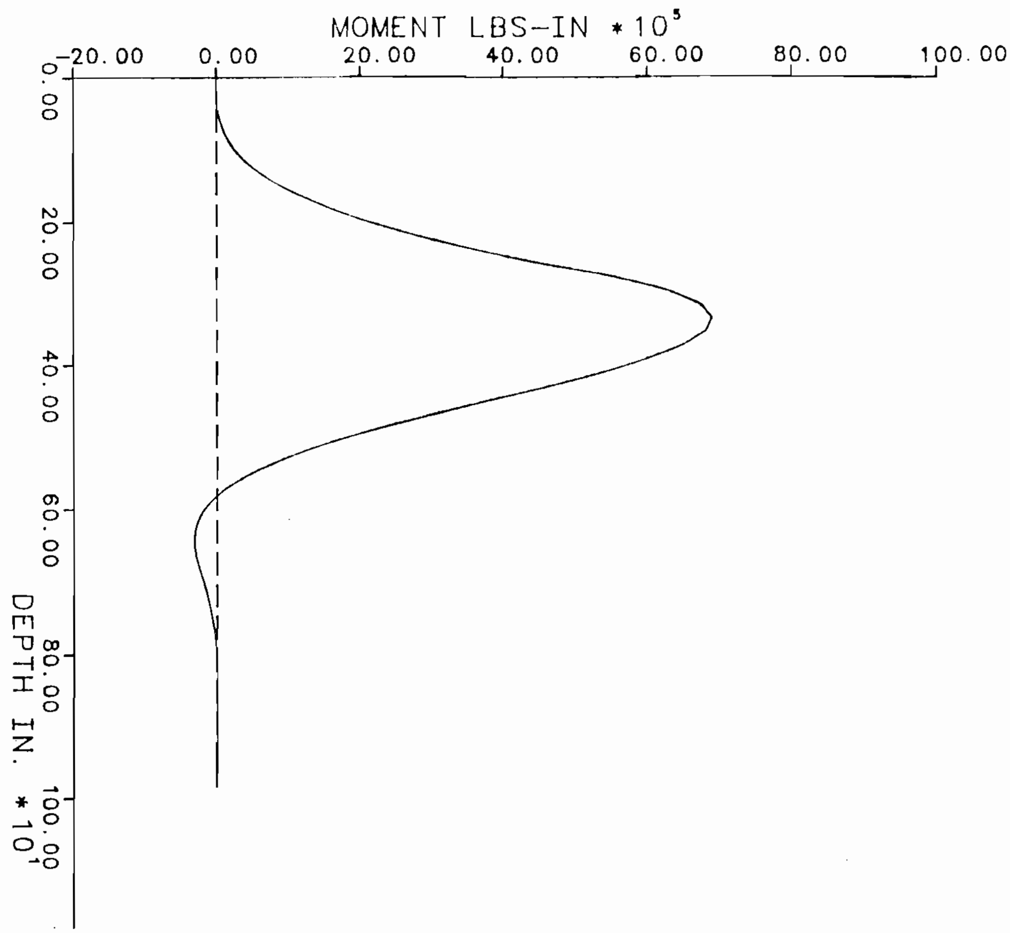

Fig. 8.7. Moment distribution curve along the drilled shaft as predicted for Case No. 2.

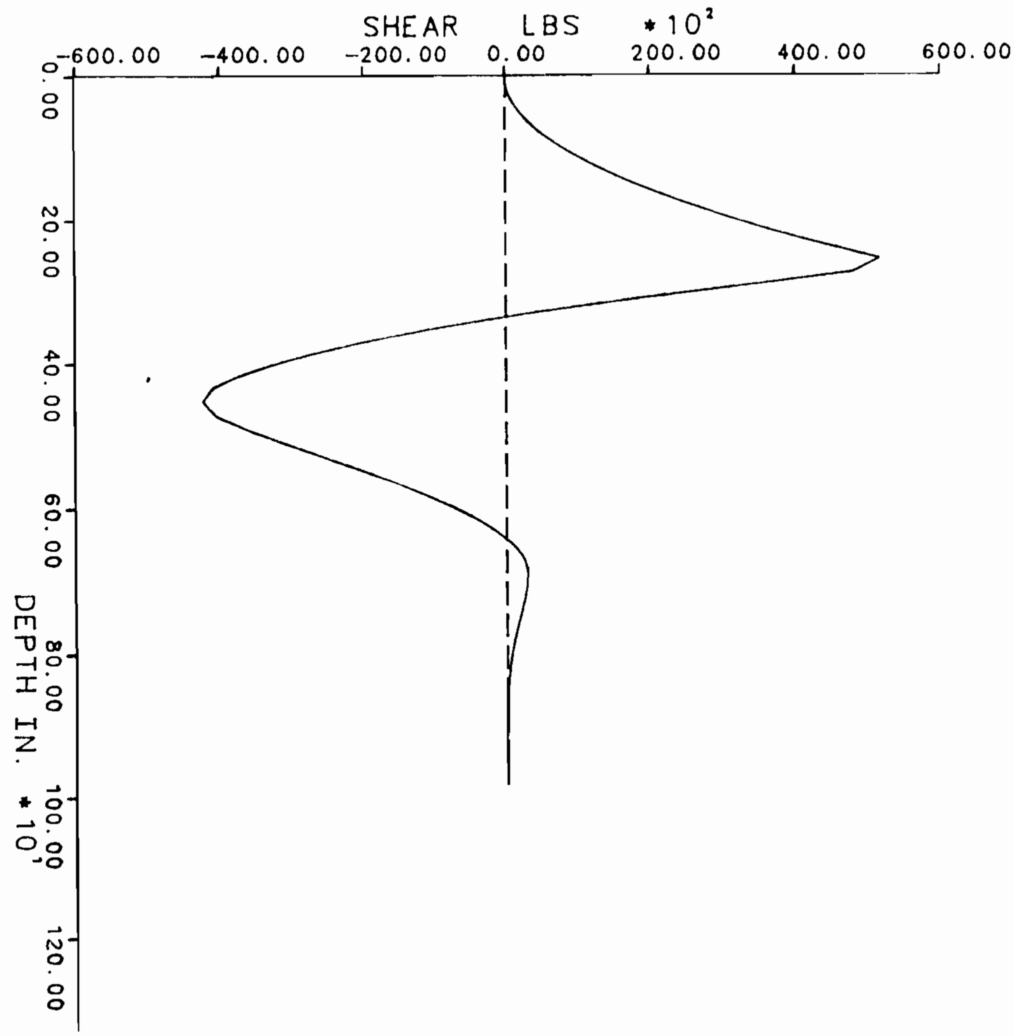

Fig. 8.8. Shear distribution curve along the drilled shaft as predicted for Case No. 2

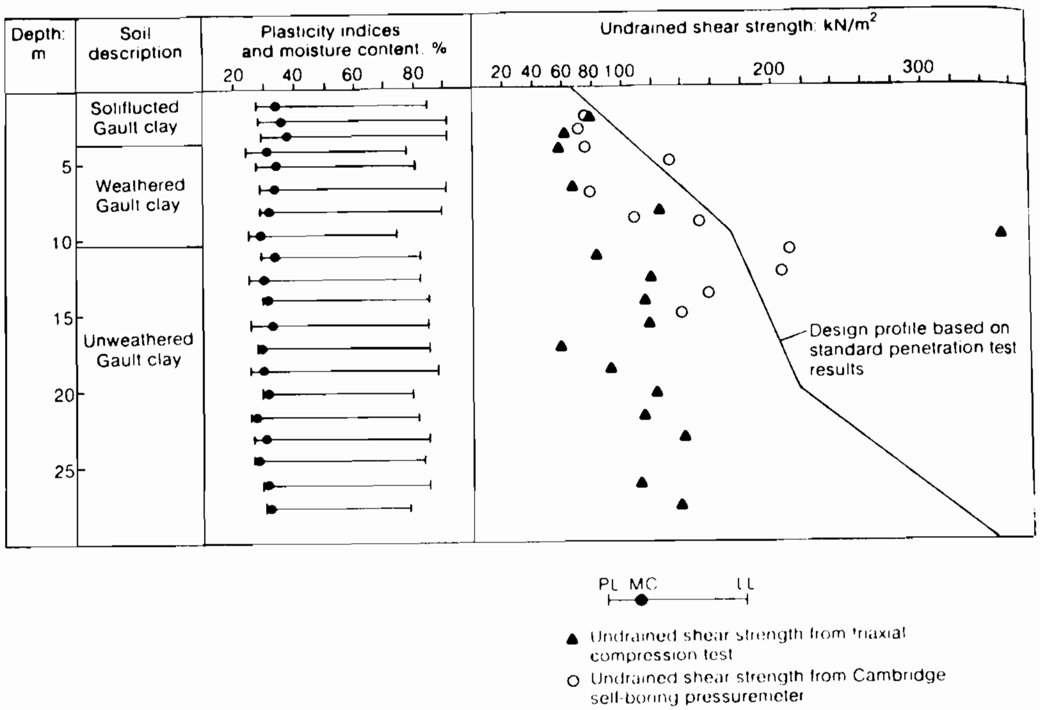

Fig. 8.9. The soil profile and strength parameters for the subsurface condition at the Dunton Green wall (after Garrett and Barnes, 1984).

the variation is that the Gault clay is a stiff and highly fissured clay and the size of the laboratory sample cannot represent the entire geologic stratum. The profile of undrained shear strength with depth determined from standard penetration tests along with the values obtained from laboratory tests on undisturbed samples and from in-situ tests using the Cambridge self-boring pressuremeter are shown in Fig. 8.9. For the drained analyses, the effective shear strength parameters were determined from laboratory tests and are presented in Table 8.1. Because a counterfort drainage system was located at every five meters along the wall, the water level remained constant near the dredge line. The diameter of the drilled shafts was 1.5 m and was spaced at 1.7 m center to center in this case study. The deflection of an instrumented area of the wall and of the retained ground were observed at the end of construction and after four years service. The unit weight of Gault clay was about 19 kN/m, and the active earth pressure at the dredge level at the dredge level for the short-term analysis can be estimated as

$$
\begin{aligned}
p_a &= K_a \gamma H - 2c\sqrt{k_a} \\
&= \gamma H - 2c \quad \text{(assume } \phi = 0,\ K_a = 1\text{)} \\
&= \gamma H \quad \text{(ignore the tensile strength)} \\
&= (19)\ (6.3) \quad \text{(earth pressure at the dredge level)} \\
&= 120\ \text{kN/m}^2
\end{aligned}
$$

The center to center spacing of drilled shafts was 1.7 m. The active pressure was assumed to vary from zero at the top of the wall to 120 x 1.7 = 204 kN/m at the dredge level. The input data prepared for computer analyses are presented in Fig. 8.10. A comparison between the measured and computed deflections is shown in Fig. 8.11, and the agreement is good. The wall deflections measured three and half years after the completion of the construction were about twice the initial deflection. Therefore, the long-term performance for drilled-shaft walls in overconsolidated clay can be predicted roughly based on this study.

TABLE 8.1. DESIGN EFFECTIVE SHEAR STRENGTH PARAMETERS (AFTER GARRETT AND BARNES, 1984)

Subdivision of Gault clay	Effective cohesion c' : kN/m^2	Effective angle of shearing resistance
Soliflucted	0	14
Cryoturbated	0	14
Weathered	13	24.5
Unweathered	13	24.5
Remoulded	10	23

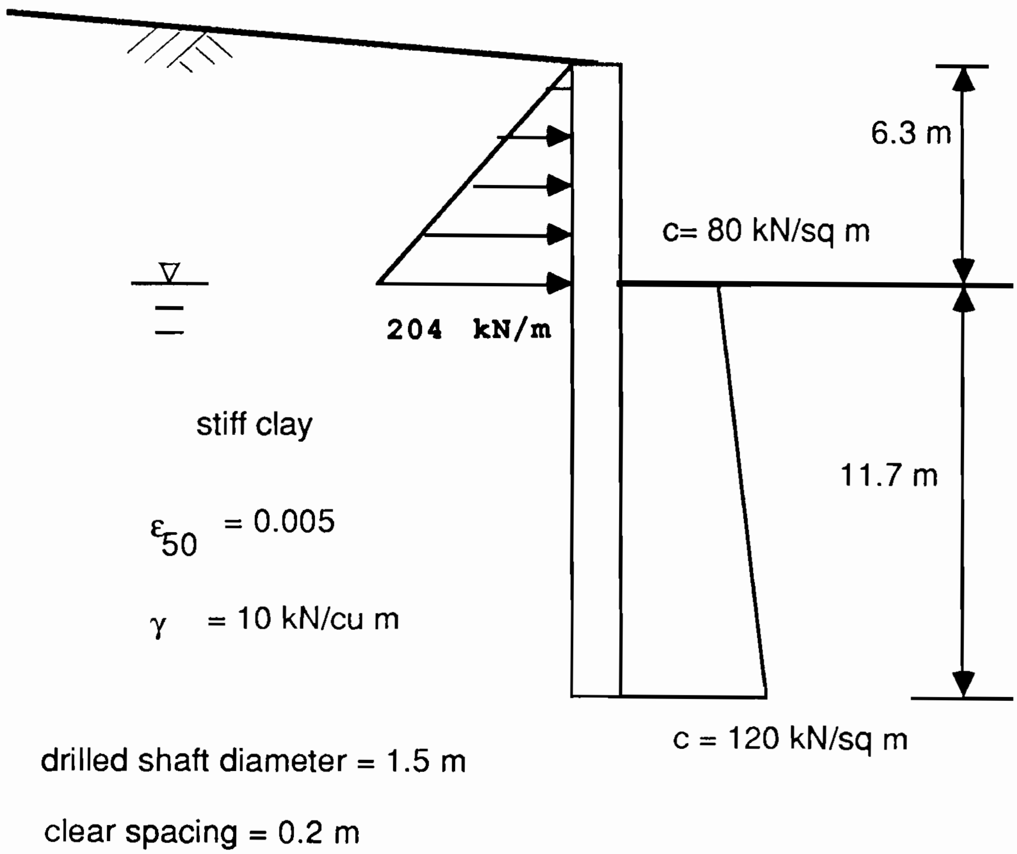

Fig. 8.10 Input parameters and earth pressure distribution on the wall, Case No. 3.

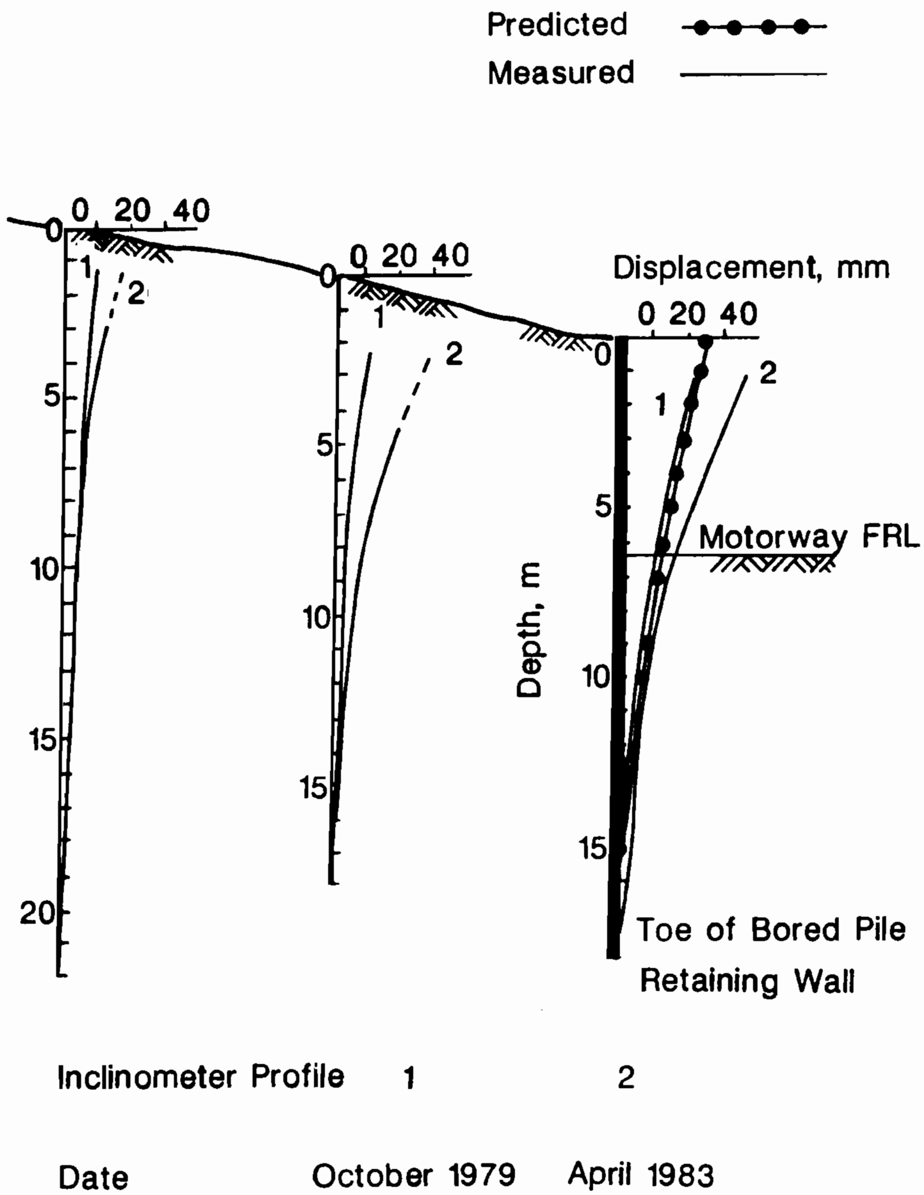

Fig. 8.11. The predicted and measured deflections on the Dunton green retaining wall.

Case No. 4--Diaphragm Wall for Underpass Construction

The measured performance of a diaphragm wall for underpass construction at Neasden Lane in North London was reported by Sills et al (1977). Actually, the problem encountered is a plate subjected to tranverse loads, but, in general, the design of diaphragm walls is simplified by treating a unit width of the wall as a beam-type structure. Thus, the p-y analysis is capable of handling the design of diaphragm walls assuming a unit width of wall is equivalent to one drilled shaft. The wall is 0.6 m in thickness, and the moment of inertia for a unit-width is about 0.018 m^4. The wall was installed to a depth of 13 meters and the total depth of excavation was 8.25 meters.

The subsurface consisted of mostly stiff fissured London clay. Relevant soil properties obtained from laboratory tests are shown in Fig. 8.12. The undrained shear strength increases linearly with depth. The moisture content is relativly low and is about 30%. The excavation was accomplished in four stages, and at end of each stage two vertical rows of tiebacks per panel were installed. Each panel was 5 m in width. All tiebacks were prestressed to 400 kN. The tieback loads were measured by load cells during excavation. Generally, the prestresses did not vary significantly during excavation. The measured deflection at the end of stage I is of most interest to this study because no tieback was installed for this stage, and the active earth pressure can be estimated.

The top 2.5 m. of soil was removed after the first stage construction and the active earth pressure acting on the cantilever portion was calculated in a manner similar to that used for the previous case. The active earth pressure acting at the dredge level is about 23.8 kN/m. The undrained shear strength employed in the analysis varied from 120 kN/m^2 at the top of the clay layer to 200 kN/m^2 at the tip of the wall. The general information regarding the soil and structural properties is presented in Fig. 8.13. The predicted deflections of wall at the end of stage I agreed well with the measured results, shown in Fig. 8.14.

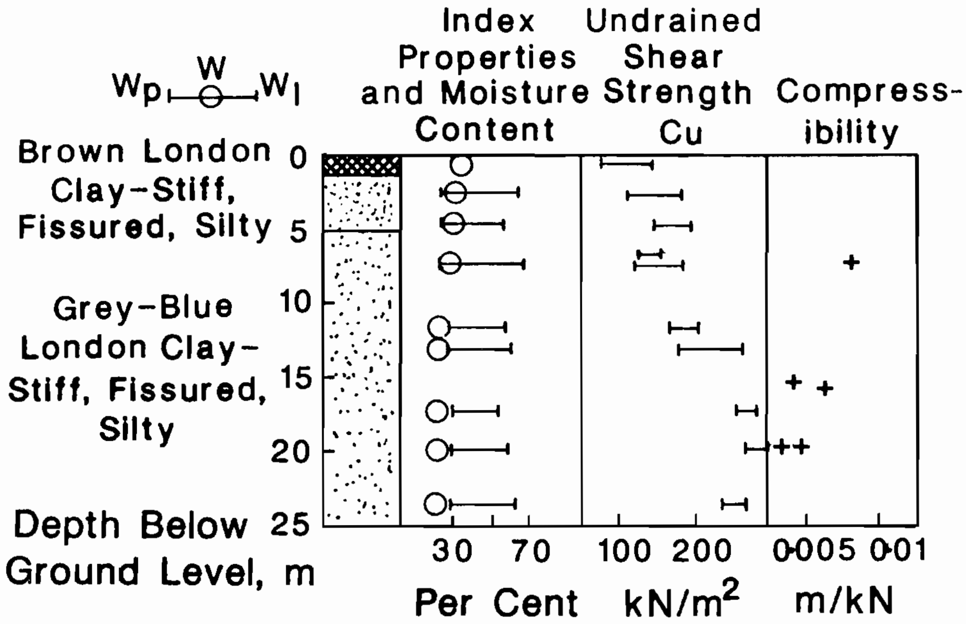

Fig. 8.12. Soil profile and strength parameters for case No. 4 (after Sills et al., 1977).

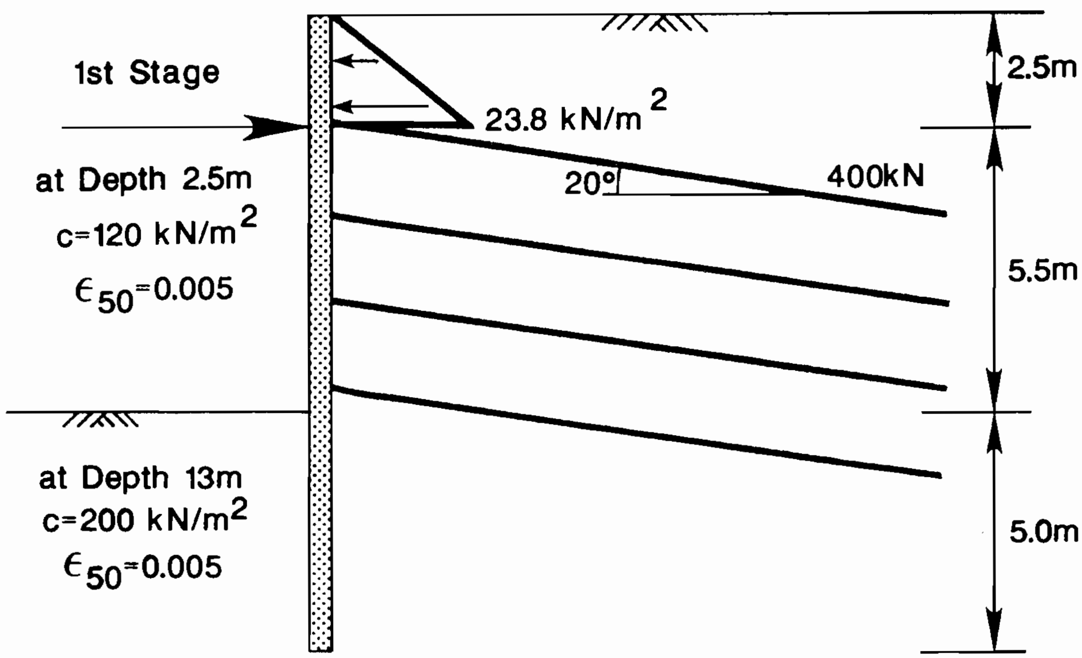

Fig. 8.13. Input parameters and earth pressure distribution on the wall, Case No. 4.

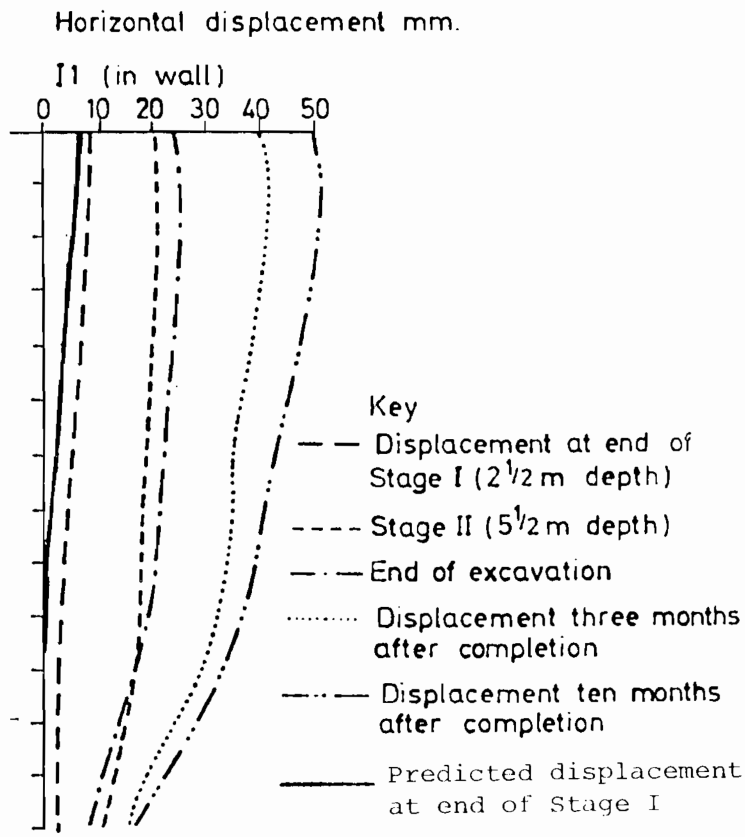

Fig. 8.14. The predicted and measured deflections on the diaphragm wall, Case No. 4.

Case No. 5--Multi-Tied Diaphragm Walls for Keybridge House

A full-scale measurement of multi-tied diaphragm walls for Keybridge House in London reported by Littlejohn and Macfarlane (1975), provides a good example for study the performance of concrete wall in cohesionless soil. A 0.61 m thick diaphragm wall was installed to a depth of 16.7 meters. Young's modulus of the wall was given as 24,500 mn/m^2. The effective depth of excavation was 14.45m, and the wall was anchored at three levels. Inclinometers were placed in the wall to measure deflections and load cells were installed to measure the loads from anchors. The readings were taken during the excavation.

The soil conditions and the retaining system are shown in Fig. 8.15. The site is covered by 8 meters of gravel overlying London clay. The first 3.05 meters of excavation was in gravel and there was no tieback to support the wall. The wall behaved as a cantilever wall and the measured deflection at the top of the wall was about 10 mm.

The active earth pressure at the dredge level during the cantilevel stage (Fig. 8.16) was calculated as

$$
\begin{aligned}
P_a &= K_a \gamma H \quad (\ \phi = 35^\circ,\ \gamma = 19.2\ \text{kN/m}\ ) \\
&= (0.27)\ (19.2)\ (3.05 + 1.67) \\
&= 24.6\ \text{kN/m}
\end{aligned}
$$

The equivalent diameter is taken as a unit meter and the flexural rigidity of wall is determined by

$$
\begin{aligned}
EI &= (2.45\times10^7\ \text{kN/m}^2)\ (\ (1)(0.61)^3\ /\ (12)\quad \text{m}^4\ ) \\
&= 4.63\times10^5\ \text{kN-m}^2
\end{aligned}
$$

The predicted deflection near the top of the wall compared with the measured results are presented in Fig. 8.17. The agreement is good for this stage, in which the performance of the wall is strongly dependent on the response of the sand layer near the ground.

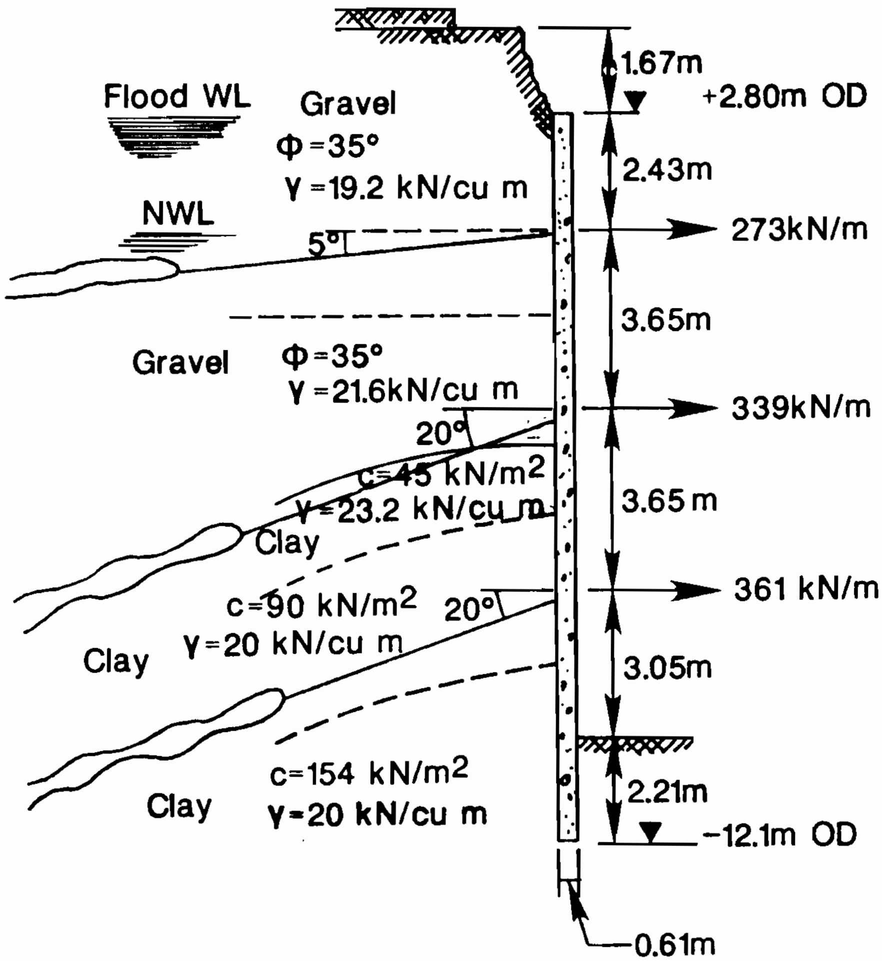

Fig. 8.15. The soil condition and retaining system for keybridge house (after Littlejohn and Macfarlane, 1975).

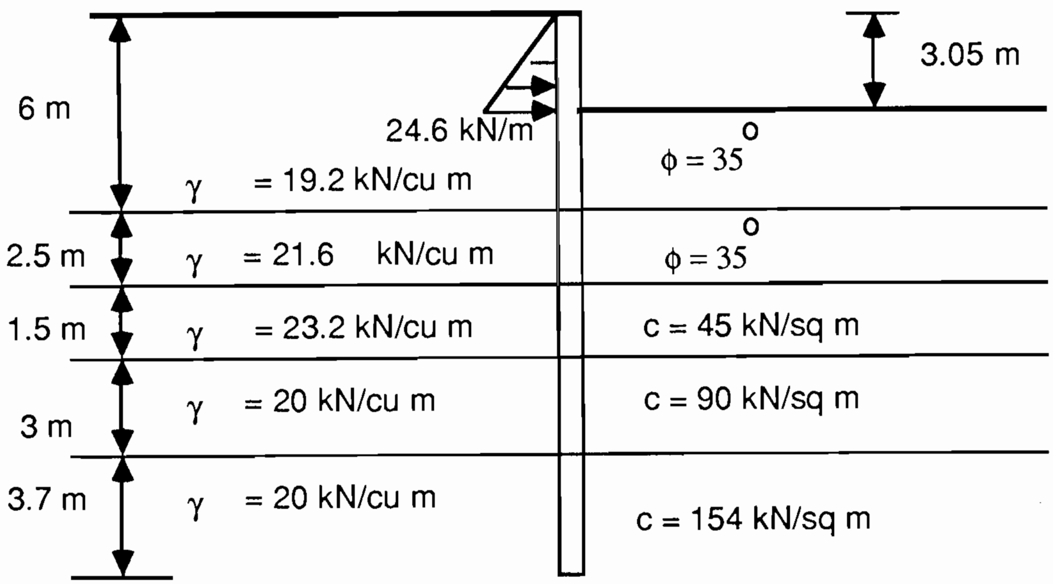

Fig. 8.16. Input parameters and earth pressure distribution on the wall at the end of first stage of excavation for Case No. 5.

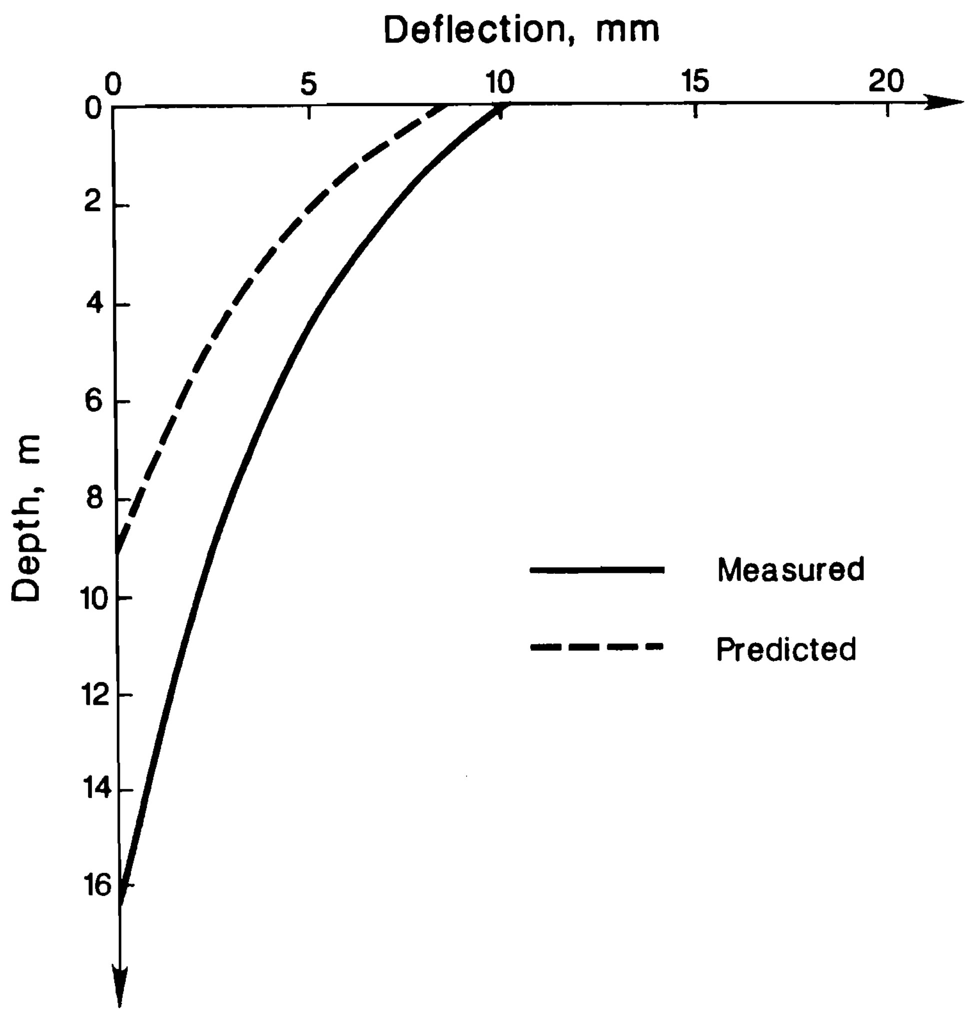

Fig. 8.17 The predicted and measured deflections on the diaphragm wall, Case No. 5.

COMMENTS ON RESULTS OF CASE STUDIES

The case studies presented in the proceeding sections include three drilled-shaft walls and two diaphragm walls. In general, agreements between experiment and analysis range from good to excellent. At present, it can not be stated with certainty that this method will be successful for every field condition. The success of the proposed method will rely on more full-scale field measurements.

The computer analysis based on the p-y method appears to be versatile for engineering design of retaining walls. The method presented in this study is limited primarily to analyses of short-term performance of drilled-shaft or diaphragm walls, but by using experience gained from the field observations, long-term behavior can be related to the short-term behavior.

CHAPTER 9. DESIGN RECOMMENDATIONS

INTRODUCTION

This chapter describes the detailed procedures of design with the recommended p-y method. From the viewpoint of practical engineeers, a good design method should be straightforward and self-explanatory. The material presented in the preceding chapters concentrated on the discussion of each individual component that is involved greatly in making the decision. A guidelines for design can be established by combining significant findings from each chapter. The step-by-step procedures of design illustrated in the following section may prove to be useful in engineering practice.

DESIGN STEPS

Assemble All of The Information on Soil Properties

All of the information on soil properties at the site should be analyzed and a soil profile should be selected for design. The information must include: stratigraphy of the site, position of water table, physical properties of sublayers, and strength parameters. If there is uncertainty about the soil properties, upper-bound values and lower-bound values may be selected.

Predict The Earth Pressure on The Wall

The active earth pressure was recommended to be used for a given wall height in this study. The drainage condition of ground water needs to be concerned. If the drained and undrained conditions both may occur in the future, the critical case should be selected. In general, the active earth pressure on the drilled-shaft wall is developed because of excavation in front of the wall. However, if the earth pressure on the wall is induced by the backfill material, the prediction of the load from the earth pressure needs to consider the method of the backfill. The state of stress behind the wall will clearly be dependent on the construction sequence.

Surcharges cause in an increase of the lateral earth pressure and should not be ignored. The lateral pressure resulting from surcharge can be estimated from the equations presented in Chapter 4.

Select a Trial Spacing Between Drilled Shafts

The selection of spacing for a drilled-shaft wall is an important issue in the design procedures. Based upon the findings of the analytical and experimental studies, soil resistance on a drilled shaft decreases with the decrease of the spacing; therefore, larger spacing allows the surrounding soil resistance to be developed more efficiently. However, selection of a large spacing can creat other problems for construction. For example, the water may seep through the gap and cause serious erosion in cohesionless soil during construction. The cantilever portion of drilled shafts may need some concrete slab to cover the exposed soil for good appearance and the large spacing generally makes the work difficult.

Results from either analytical and experimental studies indicate that the soil resistance is reduced dramatically when the clear-spacing is less than 0.5 diameters. It seems that a design spacing of 0.5 to 1.0 diameter will not lose any significant amount of soil resistance due to group effects and is acceptable for many construction procedures. Of course, selection of a proper spacing is also affected by other factors. For example, if a drilled-shaft wall is incorporated as a permanent part of the basement of building, drilled shafts, in general, are installed next to each other.

Compute Lateral Load on a Drilled Shaft and Estimate The Diameter and Flexural Rigidity of Cross Section

After the spacing has been decided, the lateral load on a drilled shaft can be computed by the product of the active earth pressure per unit width times the spacing. The diameter of a drilled shaft can be decided approximately based on the magnitude of the lateral load. The flexural rigidity is computed based on the gross-section EI for the preliminary design. Later, if the loading range is larger than 50% of the design load as defined in Chapter 5, either a equivalent constant EI-value or a nonlinear EI-value should be used for the load-deflection analysis.

Use Recommendations and Get Modified p-y Curves

The soil resistance curves recommended in Chapter 6 have been added into the design program, PYWALL. If such a comprehensive program is not available in the office, p-y curves of a single pile can be modified by following the equations presented in this study. Both the elastic group effects and shadowing effects must be taken into account.

Structural Analysis Based on The "Long" Pile Behavior

Compute the deflection, bending moment, and shear force along a drilled shaft. Check the maximum bending moment and shear on a drilled shaft to see if the structural design satisfies the ACI-Code. If not, another cross section needs to be selected. Check the deflection at the top of drilled shafts to see if the deflection is sufficient for development of active earth pressure and if the deflection such as not to cause damage of neighboring structures. Make such adjustments as necessary in dimensions of the drilled shaft.

Decide The Penetration Depth

The penetration of drilled-shafts is of importance for the deflection of drilled-shaft walls. The effects of penetration in foundation soil can be illustrated by the nondimensional method for the analysis of laterally loaded piles (Matlock and Reese, 1962). Assume that soil modulus k is a linear function of depth as $k = mx$, where m is a soil stiffness parameter and x is the depth below the ground surface. The deflection of an elastic pile acted by a lateral load P_t and moment M_t can be obtained from Eq. 9.1.

$$y = A_y \frac{P_t T^3}{EI} + B_y \frac{M_t T^2}{EI} \tag{9.1}$$

where A_y and B_y are the deflection coefficients associated with the external load P_t and M_t, respectively, and T is the relative stiffness factor. In general, T is a dimensional parameter, which relates the stiffness of the soil and the piles as

$$T = \sqrt[5]{\frac{EI}{m}} \tag{9.2}$$

How pile deflections vary with the nondimensional depth coefficient, L/T (L is the length of the pile) is shown in Fig. 9.1. The pile deflections produced by the lateral load at the ground line are significantly influenced by the pile length when L/T is less than 3. However, for a long pile, with L/T is larger than 5, pile length is insignificant to the pile deflection. Figure 9.2 shows the results of studies when the penetration of the drilled shaft is gradually reduced. The groundline deflection is unaffected by increased penetration beyond a critical depth. However, as the penetration becomes less than the critical depth, the deflection sharply increases, indicating failure. For this example, the critical depth is about 18 feet for a lateral load of 10 kips and about 24 feet for a lateral load of 30 kips. From an economic standpoint, the penetration should be as short as possible. However, using engineering judgement, penetration should be larger than the critical length to avoid excessive deflection.

The critical depth depends on the foundation soil, structural properties, and loading conditions. The study by Swan, Wright, and Reese (1986) suggests that it is more beneficial to have a shaft exhibit two points of zero deflection. From this study, it appears that an L/T of about 4.8 can give the required shaft penetration needed to obtain two points of zero deflection for a particular shaft and soil conditions. If the zero-deflection points along a drilled shaft are more than three, the penetration can be reduced.

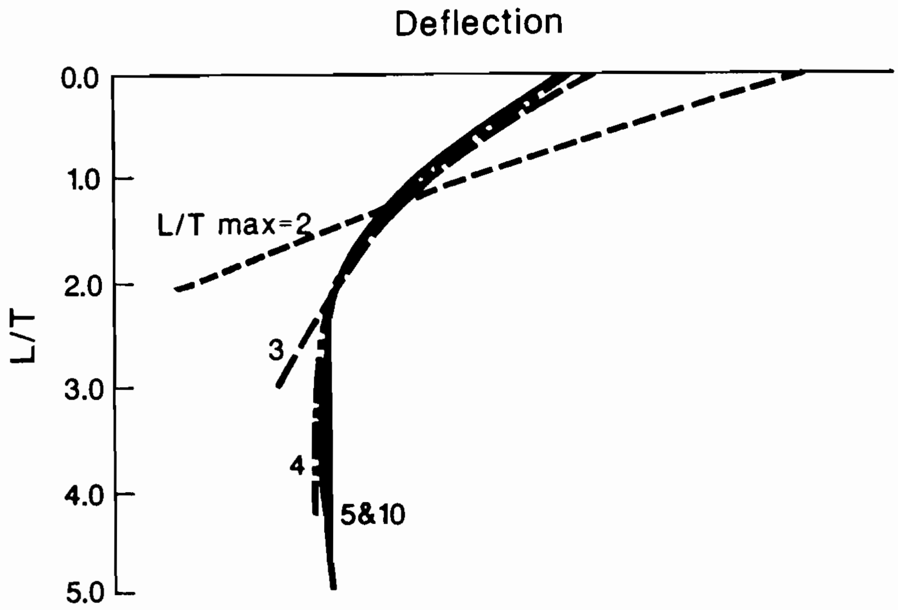

Fig. 9.1. Pile deflection versus L/T for varied length (after Swan, Wright, and Reese, 1986).

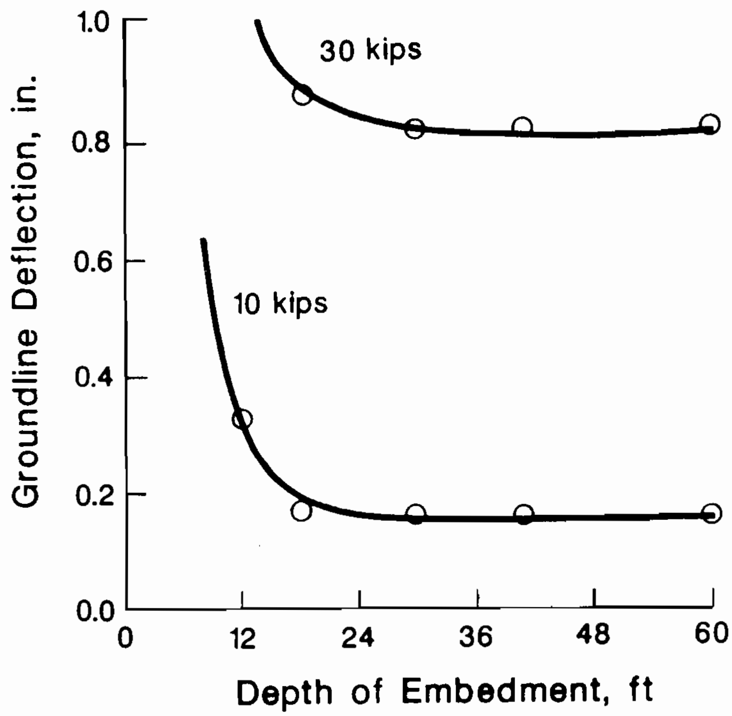

Fig. 9.2. Effect of depth of embedment of lateral deflection in sand

Adjust The Spacing and Pile Geometry if Necessary

Up to this step, the design parameters have been set up and checked out preliminarily. If the computed behavior of the wall is not adequate, adjustment needs to be made. The design parameters are influenced by each other. If the earth pressure on a drilled shaft is too large to be taken by the structure due to a wider spacing, there are two remedies that can be made. One is to reduce the spacing and the other is to change the pile geometry. Several trials may be necessary in order to find the most economical solution.

Check Overall Stability

Retaining walls may fail because of a general slope failure that causes movement as a unit of the wall and surrounding soil and the problem of overall stability should not be neglected in the analysis.

The penetration of the drilled shafts is a beneficial factor regarding the overall slope failure. The analysis of overall stability can be done by the circular arc, the wedge, or other limit-equilibrium methods with the aid of computers. A minimum safety factor of 1.5 is recommended for noncritical applications and 3.0 for critical applications. The higher safety factor should be used if there are buildings next to the wall.

A simple method to examine overall stability in cohesive soils can be done by treating the soil mass above the dredge line as a surcharge on the foundation (Fig.9.3). The safety factor can be obtained approximately from

$$F.S = \frac{5.14c}{\gamma H} \qquad (9.3)$$

where

c = the cohesive shear strength,

γ = the soil unit weight,

H = the height of the wall.

From Fig.9.3, it can be noted that if the cohesive strength is constant with depth, the safety factor is independent of the depth of penetation of the piles. In that case, the height of the wall should not be larger than

$$H_{cr} = \frac{5.14c}{\gamma\ (F.S.).}$$

However, in most situations the shear strength is not constant and increases with depth. A deep penetration of the drilled shafts will usually cause layers of soil with increased strength to come into consideration. For such complex strata, a comprehensive computer program such as SSTAB1 (Wright, 1982) can be used for the stability analysis.

Overall stability of the wall system must be considered for every application. If the safety factor is too low, additional penetration of the drilled shafts may be required.

CONCLUDING COMMENT

It is evident that the above steps need to be repeated several times to obtain an acceptable design. In addition to technical considerations, other factors, such as the construction time, construction cost, and environmental conditions, may need to be judged before a final design is selected.

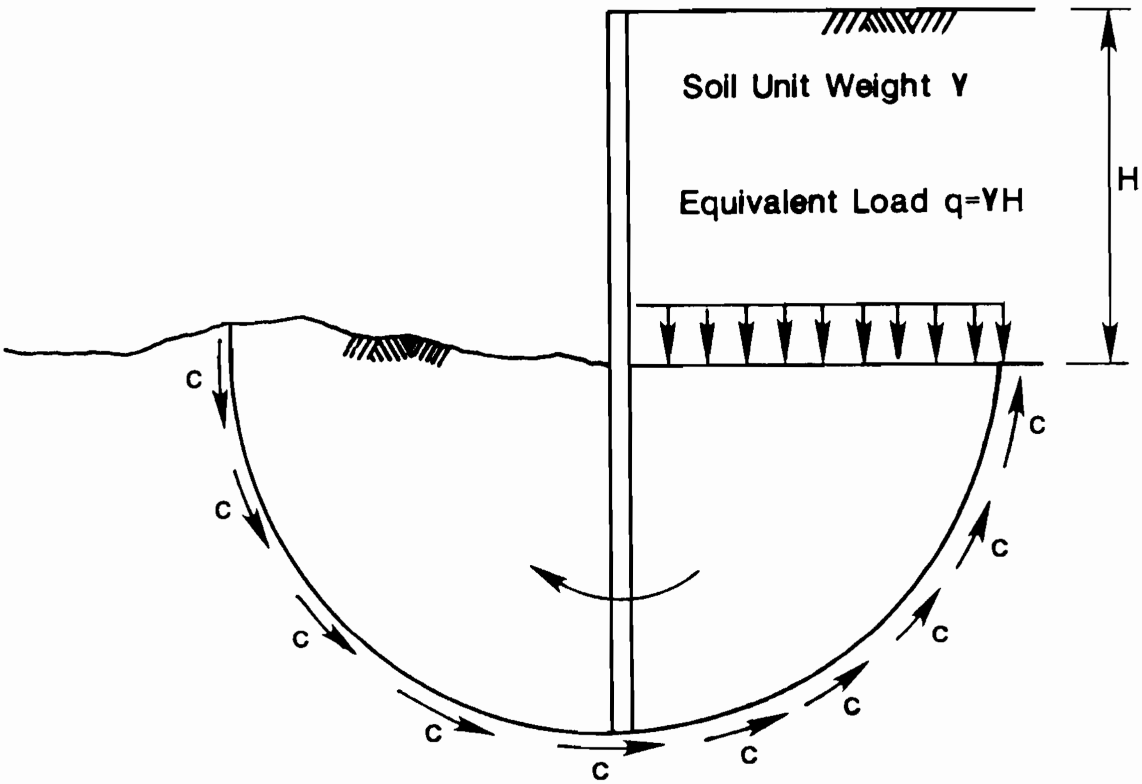

Fig. 9.3. Check of overall stability by the equivalent-load method

CHAPTER 10. CONCLUSIONS

The problem of analysis and design of retaining structures is complex because of the large number of variables involved in the soil-structure-interaction problem. To develop a rational method for the design of drilled-shaft retaining walls, the individual influence of these variables must be investigated thoroughly. Three important components for the design of drilled-shaft walls have been studied in this report. These are (1) the earth pressure acting on the wall, (2) the resistance the soil to the lateral movement of the shafts, and (3) the structural response of the drilled shafts. These studies are relevant to a complete analysis of the interaction between the soil and the structure.

In addition, small-scale experiments were conducted to verify the proposed p-y curves for piles in a row, that are derived based upon the analytical solution.

Several case studies indicate that the approach presented herein can predict the behavior of retaining structures quite well by taking into account the soil-structure-interaction. The selection of the penetration length, diameter, spacing, and flexural resistance of drilled shafts can be facilitated by the method.

Significant findings and conclusions are the following:

(1) Active earth pressure, calculated by conventional earth-pressure theory, can be used as the driving force on drilled-shaft walls. However, to achieve the active states of stress, deflections along the drilled shafts must be in the appropriate range. The selections of diameter, spacing, height of wall, and steel ratio for a concrete section have a direct influence on the magnitude of the earth pressure and are considered to be important for the design of drilled-shaft walls.

(2) To employ successfully the p-y method for the design of retaining walls, the soil-resistance curves must be modified to include group effects. The shadowing effects are significant for either the wedge-type failure or the flow-around failure at small drilled-shaft spacings. The influence of the shadowing on the ultimate soil resistance has been reflected in the proposed p-y modifications. The group effects due to elastic response are important for drilled shafts with spacing less than three diameters. The elastic effect is included in the new p-y criteria.

(3) Experimental studies indicate that the proposed p-y curves are reliable. In general, soil resistance decreases with the decrease of the spacing between piles. The maximum load that can be applied to each individual pile in a continuous wall is about one half of that on a single pile.

(4) The nonlinear flexural rigidity of concrete members must be considered in the structural analysis. The deflection and soil response are both influenced by this variation. To evaluate the flexural rigidity in response to cracks is important not only for controlling the structural behavior, but also for obtaining the correct form of soil resistance. With the correct evaluation of the flexural rigidity and the distribution of the bending moment, a highly efficient design of the reinforcement can be achieved.

(5) Case studies of three drilled-shaft walls and two diaphragm walls have shown that the proposed design method has acceptable accuracy for short-term behavior. Generally speaking, the p-y-based design can provide excellent opportunities to solve the closely linked soil-structure-interaction problem in a systematic way.

(6) Improvement in the ability to predict earth pressure and the soil response that are varying with the time is the key to a general up-grading of the analytical technique that is presented. The principal need is additional experimental work for the development of p-y curves under sustained load. Full-scale tests of instrumented drilled-shaft walls are strongly needed.

APPENDICES

APPENDIX A

EQUATIONS FOR COMPUTING LATERAL PRESSURE RESULTING FROM SURCHARGE

APPENDIX A EQUATIONS FOR COMPUTING LATERAL PRESSURE RESULTING FROM SURCHARGE

For the case of point loads, if the Poisson's ratio υ equals 0.5, the Boussinesq equation gives the following expression for the stresses perpendicular to the wall:

$$\sigma_h = \frac{3Q}{2\pi} \frac{x^2 Z}{R^5} \tag{A.1}$$

where

Q = point load,
R = distance between the load and a point on the wall,
Z = vertical distance as indicated in Fig. A.1, and
x = horizontal distance as indicated in Fig. A.1.

Spangler rewrote the above equation and included empirical terms, as follows:

$$\sigma_h = \frac{k}{x^n} \frac{x^2 Z}{R^5} \tag{A.2}$$

He found n to be equal to 0.25, and k to be equal to 1.1 for moist gravel and k to be 1.6 for dry gravel. The units of length in Eq. A.2 are feet.

Terzaghi (1954) published a paper on anchored bulkheads, where he reported some detailed studies regarding the lateral pressures resulting from surcharge. In Fig. A.2, if the value of m (the normalized distance of the surcharge from the wall) is greater than 0.4, the unit pressure along the horizontal line ab can be estimated roughly using:

$$\text{If} \quad m > 0.4 \qquad \sigma_h = \frac{1.77Q}{H^2} \frac{m^2 n^2}{(m^2 + n^2)^3} \tag{A.3}$$

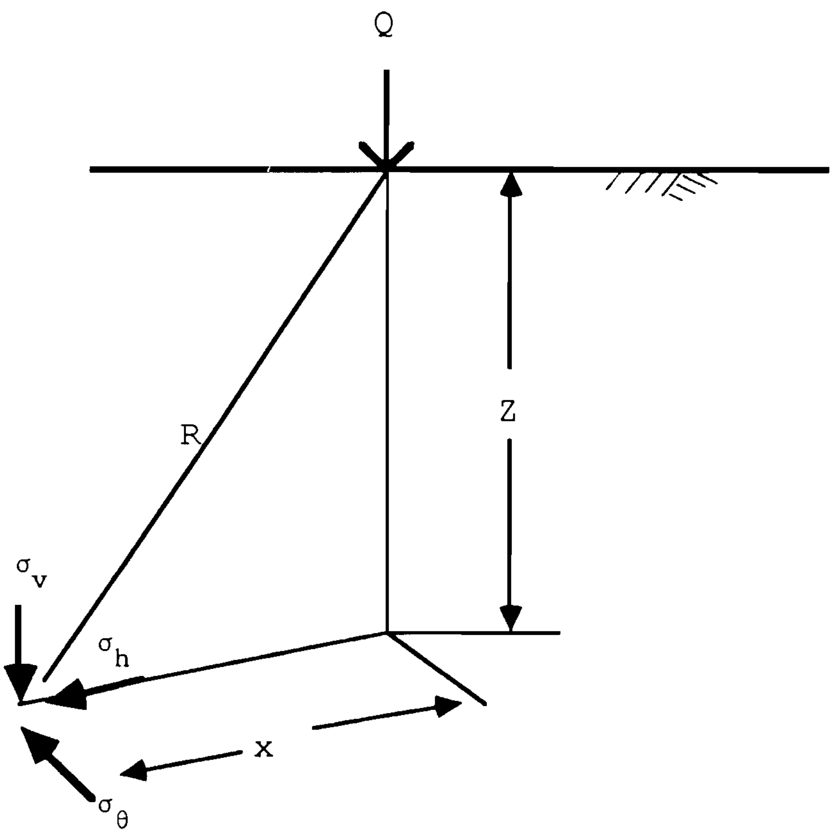

Fig. A.1. Stress due to a point load.

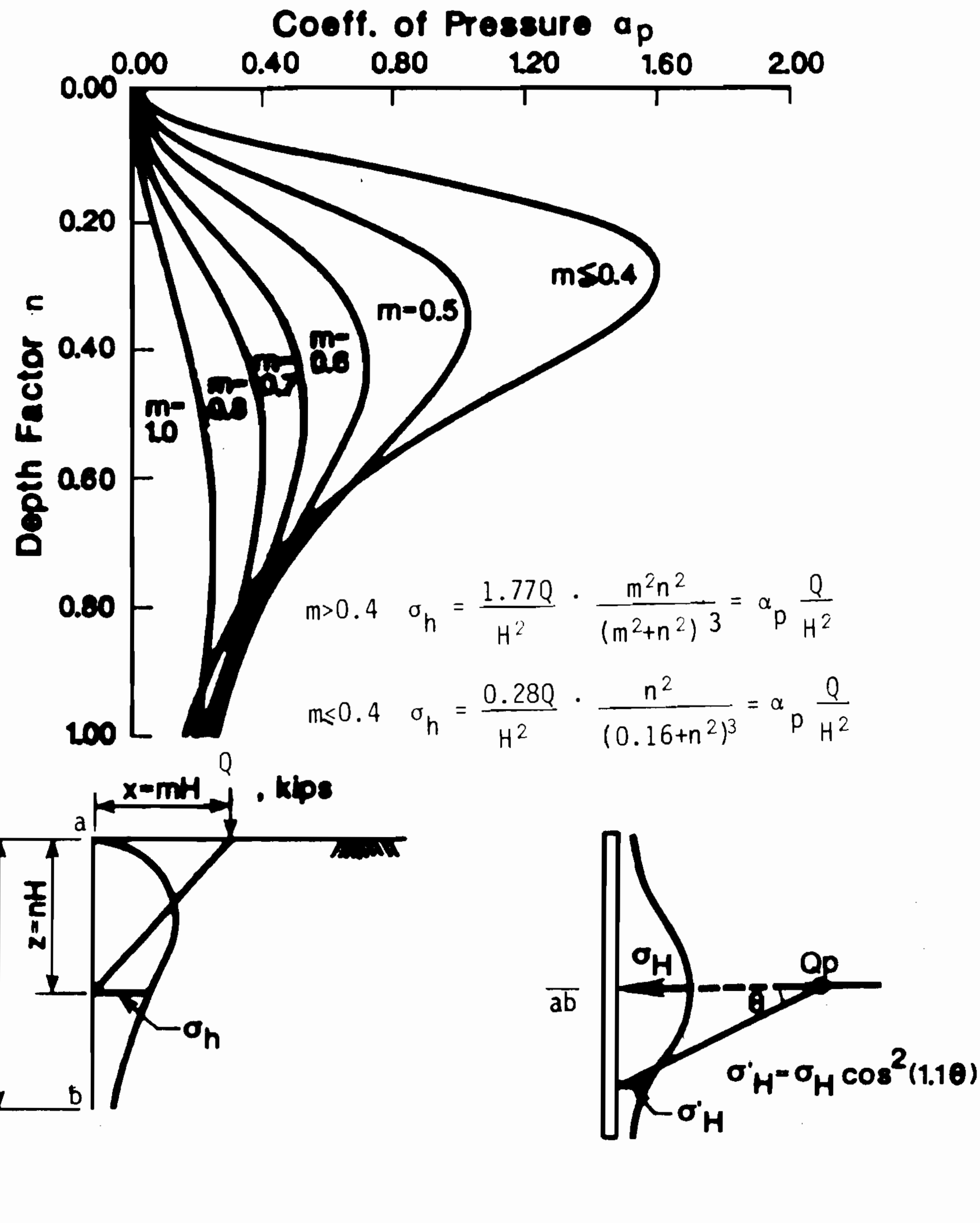

Fig. A.2. Lateral pressures resulting from point load.

All symbols in Eq. A.3 were identified in Fig. A.2. For values of m less than 0.4, a better approximation of unit pressure can be obtained using:

$$\text{If} \quad m \leq 0.4 \qquad \sigma_h = \frac{0.28Q}{H^2} \frac{n^2}{(0.16 + n^2)^3} \tag{A.4}$$

The maximum lateral pressure is in the direction perpendicular to the wall and are of most concern to the designer. The pressures at other points on the wall can be obtained by use of an empirical equation developed by Terzaghi.

$$\sigma_h' = \sigma_{h,ab} \cos^2 (1.1\theta) \tag{A.5}$$

where

$\sigma_{h,ab}$ = unit pressure on line ab,

θ = angle between line ab and point of interest selective to the point load (Fig. A.2).

A simplified design chart for computing the lateral pressure resulting from a point load, Q, on a wall with a height, H, has been developed in this study. The distribution of lateral pressure along a wall is influenced strongly by the position of the point load as shown in Fig. A.2. The lateral pressure casued by a point load at a particular position can be estimated in this figure if the dimension of the wall, normalized values, m and n, and point load Q are known.

For the case of line load, if υ = 0.5 and using the ratio m, n as defined in Fig. A.3, the Boussinesq equation for lateral stresses is

$$\sigma_h = \frac{2q}{\pi H} \frac{m^2 n}{(m^2 + n^2)^2} \tag{A.6}$$

Measured values of lateral stress from tests were found to be approximately twice of this value. Therefore, modified equations are presented for the line load (Terzaghi, 1954).

$$\text{If } m > 0.4 \qquad \sigma_h = \frac{4q}{\pi H} \frac{m^2 n}{(m^2 + n^2)^2} \tag{A.7}$$

$$\text{If } m \leq 0.4 \qquad \sigma_h = \frac{q}{H} \frac{0.203n}{(0.16 + n^2)^2} \tag{A.8}$$

The lateral stresses on a wall from the line load can be estimated by the simplified design chart as indicated in Fig. A.3.

A strip load is a load applied over a finite width such as from a highway, railroad, or earth embankment, which is parallel to the retaining structure. The resulting unit pressure on the wall can be obtained by integrating the equation of a line load. The equation that is obtained is:

$$\sigma_h = \frac{2q}{\pi} (\beta - \sin\beta \cos 2\alpha) \tag{A.9}$$

where α, β are in radians and the other terms are as identified in Fig.A.4. If the width of the strip load is assumed to be 0.1H, the distribution of the horizontal stresses on the wall at different locations can be found in Fig. A.4.

The above equations for the prediction of lateral pressures resulting from surcharge are based on limited amount of experimental data and may not be accurate. Further research work on this subject is needed. At present, these equations can be used for design purposes if used with a reasonable factor of safety.

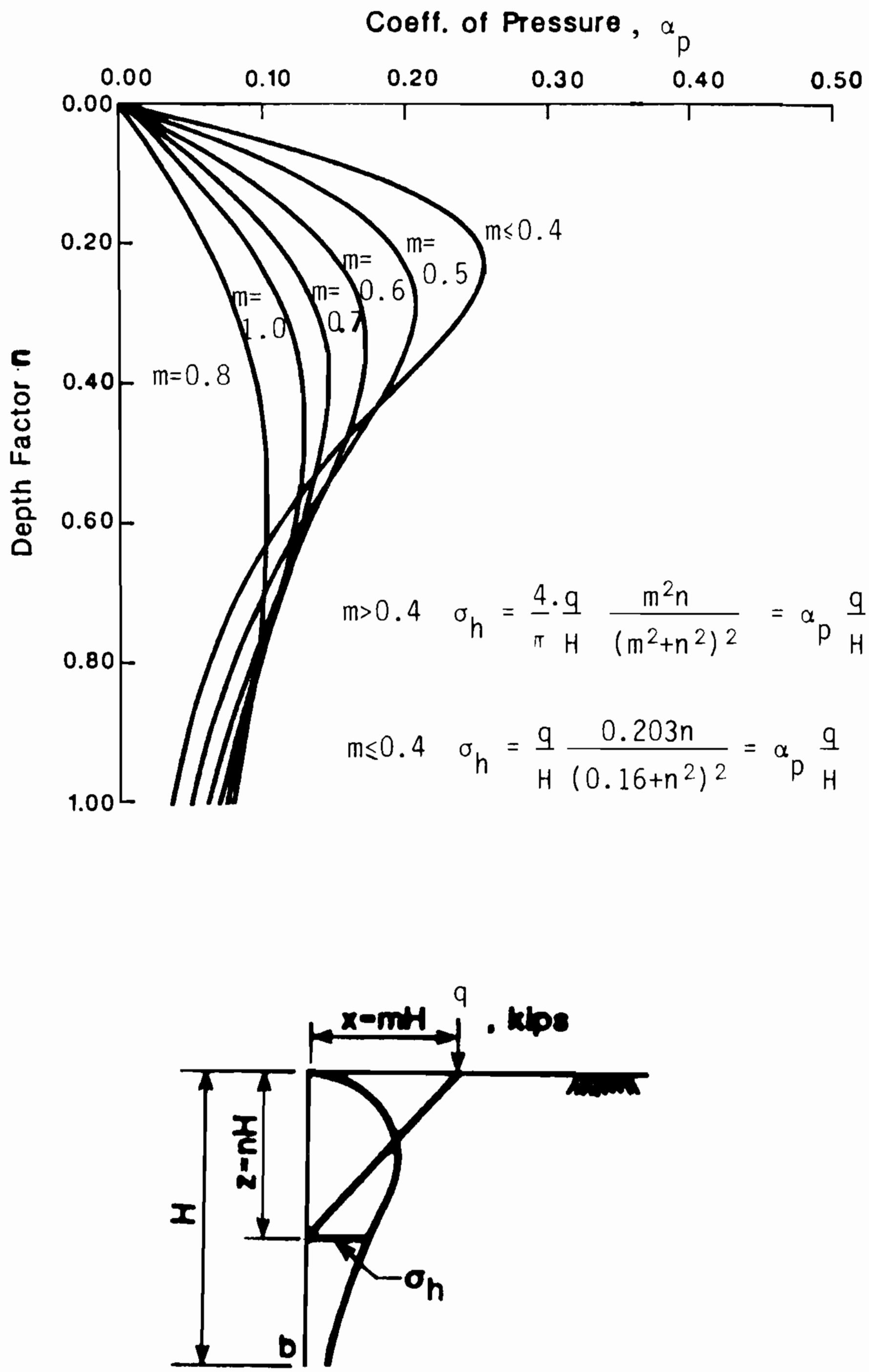

Fig. A.3. Lateral pressures resulting from line load.

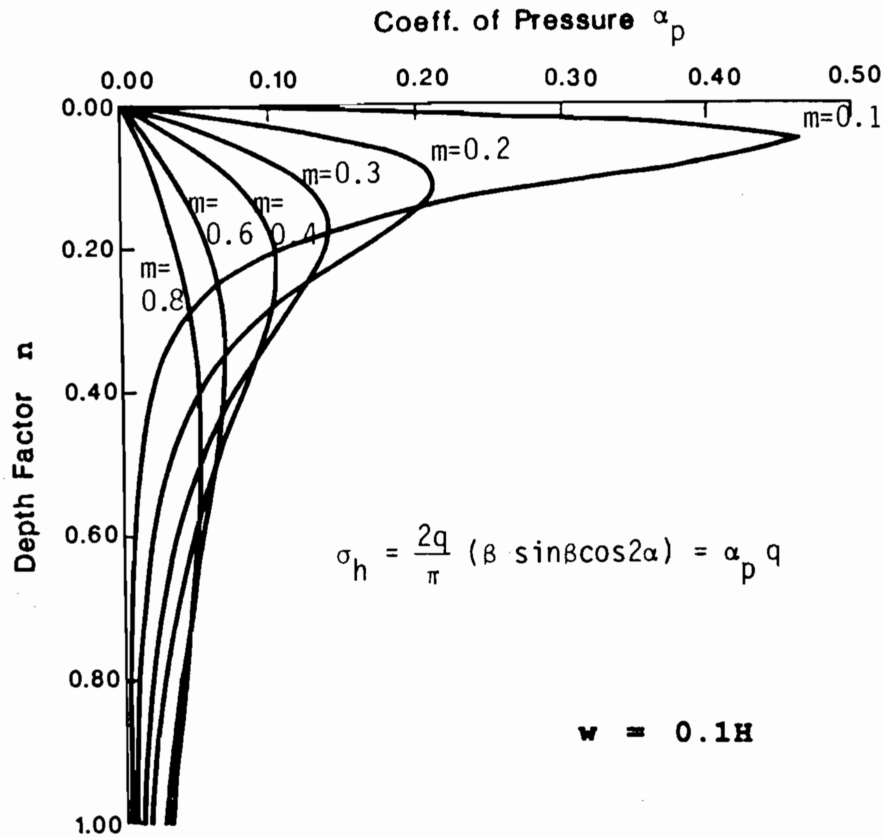

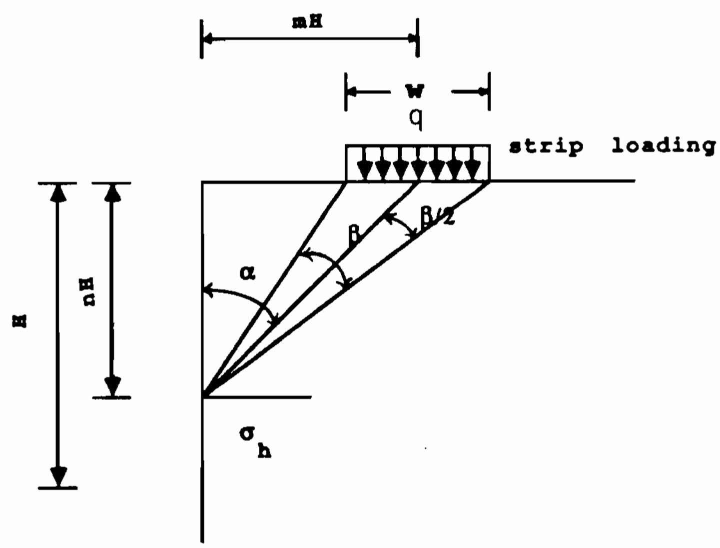

Fig. A.4. Lateral pressures resulting from strip load.

APPENDIX B

BASIC EQUATIONS FROM SLIP-LINE THEORY

APPENDIX B BASIC EQUATIONS FROM SLIP-LINE THEORY

First, the state of stress in a region of soil at failure is considered. The stresses that satisfy the condition of equilibrium in the absence of body forces for the plain-strain condition are expressed as:

$$\frac{\partial \sigma_x}{\partial x} + \frac{\partial \tau_{yx}}{\partial y} = 0$$
$$\frac{\partial \tau_{xy}}{\partial x} + \frac{\partial \sigma_y}{\partial y} = 0 \qquad \text{(B.1)}$$

The failure criterion for undrained loading of soils is given by

$$(\sigma_x - \sigma_y)^2 + 4\tau_{xy}^2 = 4c^2$$

or $\qquad$ (B.2)

$$(\sigma_1 - \sigma_3) / 2 = c$$

where

σ_1 = the maximum principal stress,

σ_3 = the minimum principal stress, and

c = the undrained shear strength.

From the Mohr diagram (Fig. B.1) the following relationships for σ_x, σ_y and τ_{xy} are found:

$$\sigma_x = q - c\sin 2\theta$$
$$\sigma_y = q + c\sin 2\theta \qquad \text{(B.3)}$$
$$\tau_{xy} = c\cos 2\theta$$

where

$$q = (1/2)(\sigma_1 + \sigma_3)$$

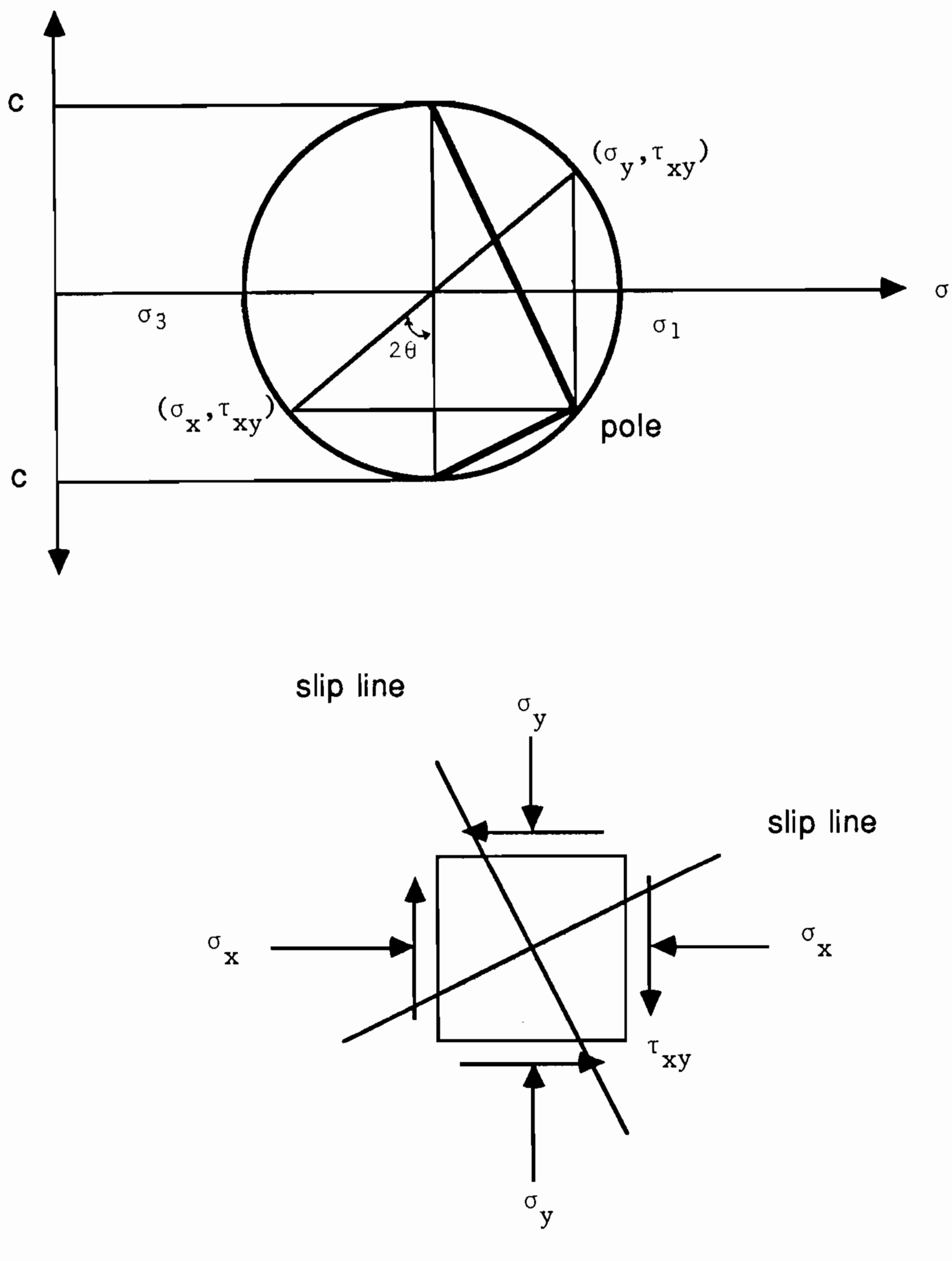

Fig. B.1. Mohr diagram for stresses

Substituting these equations into the equilibrium equations, two nonlinear partial differential equations of first order can be obtained with respect to the unknown functions q(x,y) and θ(x,y):

$$\frac{\partial q}{\partial x} - 2c \left(\cos 2\theta \frac{\partial \theta}{\partial x} + \sin 2\theta \frac{\partial \theta}{\partial y} \right) \qquad (B.4)$$

$$\frac{\partial q}{\partial y} - 2c \left(\sin 2\theta \frac{\partial \theta}{\partial x} - \cos 2\theta \frac{\partial \theta}{\partial y} \right) \qquad (B.5)$$

Eqs A.4 and A.5 govern the distribution of stresses throughout the plastic region and are hyperbolic. The mathmatical procedure used for the solution of hyperbolic partial differential equations is the method of characteristics. The characteristics of the above system of equations form two families of orthogonal curves whose directions coincide with the direction of the maximum shearing stress. These curves are known as slip-lines or can be described physically as shear-failure lines. The slopes of these two families of curves are:

$$\frac{dy}{dx} = \tan\theta, \qquad \alpha - \text{line} \qquad (B.6)$$

$$\frac{dy}{dx} = -\cot\theta, \qquad \beta - \text{line} \qquad (B.7)$$

One is called the α-lines and the other is called the β-lines.

Slip lines have a series of important properties (investigated principally by Hencky, 1923), which need to be considered:

(1) Along a slip line the pressure q and the angle θ have the following relations

$$\frac{q}{2c} - \theta = \xi \quad \text{(constant)} \qquad \text{on } \alpha - \text{line}$$

$$\frac{q}{2c} + \theta = \eta \quad \text{(constant)} \qquad \text{on } \beta - \text{line}$$

(2) The change in the angle θ and pressure q is the same for a transition from one slip line of the β-family to another along any slip line of the α-family (Hencky's first theorem).

Hencky's first theorem is illustrated in Fig.B.2. In Figure B.2 the region ABCD is bounded by two α-lines, AB and CD, and two β-lines, AD and BC. The difference in q between A and C is found from Eqs. B.8 and B.9 as

$$q_C - q_A = (q_C - q_B) + (q_B - q_A)$$
$$= 2c\,(2\theta_B - \theta_C - \theta_A) \tag{B.8}$$

also,

$$q_C - q_A = (q_C - q_D) + (q_D - q_A)$$
$$= 2c\,(-2\theta_D + \theta_C + \theta_A) \tag{B.9}$$

consequently,

$$\theta_D - \theta_A = \theta_C - \theta_B \tag{B.10}$$

and

$$\theta_B - \theta_A = \theta_C - \theta_D \tag{B.11}$$

These relations are important in the numerical and graphical construction of slip-line fields.

In the previous discussion, the failure criterion is defined for undrained soil. In many cases, the soil satisfies the Coulomb failure criterion and slip-lines change with the new criterion. Referring to the Mohr circle representation of the Coulomb condition in Fig. B.3, the following relations between stresses in this case are found.

$$\sigma_x = q\,(1 + \sin\phi\cos 2\theta) - c\cot\phi \tag{B.12}$$

$$\sigma_y = q\,(1 - \sin\phi\cos 2\theta) - c\cot\phi \tag{B.13}$$

$$\tau_{xy} = q\sin\phi\sin 2\theta \tag{B.14}$$

where, θ is again the angle to the maximum principal stress direction.

Substituting these equations into the equilibrium equations, a more general type of system of hyperbolic equations can be obtained for cohesive as well as for cohesionless materials:

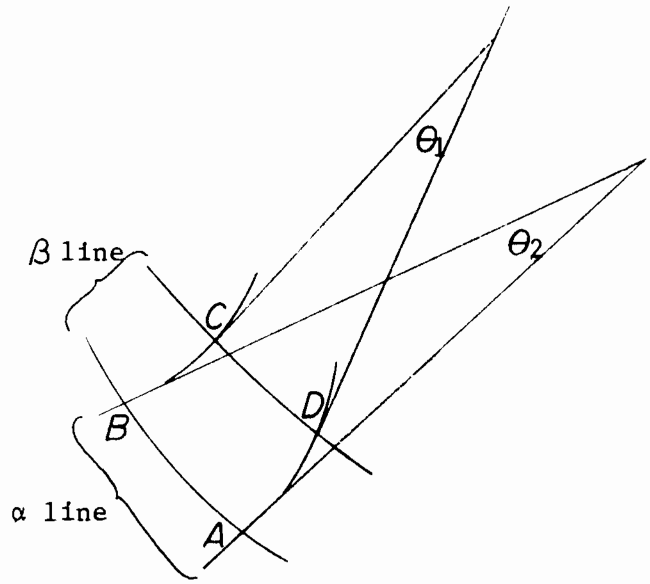

Fig. B.2. Demonstration of Hencky's first theorem.

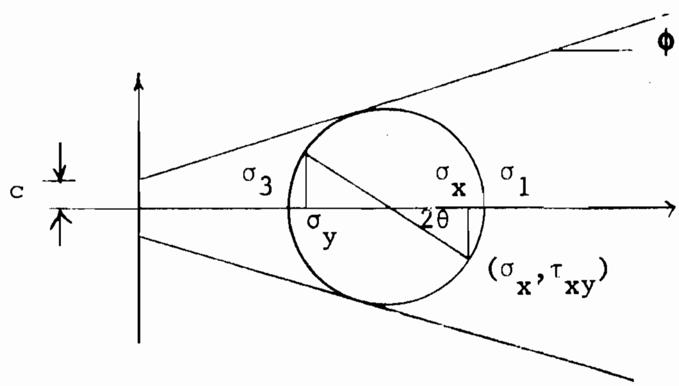

Fig. B.3. Mohr-diagram for soils satisfying Coulomb failure criterion.

$$\frac{\partial q}{\partial x}\ (\ 1 + \sin\phi\cos 2\theta\ ) - \frac{\partial \theta}{\partial x}\ (\ 2q\sin\phi\sin 2\theta\ ) \qquad \text{(B.15)}$$

$$+ \frac{\partial q}{\partial y}\ (\ \sin\phi\sin 2\theta\ ) + \frac{\partial \theta}{\partial y}\ (\ 2q\sin\phi\cos 2\theta\ ) = 0$$

$$\frac{\partial q}{\partial x}\ (\ \sin\phi\sin 2\theta\ ) - \frac{\partial \theta}{\partial x}\ (\ 2q\sin\phi\cos 2\theta\ ) + \frac{\partial q}{\partial y} \qquad \text{(B.16)}$$

$$(\ 1 - \sin\phi\sin 2\theta\ ) \quad + \frac{\partial \theta}{\partial y}\ (\ 2q\sin\phi\sin 2\theta\ ) = 0$$

Two families of slip-lines from the above system of partial-differential equations were obtained by Abbott(1950):

$$\frac{dy}{dx} = \tan\ [\ q + (\ \frac{\pi}{4} - \frac{\phi}{2}\ )\ ] \quad \alpha-\text{ line} \qquad \text{(B.17)}$$

$$\frac{dy}{dx} = \tan\ [\ q - (\ \frac{\pi}{4} - \frac{\phi}{2}\ )\ ] \quad \beta - \text{line} \qquad \text{(B.18)}$$

and

$$\frac{1}{2}\cot\phi\ \ln q + \theta = \xi \text{ (constant)} \quad \text{on } \alpha - \text{line} \qquad \text{(B.19)}$$

$$\frac{1}{2}\cot\phi\ \ln q - \theta = \eta \text{ (constant)} \quad \text{on } \beta - \text{line} \qquad \text{(B.20)}$$

The above discussion is limited in the stress field and three unknown σ_x, σ_y, and τ_{xy} need to be solved. If the boundary conditions are given only in terms of stresses, these equations are sufficient to give the stress distribution without any reference to the stress-strain relations. Problems of this type are called statically determinant. If the problem is statically determinant, the slip-line field is defined uniquely by the boundary conditions for stress and this type of problem presents no great difficulty.

If, however, the problem is not statically determinant, the boundary condition for velocity has to be considered for a unique answer. The definition of velocity comes from plasticity theory where it is common to discuss displacements in terms of an arbitrary time interval so that increments of strain and displacement are referred to as strain rates and velocities respectively. There are two equations involved in the velocity field:

$$\frac{\partial v_x}{\partial x} + \frac{\partial v_y}{\partial y} = 0 \tag{B.21}$$

$$\frac{\partial \tau_{xy}}{\sigma_x - \sigma_y} = \left(\frac{\partial v_x}{\partial y} + \frac{\partial v_y}{\partial x} \right) / \left(\frac{\partial v_x}{\partial x} - \frac{\partial v_y}{\partial y} \right) \tag{B.22}$$

The equations for stresses and velocities have to be solved in conjunction, and this is diffcult. In general, the approach to such problems is to use repeated trials. A more detailed discussion can be found in Hill (1963).

APPENDIX C

TEST DATA FROM SMALL-SCALE EXPERIMENTS

APPENDIX C TEST DATA FROM SMALL-SCALE EXPERIMENTS

TEST RESULTS FOR SOFT CLAY

Clear Spacing S = 0

Single pile		Center pile (c.p.)		Right of c.p.		Left of c.p.	
Disp.	Load	Disp.	Load	Disp.	Load	Disp.	Load
(in.)	(lb)	(in.)	(lb)	(in.)	(lb)	(in.)	(lb)
0.000	0.000	0.000	0.000	0.000	0.000	0.000	0.000
0.007	1.690	0.012	0.440	0.013	0.560	0.012	0.440
0.028	3.390	0.033	1.580	0.028	2.420	0.033	1.420
0.054	5.270	0.075	3.330	0.060	4.006	0.073	3.470
0.086	7.440	0.145	4.910	0.148	5.870	0.150	5.250
0.119	8.850	0.225	5.780	0.223	6.890	0.235	6.580
0.170	10.64	0.290	6.390	0.305	7.920	0.295	7.560

Clear Spacing S = 0.25b

Single pile		Center pile (c.p.)		Right of c.p.		Left of c.p.	
Disp.	Load	Disp.	Load	Disp.	Load	Disp.	Load
(in.)	(lb)	(in.)	(lb)	(in.)	(lb)	(in.)	(lb)
0.000	0.000	0.000	0.000	0.000	0.000	0.000	0.000
0.007	1.410	0.005	0.610	0.005	0.650	0.005	0.610
0.021	3.110	0.014	1.310	0.012	1.290	0.014	1.390
0.037	4.520	0.024	2.010	0.021	1.760	0.025	2.260
0.059	6.310	0.039	2.710	0.033	2.310	0.042	3.140
0.089	8.090	0.055	3.240	0.048	2.770	0.061	4.010

0.120	9.880	0.078	3.850	0.070	3.330	0.095	4.880
0.170	11.29	0.110	4.550	0.096	3.790	0.129	5.750
0.245	13.01	0.148	5.160	0.131	4.440	0.185	6.790
		0.190	5.780	0.170	5.090	0.230	7.580
		0.240	6.210	0.220	5.550		

Clear Spacing S = 0.50b

Single pile		Center pile (c.p.)		Right of c.p.		Left of c.p.	
Disp. (in.)	Load (lb)	Disp. (in.)	Load (lb)	Disp. (in.)	Load (lb)	Disp. (in.)	Load (lb)
0.000	0.000	0.000	0.000	0.000	0.000	0.000	0.000
0.007	1.320	0.004	0.440	0.003	0.370	0.004	0.620
0.024	2.920	0.009	1.050	0.010	1.110	0.011	1.420
0.052	4.610	0.016	1.490	0.017	1.760	0.020	1.780
0.085	6.310	0.028	2.280	0.029	2.590	0.034	3.290
0.104	7.060	0.044	3.150	0.044	3.330	0.052	4.360
0.128	7.720	0.069	4.030	0.068	4.250	0.080	5.600
0.175	9.220	0.098	5.080	0.098	5.360	0.110	6.580
0.224	10.92	0.140	6.130	0.140	6.470	0.152	7.650
0.280	12.05	0.233	7.180	0.238	7.580	0.252	8.710

Clear Spacing S = 1.0b

Single pile		Center pile (c.p.)		Right of c.p.		Left of c.p.	
Disp. (in.)	Load (lb)	Disp. (in.)	Load (lb)	Disp. (in.)	Load (lb)	Disp. (in.)	Load (lb)
0.000	0.000	0.000	0.000	0.000	0.000	0.000	0.000
0.002	0.750	0.006	0.880	0.007	1.050	0.007	0.890

0.014	2.450	0.016	1.580	0.018	2.000	0.016	1.780
0.035	3.950	0.037	2.980	0.038	3.220	0.036	3.200
0.063	5.740	0.064	4.110	0.065	4.620	0.061	4.530
0.098	7.440	0.095	5.690	0.098	5.840	0.094	6.040
0.141	9.130	0.140	7.090	0.148	7.140	0.141	7.650
0.175	10.26	0.205	8.580	0.215	8.280	0.210	9.330
0.241	12.05	0.275	9.980	0.299	9.320	0.280	10.31

Clear Spacing S = 2.0b

Single pile		Center pile (c.p.)		Right of c.p.		Left of c.p.	
Disp.	Load	Disp.	Load	Disp.	Load	Disp.	Load
(in.)	(lb)	(in.)	(lb)	(in.)	(lb)	(in.)	(lb)
0.000	0.000	0.000	0.000	0.000	0.000	0.000	0.000
0.004	1.510	0.008	1.230	0.006	0.830	0.008	1.330
0.014	3.200	0.032	3.150	0.018	2.870	0.036	3.114
0.030	4.992	0.057	4.910	0.034	4.253	0.630	4.896
0.089	8.751	0.082	6.567	0.058	5.638	0.094	6.491
0.132	10.26	0.113	7.875	0.083	6.943	0.128	8.181
0.156	11.26	0.149	9.281	0.114	8.138	0.170	9.602
0.199	12.14	0.200	11.03	0.165	10.08	0.225	11.29
0.270	13.46	0.240	11.98	0.205	11.10		

Clear Spacing S = 3.0b

Single pile		Center pile (c.p.)		Right of c.p.		Left of c.p.	
Disp.	Load	Disp.	Load	Disp.	Load	Disp.	Load
(in.)	(lb)	(in.)	(lb)	(in.)	(lb)	(in.)	(lb)
0.000	0.000	0.000	0.000	0.000	0.000		

0.010	1.600	0.013	1.840	0.013	1.600
0.030	3.390	0.032	3.330	0.030	3.290
0.053	4.990	0.057	5.080	0.052	4.800
0.084	6.590	0.089	6.830	0.080	6.490
0.120	8.280	0.136	8.750	0.120	8.180
0.161	10.07	0.187	10.48	0.173	10.40
0.219	11.76	0.235	11.64	0.222	12.05

TEST RESULTS FOR DENSE SAND

Clear Spacing S = 0.0b

Single pile		Center pile (c.p.)		Right of c.p.		Left of c.p.	
Disp. (in.)	Load (lb)	Disp. (in.)	Load (lb)	Disp. (in.)	Load (lb)	Disp. (in.)	Load (lb)
0.000	0.000	0.000	0.000	0.000	0.000	0.000	0.000
0.004	1.690	0.007	1.840	0.005	1.160	0.004	1.670
0.010	3.480	0.016	2.360	0.014	2.580	0.014	2.510
0.019	5.740	0.028	5.160	0.026	3.820	0.024	5.100
0.039	9.980	0.041	6.910	0.036	5.250	0.037	7.920
0.062	14.02	0.057	8.930	0.050	6.490	0.054	9.030
0.086	18.26	0.073	11.03	0.079	9.060	0.069	10.52
0.114	23.15	0.091	12.86	0.095	10.80	0.086	12.29
0.159	29.74	0.109	15.05	0.112	12.44	0.104	14.06
		0.128	16.80	0.130	13.87	0.123	15.46
		0.147	18.64	0.147	15.02	0.141	17.23
		0.163	20.30			0.158	18.62

Clear Spacing S = 0.25b

Single pile		Center pile (c.p.)		Right of c.p.		Left of c.p.	
Disp.	Load	Disp.	Load	Disp.	Load	Disp.	Load
(in.)	(lb)	(in.)	(lb)	(in.)	(lb)	(in.)	(lb)
0.000	0.000	0.000	0.000	0.000	0.000	0.000	0.000
0.008	1.550	0.004	1.230	0.004	1.390	0.003	1.300
0.030	5.840	0.009	2.630	0.009	2.950	0.008	2.420
0.058	10.45	0.015	3.150	0.015	3.460	0.012	3.110
0.092	14.59	0.025	5.780	0.021	5.180	0.022	4.840
0.152	21.65	0.035	5.780	5.032	6.130	0.033	5.400
0.222	28.52	0.045	7.790	0.046	8.510	0.043	7.600
		0.058	9.190	0.064	10.08	0.056	8.900
		0.071	10.50	0.080	11.38	0.070	10.20
		0.085	1.730	0.096	12.58	0.084	11.33
		0.099	12.60	0.113	14.56	0.100	12.16
		0.111	13.65	0.125	15.35	0.114	13.15
		0.128	14.26	0.141	16.74	0.130	13.91

Clear Spacing S = 0.50b

Single pile		Center pile (c.p.)		Right of c.p.		Left of c.p.	
Disp.	Load	Disp.	Load	Disp.	Load	Disp.	Load
(in.)	(lb)	(in.)	(lb)	(in.)	(lb)	(in.)	(lb)
0.000	0.000	0.000	0.000	0.000	0.000	0.000	0.000
0.005	1.690	0.005	1.400	0.003	1.420	0.006	1.420
0.035	6.580	0.010	1.750	0.008	2.220	0.009	1.780
0.084	13.08	0.017	2.710	0.017	2.760	0.016	2.490

0.144	20.05	0.027	4.200	0.024	4.810	0.024	4.620
0.175	23.58	0.035	4.810	0.032	6.400	0.036	5.250
		0.050	6.650	0.040	7.640	0.049	6.730
		0.065	8.310	0.063	9.240	0.066	8.620
		0.080	10.06	0.076	10.67	0.179	10.31
		0.096	11.38	0.092	12.09	0.095	11.70
		0.110	12.95	0.105	13.51	0.107	13.21
		0.125	14.09	0.117	14.57	0.121	14.50
		0.141	15.75	0.138	16.44	0.135	15.80

Clear Spacing S = 1.0b

Single pile		Center pile (c.p.)		Right of c.p.		Left of c.p.	
Disp. (in.)	Load (lb)	Disp. (in.)	Load (lb)	Disp. (in.)	Load (lb)	Disp. (in.)	Load (lb)
0.000	0.000	0.000	0.000	0.000	0.000	0.000	0.000
0.005	1.900	0.005	1.800	0.005	1.900	0.005	1.600
0.016	4.600	0.015	4.600	0.014	4.100	0.015	3.400
0.030	8.010	0.028	6.000	0.027	6.580	0.027	5.750
0.053	11.48	0.041	8.050	0.040	8.880	0.039	8.450
0.075	15.00	0.058	10.50	0.057	10.50	0.054	9.320
0.100	18.45	0.076	11.90	0.076	13.50	0.071	12.37
0.125	21.51	0.090	15.14	0.091	15.63	0.084	15.07
0.150	23.59	0.111	17.76	0.110	17.85	0.107	17.42
		0.131	19.69	0.129	19.61	0.125	19.51

Clear Spacing S = 2.0b

Single pile		Center pile (c.p.)		Right of c.p.		Left of c.p.	
Disp.	Load	Disp.	Load	Disp.	Load	Disp.	Load
(in.)	(lb)	(in.)	(lb)	(in.)	(lb)	(in.)	(lb)
0.000	0.000	0.000	0.000	0.000	0.000	0.000	0.000
0.004	1.500	0.004	1.840	0.004	2.220	0.005	1.820
0.011	3.200	0.015	4.380	0.003	4.620	0.012	3.850
0.020	5.270	0.027	7.400	0.031	8.230	0.023	6.400
0.040	9.600	0.043	11.03	0.054	11.83	0.035	8.710
0.063	13.93	0.064	14.44	0.079	15.44	0.049	10.93
0.096	18.54	0.090	17.85	0.112	20.07	0.073	14.58
0.116	22.77	0.119	22.14	0.145	24.41	0.097	18.22
0.160	29.27	0.144	25.38	0.176	28.21	0.120	21.65

Clear Spacing S = 3.0b

Single pile		Center pile (c.p.)		Right of c.p.		Left of c.p.	
Disp.	Load	Disp.	Load	Disp.	Load	Disp.	Load
(in.)	(lb)	(in.)	(lb)	(in.)	(lb)	(in.)	(lb)
0.000	0.000	0.000	0.000	0.000	0.000		
0.003	1.600	0.003	1.230	0.002	1.480		
0.009	3.480	0.011	2.800	0.010	3.240		
0.017	5.460	0.017	4.640	0.014	4.720		
0.039	9.040	0.024	5.860	0.022	6.660		
0.063	14.21	0.036	7.960	0.038	9.900		
0.091	18.45	0.065	12.43	0.071	15.26		
0.115	22.40	0.080	14.79	0.087	18.50		

0.161	29.18	0.100	17.76	0.109	22.29
		0.120	20.65	0.133	25.89
		0.144	24.06	0.156	29.69

Test Results for Loose Sand

Clear Spacing S = 0.0b

Single pile		Center pile (c.p.)		Right of c.p.		Left of c.p.	
Disp. (in.)	Load (lb)	Disp. (in.)	Load (lb)	Disp. (in.)	Load (lb)	Disp. (in.)	Load (lb)
0.000	0.000	0.000	0.000	0.000	0.000	0.000	0.000
0.019	1.690	0.023	1.400	0.019	1.290	0.031	1.680
0.032	3.390	0.060	3.320	0.048	2.590	0.061	3.170
0.069	5.360	0.130	4.810	0.108	3.700	0.125	4.660
0.107	7.060	0.168	5.430	0.145	4.440	0.160	5.490
0.145	8.660	0.210	6.130	0.184	5.270	0.201	6.610
0.177	10.16						

Clear Spacing S = 0.25b

Single pile		Center pile (c.p.)		Right of c.p.		Left of c.p.	
Disp. (in.)	Load (lb)	Disp. (in.)	Load (lb)	Disp. (in.)	Load (lb)	Disp. (in.)	Load (lb)
0.000	0.000	0.000	0.000	0.000	0.000	0.000	0.000
0.012	1.510	0.005	0.830	0.006	1.040	0.005	0.800
0.038	3.290	0.016	1.480	0.019	2.010	0.019	1.600
0.063	4.420	0.035	2.400	0.044	3.190	0.041	2.310
0.101	6.210	0.056	2.770	0.074	4.230	0.066	2.930
0.148	7.910	0.084	3.420	0.109	5.950	0.097	3.730

0.207	9.690	0.115	4.350	0.146	6.740	0.134	4.270
		0.133	4.720	0.167	1.740	0.154	4.710
		0.156	5.270	0.190	7.960	0.178	5.330
		0.179	5.830	0.214	8.490	0.198	5.690

Clear Spacing S = 0.50b

Single pile		Center pile (c.p.)		Right of c.p.		Left of c.p.	
Disp. (in.)	Load (lb)	Disp. (in.)	Load (lb)	Disp. (in.)	Load (lb)	Disp. (in.)	Load (lb)
0.000	0.000	0.000	0.000	0.000	0.000	0.000	0.000
0.008	1.410	0.005	0.700	0.003	0.650	0.005	0.800
0.018	2.300	0.012	1.310	0.011	1.480	0.013	1.420
0.043	3.520	0.022	2.010	0.022	2.220	0.023	2.400
0.078	4.750	0.064	3.410	0.063	3.230	0.068	3.730
0.117	6.130	0.148	4.810	0.138	4.720	0.160	5.870
0.166	8.050	0.182	5.510	0.171	5.360	0.199	6.670
0.211	9.170	0.228	6.130	0.215	6.380	0.245	7.470

Clear Spacing S = 1.0b

Single pile		Center pile (c.p.)		Right of c.p.		Left of c.p.	
Disp. (in.)	Load (lb)	Disp. (in.)	Load (lb)	Disp. (in.)	Load (lb)	Disp. (in.)	Load (lb)
0.000	0.000	0.000	0.000	0.000	0.000	0.000	0.000
0.003	0.660	0.005	1.400	0.004	1.110	0.005	1.240
0.017	2.350	0.018	2.540	0.014	2.130	0.016	2.310

0.040	4.050	0.030	3.760	0.025	2.680	0.028	3.290
0.071	5.840	0.050	4.900	0.044	3.700	0.045	4.270
0.109	7.345	0.067	5.690	0.060	4.620	0.059	5.160
0.153	9.045	0.087	6.560	0.080	5.360	0.076	6.050
0.232	11.11	0.118	7.530	0.110	6.470	0.102	6.670
		0.171	8.930	0.167	8.420	0.153	8.180
		0.249	9.890	0.249	11.00	0.230	10.22

Clear Spacing S = 2.0b

Single pile		Center pile (c.p.)		Right of c.p.		Left of c.p.	
Disp. (in.)	Load (lb)	Disp. (in.)	Load (lb)	Disp. (in.)	Load (lb)	Disp. (in.)	Load (lb)
0.000	0.000	0.000	0.000	0.000	0.000	0.000	0.000
0.009	1.510	0.021	2.450	0.006	1.020	0.008	1.510
0.028	3.200	0.043	3.760	0.032	2.090	0.029	3.640
0.058	4.800	0.072	5.340	0.065	4.165	0.063	5.600
0.092	6.490	0.105	6.740	0.094	5.270	0.100	7.560
0.135	8.370	0.137	8.490	0.123	6.380	0.140	9.160
0.188	11.48	0.167	9.450	0.148	7.210	0.175	10.49
		0.210	11.03	0.182	8.510	0.210	11.91

APPENDIX D
USER'S MANUAL OF PYWALL

SUMMARY

The problem of analysis and design of retaining structures is complex because of the large number of variables involved in the soil-structure-interaction problem. To develop a rational method for the design of drilled-shaft retaining walls, the individual influence of these variables must be investigated thoroughly. Three important components for the design of drilled-shaft walls have been studied in this report. These are (1) the earth pressure acting on the wall, (2) the resistance the soil to the lateral movement of the shafts, and (3) the structural response of the drilled shafts. These studies are relevant to a complete analysis of the interaction between the soil and the structure.

The method of analysis of drilled shafts employed in earth retaining structures are summarized in the following.

(1) Active earth pressure, calculated by conventional earth-pressure theory, is used as the driving force on drilled-shaft walls. However, to achieve the active states of stress, deflections along the drilled shafts must be in the appropriate range. The selections of diameter, spacing, height of wall, and steel ratio for a concrete section have a direct influence on the magnitude of the earth pressure and are considered to be important for the design of drilled-shaft walls.

(2) To employ successfully the p-y method for the design of retaining walls, the soil-resistance curve must be modified to include group effects. The shadowing effects are significant for either the wedge-type failure or the flow-around failure at small drilled-shaft spacings. The influence of the shadowing on the ultimate soil resistance has been reflected in the proposed p-y modifications. The group effects due to elastic response are important for drilled shafts with spacing less than

three diameters. The elastic effect is included in the new p-y criteria.

(3) The nonlinear flexural rigidity of concrete members must be considered in the structural analysis. The deflection and soil response are both influenced by this variation. To evaluate the flexural rigidity in response to cracks is important not only for controlling the structural behavior, but also for obtaining the correct form of soil resistance. With the correct evaluation of the flexural rigidity and the distribution of the bending moment, a highly efficient design of the reinforcement can be achieved.

In addition, small-scale experiments were conducted to verify the proposed p-y curves for piles in a row, that are derived based upon the analytical solution.

Small-scale experimental studies indicate that the proposed p-y curves are reliable. In general, soil resistance decreases with the decrease of the spacing between piles. The maximum load that can be applied to each individual pile in a continuous wall is about one half of that on a single pile.

Finally, several case studies indicate that the approach presented herein can predict the behavior of retaining structures quite well by taking into account the soil-structure-interaction. The selection of the penetration length, diameter, spacing, and flexural resistance of drilled shafts can be facilitated by the method.

APPENDIX D

INFORMATION ON INPUT OF DATA FOR COMPUTER PROGRAM PYWALL

D.1 INTRODUCTORY REMARKS

Data input is based on a coordinate system in which the head of the drilled shafts is the origin and the positive x-direction is downward (Fig. D1). The ground surface on the side of the excavation is below the head of the drilled shafts as shown in Fig. D1. Sign conventions are shown in Fig. D2.

The program is organized so that up to 50 problems can be analyzed in a single run; this facilitates sensitivity studies of input variable with minimum effort by the user.

Any convenient and consistent units of force and length can be used. The program is set up to label the output in one of three ways:

1. The user can designate that English units of inches and pounds will be used, and output will be labeled accordingly;
2. The user can specify that metric units of kilonewtons and meters will be used, and output will be labeled accordingly;
3. The user can use any other consistent units (the computer does not need to know which one) of force and length, and output will be labeled in terms of forces and lengths (F and L).

Several default values may be used in data input. Where the user desires to use a default value, he should leave the input blank for the relevant variable.

D.2 PREPARATION FOR INPUT

The following steps are recommended to prepare for data input.

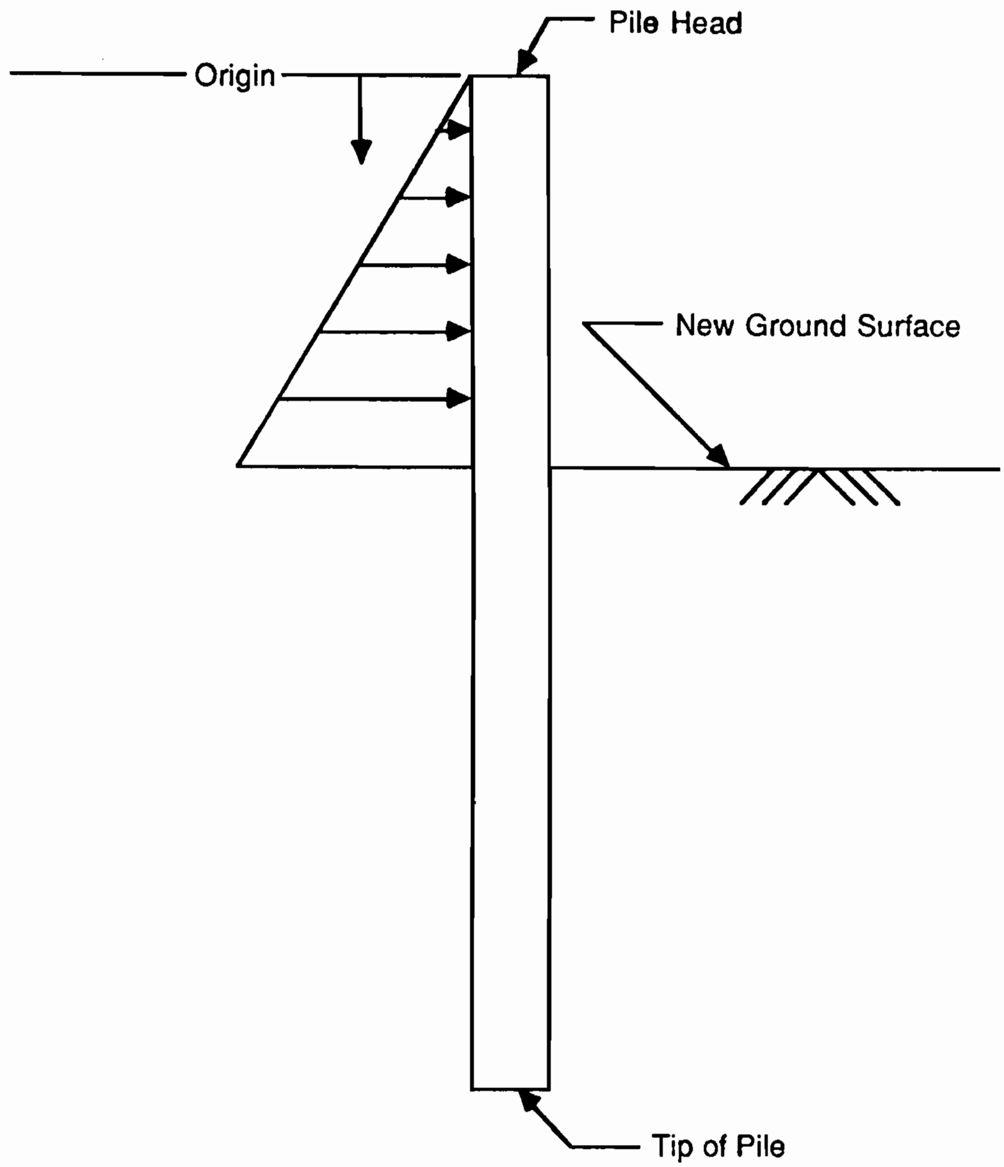

Fig. D.1. Coordinate system.

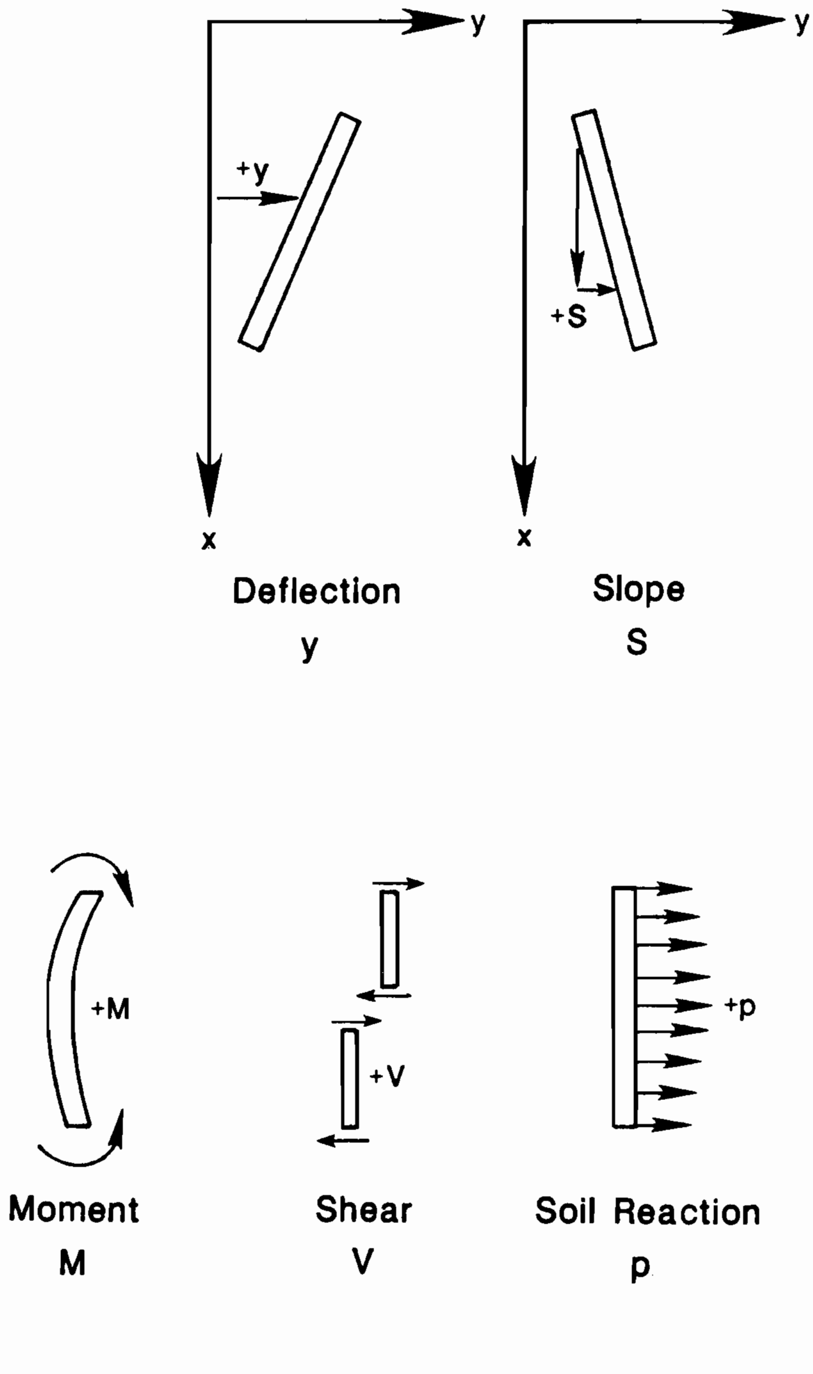

Fig. D.2. Sign convention.

1. Decide which units will be used for force and length.
2. Decide into how many increments the drilled shaft is to be divided. Up to 300 increments are allowed. Be sure to satisfy yourself that an adequate number of increments have been used to obtain a satisfactory solution.
3. Decide whether p-y curves will be input or whether they will be generated internally. If they are to be input, pick depths for input, pick the number of points to be input for each depth, and tabulate the data. Up to 30 p-y curves are allowed.
4. If p-y curves are to be generated internally, divide the soil profile into from one to nine layers; decide which of the following p-y criteria for soft clay;
   - Matlock's (1970) criteria for soft clay;
   - Reese et al.'s (1975) criteria for stiff clay below the water table;
   - Welch and Reese's (1975) criteria for stiff clay above the water surface;
   - Reese et al.'s (1974) criteria for sand;
   - Estimate undrained shear strength c and strain at 50 percent stress level ε_{50} for clay layers; estimate the angle of internal friction ϕ for sand; and estimate the slope k of a plot of maximum soil modulus E_s versus depth x for all strata.
5. Note the length of the drilled shaft, the modulus of elasticity of drilled-shaft material, and the x-coordinate of the ground surface.
6. Divide the drilled shaft into from one to ten segments with uniform cross-section. For each segment, tabulate the x-coordinate of the top of the segment, the diameter of the segment, the moment of inertia, and, the area of the cross section.
7. The earth pressure above the dredge level is distributed along the drilled shaft, tabulate up to ten points on a

plot of distributed load versus depth below top of drilled shaft.

8. Tabulate up to ten points on a plot of effective unit weight of soil versus depth. This step is not necessary if no p-y curves will be generated internally.
9. Tabulate up to ten points on plots of c, ϕ, and ε_{50} versus x. Skip this step if no p-y curves will be generated internally.
10. If p-y curves are generated internally in the program, tabulate any depths for which p-y curves are to be printed. Ordinarily, a few curves are printed for verification purposes.
11. Determine the additional loads to the top of the pile, it can be none.
    - A. Lateral load at pile head
    - B. Second boundary condition at pile head, which can be either
        - i. moment (M_t)
        - ii. slope (S_t)
        - iii. rotational restraint (M_t/S_t)
    - C. Axial load (assumed to be uniform over full length of pile).Up to 20 loading combinations can be input for each problem, e.g., to generate a load deflection curve.

D.3 LINE-BY-LINE INPUT GUIDE (See Appendix A1.6 for the input form

<u>Title Card</u>

Variable: TITLE(I)

Format: 18A4

Number of Cards: 1

Explanation: Any characters, including blanks, are allowed in this descriptive title. However, do not type the word END in columns 1 through 3 as this is used to indicate the end of the data input.

Units Cards

Variables: ISYSTM, IDUM1, IDUM2, IDUM3

Format: 4A4

Number of Cards: 1

Explanation: In columns 1 through 4, type:

ISYSTM = ENGL if English units of pounds and inches are to be used;

= METR if metric units of kilonewtons and meters are to be used;

= Anything else if some other consistent set of units for force and length are to be used (the program will not try to determine which st of units is used but will indicate units on output by F for force and L for length, e.g., stress would be F.L**2).

Input Control Card

Variables: NI, NL, NDIAM, NW, MEI

Format: 4I5

Number of Cards: 1

Explanation: NI = number of increments into which the pile is divided (maximum is 300)

NL = number of layers of soil (maximum is 9)

NDIAM = number of segments of pile with different diameter, area, or moment of inertia (maximum is 10)

NW = number of points on plot of distributed lateral load on the pile versus depth (minimum is 0, maximum is 10).

MEI =0 constant EI employed in the analysis. 1 nonlinear EI employed in the analysis

NDIAM must be > 0 for the first problem in the data deck. If NDIAM = 0 for subsequent problems, the same pile properties used in the previous problem will be used again in the subsequent problem.

Set NW = 0 if there are no distributed loads on the pile. Set NW = -1 for the second or any subsequent problem in a data deck if you want the same distributed loads to be used again.

Set NL = 0 if the same soil profile is to be used as was used in the previous problem in the data deck.

Input Control Card

Variables: NG1, NSTR, NPY

Format: 3I5

Number of Cards: 1

Explanation: NG1 = number of points on plot of effective unit weight versus depth (minimum = 2, maximum = 10)

NSTR = number of points on input curves of strength parameters (c, ϕ, ε_{50}) versus depth (minimum = 2, maximum = 10)

NPY = number of input p-y curves (minimum = 0, maximum = 30)

NG1 may equal 0 for the second or any subsequent problem in a data deck if the same unit eight plot is to be used as was used in the previous problem.

Set NPY = -1 in the second or any subsequent problem in a data deck to retain the input p-y curves from the previous problem and therefore to avoid re-reading the data.

Set NG1 = 0 and NSTR = 0 if all p-y curves are to be input by the user (if no p-y curves are to be generated internally).

Shape of cross section card

Omit this card if MEI: 0

Variables: ISHAPE

Format: I5

Number of Cards: 1

Explanation: ISHAPE = identification number of the shape of cross section of drilled shaft

= 1 for rectangular of square

= 10 for circular (without shell or core)

= 20 for circular (with shell but without core)

= 30 for circular (with shell and core or without shell and with core).

Axial load card

Omit this card if MEI = 0

Variables: PX

Format: E10.3

Number of cards: 1

Explanation : axial load at the top of the drilled shaft (F)

Material properties card

Omit this card if MEI = 0

Variables: FC, BARFY, TUBEFY, ES

Format: 4E10.3

Number of cards: 1

Explanation: FC = cylinder strength of concrete

BARFY = yield strength of reinforcement

TUBEFY = yield strength of shell or core

ES = modulus of elasticity of steel.

Dimension card

Omit this card if MEI = 0

Variables: WIDTH, OD, DT, T, TT

Format: 5E10.3

Number of Cards: 1

Explanation: WIDTH = width of section if rectangular (ϕ,ϕ if circular)

OD = outer diameter, if circular, or depth of section if rectangular

DT = outer diameter of core (ϕ,ϕ if ISHAPE is 1 or 10)

T = thickness of shell

TT = thickness of core

Rebar Cage

Omit this card if MEI = 0

Variables: NBARS, NROWS, COVER

Format: 215, E10.3

Number of Card: 1

Explanation: NBARS = number of reinforcing bars

NROWS = number of rows of reinforcing bars (a number not exceeding 50).

COVER = cover of rebar, from center of rebar to outer edge of concrete.

Area of Reinforcement Card

Omit this card if MEI = 0

Variables: AS

Format: E10.3

Number of Cards: NROW

Explanation: area of reinforcement in a row. AS(1) is for the top row, AS(2) is for the second row from the top, etc. In the cases of an odd number of bars in a circular cross section the centroidal axis is taken as the diameter passing through one bar. In this case the number of rows will be the same as the number of bars.

Distance of Row Card

Omit this card if MEI = 0 or ISHAPE = 1

Variables: XS

Format: E10.3

Number of Cards: NROW

Explanation: distance of row from centroidal axis, starting from top row downwards. Positive for rows above the axis and negative for rows below the axis.

Geometry Card

Variables: LENGTH, EPILE, XGS, SPACE

Format: 3E10.3

Number of Cards: 1

Explanation: LENGTH = length of pile(l)

EPILE = modulus of elasticity of pile (F/L^2)

XGS = depth below top of drilled shaft to the new ground surface (L)

SPACE = clear spacing between two drilled shafts (L)

Output Control Card

Variables: KPYOP, INC

Format: 2I5

Number of Cards: 1

Explanation: KPYOP = 0 if no p-y curves are to be generated and printed for verification purposes

= 1 if p-y curves are to be generated and printed for verification (see "control card for output of Internally-Generated p-y curves: card for input of depths at which p-y curves will be generated and printed)

INC = increment used in printing output

= 1 to print values at every node

= 2 to print values at every second node

= 3 to print values at every third node, etc. (up to NI + 1).

Any p-y curves generated for output are written to TAPE1.

Analysis Control Card

Variables: DBC, KOUTPT, KCYCL, RCYCL

Format: 3I5, E10.3

Number of Cards: 1

Explanation: KBC = code to control boundary condition at top of pile

= 1 for a free head (user specifies shear P_t and Moment M_t at the drilled-shaft head)

KOUTPT = 0 if data are to be printed only to depth where moment first changes sign

Run Control Card

Variables: MAXIT, YTOL, EXDEFL

Format: I5, 2E10.3

Number of Cards: 1

Explanation: MAXIT = Maximum number of iterations allowed for analysis of single set of loads. Leave blank for default value of 100 to be used.

YTOL = tolerance (L) on solution convergence. When the maximum change in deflection at any node for successive iterations is less than YTOL, iteration stops. Leave blank for default value of 1.0 E -5 to be used.

EXDEFL = value of deflection of drilled-shafts head (L) that is considered grossly excessive and which stops the run. Leave blank for a default value equal to ten times the diameter of the top of the pile.

Distributed Loads

Omit if NW = 0 or NW = -1

Variables: XW(I), WW(II)

Format: 2E10.3

Number of Cards: NW

Explanation: XW = depth (L) below top of drilled shaft to a point where distributed load is specified

WW = distributed lateral earth pressure (F/L) on drilled shaft

The program uses linear interpolation between points on the WW-XW curve to determine the distributed load at every node. For best results, points on the WW-XW curve should fall on the pile node points. Wherever no distributed load is specified, it is assumed to be zero. Data must be arranged with ascending values of XW.

Pile Properties Card

Omit if NDIAM = 0

Variables: XDIAM(I), DIAM(I), MINERT(I), AREA(I)

Format: 4E10.3

Number of Cards: NDIAM

Explanation: XDIAM = x-coordinate (depth below top of pile) of the top of a segment of pile with uniform cross-section

(L). The first depth (XDIAM(1)) must equal 0.0.

DIAM = diameter of pile corresponding to XDIAM(L). For non-circular cross-sections, use of minimum width will produce conservative results.

MINERT = moment of inertia of pile cross-section (L^4)

AREA = cross-sectional area of pile (L2). If left blank, program will compute area assuming a pipe section.

Data must be arranged with ascending values of XDIAM. Note that at a depth between XDIAM(I) and XDIAM (I + 1), the pile properties associated with XDIAM(I) will be used. For a pile with uniform cross-section, just one pile property card is needed. The last value of XDIAM need not be greater than or equal to the length of pile.

Soil Profile Card

Omit this card if NL = 0

Variables: LAYER, KSOIL, XTOP, XBOT, K, POISS, ESOIL

Format: 2I5, 5E10.3

Number of Cards: NL

Explanation: LAYER(I) = layer identification number (use 1 for the top layer, 2 for the second layer, etc.)

KSOIL(I) = code to control the type of p-y curves that will be used for L-th layer

= 1 to have p-y curves computed internally using Matlock's (1970) criteria for soft clay

= 2 to have p-y curves computed internally using Reese et al.'s (1975) criteria for stiff clay below the water table

= 3 to have p-y curves computed internally using Reese and Welch's (1975) criteria for stiff clay above the water table

= 4 to have p-y curves computed internally using Reese et al.'s (1974) criteria for sand

= 5 to use linear interpolation between input p-y curves

XTOP(I) = x-coordinate of top of layer (L)

M(I) = constant (F/L^3) in equation K=mx. This is used (1) to define initial soil moduli for the first iteration and (2) to determine initial slope of p-y curve where KSOIL = 2 or 4

POISS(I) = Poisson's ratio in the Mindlin equation

ESOIL(I) = constant elastic modulus (F/L^2) in the Mindlin equation.

Arrange data in ascending order of LAYER(I).

<u>Unit Weight Card</u>

Omit this card if NG1 = 0

Variables: XG1(I), GAM1(I)

Format: 2E10.3

Number of Cards: NG1

Explanation: XG1 = depth below top of pile to point where effective unit weight of soil is specified (L)

GAM1 = effective unit weight of soil (F/L^3) corresponding to XG1

The first depth (XG1(I)) must not be greater than the x-coordinate of the ground surface and the last depth (XG1(NG1)) must not be less than the length of pile. The program interpolates linearly between points on XG1 - GAM1 curve to determine effective unit weight of soil at a particular depth. The data must be arranged with ascending values of XG1.

<u>Strength Parameter Card</u>

Omit this card if NSTR = 0

Variables: XSTR(I), C1(I), PHI1(I), EE50(I)

Format: 4E10.3

Number of Cards: NSTR

Explanation: XSTR = x-coordinate (depth below top of pile) for which c, ϕ, and ε_{50} are specified (L)

C1 = undrained shear strength of soil (F/L2) corresponding to XSTR

PHI1 = angle of internal friction (ϕ, in degrees) corresponding to XSTR

EE50 = strain at 50 percent stress level (ε_{50}, dimensionless) corresponding to XSTR

The program uses linear interpolation to find c, ϕ, and ε_{50} at points between input XSTR's. XSTR(I) should not be greater than the x-coordinate of the ground surface and XSTR(NSTR) should not be less than the length of the pile. Arrange data with ascending values of XSTR. For clay layers (KSOIL = 1, 2, or 3), PHI1 will not be used and may be left blank. For sand layers (KSOIL = 40), C1 and EE50 are not used and may be left blank.

<u>Control Card for Input of p-y Curves</u>

Omit this card if NPY = 0 or NPY = -1

Variable: NPPY

Format: I5

Number of Cards: 1

Explanation: NPPY = number of points on input p-y curves (minimum = 2, maximum = 30)

<u>Card for Depth of p-y Curve</u>

Omit this card if NPY = 0 or NPY = -1

Variable: XPY(I)

Format: E10.3

Number of Cards: 1

Explanation: XPY = x-coordinate (depth below top of pile) to an input p-y curve (L)

Data must be arranged in ascending order of XPY. Input XPY, then data to define the associated p-y curve (see next card), then the next XPY, etc.

<u>p-y Curve Data Card</u>

Omit if NPY = 0 or NPY = -1

Variables: YP(I,J), PP(I,J)

Format: 2E10.3

Number of Cards: NPY * NPPY

Explanation: YP = deflection (L) of a point on a p-y curve

PP = soil resistance (F/L) corresponding to YP

Data must be arranged in ascending order of YP. Sequence of input is as follows:

```
   DO 30 I=1, NPY
   READ (5,10), XPY(I)
10 FORMAT (E10.3)
   READ (5,20), (YP(I,J), PP(I,J), J=1, NPPY)
```

20 FORMAT (2E10.3)

30 CONTINUE

The program interpolates linearly between points on a p-y curve and between p-y curves. The program uses the deepest p-y curve available for any nodes that extend below the depth of the deepest p-y curve.

Control Card for Output of Internally-Generated p-y Curves

Omit this card if KPYOP = 0

Variable: NN

Format: I5

Number of Cards: 1

Explanation: NN = number of depths for which internally-generated p-y curves are to be printed (maximum = 305).

Internally-generated p-y curves may be computed for selected depths and printed for verification purposes. In the analysis of pile response, a separate p-y curve is calculated at every node. Therefore, the number of p-y curves printed will have no effect on the solution.

Control Card for Depths at Which Internally-Generated p-y Curves are to be Printed

Omit this card if KPYOP = 0

Variable: XN(I)

Format: E10.3

Number of Cards: NN

Explanation: XN = x - coordinate (L) at which internally-generated p-y curves are to be generated and printed.

Card to Establish Loads on Pile Head

Variables: KOP, PT, BC2

Format: I5, 2E10.3

Number of Cards: Between 1 and 20

Explanations: KOP = 0 if only the pile head deflection, slope, maximum bending moment, and maximum combined stress are to be printed for the associated loads

= 1 if complete output is desired for the associated loads

= -1 to indicate that all pile head loads have been read and to terminate reading this card.

PT = lateral load (F) at top of pile

BC2 = value of second boundary condition

= moment (F-L) at top of pile if KBC = 1

= slope (dimensionless) at top of pile if KBC = 2

= rotational stiffness (F-L), or moment divided by slope, if KBC = 3

Set KOP = -1 to stop input of loads on pile head.

<u>Card to Stop Run</u>

Variable: TITLE(I)

Format: 18A4

Explanation: TITLE = END to stop reading data.

This is the descriptive title for the run (see explanation of first card in the data deck). If the word END is typed in columns 1-3, and column 4 is blank, the program will stop. If anything else appears in these columns, the card will be assumed to be a descriptive title for a new problem. Up to 50 problems can be analyzed in one run. If a new problem is to be read, return to the beginning of this input guide to read the title card and further data. Input is identical no matter what problem is analyzed, except that on second and subsequent problems, some parameters (NL, NDIAM, NW, NG1, NPY) can be set equal to zero (or in some cases -1), to avoid inputting redundant data.

D.4 SUMMARY

A summary of formats for input data is presented in the following tables. All integers (I-format) must be right justified, following tables. E-formats are for real values and also must be right justified.

Coding Form for PYWALL

Made by: ________________ Date: ______

Checked by: ________________ Date: ______

1.00

TITLE CARD (18 A4)																		
1	5	9	13	17	21	25	29	33	37	41	45	49	53	57	61	65	69	72

2.00

UNITS CARDS (4A 4)			
1	5	9	13

3.00

INPUT CONTROL CARD (4 I 5)			
1	6	11	16
N I	N L	N D I A M	N W

4.00

INPUT CTRL. CARD (3 I 5)		
1	6	11
NGI	NSTR	NPY

5.00

CARD 5 (2I5)	
5	10
ISHAPE	

← Identification Number of the Shape Cross Section and the Load Cases

Coding Form for PYWALL

Made by: ______________ Date: ______

Checked by: ______________ Date: ______

CARD 6 (E10.3) ← Axial Load

6.00	10
	P

CARD 7 (4E 10.3) STRENGTH AND MODULUS

7.00	10	20	30	40
	F C	B A R F Y	T U B F F Y	E S

CARD 8 (5E 10.3) SECTION SIZE

8.00	10	20	30	40	50
	W I D T H	O D	D T	T	T T

CARD 9 (215, E 10.3) ← Rebar Arrangement

9.00	5	10	20
	N B A R S	N R O W S	C O V E R

CARD 10 (E 10.3) ← Area of Reinforcement in a Row

10

AS

10.01
10.02
10.03

Repeat nrows times

CARD 11 (E 10.3) ← Distance of Row from Centroidal Axis (Required for Rectangular or Square Section)

10

XS

11.01
11.02
11.03

Repeat nrows times

PILE GEOMETRY CARD (4E 1Ø.3)				
	1	11	21	31
	LENGTH	EPILE	XGS	SPACE
12.00				

Coding Form for PYWALL

Made by: ____________________ Date: ________

Checked by: ____________________ Date: ________

Output Control Card (215)

	1	6
13.00	KPYOP	INC

	ANALYSIS CTRL CARD (215)		
	1	6	11
14.00	KBC	KOUTPT	

	RUN CONTROL CARD (I5,2E 1 Ø.3)		
	1	6	16
15.00	MAXIT	YTOL	EXDEFL

Omit this card if NW = Ø or NW = -1

	DISTRIBUTED LOADS (2E 1 Ø.3)	
	1	11
	XG1 (I)	GAM1 (I)
16.01		
16.02		
16.03		

NW Cards

Coding Form for PYWALL

Made by: ________________ Date: ________

Checked by: ________________ Date: ________

Omit this card if NDIAM = Ø

PILE PROPERTIES CARD (4E 1 Ø.3)

	1	11	21	31
	XDIAM(I)	DIAM(I)	MINERT(I)	AREA(I)
17.01				
17.02				
17.03				

NDIAM Cards

Omit this card if NDIAM = Ø

PILE PROPERTIES CARD (4E 1 Ø.3)

	1	6	11	21	31	41	51
	LAYER	KSOIL	XTOP	XBOT	K	POISS(I)	ESOIL(I)
18.01							
18.02							

NL Cards

Omit this card if NG1 = Ø

UNIT WEIGHT CARD (2E 1 Ø.3)

	1	11
	XG1(I)	GAM1(I)
19.01		
19.02		
19.03		

NGI Cards

Coding Form for PYWALL

Made by: ________________ Date: ______

Checked by: ________________ Date: ______

Omit this card if NSTR = Ø

STRENGTH PARAMETER CARD (4E 1 Ø.3)			
1	11	21	31
XSTR(I)	C1(I)	PHI1(I)	EE5Ø(I)
20.01			
20.02			

NSTR Cards

Omit this card if NPY = Ø or NPY = -1

Control Card for Input Of P-y Curves (I5)

1 5
NPPY
21.00

Omit this card if NPY = Ø or NPY = -1

Control Card for Depth Of P-y Curve (E 1 Ø.3)

XPY(I)
22.00

Omit this card if NPY = Ø or NPY = -1

P-Y CURVE DATA CARD (2E 1 Ø.3)	
1	11
YP(I, J)	PP(I, J)
23.01	
23.02	
23.03	

NPPY Cards

Repeat NPY Times

Coding Form for PYWALL

Made by: ____________ Date: ______

Checked by: ____________ Date: ______

Omit this card if KPYOP = Ø

Control Card for Output of Internally-Generated P-Y Curves (I 5)

1 – 5
NN
24.00

Omit this card if KPYOP = Ø

Control Card for Depths at which Internally-Generated P-Y Curves are to be Printed (E 1Ø.3)

1 – 10
XN (I)
25.01
25.02

CARD TO ESTABLISH LOADS ON PILE HEAD (I 5,2E1Ø.3)			
1	6	16	26
KOP	PT	BC2	
26.01			
26.02			

Maximum 20 Loadings

TITLE CARD (18 A4)

1 5 9 13 17 21 25 29 33 37 41 45 49 53 57 61 65 69 72

27.00

APPENDIX E

OUTPUT

EXAMPLE 1

(INPUT)

```
CASE NO. 1
ENGL
   50     1     1     2     0
    4     2     0
    9.84E2    3.37E6     264.0    12.0
    1     1
    1     1     1
   50  1.00E-03  20.0
  0.0         0.0
  264.0       417.0
    0.00E0    48.00     2.61E05   1810.0
    1     2     264.    994.       1000.   0.45      1000.
    0.0       .072
  264.0       .072
  264.0       .036
  994.0       .036
    264.      20.83                 0.005
   994.       20.83                 0.005
    1
  400.0
    1   4.00
   -1
END
```

EXAMPLE 1

(OUTPUT)

```
CASE NO. 1

UNITS--ENGL


                  I N P U T   I N F O R M A T I O N
                  *********************************


    DISTRIBUTED LOAD CURVE            2 POINTS
                         X,IN        LOAD,LBS/IN
                            0             0
                       264.00          .417E+03


THE LOADING IS STATIC


PILE GEOMETRY AND PROPERTIES

    PILE LENGTH                          =      984.00 IN
    MODULUS OF ELASTICITY OF PILE        =    .337E+07 LBS/IN**2
                  1 SECTION(S)

                X            DIAMETER     MOMENT OF        AREA
                                           INERTIA
                IN              IN          IN**4          IN**2
                  0
                              48.000      .261E+06       .181E+04
             984.00


SOILS INFORMATION

    X AT THE GROUND SURFACE              =      264.00 IN

    1 LAYER(S) OF SOIL

    LAYER  1
    THE SOIL IS A STIFF CLAY BELOW THE WATER TABLE
    X AT THE TOP OF THE LAYER            =      264.00 IN
    X AT THE BOTTOM OF THE LAYER         =      994.00 IN
    MODULUS OF SUBGRADE REACTION         =    .100E+04 LBS/IN**3


    DISTRIBUTION OF EFFECTIVE UNIT WEIGHT WITH DEPTH
                      4 POINTS
               X,IN     WEIGHT,LBS/IN**3
                  0         .72E-01
             264.00         .72E-01
             264.00         .36E-01
             994.00         .36E-01

    DISTRIBUTION OF STRENGTH PARAMETERS WITH DEPTH
                      2 POINTS
```

```
                X,IN         C,LBS/IN**2      PHI,DEGREES      E50
               264.00         .208E+02             0         .500E-02
               994.00         .208E+02             0         .500E-02


     FINITE DIFFERENCE PARAMETERS
         NUMBER OF PILE INCREMENTS                                   =          50
         TOLERANCE ON DETERMINATION OF DEFLECTIONS                   =     .100E-02 IN
         MAXIMUM NUMBER OF ITERATIONS ALLOWED FOR PILE ANALYSIS =               50
         MAXIMUM ALLOWABLE DEFLECTION                                =      .20E+02 IN


     INPUT CODES
         OUTPT   =  1
         KCYCL   =  1
         KBC     =  1
         KPYOP   =  1
         INC     =  1
1    CASE NO. 1


     UNITS--ENGL


                         O U T P U T   I N F O R M A T I O N
                         ***********************************




     GENERATED P-Y CURVES

         THE NUMBER OF CURVES                                 =  1
         THE NUMBER OF POINTS ON EACH CURVE                   = 17


         DEPTH BELOW GS        DIAM          C           CAVG        GAMMA          E50
               IN               IN      LBS/IN**2   LBS/IN**2   LBS/IN**3
            400.00           48.000      .2E+02      .2E+02       .6E-01      .500E-02

            AS =.58        AC =.30      Y,IN               P,LBS/IN
                                          0                    0
                                        .070             1129.755
                                        .140             1597.715
                                        .210             1860.044
                                        .280             2029.401
                                        .350             2144.223
                                        .420             2220.029
                                        .490             2265.684
                                        .560             2286.909
                                        .630             2287.679
                                        .700             2270.906
                                        .770             2238.807
                                        .840             2193.120
                                       1.400             1583.907
                                       1.960              973.770
                                       2.520              363.632
                                      28.000              363.632
```

---------- *** ----------

PILE LOADING CONDITION

LATERAL LOAD AT PILE HEAD = .400E+01 LBS
APPLIED MOMENT AT PILE HEAD = -0 LBS-IN
AXIAL LOAD AT PILE HEAD = 0 LBS

DISTRIBUTED LOAD CURVE 2 POINTS

X,IN	LOAD,LBS/IN
0	0
264.00	.417E+03

X	DEFLECTION	MOMENT	TOTAL STRESS	DISTR. LOAD	SOIL MODULUS	FLEXURAL RIGIDITY
IN	IN	LBS-IN	LBS/IN**2	LBS/IN	LBS/IN**2	LBS-IN**2
*****	**********	**********	**********	**********	**********	**********
0	.638E+00	-.807E-05	.742E-09	0	0	.880E+12
19.68	.601E+00	.787E+02	.724E-02	.311E+02	0	.880E+12
39.36	.564E+00	.122E+05	.112E+01	.622E+02	0	.880E+12
59.04	.527E+00	.484E+05	.445E+01	.933E+02	0	.880E+12
78.72	.490E+00	.121E+06	.111E+02	.124E+03	0	.880E+12
98.40	.453E+00	.241E+06	.222E+02	.155E+03	0	.880E+12
118.08	.416E+00	.422E+06	.388E+02	.187E+03	0	.880E+12
137.76	.380E+00	.675E+06	.620E+02	.218E+03	0	.880E+12
157.44	.343E+00	.101E+07	.931E+02	.249E+03	0	.880E+12
177.12	.307E+00	.145E+07	.133E+03	.280E+03	0	.880E+12
196.80	.272E+00	.199E+07	.183E+03	.311E+03	0	.880E+12
216.48	.238E+00	.265E+07	.244E+03	.342E+03	0	.880E+12
236.16	.205E+00	.344E+07	.317E+03	.373E+03	0	.880E+12
255.84	.173E+00	.438E+07	.403E+03	.404E+03	0	.880E+12
275.52	.143E+00	.548E+07	.504E+03	.950E+01	.509E+04	.860E+12
295.20	.116E+00	.630E+07	.579E+03	.950E+01	.705E+04	.880E+12
314.88	.914E-01	.680E+07	.625E+03	.950E+01	.849E+04	.880E+12
334.56	.698E-01	.701E+07	.644E+03	.950E+01	.995E+04	.880E+12
354.24	.513E-01	.695E+07	.639E+03	.950E+01	.117E+05	.880E+12
373.92	.359E-01	.666E+07	.613E+03	.950E+01	.140E+05	.880E+12
393.60	.234E-01	.618E+07	.568E+03	.950E+01	.170E+05	.880E+12
413.28	.136E-01	.555E+07	.511E+03	.950E+01	.209E+05	.880E+12
432.96	.633E-02	.482E+07	.443E+03	.950E+01	.259E+05	.880E+12
452.64	.113E-02	.402E+07	.370E+03	.950E+01	.255E+05	.880E+12
472.32	-.230E-02	.322E+07	.296E+03	.950E+01	.420E+05	.880E+12
492.00	-.431E-02	.245E+07	.226E+03	.950E+01	.448E+05	.880E+12
511.68	-.524E-02	.177E+07	.163E+03	.950E+01	.462E+05	.880E+12
531.36	-.540E-02	.118E+07	.109E+03	.950E+01	.486E+05	.880E+12
551.04	-.503E-02	.701E+06	.645E+02	.950E+01	.520E+05	.880E+12
570.72	-.435E-02	.325E+06	.298E+02	.950E+01	.568E+05	.880E+12
590.40	-.354E-02	.475E+05	.437E+01	.950E+01	.629E+05	.880E+12
610.08	-.270E-02	-.140E+06	.128E+02	.950E+01	.704E+05	.880E+12

629.76	-.192E-02	-.250E+06	.230E+02	.950E+01	.791E+05	.880E+12
649.44	-.125E-02	-.297E+06	.273E+02	.950E+01	.883E+05	.880E+12
669.12	-.712E-03	-.299E+06	.275E+02	.950E+01	.952E+05	.880E+12
688.80	-.307E-03	-.270E+06	.248E+02	.950E+01	.914E+05	.880E+12
708.48	-.198E-04	-.227E+06	.208E+02	.950E+01	.193E+05	.880E+12
728.16	.167E-03	-.180E+06	.165E+02	.950E+01	.707E+05	.880E+12
747.84	.275E-03	-.133E+06	.123E+02	.950E+01	.815E+05	.880E+12
767.52	.325E-03	-.922E+05	.848E+01	.950E+01	.861E+05	.880E+12
787.20	.333E-03	-.582E+05	.535E+01	.950E+01	.889E+05	.880E+12
806.88	.316E-03	-.320E+05	.294E+01	.950E+01	.911E+05	.880E+12
826.56	.285E-03	-.132E+05	.122E+01	.950E+01	.929E+05	.880E+12
846.24	.249E-03	-.108E+04	.992E-01	.950E+01	.944E+05	.880E+12
865.92	.211E-03	.566E+04	.520E+00	.950E+01	.953E+05	.880E+12
885.60	.177E-03	.827E+04	.760E+00	.950E+01	.958E+05	.880E+12
905.28	.145E-03	.801E+04	.737E+00	.950E+01	.958E+05	.880E+12
924.96	.118E-03	.604E+04	.555E+00	.950E+01	.952E+05	.880E+12
944.64	.928E-04	.340E+04	.313E+00	.950E+01	.936E+05	.880E+12
964.32	.694E-04	.108E+04	.990E-01	.950E+01	.906E+05	.880E+12
984.00	.464E-04	0	0	.950E+01	.851E+05	.880E+12

OUTPUT VERIFICATION

THE MAXIMUM MOMENT IMBALANCE FOR ANY ELEMENT = .155E-04 IN-LBS
THE MAX. LATERAL FORCE IMBALANCE FOR ANY ELEMENT = .116E-05 LBS

COMPUTED LATERAL FORCE AT PILE HEAD = .40000E+01 LBS
COMPUTED MOMENT AT PILE HEAD = -.80683E-05 IN-LBS
COMPUTED SLOPE AT PILE HEAD = -.18793E-02

THE OVERALL MOMENT IMBALANCE = -.331E-03 IN-LBS
THE OVERALL LATERAL FORCE IMBALANCE = .194E-05 LBS

OUTPUT SUMMARY

PILE HEAD DEFLECTION = .638E+00 IN
MAXIMUM BENDING MOMENT = .701E+07 IN-LBS
MAXIMUM TOTAL STRESS = .644E+03 LBS/IN**2
MAXIMUM SHEAR FORCE = .517E+05 LBS

NO. OF ITERATIONS = 6
MAXIMUM DEFLECTION ERROR = .911E-03 IN

1 CASE NO. 1

S U M M A R Y   T A B L E
****

LATERAL LOAD (LBS)	BOUNDARY CONDITION BC2	AXIAL LOAD (LBS)	YT (IN)	ST (IN/IN)	MAX. MOMENT (IN-LBS)	MAX. STRESS (LBS/IN**2
.400E+01	-0	0	.638E+00	-.188E-02	.701E+07	.644E+0.

EXAMPLE 2

(INPUT)

```
CASE NO. 1
ENGL
   50     1     1     2     1
    4     2     0
   10
      0.00
      4.00      60.00       0.00  29000.00
      0.00      48.00       0.00      0.00      0.00
   12     7       3.00
      1.00
      2.54
      2.54
      2.54
      2.54
      2.54
      1.00
    9.84E2    3.37E6      264.0   12.0
    1     1
    1     1     1
   50   5.00E-03  20.0
  0.0        0.0
  264.0      417.0
    0.00E0   48.00      2.61E05   1810.0
    1     2      264.     994.0      1000.    0.45      1000.
    0.0      .072
  264.0      .072
  264.0      .036
  994.0      .036
    264.      20.83             0.005
   994.      20.83             0.005
    1
  400.0
    1   4.00
   -1
END
```

NONLINEAR EI AND ULTIMATE BENDING CAPACITY OF DRILLED SHAFTS

SHAPE : CIRCULAR
DIAMETER 48.00
SHELL THICKNESS 0
CORE TUBE O.D. 0
CORE TUBE THICKNESS 0

NO. OF REBARS 12
ROWS OF REBARS 7
COVER
(BAR CENTER TO CONCR EDGE) 3.0

LAYER	AREA	ORDINATE
1	1.00	21.00
2	2.54	18.19
3	2.54	10.50
4	2.54	0
5	2.54	-10.50
6	2.54	-18.19
7	1.00	-21.00

CONCRETE CYLINDER STRENGTH 4.00KSI
REBARS YIELD STRENGTH 60.00KSI
SHELL/TUBE YIELD STRENGTH 0KSI
MODULUS OF ELAST. OF STEEL 29000.00KSI
MODULUS OF ELAST. OF CONCR 3636.62KSI
SQUASH LOAD CAPACITY 8061.45KPS

1 AXIAL LOAD = 0 KIPS

	MOMENT IN KIPS	EI KIP-IN2	PHI	MAX STR IN/IN	N AXIS IN
1	1186.8	1186818893.0	.000001	.00002	24.08
2	3201.2	640245476.2	.000005	.00012	24.08
3	3201.2	355691931.2	.000009	.00010	10.95
4	3201.2	246248260.1	.000013	.00014	10.97
5	3464.8	203813847.6	.000017	.00019	11.00
6	4272.8	203466753.9	.000021	.00023	11.02
7	5078.1	203122612.1	.000025	.00028	11.05
8	5880.2	202765913.9	.000029	.00032	11.07
9	6679.6	202411236.3	.000033	.00037	11.10
10	7475.9	202050676.4	.000037	.00041	11.12
11	8269.0	201683848.9	.000041	.00046	11.15
12	9059.0	201310362.8	.000045	.00050	11.17
13	9880.9	201650509.5	.000049	.00055	11.20
14	10640.1	200756206.6	.000053	.00059	11.20
15	14481.5	174475477.6	.000083	.00091	10.92
16	15672.4	138693889.4	.000113	.00116	10.25
17	16571.6	115885311.3	.000143	.00140	9.79
18	16878.0	97560913.8	.000173	.00161	9.32
19	17081.3	84144215.5	.000203	.00181	8.93

20	17270.8	74123673.8	.000233	.00203	8.71
21	17413.7	66211612.7	.000263	.00223	8.48
22	17543.8	59876502.5	.000293	.00244	8.32
23	17663.7	54686236.3	.000323	.00265	8.20
24	17776.7	50358880.1	.000353	.00286	8.11
25	17870.4	46659128.8	.000383	.00308	8.04
26	18151.3	43949841.3	.000413	.00330	8.00
27	17885.5	40373601.3	.000443	.00350	7.91
28	17872.2	37784746.5	.000473	.00369	7.80
29	17857.9	35502747.1	.000503	.00388	7.72

1

CASE NO. 1

UNITS--ENGL

INFUT INFORMATION
****

DISTRIBUTED LOAD CURVE   2 POINTS

X,IN	LOAD,LBS/IN
0	0
264.00	.417E+03

THE LOADING IS STATIC

PILE GEOMETRY AND PROPERTIES

PILE LENGTH = 984.00 IN
MODULUS OF ELASTICITY OF PILE = .337E+07 LBS/IN**2
1 SECTION(S)

X	DIAMETER	MOMENT OF INERTIA	AREA
IN	IN	IN**4	IN**2
0			
	48.000	.261E+06	.181E+04
984.00			

SOILS INFORMATION

X AT THE GROUND SURFACE = 264.00 IN

1 LAYER(S) OF SOIL

LAYER 1
THE SOIL IS A STIFF CLAY BELOW THE WATER TABLE
X AT THE TOP OF THE LAYER = 264.00 IN
X AT THE BOTTOM OF THE LAYER = 994.00 IN
MODULUS OF SUBGRADE REACTION = .100E+04 LBS/IN**3

DISTRIBUTION OF EFFECTIVE UNIT WEIGHT WITH DEPTH

```
                         4 POINTS
                 X,IN     WEIGHT,LBS/IN**3
                   0          .72E-01
              264.00          .72E-01
              264.00          .36E-01
              994.00          .36E-01

     DISTRIBUTION OF STRENGTH PARAMETERS WITH DEPTH
                         2 POINTS
                 X,IN        C,LBS/IN**2      PHI,DEGREES      E50
              264.00        .208E+02              0         .500E-02
              994.00        .208E+02              0         .500E-02

   FINITE DIFFERENCE PARAMETERS
       NUMBER OF PILE INCREMENTS                                =          50
       TOLERANCE ON DETERMINATION OF DEFLECTIONS                =    .500E-02 IN
       MAXIMUM NUMBER OF ITERATIONS ALLOWED FOR PILE ANALYSIS   =          50
       MAXIMUM ALLOWABLE DEFLECTION                             =     .20E+02 IN

   INPUT CODES
       OUTPT   =  1
       KCYCL   =  1
       KBC     =  1
       KPYOP   =  1
       INC     =  1
1  CASE NO. 1

   UNITS--ENGL

                        O U T P U T   I N F O R M A T I O N
                        ***********************************

   GENERATED P-Y CURVES

       THE NUMBER OF CURVES                           =  1
       THE NUMBER OF POINTS ON EACH CURVE             = 17

       DEPTH BELOW GS      DIAM        C          CAVG       GAMMA         E50
            IN              IN    LBS/IN**2  LBS/IN**2  LBS/IN**3
          400.00          48.000    .2E+02     .2E+02     .6E-01     .500E-02

          AS =.58       AC =.30    Y,IN             P,LBS/IN
                                      0                  0
                                   .070           1129.755
                                   .140           1597.715
                                   .210           1860.044
                                   .280           2029.401
                                   .350           2144.223
                                   .420           2220.029
                                   .490           2265.684
```

.560	2286.909
.630	2287.679
.700	2270.906
.770	2238.807
.840	2193.120
1.400	1583.907
1.960	973.770
2.520	363.632
28.000	363.632

---------- *** ----------

PILE LOADING CONDITION

LATERAL LOAD AT PILE HEAD	=	.400E+01	LBS
APPLIED MOMENT AT PILE HEAD	=	-0	LBS-IN
AXIAL LOAD AT PILE HEAD	=	0	LBS

DISTRIBUTED LOAD CURVE 2 POINTS

X,IN	LOAD,LBS/IN
0	0
264.00	.417E+03

X IN	DEFLECTION IN	MOMENT LBS-IN	TOTAL STRESS LBS/IN**2	DISTR. LOAD LBS/IN	SOIL MODULUS LBS/IN**2	FLEXURAL RIGIDITY LBS-IN**2
*****	**********	**********	**********	**********	**********	**********
0	.194E+01	-.435E-04	.400E-08	0	0	.119E+13
19.68	.182E+01	.787E+02	.724E-02	.311E+02	0	.119E+13
39.36	.171E+01	.122E+05	.112E+01	.622E+02	0	.119E+13
59.04	.159E+01	.484E+05	.445E+01	.933E+02	0	.119E+13
78.72	.147E+01	.121E+06	.111E+02	.124E+03	0	.119E+13
98.40	.135E+01	.241E+06	.222E+02	.155E+03	0	.119E+13
118.08	.123E+01	.422E+06	.388E+02	.187E+03	0	.119E+13
137.76	.111E+01	.675E+06	.620E+02	.218E+03	0	.119E+13
157.44	.995E+00	.101E+07	.931E+02	.249E+03	0	.119E+13
177.12	.877E+00	.145E+07	.133E+03	.280E+03	0	.251E+12
196.80	.762E+00	.199E+07	.183E+03	.311E+03	0	.251E+12
216.48	.649E+00	.265E+07	.244E+03	.342E+03	0	.251E+12
236.16	.541E+00	.344E+07	.317E+03	.373E+03	0	.240E+12
255.84	.438E+00	.438E+07	.403E+03	.404E+03	0	.213E+12
275.52	.343E+00	.548E+07	.504E+03	.950E+01	.198E+04	.209E+12
295.20	.258E+00	.632E+07	.581E+03	.950E+01	.402E+04	.206E+12
314.88	.185E+00	.675E+07	.621E+03	.950E+01	.583E+04	.205E+12
334.56	.125E+00	.678E+07	.623E+03	.950E+01	.773E+04	.205E+12
354.24	.780E-01	.643E+07	.591E+03	.950E+01	.976E+04	.206E+12
373.92	.427E-01	.579E+07	.532E+03	.950E+01	.127E+05	.209E+12
393.60	.182E-01	.494E+07	.454E+03	.950E+01	.171E+05	.213E+12
413.28	.267E-02	.398E+07	.366E+03	.950E+01	.191E+05	.222E+12
432.96	-.594E-02	.300E+07	.276E+03	.950E+01	.304E+05	.251E+12

452.64	-.991E-02	.209E+07	.192E+03	.950E+01	.313E+05	.251E+12
472.32	-.107E-01	.131E+07	.121E+03	.950E+01	.332E+05	.251E+12
492.00	-.938E-02	.671E+06	.617E+02	.950E+01	.372E+05	.119E+13
511.68	-.789E-02	.169E+06	.155E+02	.950E+01	.420E+05	.119E+13
531.36	-.634E-02	-.201E+06	.185E+02	.950E+01	.474E+05	.119E+13
551.04	-.485E-02	-.451E+06	.414E+02	.950E+01	.538E+05	.119E+13
570.72	-.351E-02	-.596E+06	.548E+02	.950E+01	.612E+05	.119E+13
590.40	-.237E-02	-.654E+06	.601E+02	.950E+01	.695E+05	.119E+13
610.08	-.144E-02	-.645E+06	.593E+02	.950E+01	.778E+05	.119E+13
629.76	-.721E-03	-.588E+06	.541E+02	.950E+01	.822E+05	.119E+13
649.44	-.194E-03	-.505E+06	.464E+02	.950E+01	.657E+05	.119E+13
669.12	.169E-03	-.413E+06	.380E+02	.950E+01	.550E+05	.119E+13
688.80	.397E-03	-.321E+06	.295E+02	.950E+01	.696E+05	.119E+13
708.48	.521E-03	-.236E+06	.217E+02	.950E+01	.740E+05	.119E+13
728.16	.567E-03	-.163E+06	.150E+02	.950E+01	.766E+05	.119E+13
747.84	.560E-03	-.102E+06	.942E+01	.950E+01	.789E+05	.119E+13
767.52	.519E-03	-.555E+05	.510E+01	.950E+01	.811E+05	.119E+13
787.20	.461E-03	-.211E+05	.194E+01	.950E+01	.831E+05	.119E+13
806.88	.395E-03	.220E+04	.203E+00	.950E+01	.849E+05	.119E+13
826.56	.330E-03	.162E+05	.149E+01	.950E+01	.863E+05	.119E+13
846.24	.271E-03	.227E+05	.209E+01	.950E+01	.871E+05	.119E+13
865.92	.219E-03	.239E+05	.220E+01	.950E+01	.873E+05	.119E+13
885.60	.174E-03	.213E+05	.196E+01	.950E+01	.868E+05	.119E+13
905.28	.137E-03	.165E+05	.152E+01	.950E+01	.854E+05	.119E+13
924.96	.105E-03	.109E+05	.100E+01	.950E+01	.827E+05	.119E+13
944.64	.768E-04	.560E+04	.515E+00	.950E+01	.782E+05	.119E+13
964.32	.502E-04	.164E+04	.151E+00	.950E+01	.703E+05	.119E+13
984.00	.242E-04	0	0	.950E+01	.424E+05	.119E+13

OUTPUT VERIFICATION

THE MAXIMUM MOMENT IMBALANCE FOR ANY ELEMENT = .919E-04 IN-LBS
THE MAX. LATERAL FORCE IMBALANCE FOR ANY ELEMENT = .889E-05 LBS

COMPUTED LATERAL FORCE AT PILE HEAD = .40000E+01 LBS
COMPUTED MOMENT AT PILE HEAD = -.43547E-04 IN-LBS
COMPUTED SLOPE AT PILE HEAD = -.60287E-02

THE OVERALL MOMENT IMBALANCE = -.321E-02 IN-LBS
THE OVERALL LATERAL FORCE IMBALANCE = .406E-04 LBS

OUTPUT SUMMARY

PILE HEAD DEFLECTION = .194E+01 IN
MAXIMUM BENDING MOMENT = .678E+07 IN-LBS
MAXIMUM TOTAL STRESS = .623E+03 LBS/IN**2
MAXIMUM SHEAR FORCE = .517E+05 LBS

NO. OF ITERATIONS = 10
MAXIMUM DEFLECTION ERROR = .413E-02 IN

L CASE NO. 1

S U M M A R Y T A B L E
****

LATERAL LOAD (LBS)	BOUNDARY CONDITION BC2	AXIAL LOAD (LBS)	YT (IN)	ST (IN/IN)	MAX. MOMENT (IN-LBS)	MAX. STRESS (LBS/IN**2)
.400E+01	-0	0	.194E+01	-.603E-02	.678E+07	.623E+03

BIBLIOGRAPHY

Abbott, M. B., An Introduction to The Method of Characteristics, American Elsevier, New York.

Al-Hussaini M. M., "Pressure Distribution Around a Laterally Loaded Pile", Journal of The University of Kuwait, Vol.9, No.1, 1982.

Bachrach B. I. and Samanta S. K., "A Numerical Method for Computing Plane Plastic Slip-Line Fields", Journal of Applied Mechanics, March, 1976.

Bjerrum, L., Frimman Clausen, C. J., and Duncan J. M., "Earth Pressures on Flexible Structures-State-of-the-Art Report," Proc., 5th Eur. Conf. Soil Mech., Madrid, 1972.

Bhushan, K., Lee, L. Jm, and Grime, D. B., "Lateral Load Tests on Drilled Piers in Sand," Drilled Piers andCaissons, Proceedings of a session sponsored by Geotechnical Engineering Division, ASCE National Convention, St. Louis, Missouri, pp. 98-113.

Bogard, D. and Matlock, H., "Procedures for Analysis of Laterally Loaded Pile Groups in Soft Clay," Proceedings, Specialty Conference on Geotechnical Engineering in Offshore Practice, ASCE April, 1983.

Bransby, P. L. and Milligan, G. W. E., "Soil Deformations Near Cantilever sheet Pile Walls," Geotechnique 25, No. 2, 1975.

Broms, B. B., "Lateral Resistance of Piles in Cohesionless Soils," Proc., ASCE, Vol. 90, No. SM 3, May, 1964b.

Broms, B. B., "Discussion on Design Method for Stabiling Piles Against Landslide-one row of Piles by Ito, T., Matsui, T., and Hong, W. P.," Soil and Foundations, Japanese Society of Soil Mechanics and Foundation Engineering, Vol. 23, No. 3, 1983.

Broms, B. B., "Lateral Resistance of Piles in Cohesive Soils," Proc., ASCE, VOl. 90, No. SM 2, March, 1964a.

Bros, B., "The Influence of Model Retaining Wall Displacements in Active and Passive Earth Pressures," Proc., 5th European Conf. on Soil Mech. and Found. Eng., Vol. I, Madrid, 1972.

Building Code Requirements and Commentary for Reinforced Concrete (ACI 318-83), American Concrete Institute, 1983.

Charke. B. G. and Wroth, C. P., "Analysis of Dunton Green Retaining Wall Based on Results of Pressuremeter Tests," Geotechnique 34, No. 4, 1984.

Clark, A. P., "Cracking in Reinforced Concrete Flexural Member," ACI Journal, V. 27, No. 8, April, 1956.

Clough, G. W. And Tsui, Y., "Performance of Tie-back Walls in Clay," Journal of The Geotechnical Division, ASCE, Vol. 100, Dec., 1974.

Cox, W. R., Dixon, D. A., and Murphy, B. S., "Lateral-Load Tests on 25.4 mm Diameter Piles in Very Soft Clay in Side-by-Side and In-Line Groups, Laterally loaded Deep Foundations: Analysis and Performance," ASTM STP 835, J. A., 1984.

Cox, W. R., Reese, L. C., and Grubbs, B. R., "Field Testing of Laterally Loaded Piles in Sand," Proceedings of Offshore Technology Conference, Houston, Texas, Vol. II, Paper No.2097, 1974.

Coyle, H. M. and Reese, L. C., "Load Transfer for Axially Loaded Piles in Clay," Journal of The Soil Mechanics and Foundations Division, ASCE, No. SM 2, March, 1966.

Dennis, N. D. and Olson, R. E., "Review and Compilation of Pile Test Results, Axial Pile Capacity ," Geotechnical Engineering Report CR83-4, Geotechnical Engineering Center, The University of Texas at Austin, Austin, Texas, 1982.

Desai, C. S. and Appel, G. C., "3-D Analysis of Laterally Loaded Structures," Proceedings, Second International Conference on Numerical Methods in Geomechanics, Blacksburg, Va., June, 1976.

Duncan, J. M. and Chang, C., "Nonlinear Analysis of stress and Strain in Soils," Journal of The Soil Mechanics and Foundations Division, ASCE, Vol. 90, No. SM 5, Sept. 1970.

Eppes, B. G., " Comparison of Measured and Calculated Stiffnesses for Beams Reinforced in Tension Only," ACI Journal, V. 31, No. 1,July, 1959.

Focht, J. A., Jr., and Koch, K. J., "Rational Analysis of the Lateral Deformance of Offshore Pile Groups," Proc., Fifty Annual Offshore Technology Conference, Paper No. 1896, Vol.II, Houston, 1973.

Garrett, C. & Barnes, S. J., "The Design and Performance of the Dunton Green Retaining Wall," Geotechnique 34, No. 4, 1984.

Gazioglu, S. M., and O'Neill, M. W., "Evaluation of p-y Relationships in Cohesive Soils," Analysis and Design of Pile Foundations, Proceedings of a symposium sponored by Geotechnical Engineering Division, ASCE National Convention, San Francisco, California, 1984.

Haliburton, T. A., "Numerical Analysis of Flexible Retaining Structures, " Proc., Journal of The Soil Mechanics and Foundations Division, ASCE, SM 6, Nov. 1968.

Hetenyi, M., Beams on Elastic Foundation, University of Michigan Press., Ann Arbor, Michigan, 1946.

Hill, R., The Mathematical Theory of Plasticity, Clarendon press, Oxford, 1950.

Ito, T. and Matsui, T., "Methods to Estimate Lateral Force Acting on Stabiling Piles," Soils and Foundations, Japanese Society of Soil Mechanics and Foundation Engineering, Vol.15, No.4, 1975.

Ito, T. Matsui, T., and Hong, W. P., "Design Method for Stabilizing Piles Against Landslide - one row of Piles," Soils and Foundations, Japanese Society of Soil Mechanics and Foundation Engineering, Vol.21, No.2, 1981.

James, E. L., and Jack, B. J., "Design Study of Diaphragm Walls, " Proc., Diaphragm Walls Anchorages, Institution of Civil Engineers, London, 1974.

Johnson, W. and Hillier, M. J., "Some Slip Line Fields for Indenting with Rotating Dies," Int. J. Mech. Sci. 2, 191, 1963.

Khadilkar, B. S. and Varma, B. S., "Analysis of Interference of Strip Footings by FEM" Proc., 9th ICSMFE, Tokyo, 1977.

Konder, R. L., "Hyperbolic Stress-Strain Response: Cohesive Soils," Journal of The Soil Mechanics and Foundations Division, ASCE, Vol. 90, No. SM 1, Feb. 1963.

Littlejohn, G. S. and Macfarlane, I. M., "A Case History Study of Multi-tied Diaphragm Walls," Proceedings I. C. Conference on Diaphragm Walls and Anchorages, London, 1975.

Matlock, H. "Correlation for Design of Laterally Loaded Piles in Soft Clay," Paper No. OTC 1204, Proc., Second Annual Offshore Technology Confer Conference, Houston, Texas, Vol. 1, 1970.

Matlock, H. and Reese, L. C., "Generalized Solution for Laterally Loaded Piles," Proc. Journal of The Soil Mechanics and Foundations Division, ASCE, Vol. 86, No. SM 5, Part I, 1960.

Mathey and Watstein, "Effect of Tensile Properties of Reinforcement on the Flexural Characteristics of Beams," ACI Journal, V. 31, No. 12, June, 1960.

Matsuo, M., Kenmochi, S., and Yagi, H., "Experimental Study on Earth Pressure of Retaining Wall Field Tests," Journal of Japanese Society of SM and FE, Vol. 18, No. 3, 1978.,

Milligan, G. W. E., "Soil Deformations Near Anchored Sheet-Pile Walls," Geotechnique 33, No. 1, 1983.

Mindlin, R. D., "Force at a Point in the Interior of a Semi-Infinite Solid," Physics, Volume 7, May, 1936, pp. 195-202.

Murchison, J. M., and O'Neill, M. W., "Evaluation of p-y Relationships in Cohesionless soils," Analysis and Design of Pile Foundations,Proceedings of symposium sponsored by Geotechnical Engineering Division, ASCE National Convention, San Francisco, California, 1984.

Myslivec, A. and Kysela, A., "Effect of Adjacent Foundation on Bearing Capacity," Proc. of Conf. on Soil Mech. and Found., Budapest,1968.

Nyman, K. J., "Field Load Tests of Instrumented Drilled Shafts in Coral Limestone," Unpublished Thesis, The University of Texas at Austin, 1980.

O'Neill, M. W., "Group Action in Offshore Piles," Proceedings, Specialty Conference on Geotechnical Engineering in Offshore Practice,American Society of Civil Engineers, April, 1983.

O'Neill, M. W., Ghazzaly, O. I., and Ha, H. B., "Analysis of Three-Dimensional Pile Groups with Nonlinear Response and Pile-Soil-Pile Interaction," Proceedings, Ninth Offshore Technology Conference, Volume II, 1977, pp. 245-256.

Owen and Hinton, Finite Elements in Plasticity: Theory and Practice, Pineridge Press Limited, Swansea, U. K>, 1980.

Parker, F., Jr., and Reese, L. C., "Lateral Pile-Soil Interaction Curves for Sand," Proceedings of the International Symposium on the Engineering Properties of Sea-Floor Soils and Their Geophysical Identification, the University of Washington, Seattle,Washington, 1971.

Poulos, H. G., "Behavior of Laterally Loaded Piles: II- Pile Groups," Proc., ASCE, Vol. 97., No. SM 5, May, 1971.

Prakash, S., "Behavior of Pile Groups Subjected to Lateral Loads," Thesis Presented to the University of Illionis, at Urbana, Ill., 1962.

Pula, O. and Rybak, C., "Plastic Interference of Strip Footings," Proc. of 10th ICSMFE, Stockholm, 1981.
Randolph, M. F, and Houlsby, G. T., "The Limiting Pressure on a Circular Pile Loaded Laterally in Cohesive Soil," Geotechnique 34, 1984.

Rauhut, J. B., " A finite-Element Method for Analysis of Anchored Bulkheads and Anchor Walls," Unpublished Thesis, The University of Texas at Austin, August, 1966.

Rix, G. J., "Correlation of Elastic Moduli and Cone Penetration Resistance," Unpublished Thesis, The University of Texas at Austin, 1984.

Reese, L. C., "Behavior of Piles and Pile Groups Under Lateral Load," Report to U.S. Department of Transportation, Federal Highway Administration, Office of Research, Development and Technology, Washington, D. C., July, 1983.

Reese, L. C., "Discussion of Soil Modulus for Laterally Loaded Piles, by McClelland, B. and Focht, J. A., Jr.," Transactions, ASCE, Vol. 123,1958.

Reese, L. C., "Handbook on Design of Piles and Drilled Shafts Under Lateral Load," Report to U. S. Department of Transportation, Federal Highway Administraion, Office of Research, Development and Technology, Washington, D. C., Report No. FHWA-IP-84-11, July, 1984.

Reese, L. C., Handbook on Design Of Piles And Drilled Shafts UnderLateral Load, a handbook prepared for U.S. Department of Transportation, Federal Highway Administration, Office of Research, Washington, D. C. July, 1984.

Reese, L. C., Cox, W. R., and Koop, F. D., "Field Testing and Analysis of Laterally Loaded Piles in Sand," Proceedings of the Fifth Offshore Technology Conference, Houston, Texas, Paper No. OTC 2080, Vol. II, 1974.

Reese, L. C., Cox, W. R., and Koop, F. D., "Field Testing and Analysis of Laterally Loaded Piles in Stiff Clay," Proceedings of the Seventh Offshore Technology Conference, Houston, Texas, Paper No. OTC 2312, Vol. II, 1975.

Reese, L. C. and Wang S, T., "Method of Analysis of Piles Under Lateral Loading," Marine Geotechnology and Nearshore and Offshore Structures, ASTM STP 923, R. C. Chaney and H. Y. Fang, Eds., American Society for Testing and Materials, Philadephia,1986.

Reese, L. C., and Welch, R. C., "Lateral Loading of Deep Foundations in Stiff Clay," Journal of the Geotechnical Engineering Division, American Society of Civil Engineers, Vol. 101, No. GT7, Proc. Paper 11456, 1975.

Richart, F. E., JR., "Analysis for Sheet-Pile Retaining Walls", Transactions, ASCE, Vol. 122, 1957.

Roscoe, K. H., Arthur, J. R. F. and James, R. G., "The Determination of Strains in Soils by an X-ray Method," Civ. Eng. and Pub.Wks. Rev. 58, No. 684.

Rowe, P. W., "Discussion on Session 3a," Proc., 5th Eur. Conf. Soil Mech., Madrid, 1972.

Rowe, P. W. "Progressive Failure and Strength of Sand Mass," Proc.,Seventh Intern, Conf. on Soil Mech. and Found, Engr., Vol. 1,1969.

Rowe, P. W., "A Theoretical and Experimental analysis of sheet pile walls," Proc., Institution of Civil Engineers, London, Jan. 1955.

Samanta, S. K., "Slip-line Field for Extrusion Cosine-Shaped Dies,"Journal of Mech. Phys. Solids, Vol. 18, 1970.

Schults, M. S., Einstein, H. H., and Azzouz, A. S., "Evaluation of Slurry Wall Construction and Design, Volume 3 Empirical Empirical Investigations of the Behavior of Diaphragm Walls," Federal Highway Administration, Office of Research and Development, Washington, D. C., 1984.

Seed, H. B. and Reese, L. C., "The Action of Soft Clay Along Friction Piles," Transactions, ASCE, Vol. 122, 1957.

Sherif, M. A., I. Ishibashi, and C. D. Lee, "Earth Pressures Against Rigid Retaining Walls," ASCE, Jour. Geot. Engr. Divi., Vol. 108, No.GT5, 1982.

Sills, G. C., Burland, J. B., and Czechowski, M. K., "Behavior of an Anchored Diaphragm Wall in Stiff Clay," Ninth ICSMFE, 1977.

Sokolovskii, V. V., Statics of Granular Media, Pergamon Press, New York, 1965.

Sowers, G. B. and Sower, G. F., Introductory Soil Mechanics and Foundations, The MacMillan Co., New York, N.Y., 1970.

Spangler, M. G., "Horizontal Pressures on Retaining Walls due to Concentrated Surface Loads," Iowa Engr. Exp. Station, Bull. 140, Iowa State University, Ames, Iowa., 1938.

Stroyer, J. R. P. N., "Earth-Pressure on Flexible Walls," J. Instn Civ. Engrs 1, Nov., 1935.

Sullivan, W. R., "Development and Evaluation of a Unified Method for the Analysis of Laterally Loaded Piles in Clay," Unpublished Thesis, The University of Texas at Austin, 1977.

Tschebotarioff, G. P., "Larger Scale Model Earth Pressure Tests on Flexible Bulkheads," Proc., ASCE, Jan. 1948.

Terzaghi, K., "Anchored Bulkheads," Transaction 119, ASCE, 1954.

Terzaghi, K., "Evaluation of Coefficients of Subgrade Reaction," Geotechnique, Volume 5, December 1955.

Terzaghi, K. ,"Large Retaining Wall Tests," Engineering News Record, Vol. 112, 1934.

Terzaghi, K. and Peck, R. B., Soil Mechanics in Engineering Practice, John Wiley & Sons, N.Y., 1967.

Terzaghi, K., "Evaluation of Coefficients of Subgrade Reaction," Geotechnique, Vol. V., 1955.

Thompson, G. R., Application of The Finite Element Method to The Development of p-y curves for Saturated Clays, Master Thesis, The University of Texas at Austin, 1977.

Waas, G., "Analysis Method for Footing Vibrations Through Layered Media," Technical Report S-71-14, U.S. Army Engineer Waterways Experiment Station, Soil and Pavements Laboratory, Visksburg, Mississippi, 1972.

Welch, R. C. and Reese, L. C., "Laterally Loaded Behavior of Drilled Shafts," Research Report No. 3-5-65-89, Center for Highway Research, University of Texas at Austin, 1972.

Williams, C. E., and Baka, J. E., "Predicted and Measured Performance of Cantilevered Retention Systems," Texas Civil Engineer, Vol. 56, No. 4, 1986.

Williams, C. E. and Focht, J. A. III, "Initial Response of Foundations on Stiff Clay," ASCE Convention and Exhibit, Pre-print 82-531, New Orleans, LA.

Williams, C. E. and Shamooelian, S., "Evaluated Performance of Cantilevered of Cantilevered Drilled Sgaft Walls," Texas Section,ASCE Fall Meeting, Houston, TX., 1980.

Winkler, E., Die Lehre von Elastizitat und Festigkeit, (On Elasticity and Fixity), Prague, 1867.

Wright, S. G., "Documenation for SSTAB1 - A General Computer Program for Slope Stability Analysis," Geotechnical Engineering Software GS82-1, Geotechnical Engineering Center, Bureau of Engineering Research, The University of Texas at Austin, Austin, Texas, 1982.

Yegian, M. and Wright, S., "Lateral Soil Resistance-Displacement Relationships for Pile Foundations in Soft Clays," Preprint Vol.II, Fifth Annual Offshore Technology Conference, Houston, Texas, 1973.